



**NTNU – Trondheim**  
Norwegian University of  
Science and Technology

# Evaluation Of Design Concepts For A Separation Monitoring Technology

**Even R Bahezre De Lanlay**  
**Rune Tungen**

Master of Energy and Environmental Engineering

Submission date: June 2014

Supervisor: Even Solbraa, EPT

Co-supervisor: Pablo Mathias Dupuy, Statoil ASA  
Oddbjørn Rekaa Nilssen, Statoil ASA

Norwegian University of Science and Technology  
Department of Energy and Process Engineering



EPT-M-2014-23

**MASTER THESIS**

for

Students Even de Lanlay and Rune Tungen

Spring 2014

**Evaluation of design concepts for a separation monitoring technology***Evaluering av designkonsepter for en separasjon-monitoreringsteknologi***Background and objective**

Statoil's Subsea Separation Technologies department addresses new ideas and problems related to separators in production systems. The performance of separation units have an impact on the downstream process equipment as well as on the specifications for the final product, e.g. low gas separation performance is giving poor gas quality increasing the risk for hydrate formation.

There are currently no existing technologies that are capable of measuring separation performance and work is therefore ongoing to develop and qualify this.

The students will work on maturing one such concept for separation performance monitoring. This implies working on detailing and validating the concept design. This will be done both by a theoretical analysis, modeling and experimental activities. The work will be based on plan and pre-study found in De Lanlay, Tungen (2013) "Early Study of Two New Technologies For Solving Separation Challenges", NTNU project thesis.

**The following tasks are to be considered:**

1. Gather design concepts, e.g. active vs. passive (vortex shedding), pipe surface geometry, diameter, length etc.
2. Assess the concepts experimentally
3. Assess the concepts theoretically
4. Conclude on robustness, reliability, accuracy, development time and considerations for installation.

-- " --

Within 14 days of receiving the written text on the master thesis, the candidate shall submit a research plan for his project to the department.

When the thesis is evaluated, emphasis is put on processing of the results, and that they are presented in tabular and/or graphic form in a clear manner, and that they are analyzed carefully.

The thesis should be formulated as a research report with summary both in English and Norwegian, conclusion, literature references, table of contents etc. During the preparation of the text, the candidate should make an effort to produce a well-structured and easily readable report. In order to ease the evaluation of the thesis, it is important that the cross-references are correct. In the making of the report, strong emphasis should be placed on both a thorough discussion of the results and an orderly presentation.

The candidate is requested to initiate and keep close contact with his/her academic supervisor(s) throughout the working period. The candidate must follow the rules and regulations of NTNU as well as passive directions given by the Department of Energy and Process Engineering.

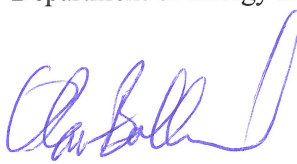
Risk assessment of the candidate's work shall be carried out according to the department's procedures. The risk assessment must be documented and included as part of the final report. Events related to the candidate's work adversely affecting the health, safety or security, must be documented and included as part of the final report. If the documentation on risk assessment represents a large number of pages, the full version is to be submitted electronically to the supervisor and an excerpt is included in the report.

Pursuant to "Regulations concerning the supplementary provisions to the technology study program/Master of Science" at NTNU §20, the Department reserves the permission to utilize all the results and data for teaching and research purposes as well as in future publications.

The final report is to be submitted digitally in DAIM. An executive summary of the thesis including title, student's name, supervisor's name, year, department name, and NTNU's logo and name, shall be submitted to the department as a separate pdf file. Based on an agreement with the supervisor, the final report and other material and documents may be given to the supervisor in digital format.

- Work to be done in lab (Water power lab, Fluids engineering lab, Thermal engineering lab)  
 Field work

Department of Energy and Process Engineering, 14. January 2014



Olav Bolland  
Department Head



Even Solbraa  
Academic Supervisor

Research Advisor:  
Oddbjørn Rekaa Nilssen, Pablo Matias Dupuy

## Abstract

Current wet gas meters used by Statoil can detect liquid volume fractions (LVFs) over 5%, but not smaller fractions. This means that there are currently no technologies capable of monitoring separation performance. It is in Statoil's interest to measure and monitor the separation performance, since too high LVFs can damage downstream process equipment and increase the risk of hydrate formation.

In this master thesis an early study of a new technology for separation performance monitoring is performed. It is based on sound measurements and the influence of liquid on sound wave propagation, i.e. acoustic damping. Other studies have showed that introducing liquid in a gas increase the attenuation of the sound amplitude.

Two different design concepts were investigated: a corrugated pipe and a smooth pipe with a loud speaker. The corrugated pipe is capable of generating sound without external sources. When gas flows through a corrugated pipe, it induces vortex shedding in the cavities. At high enough flow velocities, the frequency of the vortex shedding couples with the pipe's natural frequency. This results in a high tonal sound, or whistling. A phenomenon usually dubbed "singing riser" in the oil and gas industry as it occurs in the flexible risers transporting hydrocarbons from the seabed to the sea surface. The smooth pipe, however, has no self-generating sound source and hence a loud speaker is needed to create sound.

The design concepts are approached theoretically, by modelling and by experiment. A one-dimensional flow-acoustics model was simulated in COMSOL Multiphysics. The model failed to return realistic sound pressure levels but captured the physical phenomena occurring in a corrugated pipe well. For instance, it predicted the first mode of the pipe's natural frequency accurately.

The two designs concepts were tested experimentally for different gas flow rates and different liquid rates. The experiments strongly indicated an added acoustic damping due to liquid, even for LVFs much lower than  $1 \cdot 10^{-4}$ , and thus the main principle of the technology was supported. However, the experiments could not reveal any significant advantages in measurement accuracy for either a smooth or a corrugated design.



## Sammendrag

Dagens metoder for å måle volumetrisk væskefraksjon (LVF) i Statoil kan ikke detektere fraksjoner lavere enn 5%. Det betyr samtidig at det ikke eksisterer teknologi for å monitorere ytelsen til separatorer. Ytelsen til separatorer ønskes målt av Statoil på grunn av de potensielle skadene en for høy væskefraksjon kan påføre nedstrøm prosesseringsutstyr og den økte risikoen for hydratdannelsen som kan oppstå.

I denne masteroppgaven er det utført en studie av en ny teknologi for å monitorere ytelsen til separatorer. Denne metoden er basert på måling av lyd og hvordan væske påvirker dempingen av lydbølgene i et rør. Andre studier har vist at lyden dempes mer i en gass når den inneholder væske enn når den er helt tørr.

To forskjellige designkonsepter har blitt undersøkt; et korrugert rør og et glatt rør med en høyttaler. Det korrugerte røret kan generere lyd uten eksterne kilder (som en høyttaler). Når gass strømmer gjennom et korrugert rør, vil det bli induert en virvelavløsning i rørrillene. For høye nok gasshastigheter vil frekvensen til denne virvelavløsningen samstemme med rørets naturlige frekvens. Resultatet blir lyd i form av en høy tone, eller synging. Dette fenomenet blir ofte kalt "singing risers" i olje- og gassindustrien siden det forekommer i de fleksible rørene (risers) som transporterer hydrokarboner fra sjøbunnen til havoverflaten. Det glatte røret har på sin side ingen intern lydkilde og må derfor fungere i par med en høyttaler for at lyddemping skal kunne måles.

Designkonseptene er studert teoretisk, gjennom modellering og ved eksperiment. En én-dimensjonal stømnings-akustisk model ble simulert i COMSOL Multiphysics. Denne modellen klarte ikke å returnere realistiske verdier for lydampplituden, men modellerte frekvensene på en mer tilfredsstillende måte. Rørets fundamentale naturlige frekvens ble presist predikert.

De to designkonseptene ble testet eksperimentelt for forskjellige gasshastigheter og væskeinjeksjonsmengder. Eksperimentene indikerte sterkt en økning i den akustiske dempingen på grunn av væsken i fluidstrømmen, selv for volumetriske væskefraksjoner mye lavere enn  $1 \cdot 10^{-4}$ , og støttet dermed hovedprinsippet for teknologien. Ingen betydelige fordeler relatert til nøyaktighet for hverken det glatte eller det korrugerte røret ble imidlertid avdekket av eksperimentene.





# Acknowledgements

First and foremost, we would like to thank our Supervisor Even Solbraa along with our Co-supervisors Pablo Matias Dupuy and Oddbjørn Rekaa Nilssen from Statoil for giving us the opportunity to work with exciting new technology development. The feedback from Dupuy and Nilssen have been invaluable through the whole process. In addition, a video conference with Stefan Belfroid, an expert of the topic, was very rewarding in terms of our overall understanding.

A special thanks goes to Ole Jørgen Nydal, Martin Bustadmo and Mariana J.C. Diaz Arias, all from The Department of Energy and Process Engineering at NTNU, for facilitating our laboratory work in an excellent matter and making it easy for us to carry out the experiments. Also Tim Cato Netland from The Department of Acoustics at NTNU, who willingly rented us equipment to accurately record the sound field, deserves recognition. You have all made the work with this master thesis easier and more fruitful for us.



# Contents

<b>1</b>	<b>Introduction</b>	<b>1</b>
1.1	Procedure . . . . .	2
1.2	Design Concepts . . . . .	3
<b>2</b>	<b>Wave And Sound Theory</b>	<b>5</b>
2.1	Different Types Of Waves . . . . .	5
2.2	The Wave Equation . . . . .	6
2.3	Frequency And Amplitude Of Sound . . . . .	7
2.4	Resonance And Sound In Pipes . . . . .	8
2.4.1	Relationship To Experiment . . . . .	11
<b>3</b>	<b>Sound Generation In A Corrugated Pipe</b>	<b>13</b>
3.1	The Helmholtz Resonator . . . . .	13
3.2	Flow Over A Cavity . . . . .	15
3.3	Shear Layer Instability And Vortex Shedding . . . . .	18
3.4	Pressure In A Vortex . . . . .	19
3.5	The Corrugated Pipe . . . . .	22
3.6	The Acoustics In The Pipe . . . . .	27
3.7	The Linear Model Of Acoustics In A Corrugated Pipe . . . . .	28
<b>4</b>	<b>Acoustic Damping</b>	<b>29</b>
4.1	Acoustic Damping In A Fluid . . . . .	29
4.2	Liquid Influence On Acoustic Damping . . . . .	31
4.2.1	The Viscous And The Thermal Part Of Acoustic Damping Due To Droplets . . . . .	32
4.3	Sensitivity Analysis . . . . .	33
4.3.1	Droplet Size . . . . .	34
4.3.2	Liquid Density . . . . .	37
4.3.3	Gas Viscosity . . . . .	39
4.3.4	Sound Frequency . . . . .	41
4.4	Discussion . . . . .	46
<b>5</b>	<b>Experiment: Liquid Influence On Sound Waves In Pipes</b>	<b>47</b>

5.1	Experimental Setup . . . . .	48
5.2	Test Matrices . . . . .	50
5.3	Results . . . . .	53
5.3.1	Resonance Frequencies . . . . .	53
5.3.2	Liquid Injection - Smooth Pipe . . . . .	57
5.3.3	Liquid Injection - Closed Corrugated Pipe . . . . .	65
5.3.4	Liquid Injection - Open Corrugated Pipe . . . . .	69
5.3.5	Comparison With Theoretical Added Acoustic Damping . . . . .	74
5.3.6	Evolution Of Resonance Amplitude For Smooth Pipe . . . . .	82
5.4	Discussion . . . . .	83
5.5	Uncertainties . . . . .	86
<b>6</b>	<b>Simulation Of Flow-Acoustics Model Using COMSOL</b>	<b>89</b>
6.1	The Strouhal Number . . . . .	89
6.2	Simulation Results . . . . .	90
6.3	Incorporation Of Added Acoustic Damping . . . . .	95
<b>7</b>	<b>Discussion</b>	<b>99</b>
<b>8</b>	<b>Conclusion</b>	<b>103</b>
	<b>Bibliography</b>	<b>105</b>
	<b>List Of Figures</b>	<b>111</b>
	<b>List Of Tables</b>	<b>117</b>
<b>A</b>	<b>Fourier Analysis</b>	<b>119</b>
A.1	Fourier Transform Of Continuous Functions . . . . .	119
A.2	Discrete Fourier Transform . . . . .	120
<b>B</b>	<b>Matlab Files</b>	<b>123</b>
B.1	Sensitivity Analysis . . . . .	123
B.1.1	Droplet Size . . . . .	123
B.1.2	Liquid Density . . . . .	126
B.1.3	Gas Viscosity . . . . .	129
B.1.4	Sound Frequency . . . . .	132
B.2	Experiment . . . . .	138
B.2.1	Creating Sound . . . . .	138
B.2.2	Recording Sound . . . . .	140
B.2.3	Plotting Experimental Values . . . . .	143
<b>C</b>	<b>Risk Assessment Of Laboratory Work</b>	<b>161</b>
<b>D</b>	<b>Work Drawings For The Experiment</b>	<b>165</b>

<b>E</b>	<b>COMSOL Simulation Setup And Results</b>	<b>169</b>
E.1	Equations . . . . .	169
E.1.1	General Equations . . . . .	169
E.1.2	COMSOL Equations . . . . .	170
E.2	Boundary Conditions . . . . .	172
E.3	Parameters . . . . .	174
E.4	Solvers . . . . .	176
E.5	Results . . . . .	176



# Chapter 1

## Introduction

Pipes with a corrugated inner surface are widely used in the oil and gas industry. They are known as flexible pipes, or flexible risers, and facilitate the hydrocarbon flow between the seabed installations and the surface facilities, as they can withstand both vertical and horizontal movement. The corrugated inner layer makes the pipes flexible while making them able to resist collapsing [1]. Such pipes can emit a high tonal sound, or whistling, when gas flows through. The singing mechanism is due to flow-induced acoustics. Flow-induced acoustics occur when vortex shedding couples with the acoustic resonance in the pipe.

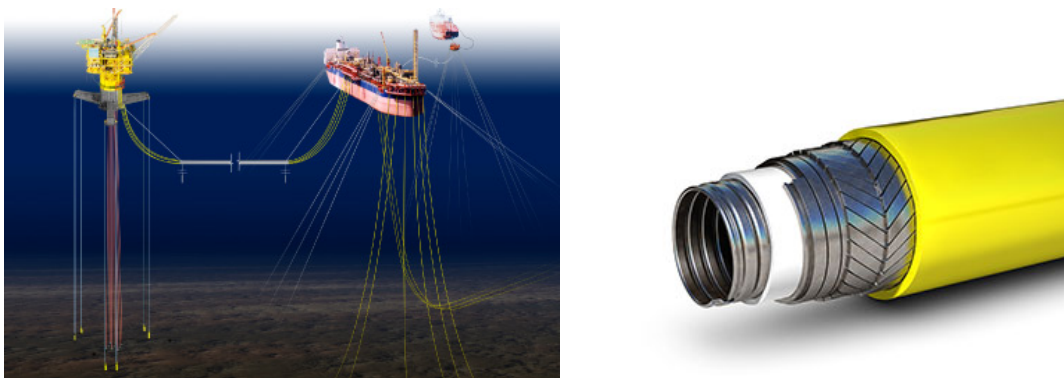


**Figure 1.1** – Flexible risers and the corrugated inner layer [2, 3].

**Singing riser** Singing riser is the expression describing the sound-emitting behaviour of flexible risers under certain conditions. The whistling occurs only in corrugated pipes; blowing air through a corrugated pipe with sufficient velocity will generate hearable sound, blowing air through a smooth pipe with the same velocity will not. The sound is hearable, meaning it has a frequency within the human hearing range, which is 20 Hz to 20 kHz [4]. The singing, or whistling, mechanism is well-known in the oil and gas

industry, because it can induce structural vibrations and mechanical stress on the riser, and eventually lead to fatigue failure of the connected topside or subsea pipe system [5].

**Liquid influence on whistling** An important issue in natural gas transport is the liquid volume fraction (LVF) - the ratio of the liquid volumetric flow rate to the gas volumetric flow rate (see equation 4.11). Current wet gas meters used in Statoil can detect LVFs over 5%, but not smaller fractions [6]. Precise knowledge of the LVF is important: if the transported natural gas is too "wet", it can inflict great damage to the costly topside process equipment as well as giving poor gas quality, increasing the risk of hydrate formation. It is therefore in Statoil's interest to measure LVFs downstream of separators more precisely than current state of the art technology is able to.

A Joint Industry Project called Flexible Risers did experiments with liquid injection in a flexible pipe at whistling conditions [5]. The experiments showed that a low volume fraction of liquid (0.03% - 0.25%) eliminates the whistling [7]. Thus, liquid appears to influence the whistling, and suggests that acoustic measurements in a corrugated pipe may lead to precise LVF measurements. This idea was proposed by Pablo Matias Dupuy and Oddbjørn Rekaa Nilssen from Statoil.

The overall objective is to develop a wet gas meter capable of measuring small fractions of liquid. At this early stage it will be difficult to conclude upon installation requirements and robustness. The main goal at this stage is to support experimentally that the liquid in a two phase flow will cause added acoustic damping and find a relationship between the added acoustic damping and the liquid quantity. To arrive at this goal, the concept of acoustic damping has to be investigated thoroughly. Another goal of the report is to document possible advantages in measurement accuracy for two different design concepts.

## 1.1 Procedure

The description of the master thesis states the following tasks:

1. Gather design concepts, e.g. active vs. passive (vortex shedding), pipe surface geometry, diameter, length etc.
2. Assess the concepts experimentally
3. Assess the concepts theoretically
4. Conclude on robustness, reliability, accuracy, development time and considerations for installation

We start out with a description of two different design concepts in Section 1.2. This is based on the NTNU project thesis "Early Study of Two New Technologies For Solving



Separation Challenges" [8]. The important characteristics and differences between the two concepts are discussed briefly.

In Chapter 2 we present a theoretical study on waves and sound waves in particular. The main focus is to describe waves mathematically and a general introduction to the concepts of sound and acoustics. Furthermore, a thorough explanation of resonance and the influence this has on sound in pipes is given.

Chapter 3 is dedicated to investigate how sound is generated in a corrugated pipe. First, a mathematical description of a flow over a single cavity is given before this is coupled with pressure oscillations and consequently acoustics. Then this theory is extended from a single cavity to a corrugated pipe and the chapter ends with the derivation of Popescu and Johansen's one-dimensional model for acoustics in a corrugated pipe [9].

After establishing the sound wave theory and sound generation in a corrugated pipe, Chapter 4 goes in depth in sound attenuation mechanisms. The acoustic damping in single phase gas is first discussed before this is augmented to acoustic damping in a pipe. Then the governing equation for added acoustic damping in two phase mist flow due to droplets is studied in depth through a sensitivity analysis. This sensitivity analysis present insight to how various parameters influence the added acoustic damping.

The liquid influence on acoustic damping is then experimentally investigated in Chapter 5 for both design concepts. The first objective was to verify that more liquid in fact results in additional damping of the sound waves. Secondly, we sought to find a relationship between the liquid in the gas flow and the damping of the sound amplitude. Then, the results from the experiment were compared to the theory from Chapter 4. The smooth and corrugated pipe were compared throughout the report to identify significant differences among the two.

In the end, Chapter 6 presents the simulation of Popescu and Johansen's one-dimensional model for flow-acoustics in a corrugated pipe is simulated with COMSOL Multiphysics. The objective was to investigate how well it predicts sound amplitude and frequency and if it could be used for design purposes.

Supporting material are presented in the appendices. This includes a description of the Fourier transform and Fourier analysis of periodic signals (Appendix A), the Matlab files used for the sensitivity analysis and experiment (Appendix B), a risk assessment of the laboratory work (Appendix C), a work drawing for the experiment setup (Appendix D) and the simulation setup up and the complete results from COMSOL (Appendix E).

## 1.2 Design Concepts

In the project thesis, two main concept design were discussed: a smooth pipe and a corrugated pipe [8]. In the corrugated pipe sound is generated from the vortex shedding in the corrugations, while for a smooth pipe a loud speaker has be installed to generate

sound. For subsea applications, the corrugated pipe offers a significant advantage as it is not subject to the reliability of the loud speaker. On the other hand, the whistling from the corrugations may be more unstable, meaning that it naturally could vary in amplitude or frequency. This problem is overcome with the smooth pipe configuration where the loud speaker can emit a sound with the constant amplitude and frequency.

As further discussed in the project thesis, the sound amplitude could be measured directly in the pipe or via an extraction tube. The extraction tube would sample a fraction of the flow, and measure the acoustic damping before re-introducing it in the main pipe. Another option is an inline installation, i.e. the components of the wet gas meter is installed directly in the main pipe. The liquid volume fraction might not be constant over the cross-section of the main pipe. This might make it necessary to have a homogenization of the flow upstream of the wet gas meter both for an extraction tube and an inline installation.

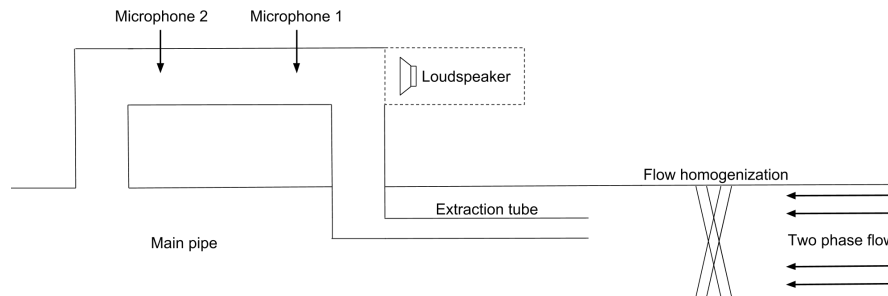


**Figure 1.2** – Sketch of an extraction tube to measure the liquid content of the gas.

Figure 1.2 shows a simple sketch of an extraction tube concept. The installation of the loud speaker is dependent on whether the measurement tube is smooth or corrugated. For an inline installation concept, the setup will be similar with two microphones used to measure the acoustic damping and possibly both a loud speaker and flow homogenization.

## Chapter 2

# Wave And Sound Theory

Several physical phenomena surrounding us in daily life can be described as waves. Ocean surface waves, radio waves and X-rays are all examples of this. Even the human voice is transported through air as waves. Waves are a fundamental part of physics and many phenomena are described with wave theory.

This chapter goes briefly through the basics of waves. First by categorizing and describing them mathematically, then by investigating sound waves in particular. Finally an explanation of sound wave propagation in pipes and the concept of resonance frequency is presented.

### 2.1 Different Types Of Waves

In general we distinguish between two different types of waves; mechanical waves and electromagnetic waves. Mechanical waves propagate through a medium and are made by displacement of the medium's particles [10]. Sound waves, for example, propagate by imposing motion on molecules creating pressure oscillations. In a gas, since gas properties are connected via an equation of state, the propagation can also be described by density variations.

Electromechanical waves, on the other hand, needs no medium. They are made by periodic oscillations of the electric or magnetic fields created by charged particles [11]. Electromagnetic waves can hence move through vacuum. Other phenomena are also described as waves, like particle behaviour in quantum mechanics. The rest of this chapter focus on the general description of mechanical waves and relates it to sound waves.

**Transverse and longitudinal waves** Two different classes of mechanical waves exist; transverse and longitudinal waves. In the first kind, the particle displacement is

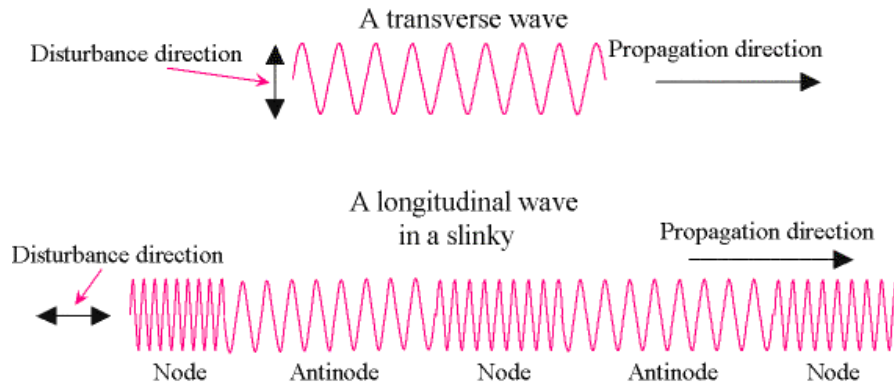


**Figure 2.1** – Illustration of longitudinal and transverse waves [12].

parallel to the direction of the wave propagation. Sound waves belongs to this class of mechanical waves. And vice versa for longitudinal waves, where the particle displacement is perpendicular to the direction of wave propagation [13]. Figure 2.1 illustrates the difference between these two wave types. A combination of the two types can also be found, e.g. water waves. It causes water particles to undergo circular motions as the waves propagate [10].

## 2.2 The Wave Equation

The wave equation can be derived from Newton's law of motion applied to an elastic string and describes the propagation of a wave in space and time [14]. The result of the derivation is given as

$$\frac{\partial^2 u}{\partial t^2} = c^2 \nabla^2 u \quad (2.1)$$

which in one dimension for cartesian coordinates reduces to

$$\frac{\partial^2 u}{\partial t^2} = c^2 \frac{\partial^2 u}{\partial x^2}. \quad (2.2)$$

In equation 2.1 and 2.2,  $t$  [s] is time,  $x$  [m] is a space variable and  $\nabla$  is the del operator and can be interpreted as a vector of the space differentials. The constant  $c$  [m/s] is the speed of propagation of the wave and  $u$  can represent different dependent variables like displacement, pressure or density [15].

This partial differential equation has the general solution

$$u(x, t) = F(x - ct) + G(x + ct). \quad (2.3)$$

In equation 2.3,  $F$  and  $G$  can be any twice differentiable function [16]. Equation 2.3 also implies that the superposition principle applies, i.e. if  $F$  and  $G$  both are solutions, then their sum  $F + G$  is also a solution. This can be simply proven. Take first

$$\frac{\partial^2(F + G)}{\partial x^2} = \frac{\partial^2 F}{\partial x^2} + \frac{\partial^2 G}{\partial x^2} \quad (2.4)$$

and

$$\frac{\partial^2(F + G)}{\partial t^2} = \frac{\partial^2 F}{\partial t^2} + \frac{\partial^2 G}{\partial t^2}. \quad (2.5)$$

Substituting this into the wave equation (Eq. 2.2) gives

$$\frac{\partial^2(F + G)}{\partial x^2} - \frac{1}{c^2} \frac{\partial^2(F + G)}{\partial t^2} = \left( \frac{\partial^2 F}{\partial x^2} - \frac{1}{c^2} \frac{\partial^2 F}{\partial t^2} \right) + \left( \frac{\partial^2 G}{\partial x^2} - \frac{1}{c^2} \frac{\partial^2 G}{\partial t^2} \right) = 0. \quad (2.6)$$

This may seem trivial, but the fact that the superposition principle applies to the wave equation has some remarkable features. Most notably, it means that two waves travelling at different speeds can pass through each other without altering each other [16]. It also means that two waves can constructively or destructively interfere. For example, two standing waves of opposite amplitudes will cancel each other out. This fact has significant implications. For instance, it is actually the technology behind active noise cancelling headphones [17].

Although waves in all kind of forms can exist, many waves, including sound waves, can be described by trigonometric functions. That is, the dependent variable,  $u$ , undergoes cyclic variations as trigonometric functions. The functions  $F$  and  $G$  can thus be written as sine or cosine functions. Hence, the general solution of the wave equation can then be stated as

$$u(x, t) = A \cos(x - ct) + B \cos(x + ct). \quad (2.7)$$

For sound waves, the speed of the wave propagation,  $c$  [m/s], is simply the speed of sound. The speed of sound is dependent of the medium through which the wave propagates.

## 2.3 Frequency And Amplitude Of Sound

When you experience sound, it is common to experience two different aspects; the amplitude and the pitch of the sound. In a purely mathematical sense, pitch is the frequency of the sound wave, though pitch can be subjective and include the perception of the sound. Nonetheless, the human hearing is able to distinguish between different sound pitches (i.e. frequencies) [18].

The frequency,  $f$  [Hz], of the sound wave is the number of full oscillations per unit time and is given by

$$f = \frac{c}{\lambda}. \quad (2.8)$$

In equation 2.8,  $c$  [m/s] is the speed of sound and  $\lambda$  [m] is the wave length. The wave length can be measured as the distance between two wave crests.

The amplitude of the sound is the magnitude of the pressure variation around the ambient condition. A common unit for sound amplitude is the decibel, shortened dB, defined as

$$\text{dB} = 20 \log_{10} \left( \frac{p_{rms}}{p_{ref}} \right). \quad (2.9)$$

In equation 2.9,  $p_{rms}$  [Pa] is the root mean square of the pressure deviation from the ambient pressure over the measurement time interval, while  $p_{ref}$  [Pa] is a reference pressure dependent on the medium. In air, the reference pressure is set to 20  $\mu\text{Pa}$ , and the value is then usually denoted Sound Pressure Level (SPL). This reference means that a pressure deviation of only 1 Pa gives a sound amplitude of 94 dB [19]. The reference pressure is defined such that 0 dB corresponds to approximately the threshold of human hearing. The decibel level of some common sounds are given in table 2.1.

Event	Sound Pressure Level [dB]
Threshold of hearing	0
Country Park	30
Soft whispering at 2 meters	40
Activity in business office	50
Conversation in quiet room	60
Moderate road traffic	70
Diesel freight train at high speed	80
Discotheque	100
Ship's engine room	120

**Table 2.1** – Sound Pressure Level [dB] of some common sounds [20].

## 2.4 Resonance And Sound In Pipes

Every system has a natural frequency based on its physical properties. The terms natural frequency and resonance frequency is used interchangeably in this report, even though, strictly speaking, the latter usually denotes the frequency of an applied force if it is

equal to the natural frequency of the system. Natural frequency is the frequency a system tends to oscillate in the absence of damping or driving force [21]. Resonance is a physical phenomenon that occurs when an oscillating force is applied to a system with the same (or close to the same) frequency as the natural undamped frequency of the system itself.

For the simple example of the mass-spring system, the natural frequency is related to the mass connected to the spring and the stiffness of the spring. If you displace the mass from equilibrium and then release, the system will oscillate with its natural frequency and slowly decay towards equilibrium. If an oscillating force is applied to the system, i.e. if you push the mass with the same frequency as the natural frequency, the displacement from equilibrium will increase with time [22]. Finally, this may result in a mechanical breakdown of the system.

Similarly, a pipe open in both ends has a natural frequency. In fact it has a set of different resonance frequencies. To derive the resonance frequencies of a pipe, first consider a pipe open in one end and closed in the other. If you "push" the air in the open end with an oscillating force you will cause oscillating air particle displacements in the pipe. At the closed end, you will have no displacement of the air particles. Figure 2.2 illustrates this. The amplitude corresponds to the maximum displacement of the air particles from their initial condition. The air particles can not move horizontally at the closed end, while maximum displacement in both directions is possible at the open end.

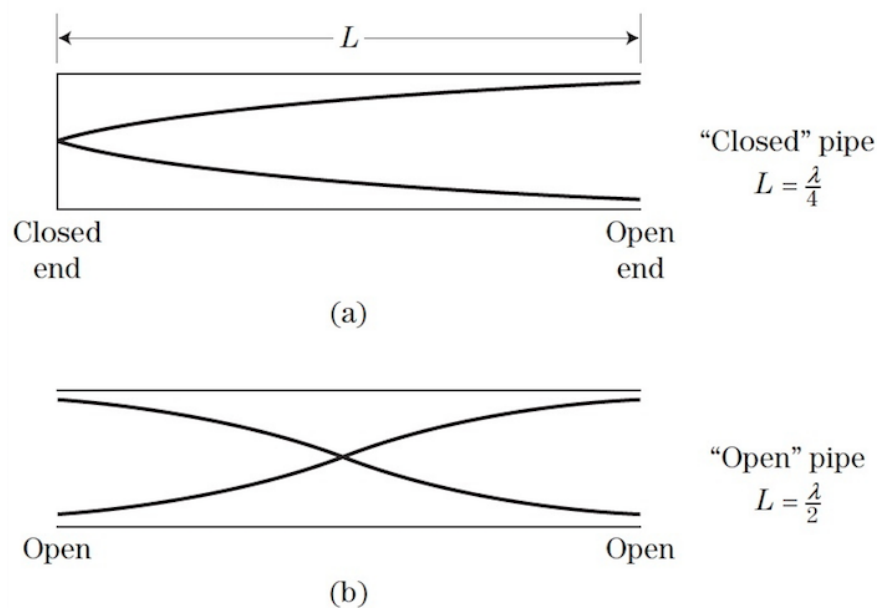


**Figure 2.2** – Displacement amplitude of air particles of the fundamental standing waves in (a) closed and (b) open pipes [23].

For an open tube, air particle displacement is possible at either end of the pipe. This is

illustrated in figure 2.2 we can see that maximum displacement is possible at both ends of the pipe. Figure 2.2 shows the fundamental mode, that is the lowest resonance frequency. The result is that half a wavelength can fit in an open pipe, while a quarter of a wavelength can fit in a closed pipe. Hence, the first (lowest) natural frequency can be calculated for a closed and open pipe as

$$\begin{aligned} f_{closed}^1 &= \frac{c}{4L} \\ f_{open}^1 &= \frac{c}{2L}. \end{aligned} \quad (2.10)$$

In equation 2.10,  $f$  [Hz] is the frequency,  $c$  [m/s] is the speed of sound and  $L$  [m] is the length of the pipe. The pressure in the pipe oscillates with a phase shift of  $\pi$  radians with respect to the displacement as seen in figure 2.3. Consider a point where the air particles does not move, for instance at the closed end of a pipe. The neighbouring air particles move towards and away from that point with the frequency of the oscillation. Maximum pressure occurs when the neighbouring air particles are as close to the point as they can be. Consequently, minimum pressure occurs when the neighbouring air particles are furthest away from the point. This is an antinode of the pressure fluctuations, i.e. a point with the largest pressure variation, but no particle displacement.

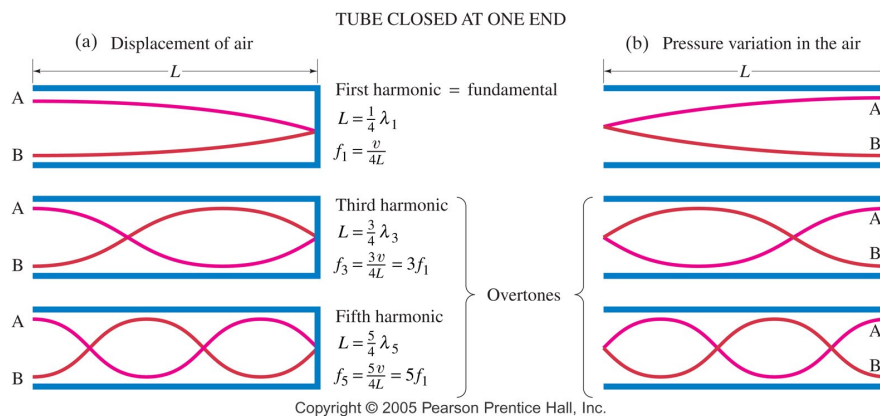


**Figure 2.3** – Fundamental modes of a standing wave in a tube closed in one end, showing both (a) the displacement of air and (b) the pressure variations [24].

Similarly, the air particles have the maximum displacement halfway between the pressure antinodes. But since the immediate neighbouring air particles move with the same velocity, there will be no variation of pressure at this point. Hence, this is a node of the pressure fluctuations [24]. This relationship between air particle displacement and pressure variation is shown in figure 2.3.

Figure 2.3 also highlights a different fact: the pipe has several resonance frequencies. In addition to the fundamental frequency, all odd integer multiples of this frequency are also resonance frequencies for a closed pipe. For an open pipe, this is true for all



integer multiples of the fundamental resonance frequency, it is basically just a question of matching the boundary conditions. Hence, the resonance frequencies are given as

$$\begin{aligned} f_{closed} &= \frac{(2n-1)c}{4L} \\ f_{open} &= \frac{nc}{2L} \\ n &= 1, 2, 3, \dots \end{aligned} \quad (2.11)$$

From equation 2.11 we can observe that for a long pipe ( $L \rightarrow \infty$ ), all frequencies become resonance frequencies. The number  $n$  [-] is called frequency mode.

### 2.4.1 Relationship To Experiment

Previous studies have shown that the pressure antinode in the open end is not located exactly at the end of the pipe, but rather a small distance outside [25]. This end correction has few references in literature, but is in the area of 0.3 to 0.46 times the diameter for a closed tube and the double for an open tube [26, 27]. From this we are able to calculate the expected resonance frequencies with the formulas [27]:

$$\begin{aligned} f_{closed} &= \frac{(2n-1)c}{4(L+0.46D)} \\ f_{open} &= \frac{nc}{2(L+0.92D)} \\ n &= 1, 2, 3, \dots \end{aligned} \quad (2.12)$$

Here,  $D$  [m] is the diameter of the pipe. For corrugated pipes, a correction due to the cavities is needed [15]. This is done by modifying the speed of sound to the effective speed of sound

$$c_{eff} = c \sqrt{\frac{V_{in}}{V_{tot}}}. \quad (2.13)$$

In equation 2.13,  $V_{in}$  [m<sup>3</sup>] is the volume of the pipe without the corrugations, while  $V_{tot}$  [m<sup>3</sup>] is the total volume of the pipe with the corrugations. Finally, we get the theoretical resonance frequencies for our experiment:

$$\begin{aligned} f_{smooth} &= \frac{(2n-1)c}{4(L+0.46D)} \\ f_{corrugated} &= \frac{(2n-1)c_{eff}}{4(L+0.46D)} \\ n &= 1, 2, 3, \dots \end{aligned} \quad (2.14)$$

In the experiment, the pipe lengths are given and we can thus calculate a theoretical resonance frequency. By spanning through all frequencies and identifying amplitude peaks, we can compare the theoretical value with our experiment. The pipes are sealed in one end by the loud speaker in the experiment, meaning they are closed pipes, except for the additional experiment on the open corrugated pipe (see Chapter 5).

## Chapter 3

# Sound Generation In A Corrugated Pipe

In this chapter, we present theory related to the sound generated in a corrugated pipe. We begin with the fundamentals of cavity resonance, continue to cavity resonance due to a grazing flow and finish with acoustic resonance in a corrugated pipe.

Theory concerning sound generated in corrugated pipes is still an area of research so few sources are found in literature. The aim in this chapter is therefore to present the information gathered in various scientific articles in a comprehensive manner, from fundamentals concepts to specific theory. We present models attempting to quantify the different phenomena occurring when a medium flows over a cavity or in a corrugated pipe. As this is still an emerging scientific area, a general, widely accepted theory has yet to be adopted. Despite this, the models presented in this chapter are valuable in terms of understanding the phenomena behind sound generation in a corrugated pipe.

### 3.1 The Helmholtz Resonator

Helmholtz resonance is the phenomenon of resonance in a cavity. The name comes from a device created by Hermann von Helmholtz (1821-1894) in the 1850s (figure 3.1).

**Harmonic oscillator** To begin with, we repeat the damped harmonic oscillator in its simplest form. For a damped harmonic oscillation, the balance of forces becomes:

$$F = -kx - F_f = -kx - c\dot{x} = m\ddot{x}. \quad (3.1)$$



**Figure 3.1** – Helmholtz resonator based on Hermann von Helmholtz original design [28].

It can be rewritten into the form:

$$\ddot{x} + 2\zeta\omega_0\dot{x} + \omega_0^2x = 0 \quad (3.2)$$

with the damping ratio,  $\eta$  [-], being

$$\eta = \frac{c}{2\sqrt{mk}} \quad (3.3)$$

and the undamped angular frequency  $\omega_0$  [rad/s] given by

$$\omega_0 = \sqrt{\frac{k}{m}}. \quad (3.4)$$

Here,  $x$  [m] is the displacement from equilibrium,  $c$  [N · s/m] is the viscous damping coefficient,  $m$  [kg] is the mass and  $k$  [N/m] is the force (spring) constant [29].

**Acoustical mass-spring system** The Helmholtz resonator can be seen as an acoustical mass-spring system, because the volume of the bottle acts as a spring, while the inertia of the flow (mass) is concentrated in the neck [15].

If the neck has a uniform cross section  $S$  [m<sup>2</sup>] and a length  $L$  [m] the mass  $m$  [kg] is:

$$m = \rho_0SL \quad (3.5)$$

where  $\rho_0$  [kg/m<sup>3</sup>] is the (reference) density.



**Figure 3.2** – The Helmholtz resonator as an acoustical mass-spring system.

The spring constant  $k$  of the system is obtained by starting from the mass conservation law, assuming a uniform density within the volume:

$$\frac{\Delta\rho}{\rho_0} = -\frac{\Delta V}{V} = -\frac{S\Delta x}{V} \quad (3.6)$$

where  $\Delta x$  is the acoustic fluid displacement in the neck. The uniform density assumption is in agreement with the fact that we neglect inertia in the volume of the resonator, implying a uniform pressure. This is the same assumption as for a massless spring, which implies that the tension is uniform over the spring [15]. Assuming an adiabatic compression, we have the speed of sound  $c_0 = \sqrt{\Delta p / \Delta \rho}$  [m/s], thus  $\Delta p = c_0^2 \Delta \rho$  [Pa]. The force acting on the fluid in the neck is therefore:

$$F = S\Delta p = -S\rho_0 c_0^2 \frac{S\Delta x}{V} = -k\Delta x. \quad (3.7)$$

Hence, the spring constant  $k$  [N/m] is

$$k = \rho_0 c_0^2 \frac{S^2}{V}. \quad (3.8)$$

For such a system, it follows that the resonance frequency,  $\omega_0$  [rad/s], is given by

$$\omega_0 = \sqrt{\frac{k}{m}} = \sqrt{\frac{\rho_0 c_0^2 \frac{S^2}{V}}{\rho_0 S L}} = c_0 \sqrt{\frac{S}{V L}}. \quad (3.9)$$

The resonance frequency, described in Section 2.4, will be explained further throughout the chapter.

## 3.2 Flow Over A Cavity

We now consider the mechanisms related to a flow over a cavity. First, we present Hémon et al.'s linear resonator model in order to understand cavity resonance theory [30].

**Linear resonator model** The Helmholtz resonator has been widely investigated from an acoustical point of view. The displacement  $\zeta$  [m] of the air layer in the neck section can be described by the basic equation (figure 3.3)

$$\rho A_c H \ddot{\zeta} + \rho c A_c (2R_0 + R_1 + \beta H_c) \dot{\zeta} + \rho c^2 \frac{A_c^2}{V} \zeta = \xi A_c p_c \quad (3.10)$$

where the acoustic pressure  $p_c$  [Pa] acts as the excitation force for the resonator,  $c$  [m/s] is the speed of sound,  $\xi$  [-] is a dimensionless parameter and  $R_0$  [-],  $R_1$  [-] and  $\beta$  [1/m] are damping parameters.  $A_c$  [m<sup>2</sup>] is the area of the neck section,  $V$  [m<sup>3</sup>] is the volume of the corrugation and  $H$  [m] and  $H_c$  [m] are related to the neck thickness as shown in figure 3.3.

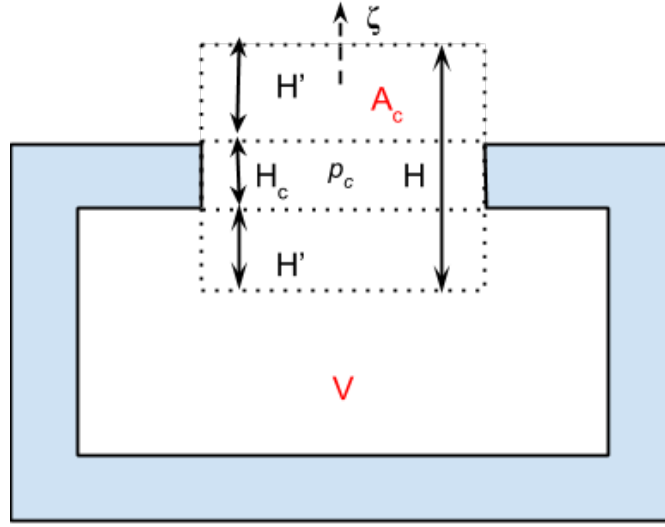


**Figure 3.3** – Sketch of the resonator.

The displacement of the air layer  $\zeta$  [m] is linked to the acoustic pressure  $p_v$  [Pa] through the relation

$$\zeta = \frac{V}{A_c \rho c^2} p_v. \quad (3.11)$$

By substituting equation 3.11 into equation 3.10, we obtain the basic equation for the cavity pressure

$$\frac{VH}{A_c c^2} \ddot{p}_v + (2R_0 + R_1 + \beta H_c) \frac{V}{A_c c} \dot{p}_v + p_v = \xi p_c. \quad (3.12)$$

As seen from figure 3.3, the term  $H$  [m] is composed of the thickness of the neck  $H_c$  [m]

increased by the thickness  $H'$  [m] of the air layers which are entrained. For noncircular holes, Crighton et al. provide the relation

$$H' = \frac{0.85A_c^{0.75}}{\sqrt{l_c}}, \quad (3.13)$$

where  $l_c$  [m] is the circumference of the opening [31].

The term  $R_0$  [-] represents radiation damping, which is the power lost to the surroundings and the cavity. It is proportional to the square of the angular frequency  $\omega$  [rad/s] and given by

$$R_0 = \frac{\omega^2 A_c}{2\pi c^2}. \quad (3.14)$$

$R_1$  [-] is the power lost due to cavity wall impedance and  $\beta$  [-] is a dissipation factor due to viscous effects along the wall. These two damping terms are numerically much smaller than  $R_0$  [-] and can be neglected. Eventually, the basic equation for the resonator becomes

$$\ddot{p}_v + \frac{\omega^2 A_c}{\pi(H_c + 2H')c} \dot{p}_v + \frac{c^2 A_c}{V(H_c + 2H')} p_v = \xi \frac{c^2 A_c}{V(H_c + 2H')} p_c. \quad (3.15)$$

Rearranging equation 3.15 with the harmonic oscillator in mind, the resonator's natural frequency  $\omega_r$  [rad/s] is introduced

$$\omega_r = c \sqrt{\frac{A_c}{V(H_c + 2H')}}. \quad (3.16)$$

This implies a reduced damping  $\eta_r$  [-], since every element of equation 3.15 must be maintained:

$$\eta_r = \omega^2 \omega_r \frac{V}{2\pi c^3}. \quad (3.17)$$

Finally, equation 3.15 reduces to

$$\ddot{p}_v + 2\eta_r \omega_r \dot{p}_v + \omega_r^2 p_v = \xi \omega_r^2 p_c. \quad (3.18)$$

Equation 3.18 is a standard damped oscillator with an excitation term, which readily can be seen when comparing it to equation 3.2. It is also worth noticing equation 3.16's coherence with equation 3.9.

### 3.3 Shear Layer Instability And Vortex Shedding

In order to fully grasp the theory of a flow past a cavity, we must account for two physical phenomenas: shear layer instability and vortex shedding.

**Shear layer instability** The shear layer describes a region of a flow where the velocity gradient is significant and the viscous shear stresses are important. For a Newtonian fluid<sup>1</sup>, the viscous shear stress is defined by

$$\tau = \mu \frac{\partial u}{\partial y} \quad (3.19)$$

where  $\mu$  [Pa · s] is the viscosity,  $u$  [m/s] the velocity and  $y$  [m] is normal to the flow direction [33].

The shear layer thickness can be defined in several ways. A general definition is the height from the surface to a point where the flow reaches approximately the "free stream velocity" [32]. The most common example of a shear layer arises when a fluid passes over a solid surface and forms a boundary layer. In this case, the velocity distribution in the shear layer is approximated by a universal velocity profile (figure 3.4) [34].

Another example is the free shear layer, which is not attached to a solid boundary. It arises in the lee of a structure placed in a flow. The free shear layer develops between the free stream velocity  $U_0$  [m/s] and the near zero velocity region occurring within the wake region.

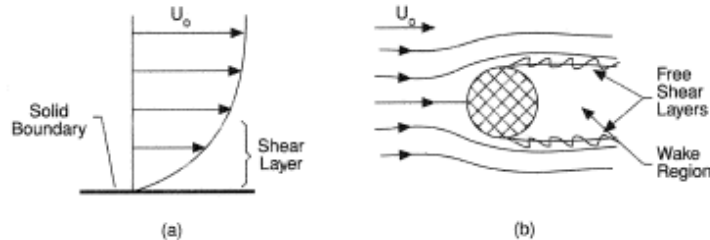


**Figure 3.4** – a) Shear layer over a solid boundary, b) Free shear layer [33].

In a Helmholtz resonator, the fluid flows past a cavity. The shear layer separated from the upstream corner can become unstable in the presence of a downstream corner. The downstream corner is called the impingement edge, meaning it triggers the shear layer instability, illustrated in figures 3.5 and 3.7 [35]. The instability of the shear layer creates the shedding of vortices in the cavity.

<sup>1</sup>Newtonian fluids are defined as having a viscous shear stress proportional to the strain rate (i.e. the normal velocity gradient) [32].



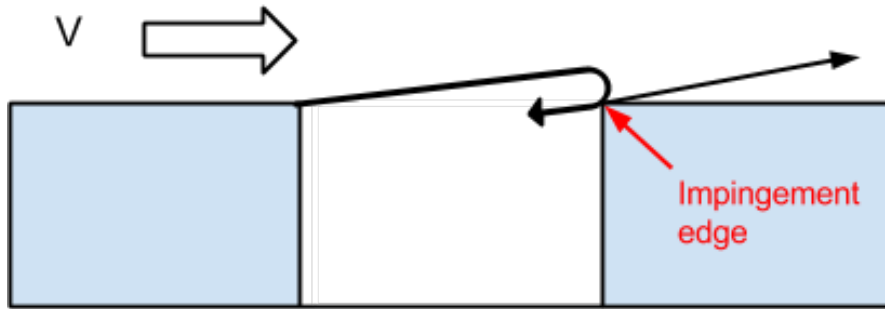


**Figure 3.5** – Shear layer instability over a cavity.

**Vortex shedding** Vortex shedding is an oscillating flow pattern. It can occur when a fluid flows past a cylindrical body, depending on the flow velocity and the shape of the body. The flow detaches periodically at the back of the body and creates alternating vortices, as seen in figure 3.6. Vortex shedding is described by the Strouhal number  $St$

$$St = \frac{fL}{U}. \quad (3.20)$$

Here,  $f$  [Hz] is the frequency of the vortex shedding (number of vortices per second),  $L$  [m] the characteristic length and  $U$  [m/s] the velocity of the fluid. The Strouhal number is a dimensionless number that describes oscillating flow mechanisms, and depends on the shape of the body and the Reynolds number. In a cavity the vortex shedding denotes the cyclic formation and destruction of vortices that occurs.

### 3.4 Pressure In A Vortex

The Navier-Stokes equations are used to derive the pressure and velocity fields in a fluid flow [32]. Starting from Newton's second law of motion applied to a differential fluid volume under the continuum assumption<sup>2</sup> the Navier-Stokes equations for incompressible Newtonian fluids is given as

$$\rho \left( \frac{\partial \vec{v}}{\partial t} + \vec{v} \cdot \nabla \vec{v} \right) = -\nabla p + \mu \nabla^2 \vec{v} + \vec{f}. \quad (3.21)$$

The expression in the parenthesis on the left hand side of equation 3.21 is often written as the material derivative of the velocity ( $D\vec{v}/Dt$ ), making the resemblance with Newton's

<sup>2</sup>In continuum mechanics the mass is modelled as continuous rather than consisting of discrete particles. This assumption is generally valid when the distance between particles is small compared to the size of the system studied [32].

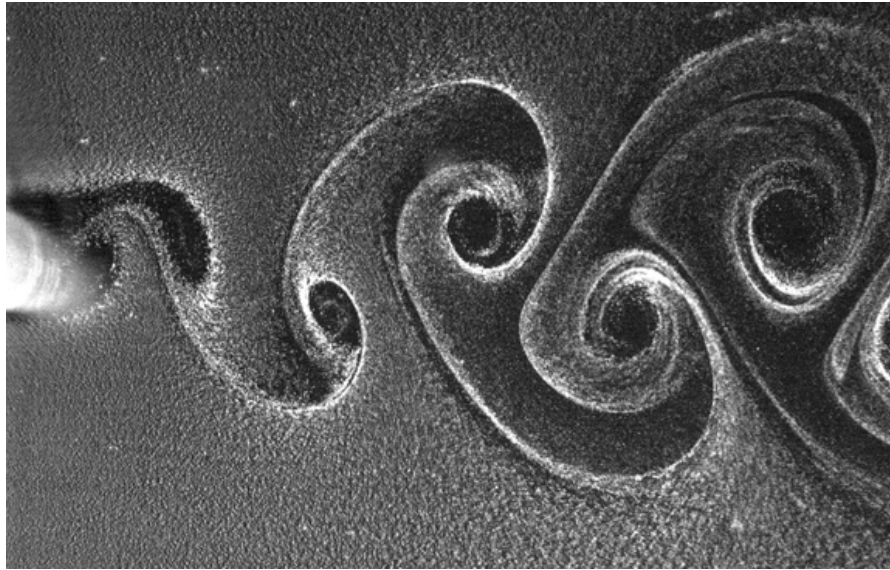


**Figure 3.6** – Vortex shedding in the wake of a cylindrical body [36].

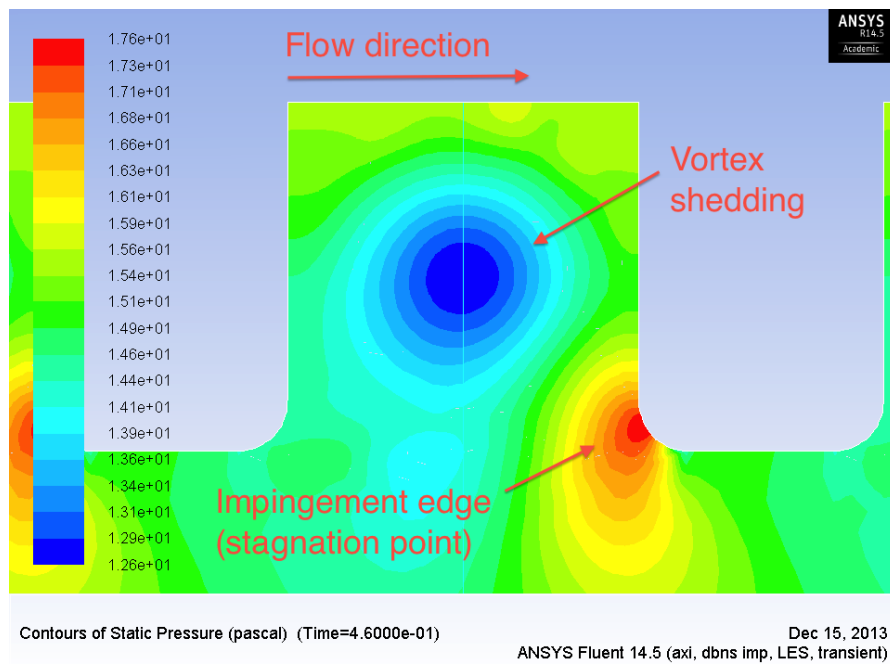


**Figure 3.7** – CFD simulation over a single cavity [8].

second law of motion more apparent [32]. In equation 3.21,  $\rho$  [kg/m<sup>3</sup>] is the fluid density,  $\vec{v}$  [m/s] is the velocity,  $p$  [Pa] is the pressure,  $\mu$  [Pa · s] is the fluid viscosity, the body force per unit volume (usually gravitational or centrifugal force) is  $\vec{f}$  [N/m<sup>3</sup>] and  $\nabla$  is

the del operator as in equation 2.1.

In the cavities of a corrugated pipe, the vortices generated can be considered to be irrotational. This is usually named a free vortex. For a free vortex, the tangential velocity is inversely proportional to the distance from the centre of the vortex. Physically this is not possible as the velocity approaches infinity at the centre of the vortex, hence this model is only valid outside a core region [32].

In two dimensions, the cylindrical Navier-Stokes equation for the radial direction when assuming no radial velocity becomes

$$\frac{1}{\rho} \frac{\partial p}{\partial r} = \frac{v_{\theta}^2}{r} - g \cos \theta. \quad (3.22)$$

Noting that  $\cos \theta = \partial z / \partial r$ , we can integrate equation 3.22 to find the pressure field

$$\int \frac{\partial p}{\rho} = \int \left( \frac{v_{\theta}^2}{r} - g \frac{\partial z}{\partial r} \right) \partial r. \quad (3.23)$$

Using the assumption that the density variation is negligible and the fact that the tangential velocity of a free vortex is inversely proportional to the distance from the centre, namely

$$v_{\theta} = \frac{\Gamma}{r} \quad (3.24)$$

with  $\Gamma$  being the constant of proportionality (which can vary in time), we have

$$\int \frac{\partial p}{\rho} = \int \left( \frac{\Gamma^2}{r^3} - g \frac{\partial z}{\partial r} \right) \partial r = \int \left( \frac{\Gamma^2}{r^3} \right) \partial r - \int g \partial z. \quad (3.25)$$

Neglecting the density variation as this can be assumed to be small relative to the change in pressure, the integration yields

$$\frac{p(r, z, t)}{\rho} = \frac{\Gamma(t)^2}{2r^2} - gz + C(z, t). \quad (3.26)$$

Notice here the close connection to the Bernoulli equation. In fact we could have derived equation 3.26 from Bernoulli's principle [37]. Setting the minimum value of the pressure to  $p_{min}$  when the circulation,  $\Gamma(t)$ , is zero, as well as neglecting the influence of gravity, we get

$$\frac{p(r, t)}{\rho} = \frac{p_{min}}{\rho} + \frac{\Gamma(t)^2}{2r^2}. \quad (3.27)$$

The strength of the vortex is generated by the instability in the shear layer above the corrugation. The vortices in the corrugations varies in strength with time and hence  $\Gamma$  is also a function of time. As  $\Gamma$  increases, so does the pressure in each point of the vortex, the frequency of the variation of  $\Gamma$  is then the vortex shedding frequency.

**Circulation** The relationship between  $\Gamma$  and vorticity can be derived using Stokes' theorem and circulation of the flow. The vorticity, the curl of the flow, is related to the velocity as  $\vec{\omega} = \nabla \times \vec{v}$ . It can be interpreted as the magnitude of the fluid particle's spin around its own axis [32]. Denote the circulation  $\Gamma$ , it is defined as

$$\Gamma = \oint_C \vec{v} \cdot d\vec{l}. \quad (3.28)$$

Hence, by Stokes' theorem we can write the circulation as

$$\Gamma = \oint_C \vec{v} \cdot d\vec{l} = \iint_S \nabla \times \vec{v} \cdot d\vec{S} = \iint_S \vec{\omega} \cdot d\vec{S}. \quad (3.29)$$

Generally, the average vorticity can be seen as the circulation divided by the area,  $A$ , enclosed by the curve  $C$ . As the integration area approaches zero, we get the definition of the vorticity [38]. It is thus given as

$$\vec{\omega} \equiv \lim_{A \rightarrow 0} \left( \frac{1}{A} \oint_C \vec{v} \cdot d\vec{l} \right). \quad (3.30)$$

### 3.5 The Corrugated Pipe

Popescu and Johansen proposed a one-dimensional flow-acoustics model that couples the acoustics of the pipe with the vortex shedding in the corrugations [9]. We will in the following sections present the theory behind the model. The model has been simulated in COMSOL Multiphysics and the results are presented in Chapter 6.

**From a cavity to a corrugated pipe** When the frequency of the vortex shedding couples with the natural frequency of the pipe, resonance occurs. For a given geometry of a corrugated pipe, the Strouhal is approximately constant [9]. Thus, the velocity of the flow controls the frequency of the vortex shedding (equation 3.20). Higher velocities induces higher frequencies of vortex shedding. When the frequency of the vortex shedding reaches the next mode of the pipe's natural frequencies (equation 2.14), a distinct shift in pitch is heard, and the system now resonates at a higher frequency mode.

Our first interest is the acoustic pressure in the corrugations. The acoustic pressure in the corrugations couples with the acoustic pressure in the pipe at resonance frequencies,

enhancing the overall acoustic power. This acoustic power drives the flow, creating a feed-back system (figure 3.8). Consequently, the regime becomes self-sustained.

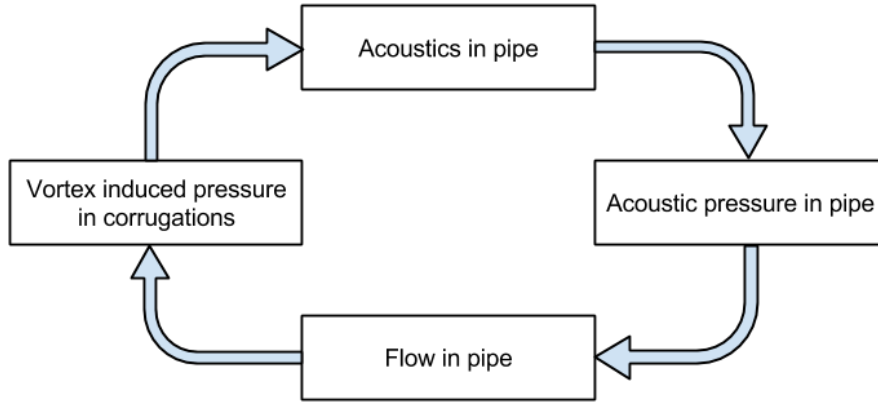


**Figure 3.8** – Block diagram illustrating the feedback mechanism between the flow and the acoustic field [35].

We start with Hémon et al.'s equation 3.18 for cavity resonance [30]:

$$\ddot{p}_v + 2\eta_r\omega_r\dot{p}_v + \omega_r^2 p_v = \xi\omega_r^2 p_c. \quad (3.18 \text{ revisited})$$

First of all, the frequency term must be reconsidered. In a corrugated pipe, the acoustic pressure in the corrugation is no longer controlled by the cavity's natural frequency  $\omega_r$ . The main resonator of the system is the pipe itself. At resonance conditions the frequency of vortex shedding equals the pipe's natural frequency. Thus,  $\omega_r$  is interchanged with  $\omega$  - the frequency at which resonance occurs.

$$\ddot{p}_v + 2\eta_r\omega\dot{p}_v + \omega^2 p_v = \xi\omega^2 p_c. \quad (3.31)$$

The excitation force of the oscillator must also be reconsidered. In equation 3.18, the acoustic pressure in the cavity  $p_v$  is excited by the acoustic pressure in the neck  $p_c$ , which again depends on surrounding pressure. In the corrugated pipe, however, the acoustic pressure in the corrugations depends on the pressure in the pipe. Popescu and Johansen propose to replace the acoustic pressure from the neck by the derivative of acoustic pressure from the pipe. The authors write that this is in accordance with Howe's analogy on vortex sound, because the acoustic energy generation can be deduced based on the acoustic velocity in the source region [9]. For a thorough explanation of Howe's analogy, see Hirschberg p. 51-63 [15]. We get then the following equation:

$$\ddot{p}_s + 2\eta_r\omega\dot{p}_s + \omega^2 p_s = \xi\omega\dot{p}. \quad (3.32)$$

where  $p_s$  [Pa] is the pressure in the corrugation and  $p$  [Pa] is the acoustic pressure in the pipe. We also notice that  $\omega$  on the right-hand side of the equation is no longer squared. This makes the units [Pa/s<sup>2</sup>] on the right-hand side of the equation coherent with the left-hand side, but no physical explanation is given in Popescu and Johansen's paper.

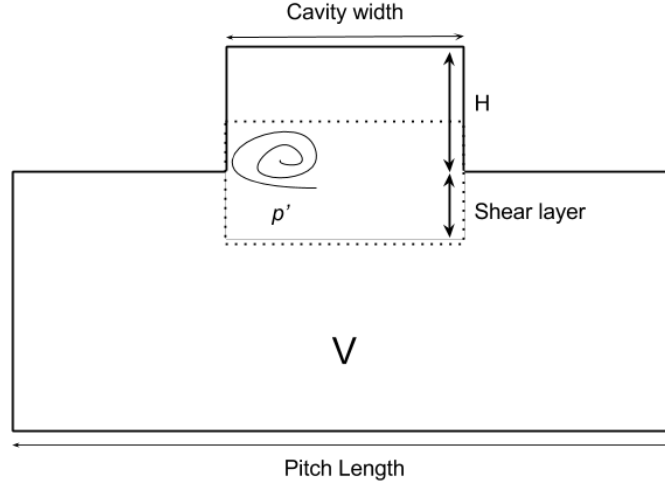


**Figure 3.9** – Sketch of the corrugation.

Furthermore, we know that the regime is self-sustained due to the feed-back mechanism. In order to describe a self-sustaining regime, the van der Pol oscillator is introduced.

**Van der Pol oscillator** The van der Pol oscillator is an oscillator with non-linear damping. It is governed by the following second order differential equation [39]:

$$\ddot{q} + \epsilon(q^2 - 1)\dot{q} + q = 0 \quad (3.33)$$

where  $q$  is the dynamic variable and  $\epsilon$  is a positive parameter. When  $q$  is small, the quadratic term  $q^2$  is negligible and the system becomes a linear differential equation. When  $q$  is large, the quadratic term  $q^2$  becomes dominant and the damping becomes positive.

The equation is credited to Balthazar van der Pol (1889-1959), a dutch physicist. Originally, it described a simple self-oscillating electrical triode circuit.

Noack et al. proposed a model for the formation of vortex cells behind a slender body by using the van der Pol oscillator [40]. This is often referred to as the "van der Pol analogy". By cells, we mean the presence of regions where the shedding of vortices are constant. For a constant flow velocity, consequently, the Strouhal number becomes constant as well. In Noack et al.'s model, equation 3.33 is assumed as the equation of

motion for the displacement of the fluid layer. We multiply the equation with the mass of the fluid layer  $\rho_0 S \Delta z$  and introduce  $\omega$  as the frequency of the vortex shedding:

$$\rho_0 S \Delta z (\ddot{q} + \epsilon \omega (q^2 - 1) \dot{q} + \omega^2 q) = 0. \quad (3.34)$$

Note the resemblance with Section 3.1 and equation 3.5. The first term may be interpreted as the inertia, i.e mass times acceleration, the last one as Hooke's restoring force and the non-linear term as an excitation force.

In a corrugated pipe, one vortex is created in each corrugation, meaning we have one oscillator for each corrugation. A viscous coupling should be introduced between the formation of these oscillators. In order to do so, we assume the existence of a weightless Newtonian fluid with dynamic viscosity  $\mu$  [Pa · s] between the number of oscillators  $i$ . The force between them can be derived from the Navier-Stokes equation:

$$f_{i\pm 1 \rightarrow i} = \mu S_i \left( \frac{\dot{q}_{i\pm 1} - \dot{q}_i}{\Delta z} \right). \quad (3.35)$$

This is the same force as the force between two moving parallel plates with a Newtonian fluid between them.

The forces of the right and left neighbors on the  $i$ th oscillator have to be added on the right hand side of equation 3.34. Thus, we get an equation of motion for a system of coupled oscillators:

$$\rho_0 S_i \Delta z (\ddot{q} + \epsilon \omega (q^2 - 1) \dot{q} + \omega^2 q) = \mu S_i \left( \frac{\dot{q}_{i+1} - 2\dot{q}_i + \dot{q}_{i-1}}{\Delta z} \right). \quad (3.36)$$

Dividing this equation by  $\rho_0 S_i \Delta z$  and applying the limit to the central difference

$$\lim_{\Delta z \rightarrow 0} \frac{f(z + \Delta z) - 2f(z) + f(z - \Delta z)}{\Delta z^2} = \frac{d^2 f}{dz^2}, \quad (3.37)$$

we obtain the corresponding continuous equation

$$\frac{\partial^2 q}{\partial t^2} + \epsilon \omega (q^2 - 1) \frac{\partial q}{\partial t} + \omega^2 q = v \frac{\partial^3 q}{\partial t \partial z^2} \quad (3.38)$$

with the kinematic viscosity  $v = \mu / \rho$  [m<sup>2</sup>/s].

This is a parabolic differential equation for  $q(z, t)$  with diffusion of the velocity

$$u = \frac{\partial q}{\partial t}. \quad (3.39)$$

In Popescu and Johansen's model, the dynamical variable  $q$  is replaced by the acoustic pressure in the corrugations  $p_s$ . In order to make the units coherent, they divide the non-linear term by  $\rho_0 U^2$ . Thus, the term remains dimensionless, as in Noack et al.'s van der Pol oscillator. Using equations 3.32 and 3.38, we get

$$\ddot{p}_s + 2\eta_r \left\{ \left( \frac{p_s}{\rho_0 U^2} \right)^2 - 1 \right\} \omega \dot{p}_s + \omega^2 p_s - v \frac{\partial^3 p_s}{\partial t \partial z^2} = \xi \omega \dot{p}. \quad (3.40)$$

Popescu and Johansen also introduce two coefficients,  $A$  and  $B$ , to account for the dynamics in a corrugated pipe:

$$\ddot{p}_s + 2A\eta_r \left\{ \left( \frac{p_s}{B\rho_0 U^2} \right)^2 - 1 \right\} \omega \dot{p}_s + \omega^2 p_s - v \frac{\partial^3 p_s}{\partial t \partial z^2} = \xi \omega \dot{p}. \quad (3.41)$$

**Coefficient A** The authors conclude that in order to have a stronger signal from the source, the shear layer has to be thinner. The shear layer thickness (in consequence also the boundary layer) controls the way in which the sound pressure propagates through the system, which is the role of coefficient  $A$  in equation 3.41. Coefficient  $A$  is therefore proportional to the thickness of the boundary layer. Popescu and Johansen propose an empirical value for  $A$  in their work:

$$A = 0.5 \cdot BLR \quad (3.42)$$

where  $BLR$  is the ratio between the boundary layer thickness and the radius of the pipe. If  $BLR$  is close to one, we deal with only turbulent flow. In this case, there is no feedback mechanism and the corrugated pipe does not whistle.

**Coefficient B** Furthermore, Popescu and Johansen argue that the shape and the volume of the cavity will affect the acoustic pressure field variations. The role of coefficient  $B$  in equation 3.41 is to incorporate these parameters. The authors admit that they do not have a very well defined procedure to obtain the value of parameter  $B$ . They choose in their work an empirical value of  $B$  as the ratio of the volume of the cavity to the volume of the pipe (with a length corresponding to the cavity opening).

We propose to use Nakiboglu et al.'s ratio, which is the ratio of the pipe diameter to the cavity width and the radius of the upstream edge of the cavity [41]:

$$B = \frac{D}{W + r_{up}}. \quad (3.43)$$

Nakiboglu et al. has showed good agreement between theory and experiment when comparing the Strouhal number to the ratio  $D/(W + r_{up})$ .



Finally, the acoustic pressure in the pipe corrugation can be described by the equation:

$$\ddot{p}_s + 2A\eta_r \left\{ \left( \frac{p_s}{B\rho_0 U^2} \right)^2 - 1 \right\} \omega \dot{p}_s + \omega^2 p_s - v \frac{\partial^3 p_s}{\partial t \partial z^2} = \xi \omega \dot{p} \quad (3.44)$$

where, in accordance to Hémon et al.'s linear resonator model (equation 3.17), and accounting for the interchange of  $\omega_r$  and  $\omega$ , the reduced damping is

$$\eta_r = \omega_r^2 \omega \frac{V}{2\pi c^3}. \quad (3.45)$$

The excitation term in equation 3.44 is defined empirically:

$$\xi = \frac{\omega}{\omega_r} \frac{|p|}{|p + p_s|}. \quad (3.46)$$

### 3.6 The Acoustics In The Pipe

Equation 3.44, contains two unknowns, namely  $p_s$  and  $\dot{p}$ . We need additional equations to describe the pressure in the pipe,  $p$ . In the pipe, the acoustic behavior can be described as a lossless medium moving with a constant velocity, quantified through a linear wave equation:

$$\begin{cases} \frac{\partial(\rho_0 u)}{\partial t} + U \frac{\partial(\rho_0 u)}{\partial z} + \frac{\partial p}{\partial z} = F(z, t), \\ \frac{\partial p}{\partial t} + U \frac{\partial p}{\partial z} + \rho_0 c_0^2 \frac{\partial u}{\partial z} = 0 \end{cases} \quad (3.47)$$

where  $u$  [m/s] is the acoustic velocity,  $p$  [Pa] the acoustic pressure,  $U$  [m/s] the average flow velocity,  $\rho_0$  [kg/m<sup>3</sup>] the reference density and  $c_0$  [m/s] the speed of sound [9].

The source term on the right hand side is:

$$F(z, t) = G \frac{\partial p_s}{\partial z} \quad (3.48)$$

where  $p_s$  [Pa] is the acoustic pressure in the corrugations, from equation 3.44, and  $G$  is a constant coefficient.

**Coefficient G** The constant coefficient  $G$  depends on the mouth area of the cavity. Popescu and Johansen introduce the coefficient since the feedback mechanism depends

on the contact area between the cavity flow and the pipe flow. They establish the empirical value of  $G$  to be the ratio of the cavity width to the cavity pitch length:

$$G = \frac{\text{Cavity width}}{\text{Cavity pitch length}}. \quad (3.49)$$

### 3.7 The Linear Model Of Acoustics In A Corrugated Pipe

Together, equation 3.44 and 3.47 becomes a system of partial differential equations. They can be solved using a numerical scheme or with a modelling software like COMSOL. A sophisticated differential scheme has to be used to solve the system numerically, i.e. central difference does not provide the numerical stability or accuracy required. In Chapter 6, the results from solving the system using COMSOL with the appropriate boundary conditions are presented.

## Chapter 4

# Acoustic Damping

This chapter is dedicated to the concept of acoustic damping, which is the main working principle of the wet gas meter. First, we state shortly how sound waves are attenuated in mediums (fluids in particular). Then, we explore the influence liquid has on sound wave attenuation and present a governing equation for acoustic damping due to droplets in a flow. A sensitivity analysis of the equation is performed in order to investigate how the different parameters influence the acoustic damping.

### 4.1 Acoustic Damping In A Fluid

Since sound waves, or acoustic waves, can be seen as transportation of energy, the energy is gradually converted from acoustic energy to heat by the viscosity of the medium [42]. Generally, the acoustic damping is defined as the exponential decay of the sound amplitude [43]:

$$A(z) = A_0 e^{-\alpha_0 z}. \quad (4.1)$$

In equation 4.1  $A$  [dB] is the amplitude of the sound wave,  $A_0$  [dB] is the starting (or maximum) amplitude,  $\alpha_0$  [1/m] is the acoustic damping coefficient and  $z$  [m] is the space variable in the direction of the sound wave. As seen in the equation, the damping coefficient can have values greater than 1.

The value of the acoustic damping coefficient can be estimated by the Stokes' law of sound attenuation [42]. The Stokes' law of sound attenuation applies to a isotropic and homogenous Newtonian fluid and is given by

$$\alpha_0 = \frac{2\mu f^2}{3\rho c^3} \quad (4.2)$$

where  $\alpha_0$  [1/m] is the damping coefficient,  $\mu$  [Pa · s] is the viscosity of the fluid,  $f$  [Hz] is the sound frequency,  $\rho$  [kg/m<sup>3</sup>] is the fluid density and  $c$  [m/s] the speed of sound. It should be noted that the formula has later been modified to account for volume viscosity, which is important when the compressibility of the fluid no longer can be ignored [44].

Sound waves do not travel indefinite, but decay in the medium they travel in. The decay of the sound waves is dependent of the properties of the fluid. Increased viscosity will for instance increase the acoustic damping. In addition to damping, sound waves are subject to other physical phenomena, like absorption and reflection [45]. These phenomena are not studied further in this chapter.

**Acoustic damping in pipes** Stokes' law of sound attenuation is not valid when describing acoustic damping in pipes. In a smooth pipe with turbulent single phase gas flow, the main attribution to the acoustic damping is the viscous-thermal effects at the wall. In Peters et al.'s work, the acoustic damping coefficient  $\alpha_0$  for a smooth pipe is given by the Kirchhoff model [46]:

$$\alpha_0 = \frac{\pi D}{2Ac_0} \sqrt{\frac{\pi f \mu}{\rho_0}} \left( 1 + \frac{\gamma - 1}{\sqrt{Pr}} \right) \quad (4.3)$$

where  $\alpha_0$  [1/m] is the damping coefficient,  $f$  [Hz] the frequency,  $\gamma$  [-] the isentropic coefficient,  $D$  [m] the tube diameter,  $A$  [m<sup>2</sup>] the tube area,  $\mu$  [Pa · s] the gas viscosity,  $\rho_0$  [kg/m<sup>3</sup>] the steady state gas density, and  $Pr$  [-] is the Prandtl number defined as

$$Pr = \frac{c_p \mu}{\kappa} \quad (4.4)$$

where  $c_p$  [J/kg · K] is the heat capacity and  $\kappa$  [W/m · K] the thermal conductivity.

To account for turbulent flow, the damping coefficient is adapted such that:

$$\alpha_0 = \alpha_0 \frac{\delta_{ac}}{\delta_{visc}} \quad \text{if} \quad \frac{\delta_{ac}}{\delta_{visc}} > 1 \quad (4.5)$$

where the acoustic boundary layer  $\delta_{ac}$  and the viscous boundary layer  $\delta_{visc}$  are defined as:

$$\delta_{ac} = \sqrt{\frac{2\mu}{\rho_0 \omega}} \quad \text{and} \quad \delta_{visc} = 10 \frac{\mu}{\rho_0 u^*} \quad (4.6)$$

where the angular frequency is  $\omega$  [rad/s] and the friction velocity is  $u^* = \sqrt{0.5C_f}$  [-] with the Fanning friction coefficient  $C_f$  [-].

The Kirchhoff model can be used to determine acoustic damping for dry gas flow in a smooth pipe. However, it is not valid for corrugated pipes, since the pressure drop in

corrugated pipes is primarily due to separation in the corrugations. Furthermore, it is only valid for single phase gas flow, and can not predict acoustic damping when liquid is introduced in the gas flow.

## 4.2 Liquid Influence On Acoustic Damping

In two phase flow consisting of gas and liquid, the sound attenuation is also influenced by the presence of liquid. Belfroid et al. has performed substantial work on the subject of liquid influence on the sound generated in a corrugated pipe [1, 7, 47, 48]. In their articles, they point out three mechanisms that could explain the effect of liquid on the whistling mechanism:

1. The corrugations are filled up by liquid, meaning that the source strength in the corrugations decreases with lower cavity depth [49].
2. Additional damping of the sound due to the presence of droplets (mist flow) [50].
3. Reduction of the source strength due to droplets on the wall. The droplets thicken the shear layer, which results in a lower source strength in the corrugation [47].

The first and third mechanisms are difficult to quantify. The second, however, has been investigated more in depth. Howe first described the damping due to droplets in the flow (mist flow),  $\alpha$ , [50]. This was adopted by Belfroid et al. to become

$$\alpha = \frac{2\pi}{\lambda} \frac{\alpha_p}{2} \left( \underbrace{\frac{\omega\tau_\eta}{1 + (\omega\tau_\eta)^2}}_{\text{Viscous}} + \underbrace{\frac{c_s(\gamma - 1)}{c_p} \frac{\omega\tau_t}{1 + (\omega\tau_t)^2}}_{\text{Thermal}} \right) \quad (4.7)$$

where

$$\tau_\eta = \frac{m}{3\pi\mu d_p} \quad \text{and} \quad \tau_t = \frac{mc_s}{2\pi\kappa d_p}. \quad (4.8)$$

In equations 4.7 and 4.8,  $\lambda$  [m] is the wave length,  $\alpha_p$  [-] is the liquid/gas mass ratio,  $c_s$  [J/kg · K] the specific heat of the liquid,  $c_p$  [J/kg · K] the specific heat of the gas,  $\gamma$  [-] the isentropic constant,  $\omega$  [rad/s] the angular frequency,  $\mu$  [Pa · s] the gas viscosity,  $\kappa$  [W/m · K] the thermal conductivity,  $m$  [kg] the droplet mass and  $d_p$  [m] the droplet diameter. The viscous and thermal effects of the damping are highlighted in the equation.

In the following, we have modified equation 4.7 slightly. The original equation from Howe was given in terms of damping per wavelength [50]. In addition  $\omega$ , the sound frequency was given in Hz. Belfroid et al. modified this to become the damping per meter by dividing with the wavelength  $\lambda$  and multiplied by  $2\pi$  to use  $\omega$  in rad/s instead.

For convenience we have used a mix of these two with  $\omega$  in Hz, but the damping given per meter. The governing equation for damping due to droplets then becomes

$$\alpha = \frac{\alpha_p}{2\lambda} \left( \underbrace{\frac{\omega\tau_\eta}{1 + (\omega\tau_\eta)^2}}_{\text{Viscous}} + \underbrace{\frac{c_s(\gamma - 1)}{c_p} \frac{\omega\tau_t}{1 + (\omega\tau_t)^2}}_{\text{Thermal}} \right) \quad (4.9)$$

where  $\tau_\eta$  and  $\tau_t$  are defined as in equation 4.8.

#### 4.2.1 The Viscous And The Thermal Part Of Acoustic Damping Due To Droplets

In equation 4.9 two different sources of damping appear: one accounting for the damping due to viscous effects and the other accounting for the damping due to thermal effects. In the sensitivity analysis, the ratio of these terms with respect to the changing parameter has been investigated.

To illustrate the viscous and thermal acoustic damping, consider the sound waves as pulses of energy. In fact, waves are energy transport without transport of matter. The energy transported is proportional to the square of the amplitude [51]. The energy in the sound waves is used to move the particles in the medium. In dry gas, this energy is used to move the gas particles along the direction of propagation of the sound wave and consequently create pressure oscillations (see Section 2.4). When liquid droplets are introduced in the flow, this energy has to be used to displace liquid molecules as well. The energy losses come from two different effects. The viscosity effects describe the energy consumed in moving a fluid, while the thermal effects describe the energy converted to heat at the surface of the droplets [50].

For droplets of small diameters (typically  $<100 \mu\text{m}$ ) with relative velocity (relative to the gas velocity) equal to the acoustic velocity, the Reynolds number is small enough for the drag to be dominated by viscosity [50]. The motion of the particles are hence governed by Stokes' drag law. Stokes drag law is stated as

$$F_D = 3\pi\mu d_p V \quad (4.10)$$

and is hence the force needed to move a spherical droplet through a fluid at a given velocity [52]. The Stokes relaxation time, that is the time constant for the exponential decay of the particle velocity due to drag, is found in the  $\tau_\eta$ -term in equation 4.9.

The pressure fluctuations in the medium created by the sound waves, may in turn cause temperature fluctuations in the bulk of the gas (if the medium is gas) as these are related through an equation of state. This means that heat can be transferred from the bulk of the gas to the droplets. Howe showed how the entropy perturbation is related to the

net heat flux between the droplets and the gas, the result being the thermal term in equation 4.9 [50].

### 4.3 Sensitivity Analysis

The acoustic damping due to liquid droplets present in a gas flow (hereafter added acoustic damping) was studied in Section 4.2. In the following we present a parametric study, or sensitivity analysis, of equation 4.9. The objective is to highlight how various parameters influence the added acoustic damping. The Matlab files used in the analysis can be found in Appendix B.

Parameter	Description	Value	Unit
$c_{gas}$	Speed of sound in gas	343.3	m/s
$\mu$	Gas viscosity	$1.802 \cdot 10^{-5}$	Pa · s
$\rho_g$	Gas density	1.225	kg/m <sup>3</sup>
$c_p$	Gas specific heat	1007.0	J/kg · K
$\gamma$	Isentropic constant	1.4	-
$\kappa$	Gas thermal conductivity	$2.476 \cdot 10^{-2}$	W/m · K
$\rho_l$	Liquid density	999.1	kg/m <sup>3</sup>
$c_s$	Liquid specific heat	4188.5	J/kg · K
$\omega$	Sound frequency	200.0	Hz
$d_p$	Droplet diameter	$1.0 \cdot 10^{-4}$	m
$d_{pipe}$	Pipe diameter	$3.5 \cdot 10^{-2}$	m
Liquid Rate	Rate of liquid injected	20.0	ml/min
$U$	Average gas velocity	3.0	m/s

**Table 4.1** – Paramteres used in the sensitivity analysis. Air and water at 1 atm and 15°C have been used for gas and liquid properties respectively [32, 53].

Gas properties from McGraw & Hill and liquid properties from NIST were used as baseline [32, 53]. All the fluid properties used are presented in table 4.1. The partial derivatives of the governing equation (4.9) for added acoustic damping was calculated using Maple 18. However, the results were rather complex equations of the fifth order, presenting no real insight in how the different variables changed the equations. They are therefore out of the analysis.

The air and water properties are coherent with the ones used in the experiment in Chapter 5. Even so, similar trends are expected for other gases and fluids, as different properties would only shift or stretch the curves horizontally or vertically. The main uncertainty regarding equation 4.9 is the droplet size, since the droplet size distribution is generally unknown in a flow.

**Parameters** Belfroid et al. investigated the influence of liquid rate on the acoustic damping term [1, 54]. The liquid rate only appears in the  $\alpha_p$  term in equation 4.9, Hence, it varies linearly with the liquid rate. For other parameters appearing in the equation the relationship is more complex. By using Matlab, we were able to qualitatively evaluate the dependence based on graphical plots. The parameters we chose to investigate, in addition to liquid rate, were:

1. Droplet size
2. Liquid Density
3. Gas Viscosity
4. Sound Frequency

To facilitate the comparison with the experiment, the liquid rate is given in ml/min. This can easily be related to the liquid volume fraction (LVF), which is widely used in engineering applications. Part per million by volume (ppmv), which is the equal to the LVF times  $1 \cdot 10^6$ , is also used to describe such small quantities. Table 4.2 gives the relation between liquid rate, LVF and ppmv for the gas density, gas velocity and pipe diameter used in the sensitivity analysis. LVF is calculated with the simplified formula

$$LVF = \frac{\dot{m}_{liquid} \rho_g}{\dot{m}_{gas} \rho_l}. \quad (4.11)$$

In equation 4.11,  $\dot{m}_{liquid}$  [kg/s] and  $\dot{m}_{gas}$  [kg/s] denote the mass flow of liquid and gas respectively, while  $\rho_l$  [kg/m<sup>3</sup>] and  $\rho_g$  [kg/m<sup>3</sup>] are the liquid and gas densities. Note that the mass of the liquid is considered to be small enough to be neglected in the denominator.

Liquid Rate [ml/min]	LVF [-]	ppmv [-]
1	$5.7743 \cdot 10^{-6}$	5.8
2.5	$1.4436 \cdot 10^{-5}$	14.4
5	$3.1759 \cdot 10^{-5}$	31.8
10	$5.7743 \cdot 10^{-5}$	57.7
20	$1.1549 \cdot 10^{-4}$	115.5
40	$2.3097 \cdot 10^{-4}$	231.0
100	$5.7743 \cdot 10^{-4}$	577.4

**Table 4.2** – Relationship between liquid rates used in the analysis, LVF and ppmv.

### 4.3.1 Droplet Size

In a real mist flow numerous droplet sizes will be present. The number of droplets of a given size will vary, meaning we have a droplet size distribution. Clearly, the added



acoustic damping is dependent on the droplet size as it appears in both  $\tau_t$  and  $\tau_n$ . In addition it also appears in  $m$ , the droplet mass, to the third power since the droplets are assumed to be spherical.

The droplet size was varied from 0.1 nm to 100  $\mu\text{m}$  and the liquid rate from 1 to 100 ml/min. These ranges are aligned with the experiment conducted and capture graphically the trends of the added acoustic damping when the droplet size is varied. The other properties were kept constant according to table 4.1.

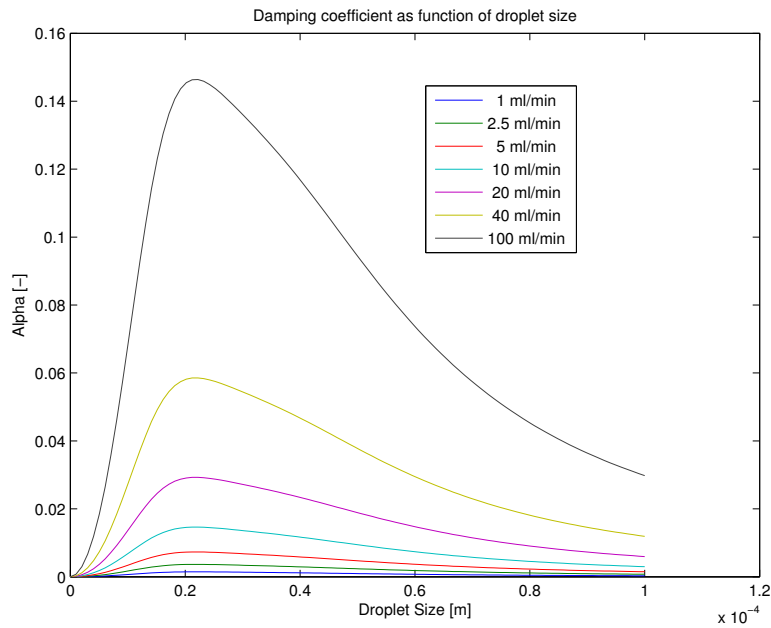


**Figure 4.1** – Added acoustic damping as a function of droplet size for different liquid rates.

From figure 4.1, we can identify a maximum added acoustic damping for the same droplet size for all liquid rates. This droplet size was calculated with Matlab to 22.2  $\mu\text{m}$  for the properties used in this analysis. It should also be noted that the damping is small for very small droplets as well as for larger droplets (towards 100  $\mu\text{m}$ ). The same effects are also identified in 3D in figure 4.2.

From figure 4.3 we can see that the ratio between the viscous and the thermal part of the equation is independent of the liquid rate. This because the liquid rate only appears outside the parenthesis in equation 4.9 and thus only influence the absolute value of the damping. This can be observed for all the parameters investigated. Furthermore, it also means that the acoustic damping varies linearly with the liquid rate as shown by Belfroid et. al. [1, 54].

We observe from figure 4.3 that the ratio between the viscous and thermal part in equation 4.9 approaches a constant value around 2.75 for droplet sizes larger than ap-

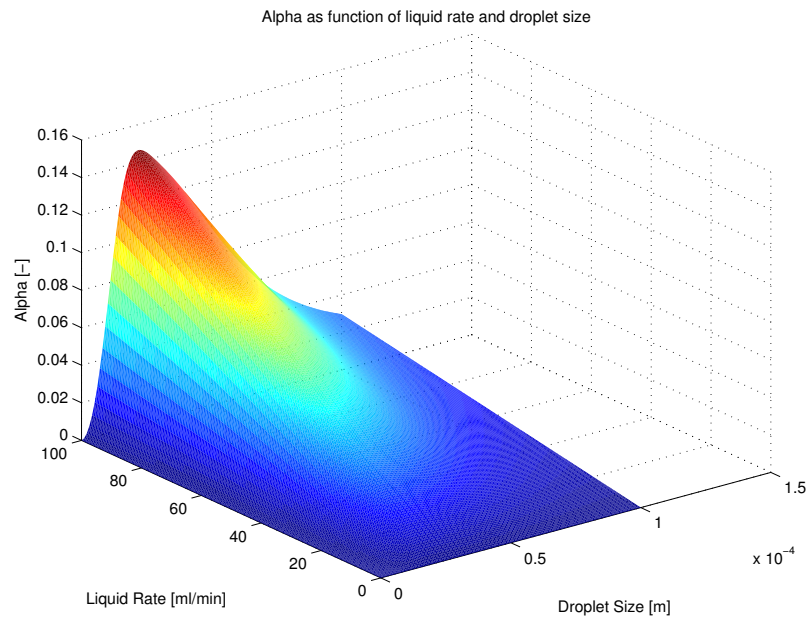


**Figure 4.2** – 3D-plot of acoustic damping as a function of droplet size and liquid rate.

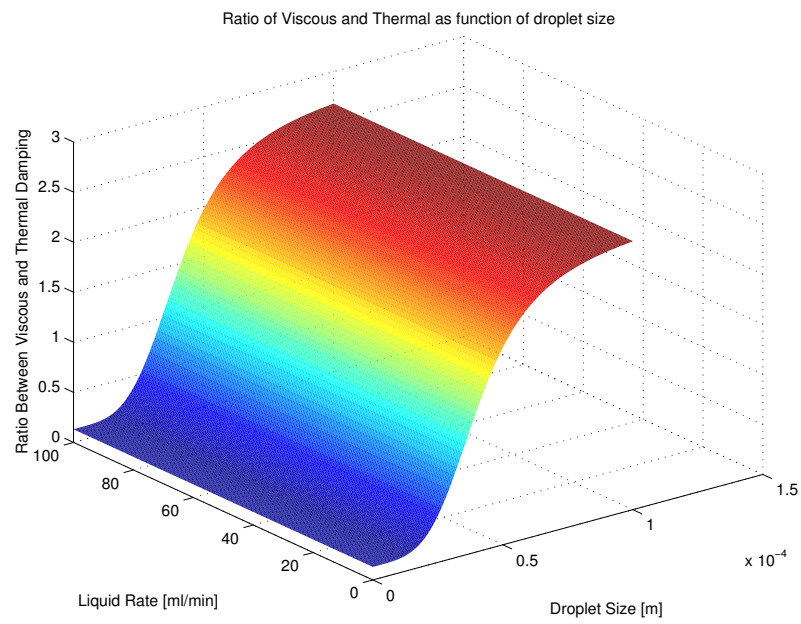


**Figure 4.3** – Ratio between the viscous and thermal term in equation 4.9 as a function of droplet size and liquid rate.

proximately  $100\ \mu\text{m}$ . Shown mathematically, when the terms  $\omega\tau_\eta$  and  $\omega\tau_t$  grow large,  $(1 + \omega\tau_\eta) \rightarrow \omega\tau_\eta$  and  $(1 + \omega\tau_t) \rightarrow \omega\tau_t$ , the ratio between the viscous and the thermal part approaches the limit

$$\lim_{\omega\tau_\eta, \omega\tau_t \rightarrow \infty} \left( \frac{\frac{\omega\tau_\eta}{1+(\omega\tau_\eta)^2}}{\frac{c_s(\gamma-1)\omega\tau_t}{c_p(1+(\omega\tau_t)^2)}} \right) = \frac{\omega\tau_t c_p}{c_s(\gamma-1)\omega\tau_\eta} = \frac{3\mu c_p}{2(\gamma-1)\kappa} \approx 2.7498. \quad (4.12)$$

### 4.3.2 Liquid Density

When analyzing the influence of the liquid density, the droplet size was fixed to  $100\ \mu\text{m}$ . The liquid density spanned from  $100\ \text{kg/m}^3$  to  $4000\ \text{kg/m}^3$ . This range should cover physical applications and capture the trends in the added acoustic damping.

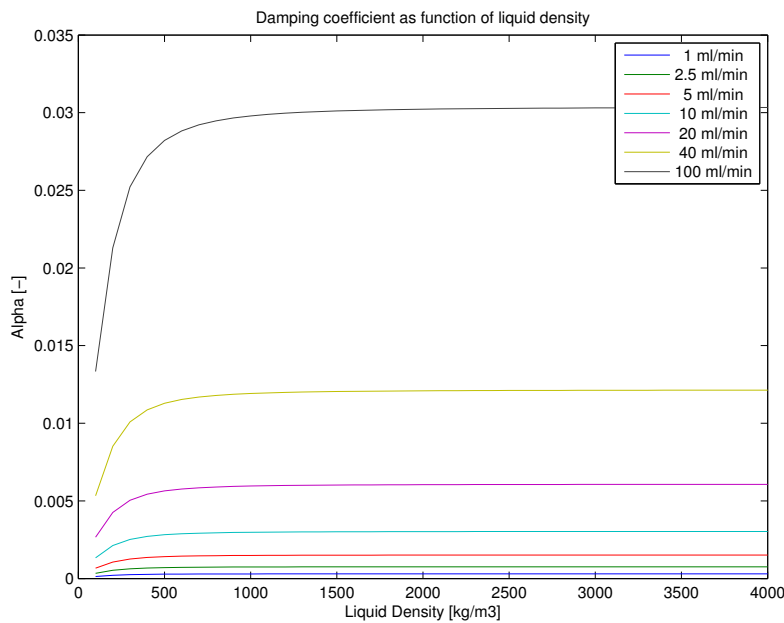


**Figure 4.4** – Added acoustic damping as a function of liquid density for different liquid rates.

From figure 4.4, we observe that the added acoustic damping is more or less constant for liquid densities greater than  $600\ \text{kg/m}^3$ . Since the droplet size was fixed to  $100\ \mu\text{m}$ , the absolute value of the added acoustic damping is not as large as we could see in section 4.3.1.

The same effect can be identified in figure 4.5; the added acoustic damping coefficient is constant for larger liquid densities. In addition it increases linearly with liquid rate, a tendency observed throughout the analysis.

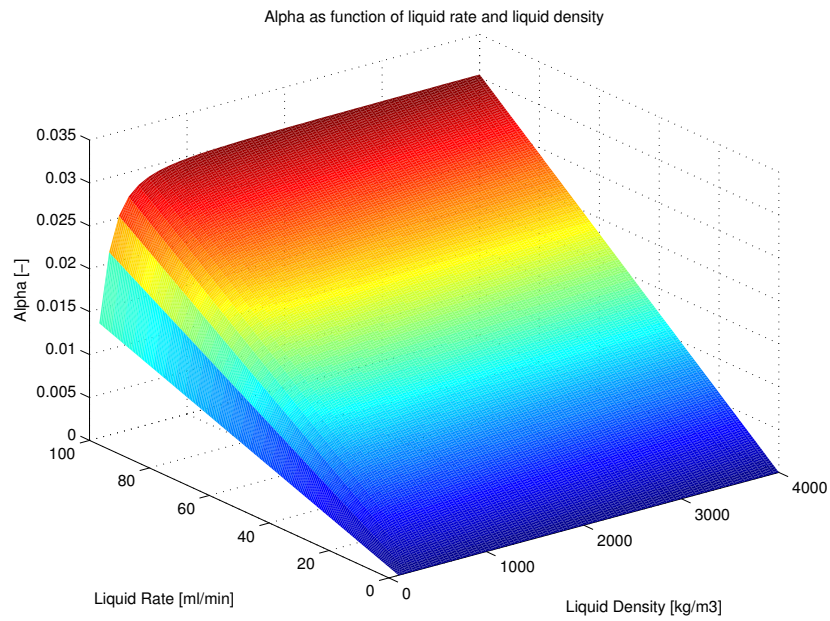


**Figure 4.5** – 3D-plot of acoustic damping as a function of liquid density and liquid rate.

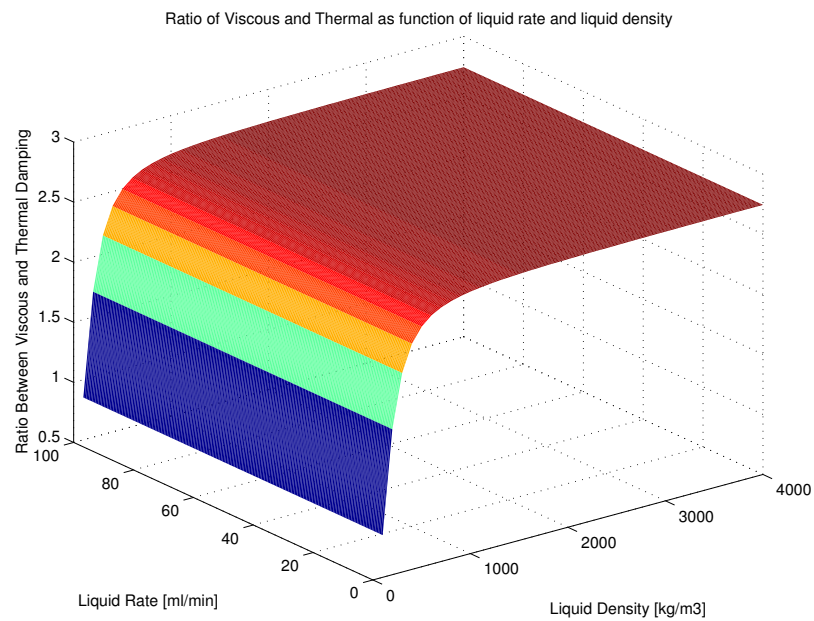


**Figure 4.6** – Ratio between the viscous and thermal term in equation 4.9 as a function of liquid density and liquid rate.

The ratio between the viscous and the thermal part of the damping approaches the same constant value of 2.75. This is in accordance with equation 4.12. At densities larger than about  $100 \text{ kg/m}^3$ , the ratio can be assumed constant with reasonable accuracy.

### 4.3.3 Gas Viscosity

Similar to the study of liquid density, the droplet size was fixed to  $100 \mu\text{m}$  when investigating the influence of gas viscosity. The gas viscosity was varied from  $1 \cdot 10^{-7}$  to  $1 \cdot 10^{-4} \text{ Pa} \cdot \text{s}$ .

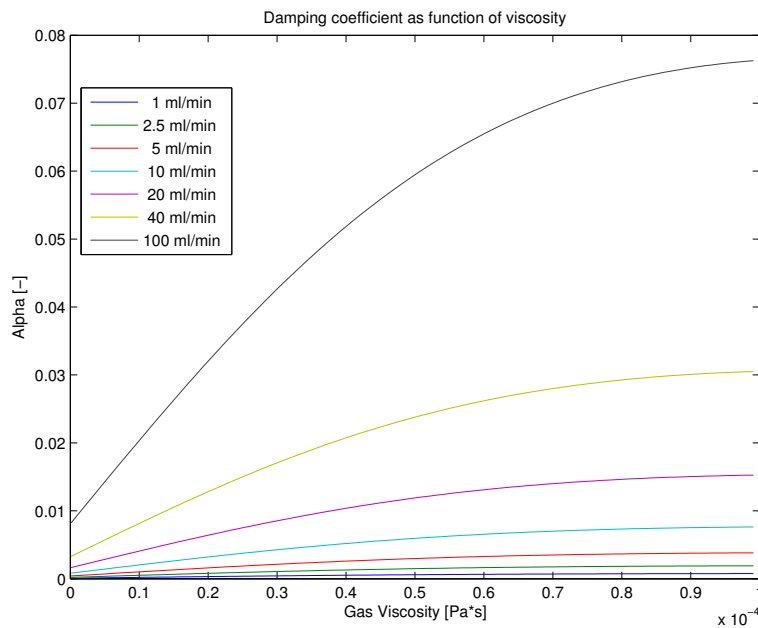


**Figure 4.7** – Added acoustic damping as a function of gas viscosity for different liquid rates.

In figure 4.7, we observe a significant increase in damping when there is an increase in viscosity. Hence, different gases give different values of acoustic damping. Viscosity is also a function of temperature, implying that the operation conditions affect the added acoustic damping of a given fluid.

Though it is not evident in figure 4.8, the added acoustic damping varies linearly with the liquid rate as for the other parameters. The acoustic damping can be relatively large even for low liquid rates, but the increase in the damping coefficient slows down as the gas viscosity increases.

As expected, the ratio between the viscous and thermal term in equation 4.9 does not approach a constant value. Instead, it increases rapidly with increasing gas viscosity.

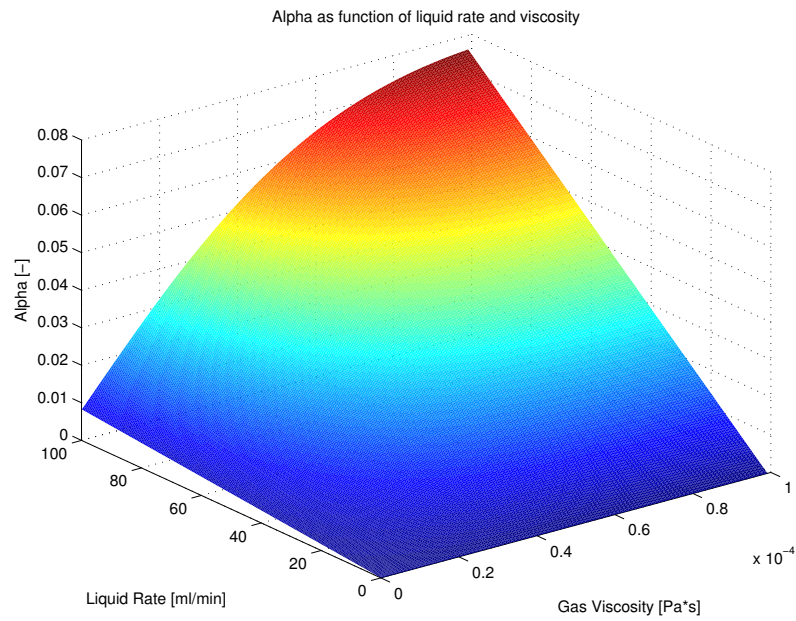


Figure 4.8 – 3D-plot of acoustic damping as a function of gas viscosity and liquid rate.

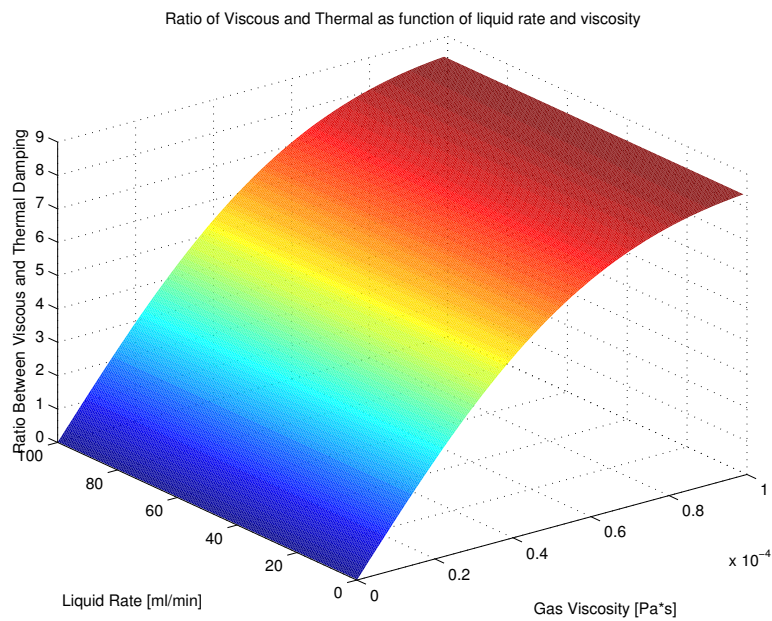


Figure 4.9 – Ratio between the viscous and thermal term in equation 4.9 as a function of gas viscosity and liquid rate.

Higher viscosity means larger drag force, and the viscous term dominates the thermal term for larger gas viscosities, as discussed in Section 4.2.1.

#### 4.3.4 Sound Frequency

We studied how the sound frequency changed with both liquid rate and droplet size. As the sound waves can be interpreted as pressure oscillations, the sound frequency denotes the frequency of these fluctuations. The frequency range investigated was 0 Hz to 2 kHz. We could also have investigated higher frequencies, but they would suppress the trends at the lower frequencies, since the added acoustic damping coefficient (for a given liquid rate) approached a constant value for quite low frequencies.

##### 4.3.4.1 Liquid Rate

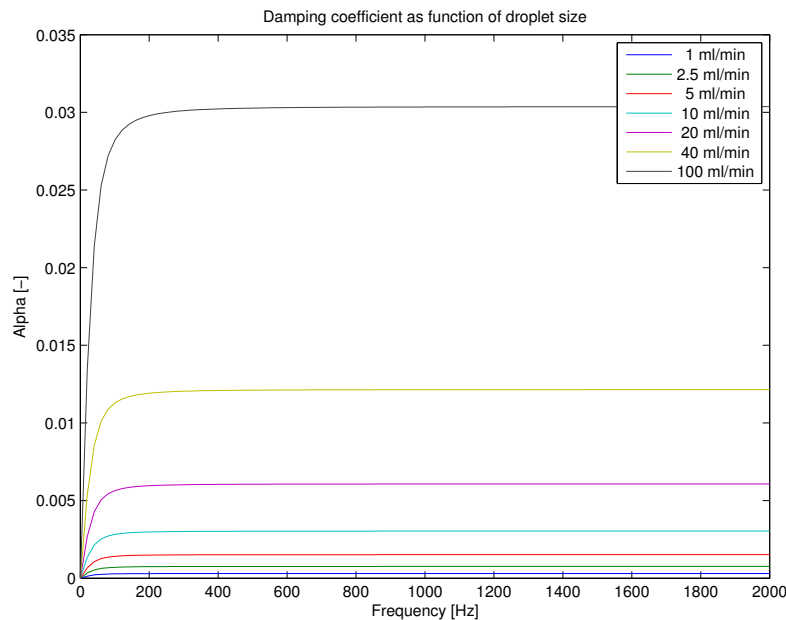


**Figure 4.10** – Added acoustic damping as a function of frequency for different liquid rates.

From figure 4.10, we observe that the added acoustic damping is approximately independent of sound frequency above 200 Hz. The same relationship is also shown in 3D in figure 4.11, where the linear relationship between the liquid rate and the added acoustic damping once again can be seen.

Figure 4.12 shows the ratio between viscous and thermal damping as a function of liquid rate and frequency. We can see that the ratio again approaches 2.75 as the frequency

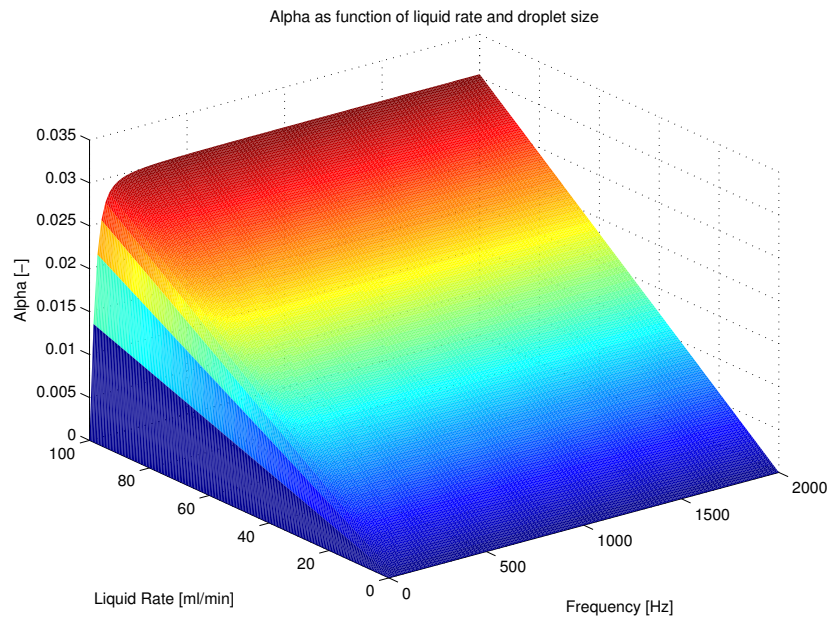


**Figure 4.11** – 3D-plot of acoustic damping as a function of frequency and liquid rate.

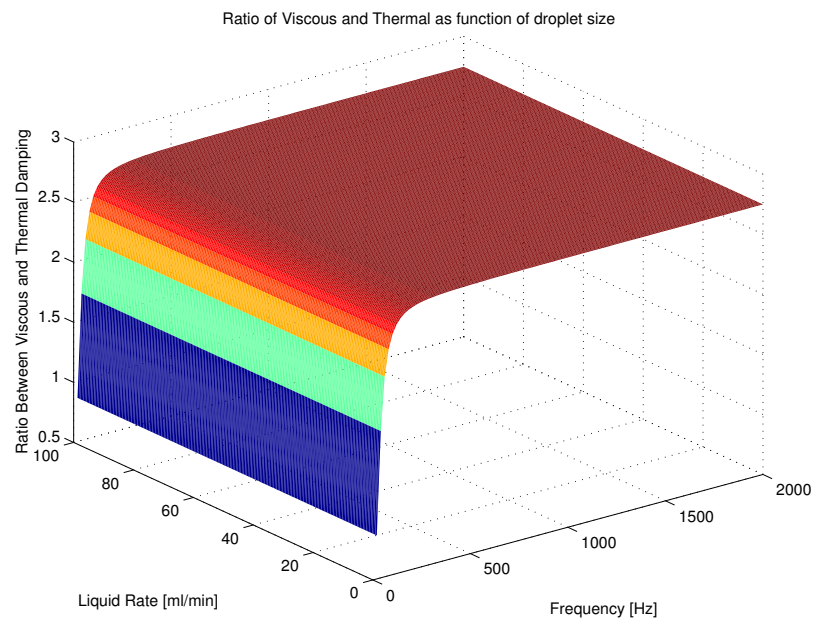


**Figure 4.12** – Ratio between the viscous and thermal term in equation 4.9 as a function of frequency and liquid rate.



increases, coherent to what we have discussed in Section 4.3.1.

#### 4.3.4.2 Droplet Size

Finally, the frequency and droplet size were varied together, keeping the liquid rate fixed at 20 ml/min. The frequency varied from 0 to 2 kHz while the droplet size spanned from 0.1 nm to 100  $\mu\text{m}$ .

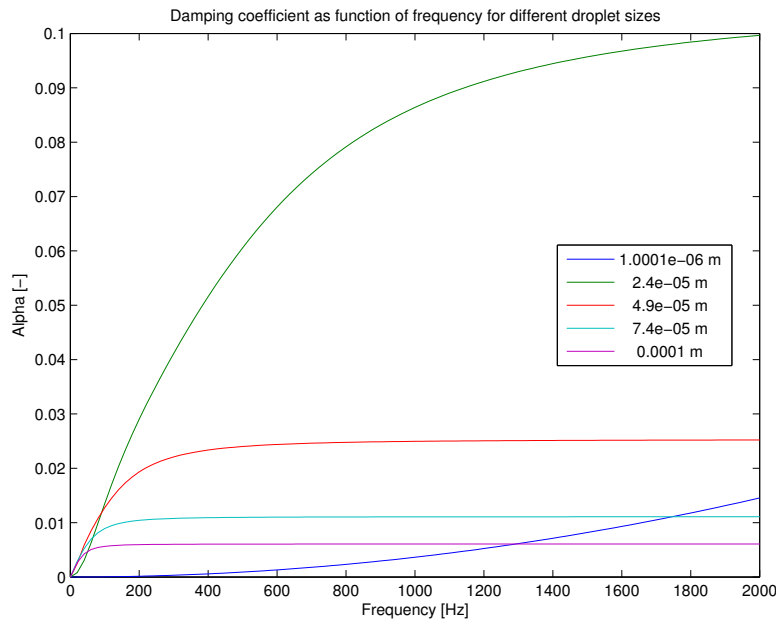


**Figure 4.13** – Added acoustic damping as a function of frequency for different droplet sizes.

It seems difficult to identify any trends in figure 4.13, but the ambiguous result (i.e. highest added acoustic damping for a middle droplet size) comes from the fact that the added acoustic damping peaks at a given droplet size. This was established in section 4.3.1. However, as we can see in figure 4.14, the droplet size with the highest damping coefficient is dependent of the frequency.

The relationship is better seen in the 3D-plot in figure 4.15. In this figure we can see that the acoustic damping generally increases with frequency, while it varies with the droplet size in the same manner as seen in figure 4.14.

In figure 4.16 and 4.17 the ratio between viscous and thermal damping is shown. As for the other parameters, we can see that the ratio approach 2.75 for larger droplet sizes and frequencies. The horizontal line in figure 4.17 for a droplet size of 1.0001  $\mu\text{m}$  appears because the absolute variations are very small compared to the other droplet sizes shown in the same figure.

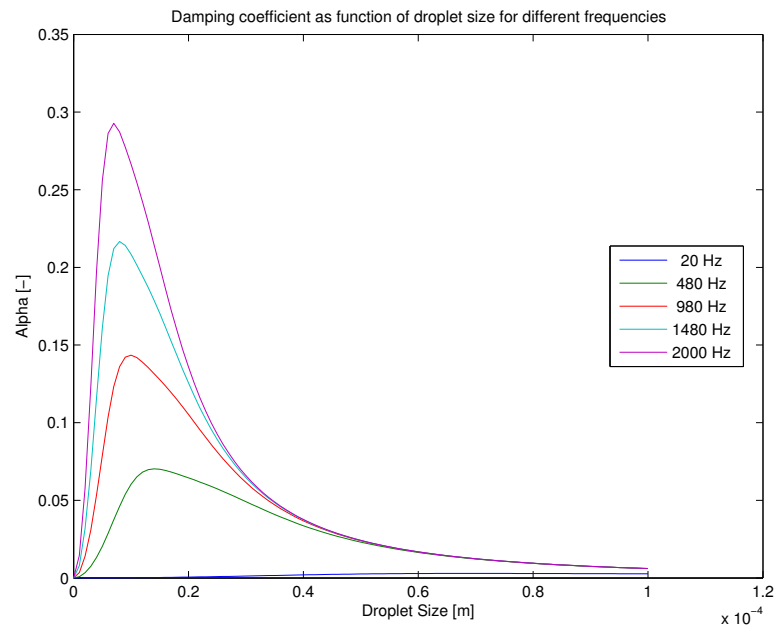


Figure 4.14 – Added acoustic damping as a function of droplet size for different frequencies.

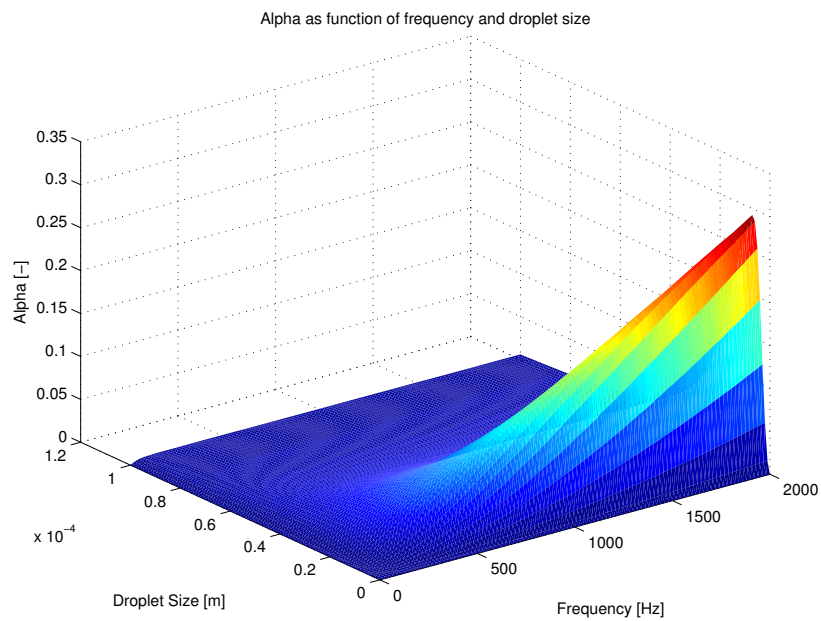
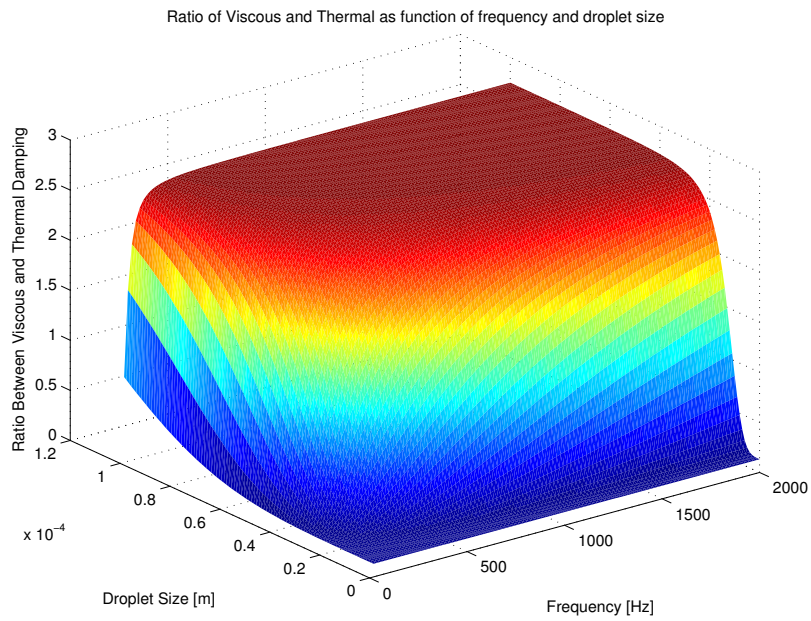
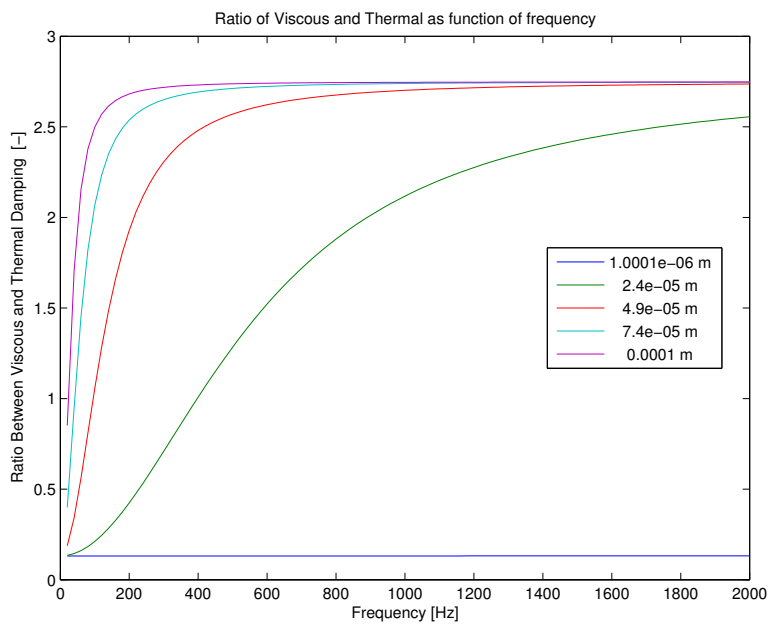


Figure 4.15 – 3D-plot of acoustic damping as a function of frequency and droplet size.



**Figure 4.16** – Ratio between the viscous and thermal term in equation 4.9 as a function of frequency and droplet size.



**Figure 4.17** – Two-dimensional plot of the ratio between the viscous and thermal term in equation 4.9 as a function of frequency for different droplet sizes.

## 4.4 Discussion

It is apparent that a whole range of different fluid properties strongly influence the added acoustic damping. Notably, the droplet size had a major influence, with a peak added acoustic damping coefficient around  $22.2\ \mu\text{m}$ . This critical droplet size is further dependent on the frequency, as seen in figure 4.14. The droplet size distribution is difficult to estimate and rarely fully known in application. Work is being done in this area, but not for low LVFs. Opdal et al. used nuclear magnetic resonance to estimate the size distribution of water droplets in crude oil, but for water cuts from 10% to 40% [55]. Without knowing the droplet size distribution it could be difficult to predict the added acoustic damping coefficient theoretically. Such a theoretical prediction would simplify the making of a wet gas meter, as it would have been possible to compare the measurement with theory directly.

The acoustic damping coefficient was directly proportional to the liquid rate, as we can see from equation 4.9. Isolated, neglecting other damping effects, it means that a measurement of the acoustic damping with all gas and liquid properties known (including the droplet size distribution) could predict the liquid flow rate (and thus the LVF). Or, if the droplet size distribution can be assumed to be constant over time, the increase in LVF can be estimated by measuring the sound attenuation. For the corrugated pipe, other damping mechanisms are also expected in application, like liquid on the wall and fill-up of the corrugations, which both decrease the strength of the sound source [49, 47].

In the sensitivity analysis we also saw how the ratio between the viscous and thermal part of the equation for added acoustic damping approached a constant value. This does not mean that the added acoustic damping is less prone to temperature variations since most fluid properties are dependent of temperature. With the viscous term being larger than the thermal term it means that the added acoustic damping is more sensitive to changes in the viscous term than in the thermal term. That is, more sensitive to viscosity changes than changes in thermal conductivity or heat capacity.

The most important result, perhaps, is that changing only one property influences the added acoustic damping significantly. A precise knowledge of the flow and its properties is therefore needed to estimate the added acoustic damping for a given operating condition. At the very least, a wet gas meter based on the sound attenuation principle has to be calibrated with real fluids before being installed. However, since the properties in a given reservoir may change over time, this may not suffice either.

## Chapter 5

# Experiment: Liquid Influence On Sound Waves In Pipes

Only a limited number of experimental results concerning the acoustic damping due to droplets exist in literature. Belfroid et al. conducted an experiment regarding liquid influence on acoustic damping and reported promising results [1]. Their results indicated a close to linear relationship between the liquid injection and the acoustic damping. However, the results were obtained for LVFs in the range  $7.1 \cdot 10^{-6}$  to  $1.2 \cdot 10^{-4}$ . In this experiment we wanted to further investigate the effect of acoustic damping for even smaller LVFs. The lowest LVF in our experiment was therefore  $4.3 \cdot 10^{-6}$  and the largest  $5.8 \cdot 10^{-4}$ , with more runs focused in the lower end of the range. The lower limit of the LVF range was limited by the operational capacity of the rotameters. Finding a robust relationship between the liquid injection, or the LVF, and the acoustic damping is fundamental for a wet gas meter to be based upon attenuation of sound waves.

The goal of the experiment was to investigate the relationship between sound amplitude and frequency and the liquid present in the gas flow. For simplicity, air and water have been used as fluids. In Section 4.3, we saw that the additional damping due to droplets in the gas flow was strongly influenced by the properties of the fluid. These relationships were not linear for all properties and therefore the results can not be transferred to other fluids directly.

The experiment was carried out in different steps. First, the resonance frequencies of the pipes were identified. The results were used to determine which frequencies we should use when measuring the added acoustic damping in the smooth pipe. For the corrugated pipe, however, the results were used to check whether the whistling jumped in frequency modes with increasing flow velocities, as described in theory. Then, liquid was injected with a needle and syringes of different sizes while the amplitude and frequency of the sound waves were measured.

A simple risk assessment was performed in association with the work in the laboratory.

Due to the relative harmless nature of the experiment, this was not carried out in a comprehensive matter. The risk assessment can be found in Appendix C.

## 5.1 Experimental Setup

Two different designs were investigated in the experiment; a smooth pipe and a corrugated pipe. For the smooth pipe, a loud speaker was installed in one end to generate the sound. For the corrugated pipe, the sound was generated by the vortex shedding in the cavities as described in Sections 3.2 and 3.3. A microphone close to the outlet of the pipe recorded the sound field in the flow (figure 5.1). The equipment used in the experiment is listed in table 5.1.

Equipment	Description
Smooth pipe	Transparent acrylic pipe, 3.5 cm diameter
Corrugated pipe	White conduit pipe, 2.5 cm diameter
Microphone	Brüel og Kjær 4191 28113972
Loud speaker	Kitsound Mini Speaker
Amplifier	Norsonic Front End type 336
Sound card	Echo Audiofire 4
Liquid injection	Terumo syringe and needle (1, 2.5, 5, 10, 20, 40 ml/min)
Rotameter 1	ABB Model D10A11 (6.9 m <sup>3</sup> /h)
Rotameter 2	Fischer & Porter D-3400 (7.0 m <sup>3</sup> /h)

**Table 5.1** – Equipment used in the experiment.

To account for time variance, each set of conditions were run multiple times. By doing this, we were able to check the robustness of the experiment, i.e. if the variation for the independent set of conditions were large. A sketch of the experimental setup can be seen in figure 5.2 and a picture of the test rig can be seen in figure 5.3.

The section where air and liquid are injected and mixed was made from a solid acrylic cylinder, a bolt. Air was injected through a bended pipe and the liquid was injected via needles from the top of the acrylic cylinder (figure 5.4).

We mounted the loud speaker at the upstream end of the acrylic cylinder. A rubber ring and rubber cover made sure the end was air tight in order to avoid inflow due to the ejector effect<sup>1</sup>. At the downstream end of the acrylic cylinder two different pipes were mounted, one corrugated and one smooth. The work drawing of the acrylic cylinder can be seen in Appendix D.

<sup>1</sup>An ejector converts pressure energy to kinematic energy according to Bernoulli's principle. This generates a low pressure zone which in turn can create a flow of (another) fluid towards this zone [56]

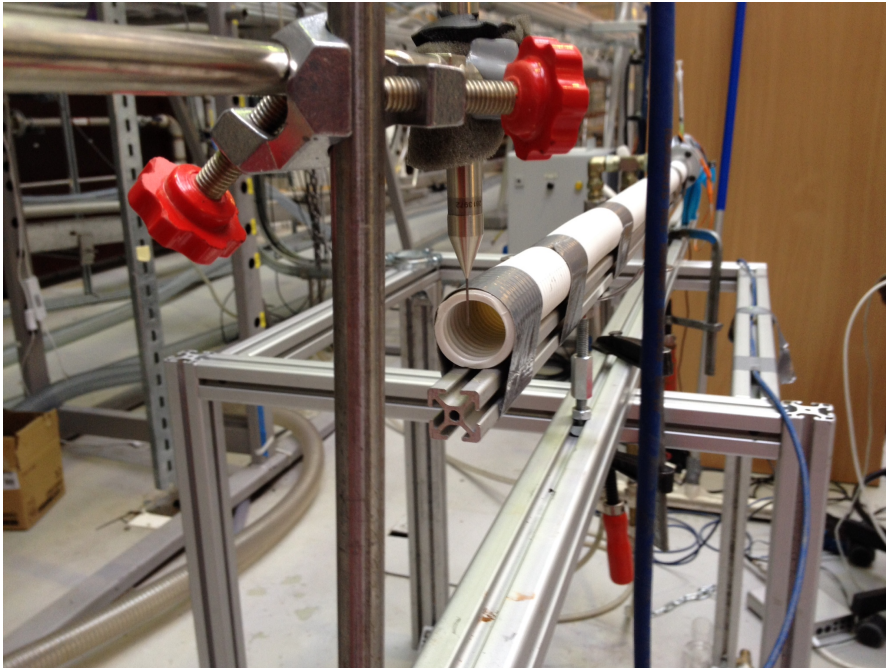


**Figure 5.1** – The probe microphone was borrowed from the Department of Acoustics at NTNU and placed at the outlet of the pipe.

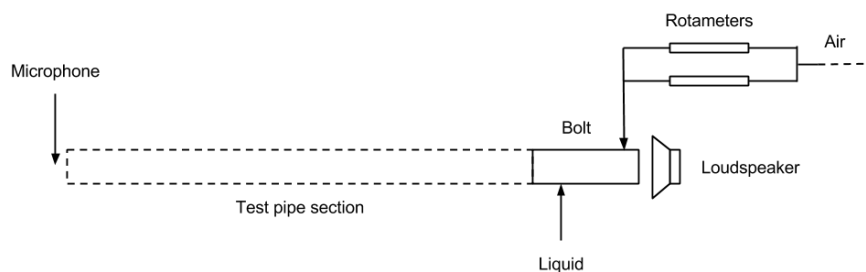


**Figure 5.2** – Sketch of the experimental setup.

The air flow was controlled by two rotameters with a capacity of 6.9 and 7.0 m<sup>3</sup>/h. Pressurized air was taken from the wall outtake and split in two before reaching the two rotameters operating in parallel. The liquid was injected with needles of different sizes, ranging from 1 to 40 ml using a stop watch to control the rate (figure 5.5). A dedicated test bench in the laboratory of the Department of Energy and Process Engineering was used for the experiment.

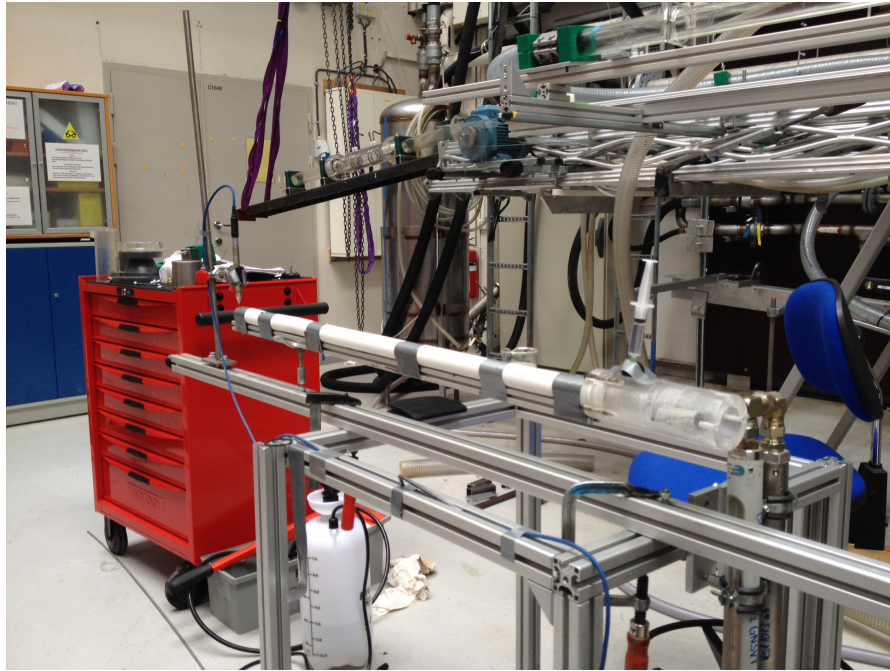


**Figure 5.3** – Picture of the test rig. On the lower right hand side the two parallel rotameters can be seen next to the needle and mixing unit. The microphone can be seen at the outlet of the pipe, on the left hand side of the picture.

## 5.2 Test Matrices

Tables 5.2 to 5.4 show the test matrices of the experiment. The flow velocities were, as mentioned, limited by the operating capacity of the rotameters, setting a restriction for the lower limit of the LVF. Each set of conditions were run for 20 seconds. The duration of the runs was somewhat limited by the capacity of the smallest syringe. However, longer runs could endanger the consistency of the liquid rate injection. Furthermore, we regarded the duration as long enough to average out noise and other time variant effects.

Air Flow Rates [ $\text{m}^3/\text{h}$ ] ([m/s])	Liquid Rates [ml/min]	Frequencies [Hz]
5.52 (1.59)	0	373
9.70 (2.80)	1	445
11.10 (3.20)	2.5	550
12.50 (3.61)	5	
13.90 (4.01)	10	
	20	
	40	

**Table 5.2** – Test matrix for smooth pipe.



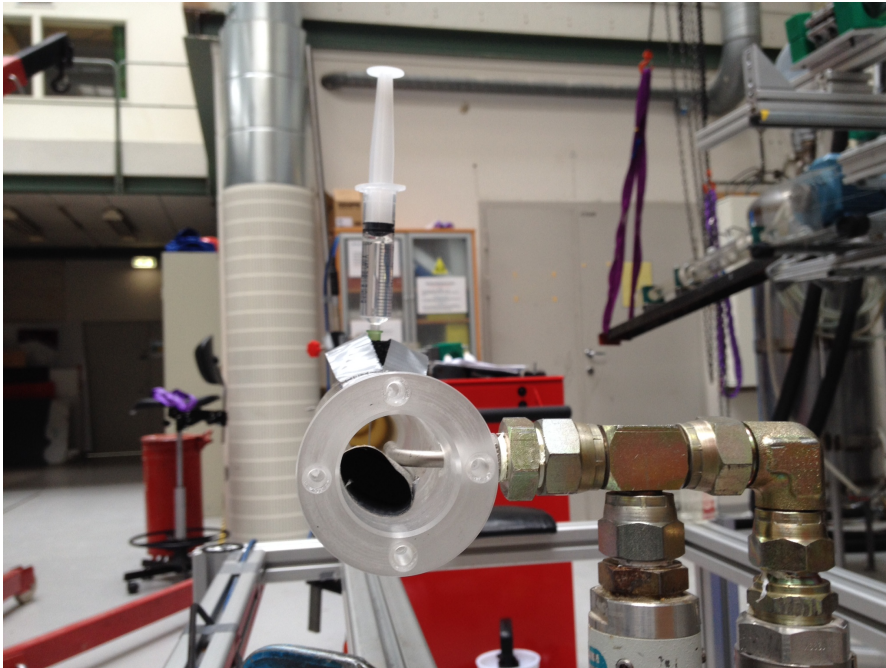


**Figure 5.4** – The mixing unit with the bended pipe and the needle.

For the smooth pipe we had three test variables: air flow velocity, liquid rate and frequency. We tested five different flow velocities together with seven liquid rates and three frequencies. Each set of conditions were given three runs, making it a total of 305 runs.

Since the loud speaker was not used to generate sound for the corrugated pipe, the frequency was no longer a free variable. This removed one test variable, but we increased the number of flow velocities to see if we could identify singing for low flow velocities. In total, we tested eight different flow velocities and seven liquid rates. Since we could not control the frequency ourselves, the amplitudes were measured at slightly varying frequencies and therefore expected to vary more. With this in mind, we increased the number of runs for each set of conditions to four, making it a total of 224 runs.

The whistling was difficult to identify from the frequency plots for the closed corrugated pipe, but a small test with both ends open revealed that the whistling was far more distinct than with one end closed. We therefore investigated the corrugated pipe with both ends open to see how the liquid influenced the amplitude of the whistling in that specific case. Unfortunately, due to the ejector effect, we could not determine the exact flow rate through the pipe. Therefore, the percentage values in table 5.4 indicate the percentage level in terms of capacity at which rotameter 1 (capacity  $6.9 \text{ m}^3/\text{h}$ ) was adjusted to. We tested three different flow rates and four liquid rates. Due to a more consistent measurement frequency compared to the closed corrugated pipe, we reduced the number of runs per test condition to three, making it a total of 36 runs.

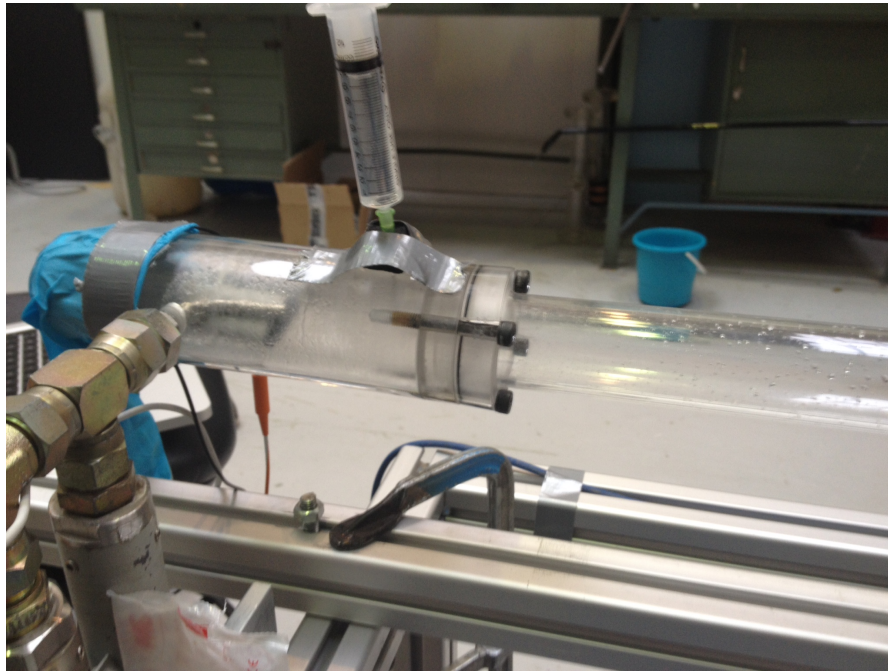


**Figure 5.5** – Different needle sizes were used to inject different liquid rates. The rubber on the left hand side of the mixing unit was pulled over the microphone in order to make the end air tight.

Air Flow Rates [ $\text{m}^3/\text{h}$ ] ([m/s])	Liquid Rates [ml/min]
4.14 (2.34)	0
5.52 (3.12)	1
6.90 (3.90)	2.5
8.30 (4.70)	5
9.70 (5.49)	10
11.10 (6.28)	20
12.50 (7.07)	40
13.90 (7.87)	

**Table 5.3** – Test matrix for corrugated pipe with upstream end closed.

Air Flow Rates [%]	Liquid Rates [ml/min]
60%	0
80%	1
100%	2.5
	5

**Table 5.4** – Test matrix for corrugated pipe with both ends open. Air flow rates given in percentage of  $6.9 \text{ m}^3/\text{h}$ .

## 5.3 Results

As mentioned in Section 5.2, each test condition were run multiple times to investigate how repeatable the experiment was. The variance and standard deviation for each set of conditions could then be calculated to quantify the variation from the mean. Table 5.5 lists the average variance and standard deviation of SPL in the experiment, split up for each of the different pipe configurations. Note that the values are given in absolute terms, but since the SPL is in the order of 50-60 dB, all the relative variances and standard deviations were less than 2%. This indicates that the experiment was robust and the variation for each test condition was averaged out by running multiple runs.

The absolute values of the amplitude of the sound waves are not considered important. Both the amplifier and the sound card were set up to maximize the sound (except for low frequencies) so that amplitude peaks could be identified more easily. The values of the SPL (or amplitude) are therefore not as they would be perceived in reality, but this was not considered critical as we were interested in how the amplitude was damped (i.e. the differences), not its exact value. The most important point was to maintain an identical setup throughout the whole experiment. In addition the SPL was calculated without a reference value (see Section 2.3), meaning they are not comparable to the sound pressure levels given in table 2.1 directly. The Matlab scripts used to generate sound at specific frequencies and record sound through the microphone are found in Appendix B.2.

Pipe	Variance [dB <sup>2</sup> ]	Standard Deviation [dB]
Smooth 373 Hz	0.1244	0.3527
Smooth 445 Hz	0.1370	0.3701
Smooth 550 Hz	0.7137	0.8448
Closed corrugated	0.7251	0.8515
Open corrugated	0.9225	0.9605

**Table 5.5** – Average variance and standard deviation for the measured SPL [dB] in the experiments.

### 5.3.1 Resonance Frequencies

From the equations in section 2.4.1, we can calculate the theoretical resonance frequencies of the pipes and compare this to experimental values. The test was done with the loud speaker spanning frequencies from 60 Hz to 1 kHz, with steps of 1 Hz per second at the upstream end of the pipe. The sound was recorded with a microphone at the downstream end using Matlab. With a Fourier transform of the recorded sound vector, we were able to identify the resonance frequencies as peaks in the frequency plot. A short introduction to the Fourier transform and Fourier analysis of signals are given in Appendix A.

### 5.3.1.1 Smooth Pipe

The speed of sound needed for the calculation in equation 2.14 was estimated using the formula for speed of sound for an ideal gas

$$c = \sqrt{\frac{\gamma RT}{M}}. \quad (5.1)$$

In equation 5.1,  $c$  [m/s] is the speed of sound,  $\gamma$  [-] is the adiabatic constant (ratio of specific heats),  $R$  [J/mol · K] is the universal gas constant,  $T$  [K] is the absolute temperature and  $M$  [kg/mol] is the molecular mass of air.

Mode	Calculated [Hz]	Experiment [Hz]	Difference
1	73.6	74.2	0.82%
2	220.8	218.5	-1.04%
3	368.0	365.9	-0.57%
4	515.2	516.0	0.16%
5	662.4	666.0	0.54%
6	809.6	816.0	0.79%
7	956.8	963.9	0.74%

**Table 5.6** – Resonance frequencies [Hz] of the smooth pipe.

In table 5.6, we observe that the experiment is very well in agreement with the predicted resonance frequencies for the smooth pipe. Uncertainties in measurements and the correction factor taken in to account, this agreement clearly underlines the fact that resonance frequency is a geometrical property (for a constant speed of sound). It should be noted, as we can see in figure 5.6, that the resonance frequency for the fundamental mode was not observed in the plot, but the maximum amplitude between 60 Hz and 80 Hz was found at 74.2 Hz. The other resonance frequencies are clearly identified as peaks in the plot. Significant low frequency noise can be observed between 0 Hz and approximately 50 Hz. This can safely be neglected from the results as the sound emitted had a starting frequency of 60 Hz.

The average distance (in Hz) between each resonance frequency was 147.2 Hz and 148.3 Hz for the calculated resonance frequencies and the experiment respectively. A difference of 0.74%. The average absolute difference between the calculated values and the experiment was 0.65%.

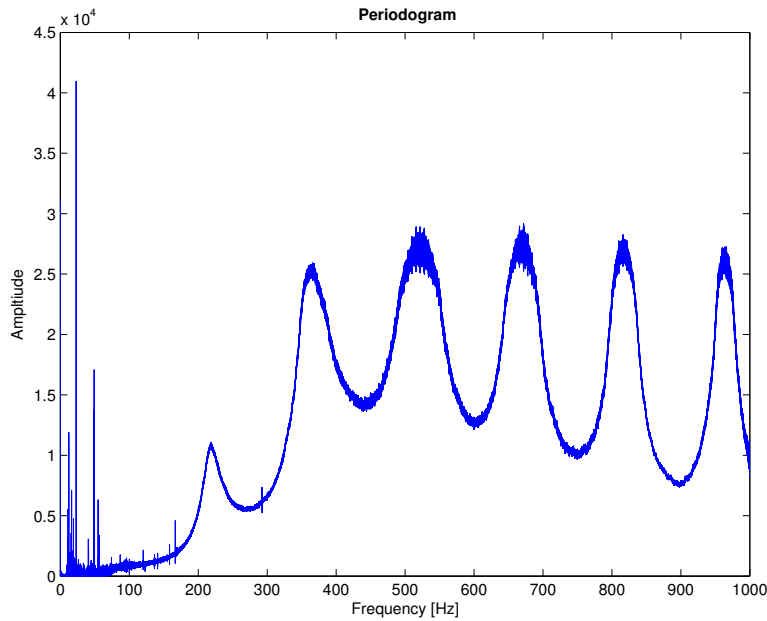


**Figure 5.6** – Amplitude of the Fourier transform as function of frequency for the smooth pipe.

### 5.3.1.2 Corrugated Pipe

As described in Section 2.4.1, Hirschberg proposed to modify the speed of sound to account for the cavities when dealing with sound propagation in a corrugated pipe [15]. The formula used for the effective speed of sound is

$$c_{eff} = c \sqrt{\frac{V_{in}}{V_{tot}}} \quad (2.13 \text{ revisited})$$

where  $c$  [m/s] is the speed of sound of the medium,  $V_{in}$  [m<sup>3</sup>] is the inner volume of the pipe without the corrugations and  $V_{tot}$  [m<sup>3</sup>] is the total volume of the pipe with the corrugations.

The bolt is added to the end of the pipe and is included in the pipe length for the smooth pipe. For the corrugated pipe, both the total pipe volume with and without the bolt were used to calculate the resonance frequencies. The effective speed of sound calculated without the bolt gave best match with the experimental resonance frequencies.

Data for the corrugated pipe is shown in table 5.7. With these properties,  $c_{eff}$  was calculated to 274.8 m/s and 304.8 m/s with and without the bolt, respectively. The Fourier transform of the recorded sound in the corrugated pipe is shown in figure 5.8.

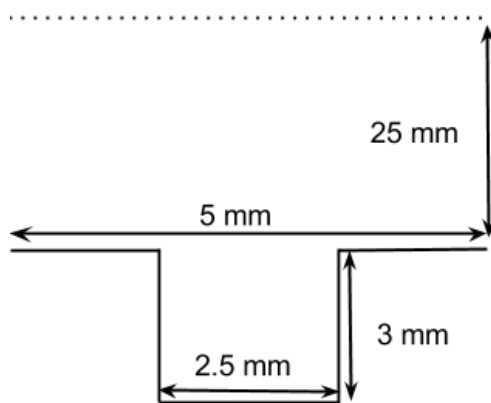


**Figure 5.7** – Sketch of a corrugation in the corrugated pipe.

Property	Value [m]
Total pipe length	1.1430
Corrugated pipe length	1.0000
Bolt length	0.1430
Bolt diameter	0.0035
Pipe diameter	0.0250
Pitch length	0.0050
Cavity width	0.0025
Cavity depth	0.0030
Number of corrugations	199

**Table 5.7** – Geometric properties of the corrugated pipe.

The resonance frequencies are easily identified as amplitude peaks and we can also see similar low-frequency noise as for the smooth pipe.

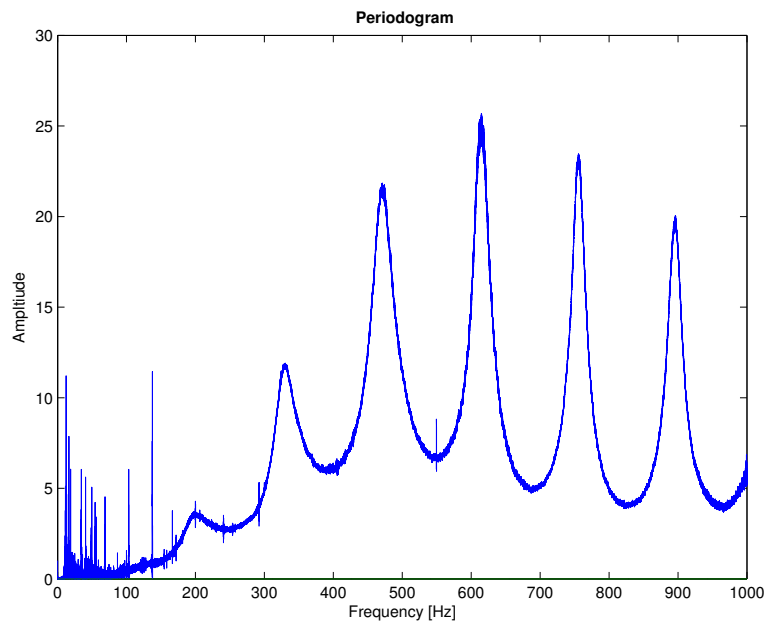


**Figure 5.8** – Amplitude of the Fourier transform as function of frequency for the corrugated pipe.

The difference in amplitudes in figure 5.6 and 5.8 comes from the fact that the Fourier transform of the latter is not divided by the time vector length. This does not influence the identification of the resonance frequencies. See Appendix A for further information

about the Fourier transform.

Mode	Calculated [Hz] (without bolt)	Experiment [Hz]	Difference
1	66.0	-	-
2	198.0	200.0	1.01%
3	330.0	330.1	0.05%
4	462.0	471.1	1.97%
5	594.0	614.9	3.52%
6	726.0	755.7	4.10%
7	858.0	896.2	4.46%
8	990.0	-	-

**Table 5.8** – Resonance frequencies [Hz] of the corrugated pipe. Speed of sound calculated without the bolt.

Mode	Calculated [Hz] (with bolt)	Experiment [Hz]	Difference
1	59.5	-	-
2	178.5	200.0	12.02%
3	297.6	330.1	10.95%
4	416.6	471.1	13.08%
5	535.6	614.9	14.80%
6	654.6	755.7	15.44%
7	773.7	896.2	15.86%
8	892.7	-	-

**Table 5.9** – Resonance frequencies [Hz] of the corrugated pipe. Speed of sound calculated with the bolt.

We can see from table 5.8 that a reasonable match with theory is made. Although the relative difference without the bolt is not that significant (in the area of 3-4%), it is still around 40 Hz for mode 7.

The average distance between the frequency modes was found in the experiment to be 139.2 Hz, while in theory was calculated to be 119.0 Hz and 132.0 Hz with and without the bolt, respectively. The percentage difference between experiment and theory was then 16.97% and 5.45%.

### 5.3.2 Liquid Injection - Smooth Pipe

Liquid was introduced in the gas flow at different liquid rates, ranging from 1 to 40 ml/min. For the smooth pipe, a loud speaker was used to play sound. This allowed us to

decide the frequency of the sound emitted as we wanted. We chose in our experiment to use the following frequencies: 373 Hz, 445 Hz and 550 Hz. This because they each represent a different part of the curve in the Fourier transform (figure 5.6). 373 Hz is a resonance frequency, meaning a local maximum in the Fourier transform. 445 Hz, on the other hand, is a local minimum, while 550 Hz is approximately in the middle between a local maximum and a local minimum. These choices allowed us to investigate if we could find any fundamental differences between a resonance frequency and other frequencies in terms of added acoustic damping. In addition, to see if we could find significant differences in variance between the runs for the three frequencies.

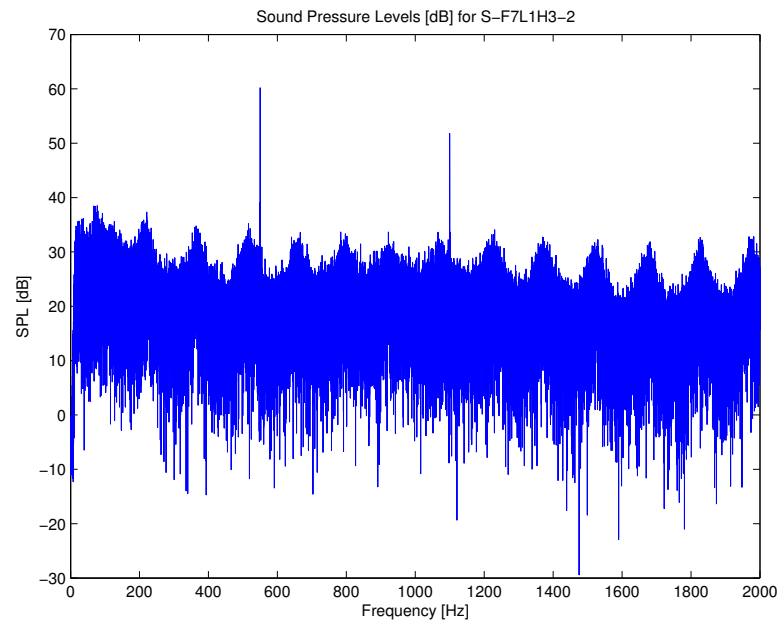


**Figure 5.9** – The frequency spectrum of the Sound Pressure Level [dB] for the smooth pipe. Flow velocity 3.2 m/s, liquid rate 0 ml/min and frequency 550 Hz. This plot is for run 2.

In figure 5.9 the SPL [dB] as a function of frequency is plotted, i.e. the Fourier transform of the recorded sound converted to decibel. The frequency of the emitted sound from the loud speaker is the vertical line at 550 Hz and we can see that it resonates at 1 100 Hz as well. The resonance frequencies of the pipe are seen as local maxima and we can clearly see that 550 Hz is approximately in the middle between a local maximum and local minimum.

**Variance plots** Figures 5.10 to 5.12 show the sound pressure level as a function of liquid rate for 373 Hz, 445 Hz and 550 Hz respectively. The tendency is the same for each frequency; the SPL reduces when the liquid rate increases. Interestingly, the lowest



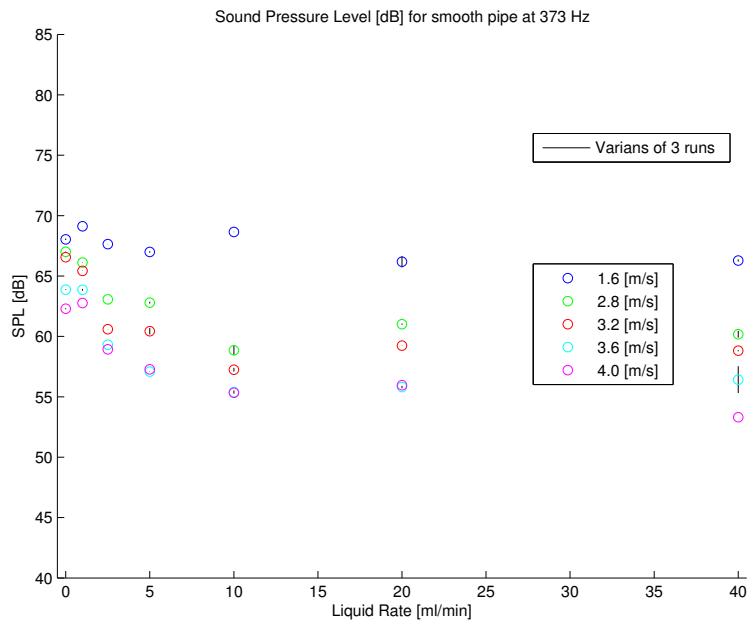


**Figure 5.10** – Sound pressure level [dB] as a function of liquid rate [ml/min] at a frequency of 373 Hz for different flow velocities. The variance over 3 runs is shown.

flow velocity (1.6 m/s) has approximately the same SPL value for all frequencies, but regarding the highest flow velocity (4 m/s) we can observe larger differences between the frequencies. For example, at liquid rate of 10 ml/min the SPL for 373 Hz is approximately 55 dB, while the SPL for 445 Hz is around 50 dB. This underlines the fact that the amplitude is higher at resonance frequencies, even though the loudspeaker emits the same sound level for all frequencies.

From figures 5.10 to 5.12, indications that the SPL decreases the most for the first four liquid rates can be observed. It is also noticeable how the difference between the four highest flow velocities decreases as the frequency increases. For 550 Hz, in figure 5.12 they are almost aligned.

**Normalized plots** Figures 5.13 to 5.15 show the SPL normalized to the non-liquid SPL as a function of liquid rate. This makes the comparison between different flow rates easier, since all of them start at the SPL of 1. We can clearly see that the reduction in SPL is most significant at small liquid rates, from 0 to 5 ml/min. It flattens out for the larger liquid rates, from 10 to 40 ml/min. This trend is observed for all flow velocities at all three frequencies, but not that distinct for the lowest flow velocity.

For all three frequencies the reduction in SPL is considerably smaller for the lowest flow velocity compared to the other four flow velocities. For example, at 373 Hz (figure

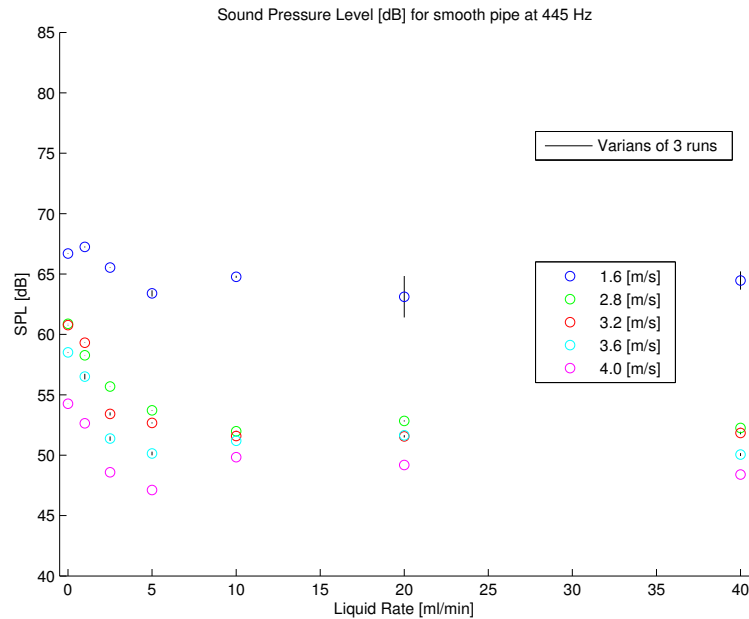


**Figure 5.11** – Sound pressure level [dB] as a function of liquid rate [ml/min] at a frequency of 445 Hz for different flow velocities. The variance over 3 runs is shown.

5.13), the reduction in SPL at flow velocity 1.6 m/s is approximately 2%, while at flow velocity 4 m/s it is approximately 15%. From the plots, it does not seem as the highest flow velocity induces the largest added acoustic damping, or vice versa (except for the lowest flow velocity, which always reduces the least). This contradicts the hypothesis that higher LVF give larger added acoustic damping, since that would mean that the lowest flow rates would have the largest added acoustic damping.

**LVF plots** SPL as a function of LVF are shown in figures 5.16 to 5.18. Naturally, we get higher LVF for lower flow rates, as the LVF is a property that describes the relationship between liquid and gas volume (see Section 4.3), and the volumetric gas flow rate increases with velocity. Again, it is interesting to see that the SPL reduces significantly for very small LVFs. For example, at flow rate 4 m/s and frequency 550 Hz, in figure 5.18, the SPL reduces approximately 7 dB from no-liquid condition to a LVF equal to  $0.25 \cdot 10^{-4}$ , that is from 0 to 25 ppmv. We also observe in the same figure that the damping of the SPL for 550 Hz is coherent for all flow rates, except for the lowest one. That is, the added acoustic damping is merely a function of LVF and independent of flow velocities (not including the lowest). This relationship is not seen for the other frequencies.

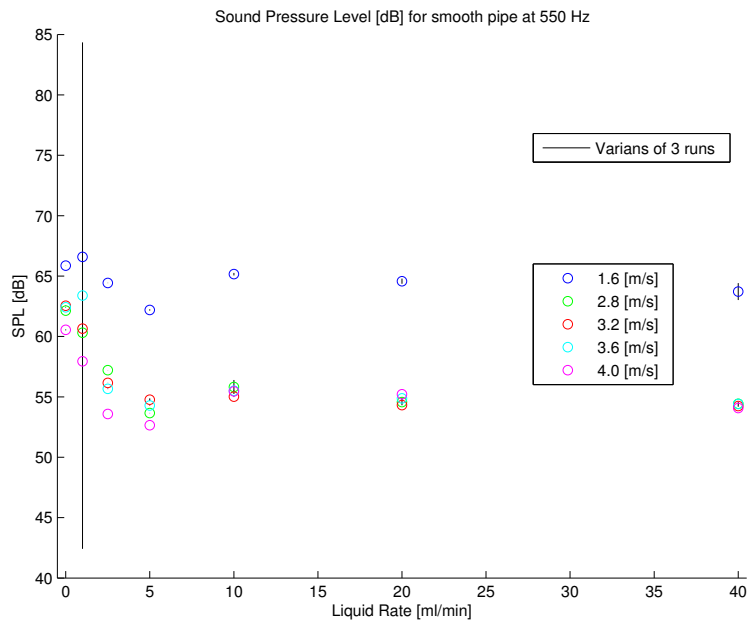


**Figure 5.12** – Sound pressure level [dB] as a function of liquid rate [ml/min] at a frequency of 550 Hz for different flow velocities. The variance over 3 runs is shown.

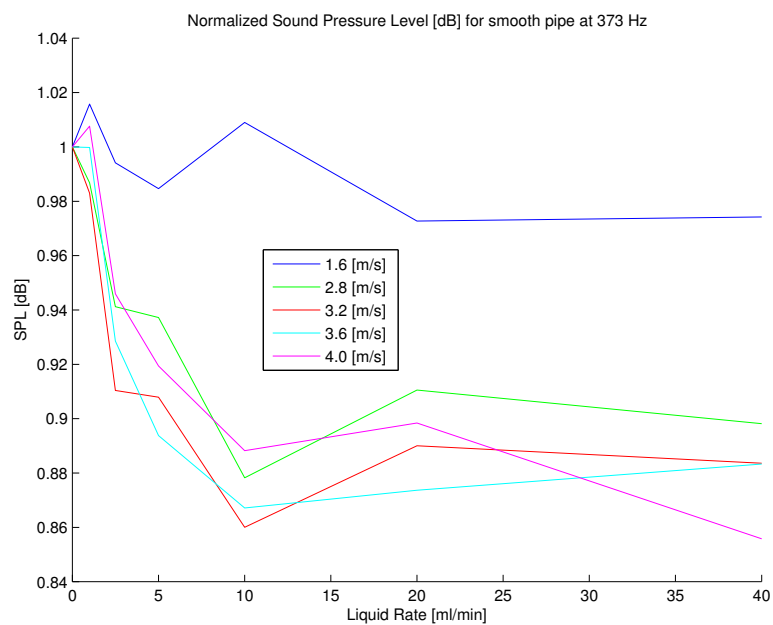


**Figure 5.13** – Normalized sound pressure level [dB] as a function of liquid rate [ml/min] at a frequency of 373 Hz for different flow velocities, illustrated with lines.

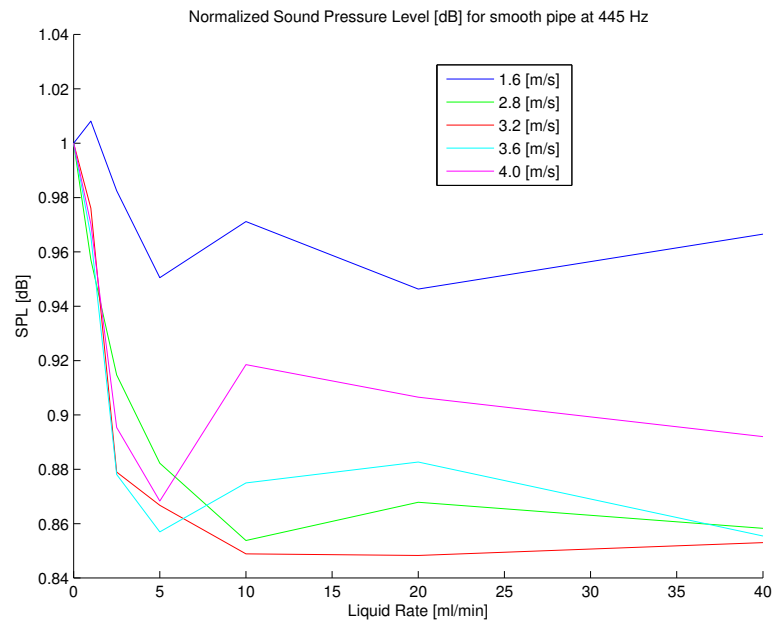


**Figure 5.14** – Normalized sound pressure level [dB] as a function of liquid rate [ml/min] at a frequency of 445 Hz for different flow velocities, illustrated with lines.

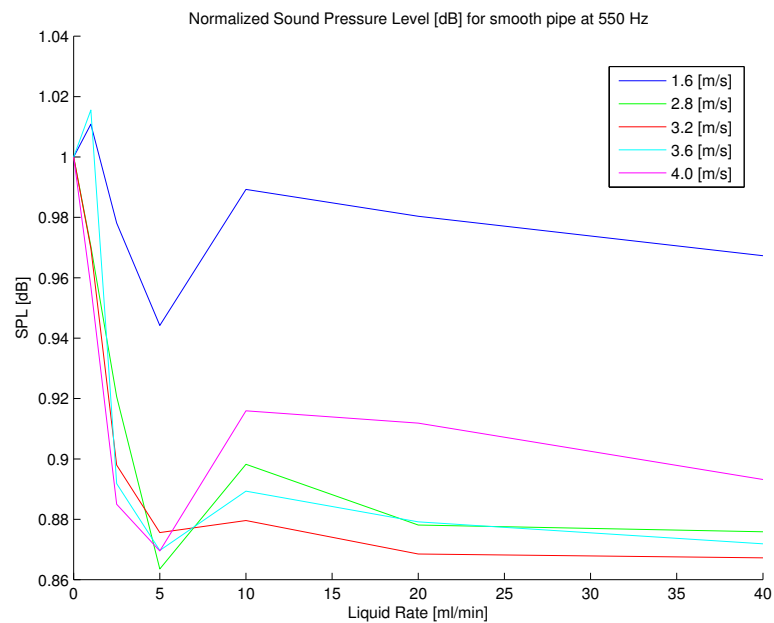


**Figure 5.15** – Normalized sound pressure level [dB] as a function of liquid rate [ml/min] at a frequency of 550 Hz for different flow velocities, illustrated with lines.

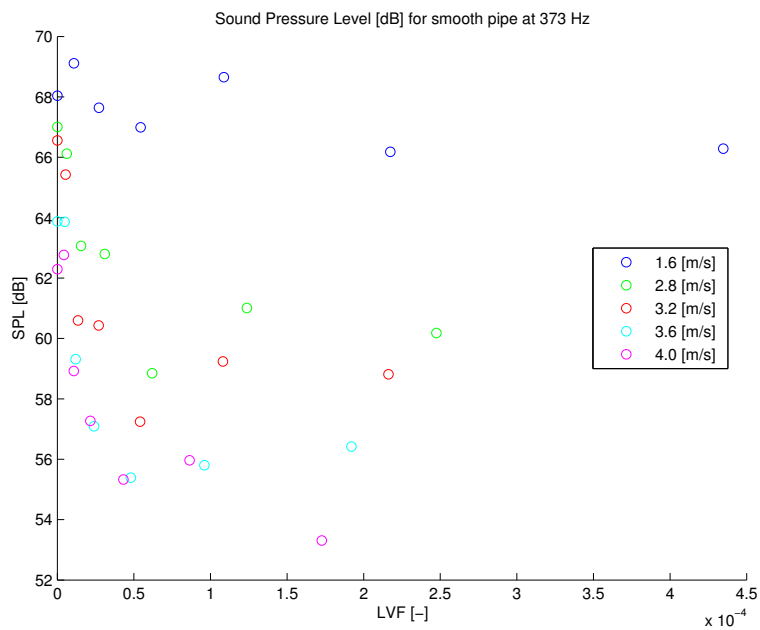


**Figure 5.16** – Sound pressure level [dB] as a function of LVF at a frequency of 373 Hz for different flow velocities.

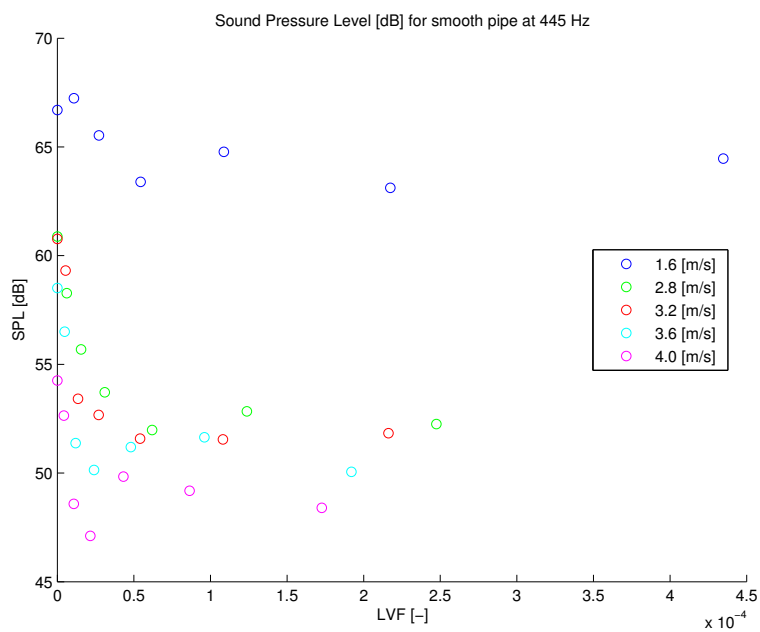


**Figure 5.17** – Sound pressure level [dB] as a function of LVF at a frequency of 445 Hz for different flow velocities.

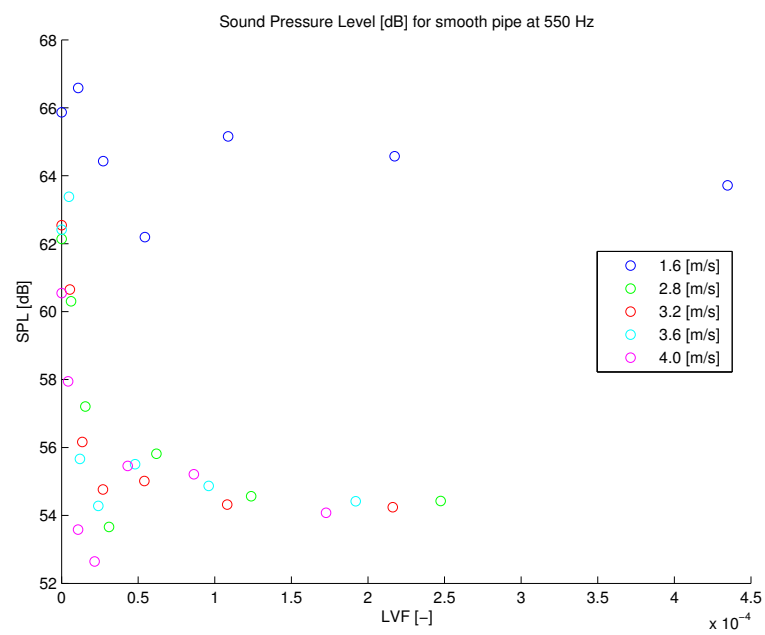


**Figure 5.18** – Sound pressure level [dB] as a function of LVF at a frequency of 550 Hz for different flow velocities.

### 5.3.3 Liquid Injection - Closed Corrugated Pipe

The experiment for the corrugated pipe was carried out in the same manner as for the smooth pipe. However, no sound was played from the loud speaker as sound was expected to be generated from the vortex shedding in the corrugations. The whistling was disguised by the noise generated in the upstream piping, but was still hearable. This is illustrated in the frequency plot in figure 5.19 where it is hard to identify a distinct amplitude maximum.

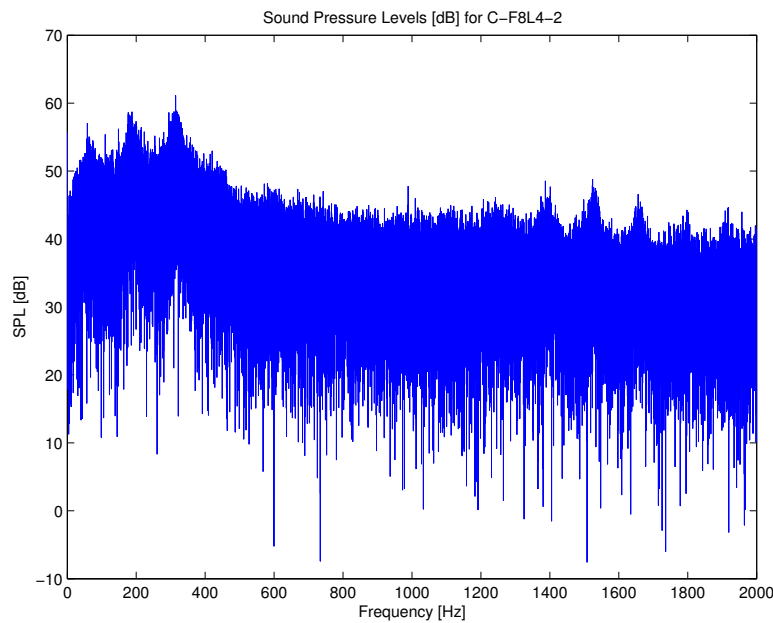


**Figure 5.19** – The frequency spectrum of the Sound Pressure Level [dB] for the closed corrugated pipe. Flow velocity 6.28 m/s and liquid rate 5 ml/min. This plot is for run 2.

Although whistling was heard, it was hard to identify in the frequency plots. This is due to the fact that the noise generated from the upstream piping was amplified at resonance frequencies and made it difficult to distinguish between whistling and amplified noise. In figure 5.19, we can see several resonance frequencies with comparable amplitudes. By measuring the amplitude of the resonance frequency with the highest amplitude, we were still able to measure the influence of liquid, even though it was unsure whether this was the whistling frequency or not. In addition, for a given flow velocity, the highest amplitude did not always occur at the same frequency. In these cases, we measured the amplitude of the frequency used previously for this flow velocity.

**Variance plot** Figure 5.20 shows the variance of the four runs at liquid rate. The average variance for all conditions together was 0.7251 as stated in table 5.5. From

this plot it is hard to identify any clear trend in the added acoustic damping. For the six highest flow velocities it looks as if the SPL is more or less constant, while the two lowest flow velocities have significant decrease in SPL for the lowest liquid rates before the decrease slows down and the SPL is constant. This is the same trend we saw for the highest four flow velocities in the smooth pipe.

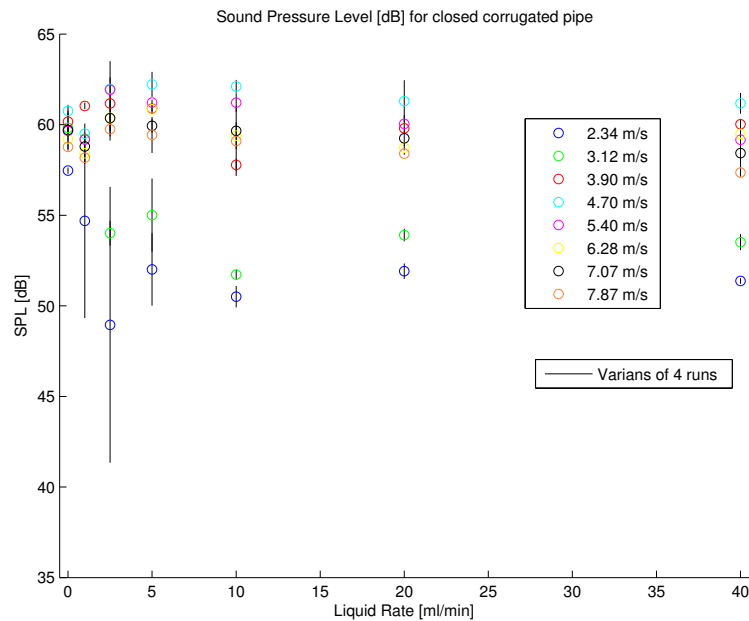


**Figure 5.20** – Average sound pressure level [dB] as a function of liquid rate [ml/min] for different flow velocities for closed corrugated pipe. The variance over 4 runs is also shown as a vertical line.

**Normalized plot** In figure 5.21, where the sound pressure levels are normalized to the SPL for no liquid injection, we can observe a small decrease in SPL with respect to the liquid rate. This was also observed for the smooth pipe, but the decrease is much less for the closed corrugated pipe. As mentioned, we clearly can see that the SPL for the two lowest flow velocities decreases sharply for the lower liquid rates and then levels out for higher liquid rates. This is reversed from the smooth pipe where the highest flow velocities had the same development.

**LVF plot** The trend observed for the smooth pipe with sound frequency 550 Hz was not seen for the corrugated pipe. This can be seen in figure 5.22, where the variation at similar LVFs is larger than the added acoustic damping in total. Hence, no clear trend between SPL and LVF could be observed for the corrugated pipe.



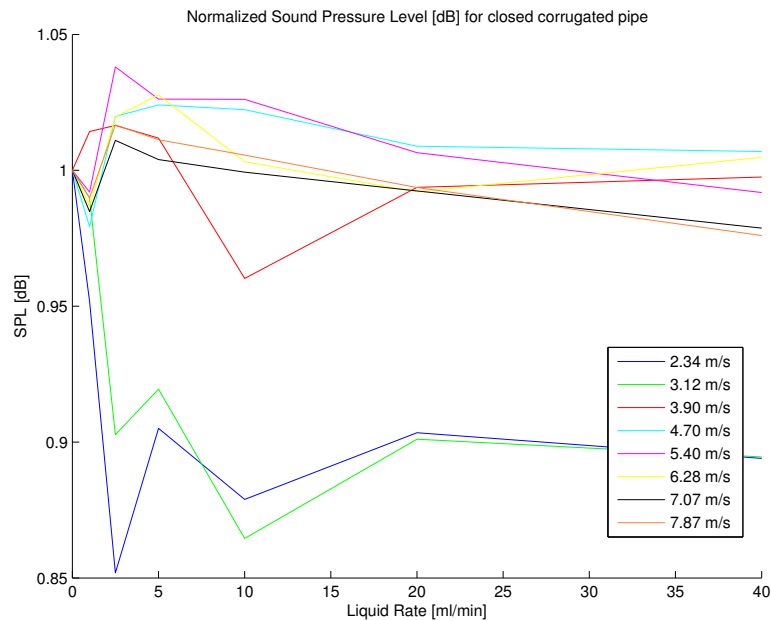


**Figure 5.21** – Normalized sound pressure level [dB] as a function of liquid rate [ml/min] for different flow velocities for closed corrugated pipe.

**Frequency plot** Figure 5.23 shows the frequencies with the highest amplitude, i.e. the frequencies where the amplitude was measured, for all runs on all flow velocities. From this plot we can observe that the results are very well in agreement with the resonance frequencies from Section 5.3.1.2. Contrary to what we expected, the frequency does not jump from mode to the next as the flow velocity increases. In fact, the two highest frequencies were found for the two lowest flow velocities.

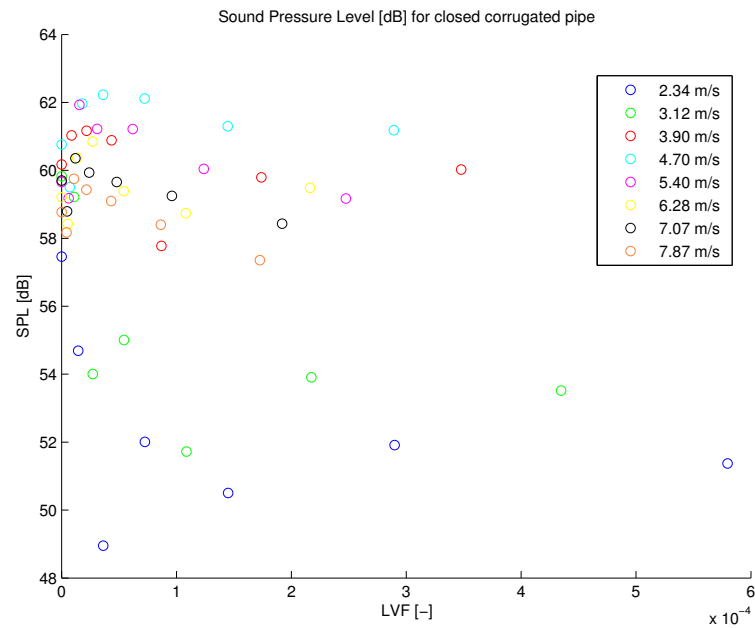


**Figure 5.22** – Average sound pressure level [dB] as a function of LVF [-] for different flow velocities for closed corrugated pipe.

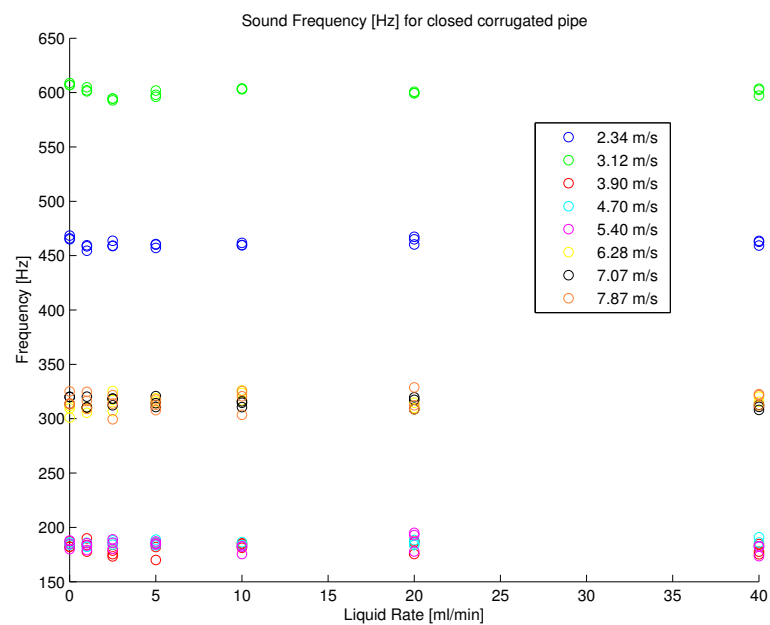


**Figure 5.23** – Frequency [Hz] as a function of liquid rate [ml/min] for different flow velocities for closed corrugated pipe.

### 5.3.4 Liquid Injection - Open Corrugated Pipe

To further investigate how liquid injection influence the whistling amplitude (and possibly frequency), we conducted an additional experiment with an open corrugated pipe. By removing the loud speaker, we got an open corrugated pipe and now whistling could clearly be heard even at low flow rates. Unfortunately, the ejector effect caused additional air to be sucked in to the pipe. This made the air flow rate and consequently the velocity an unknown quantity. Furthermore, the LVF could thus not be calculated.

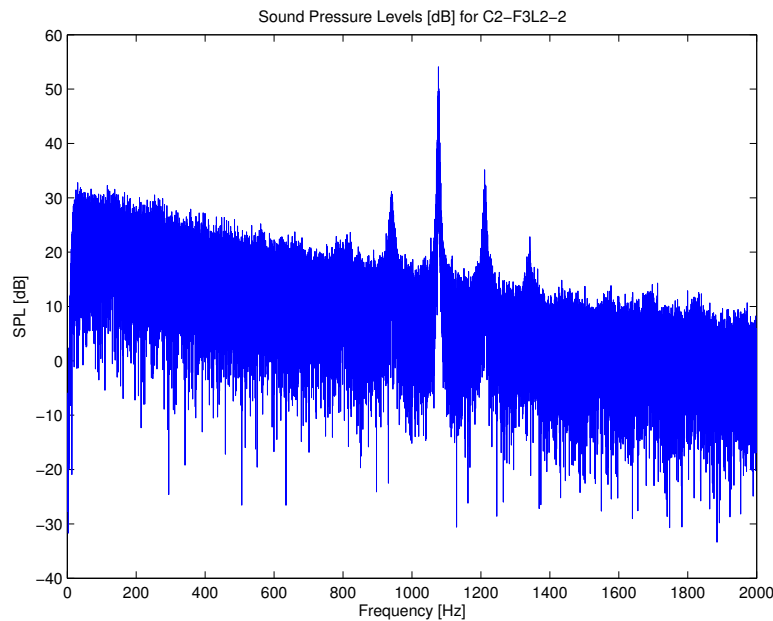


**Figure 5.24** – The frequency spectrum of the Sound Pressure Level [dB] for open corrugated pipe. Flow rate is equal to 60% of maximum for rotameter 1 and the liquid rate is 1 ml/min. The plot is for run 2.

In figure 5.24 the whistling is illustrated by the peak of the SPL at 1076.6 Hz. Notice how the two neighbouring resonance frequencies also can be identified. This indicates that the whistling consists of more than one frequency, contrary to what has been reported in literature [1, 9, 54].

**Variance plot** It can be observed from figure 5.25 that we experienced a larger variance between the runs for this setup. Even though the relative variance is small, it is of the same order of magnitude as the total added acoustic damping (between 0 ml/min and 5 ml/min). However, there were only a few runs that created these relatively large variances and the overall variance was small. From the plot, indications of a similar trend as for the smooth pipe can be seen. The SPLs decrease more for the lowest liquid

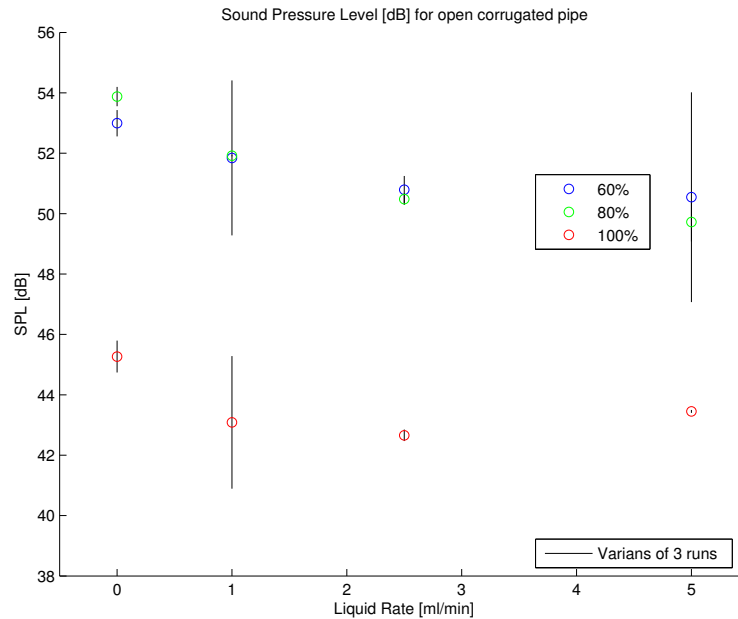


**Figure 5.25** – Average Sound Pressure Level [dB] as a function of liquid rate [ml/min] for different flow rates for open corrugated pipe. The variance over 3 runs is also shown as a vertical line.

rates before the decrease slows down at higher liquid rates.

**Normalized plot** From figure 5.25 we can observe a similar trend for all flow rates. This is seen even clearer in figure 5.26 were the SPLs are normalized, The same trend reported for other pipe configurations can be observed; the SPL decrease sharply for the lowest flow rates before they tend to flatten out. The flattening of the damping is not as clearly observed in this case as the maximum liquid rate is 5 ml/min.

**Frequency plot** In figure 5.27 we notice that the whistling frequency for each flow rate is constant, except for two runs at 2.5 ml/min and 60% flow rate. The reason for this is that 60% flow rate was exactly at the border line between two frequencies and just a small change in the flow rate could change the frequency. This can be seen in figure 5.28, which shows the frequency spectrum of the recorded sound at this flow rate. Here, two different frequencies (934.3 Hz and 1069.0 Hz) have nearly the same amplitude. This means that a small decrease in the flow rate would shift the peak frequency from 1069.0 Hz to 934.3 Hz.

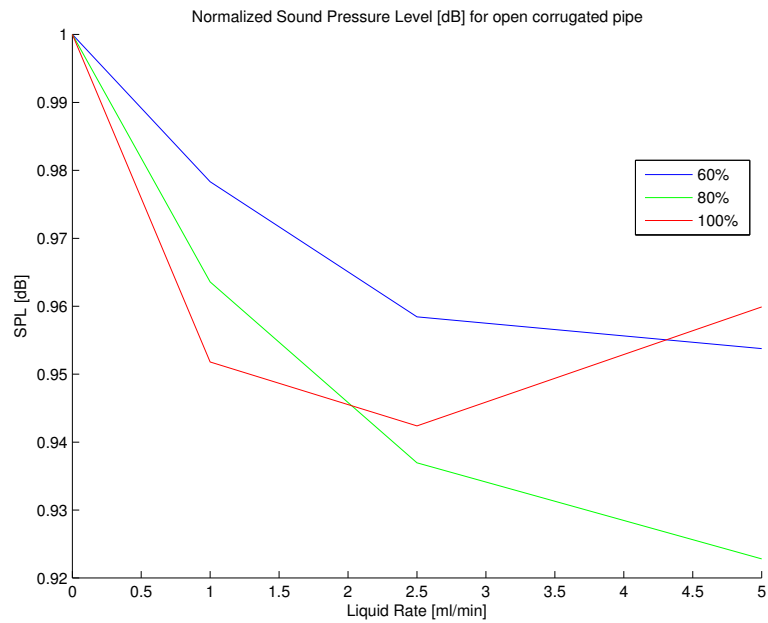


**Figure 5.26** – Normalized Sound Pressure Level [dB] as a function of liquid rate [ml/min] for different flow rates for open corrugated pipe.

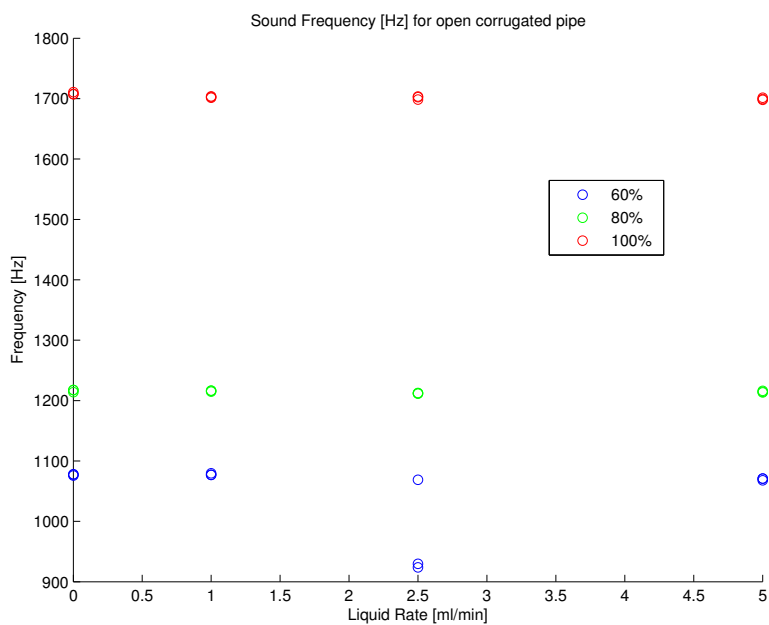


**Figure 5.27** – Frequency [Hz] as a function of liquid rate [ml/min] for different flow rates for open corrugated pipe.

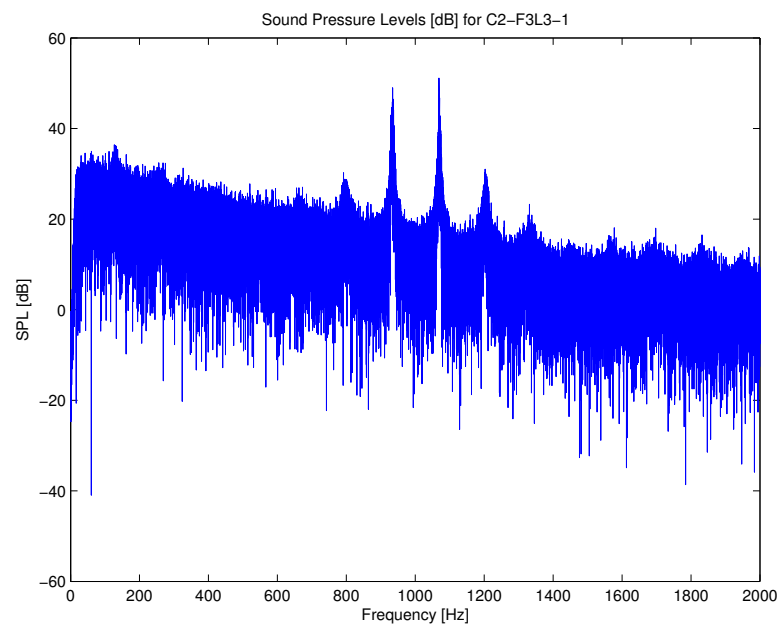


**Figure 5.28** – The frequency spectrum of the Sound Pressure Level [dB] for open corrugated pipe. Flow rate is equal to 60% of maximum for rotameter 1 and the liquid rate is 2.5 ml/min. The plot is for run 1.

### 5.3.4.1 Interval SPL - Open Corrugated Pipe

For both the corrugated pipes, the measured frequency and amplitude are not exactly identical for each run. We have therefore investigated how the average SPL for an interval  $\pm 10$  Hz around the peak frequency is dampened due to liquid. For the three flow rates for the open corrugated pipe, the peak frequencies was approximately 1073 Hz, 1214 Hz and 1702 Hz respectively. However, as mentioned in Section 5.3.4, we did not have a completely consistent frequency mode for the lowest flow rate. I.e. some of the measurements were taken at a different frequency than the rest, see figure 5.27. This did not influence the maximum amplitude significantly, but it had a bigger impact when we calculated the average amplitude around the frequency. Therefore, the lowest flow rate has been omitted from this part of the results.

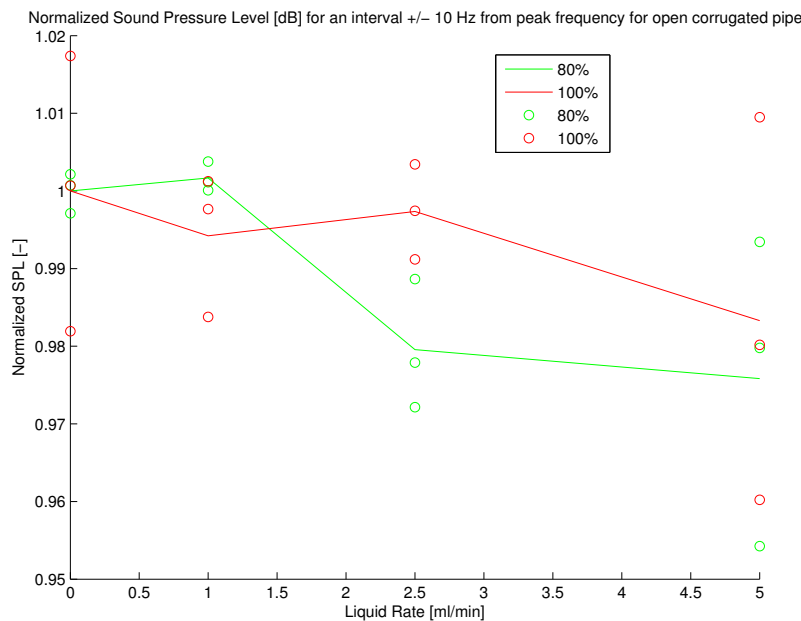


**Figure 5.29** – Normalized Sound Pressure Level [dB] as a function of liquid rate [ml/min] for an interval  $\pm 10$  Hz around the peak frequency. Open corrugated pipe.

The lines in figure 5.29 represent the average SPLs for each LVF while the circles represent each run, both normalized to the average SPL for no liquid. We can see that the damping was much less in percentage for the interval than it was for the single peak frequency. The average SPLs show a close to linear decrease, but we can also observe that the variation between the runs at each test condition is large compared to this average decrease in SPL. This means that it would be difficult to estimate the LVF even if the normalized SPL and the flow rate is known. Also, the variances of these measurement are not less than the variances of the measurements of the single peak frequency. Hence, this approach does not seem to offer any advantages regarding robustness.

### 5.3.5 Comparison With Theoretical Added Acoustic Damping

In Chapter 4 the acoustic damping and the influence of liquid was investigated. The acoustic damping was defined in equation 4.1. If we add the acoustic damping coefficient due to liquid we have two acoustic damping coefficients;  $\alpha_0$  and  $\alpha$ . The first corresponds to the damping without liquid and the latter accounts for the damping due to liquid. Assuming they do not influence each other, the equation for exponential decay of a sound wave then becomes

$$A(z) = A_0 e^{-(\alpha_0 + \alpha)z}. \quad (5.2)$$

Assuming that the damping without liquid is constant for a given flow rate and knowing that the measuring point is at a fixed distance,  $z_0$ , we can rearrange to calculate the additional damping due to liquid in the experiment by the formula:

$$\alpha = \frac{1}{z_0} \ln \left( \frac{A_{ref}}{A} \right). \quad (5.3)$$

In equation 5.3,  $\alpha$  [1/m] is the damping coefficient due to liquid,  $z_0$  [m] is the distance from the loud speaker to the microphone,  $A_{ref} = A_0 e^{-\alpha_0 z_0}$  [dB] is the reference amplitude without liquid and  $A$  [dB] is the measured amplitude of the sound. Note that  $A_{ref}/A$  is the inverse of the normalized SPL.

The experimental value of the additional damping was compared to the theoretical value calculated from equation 4.9. Note that the theoretical value only accounts for the added acoustic damping due to droplets in the flow. The average values of all runs for each liquid rate were used to calculate the experimental added damping ( $A$  in equation 5.3). The theoretical value of  $\alpha$  was calculated using the frequency, flow rate and liquid rate for each set of test conditions. However, since the droplet size was unknown, the theoretical value of  $\alpha$  for three different droplet sizes is plotted. These are plotted as lines in figures 5.33 to 5.39. For the smooth pipe and the closed corrugated pipe the droplet sizes shown are 1  $\mu\text{m}$ , 10  $\mu\text{m}$  and 100  $\mu\text{m}$ . This is changed for the open corrugated pipe to 10  $\mu\text{m}$ , 50  $\mu\text{m}$  and 100  $\mu\text{m}$  to better illustrate the span in the theoretical damping.

#### 5.3.5.1 Added Acoustic Damping - Smooth Pipe

From figure 5.30 to 5.32, we can see that the measured damping exceeds the theoretical damping for a smooth pipe. This illustrates, that even for a smooth pipe where corrugation fill up does not occur (and attenuate the sound source), we have more effects influencing the the added acoustic damping than predicted from equation 4.9 (droplets in mist flow). During the experiments we could observe liquid droplets deposit on the pipe wall. These droplets could influence the sound field in addition to the mist flow.



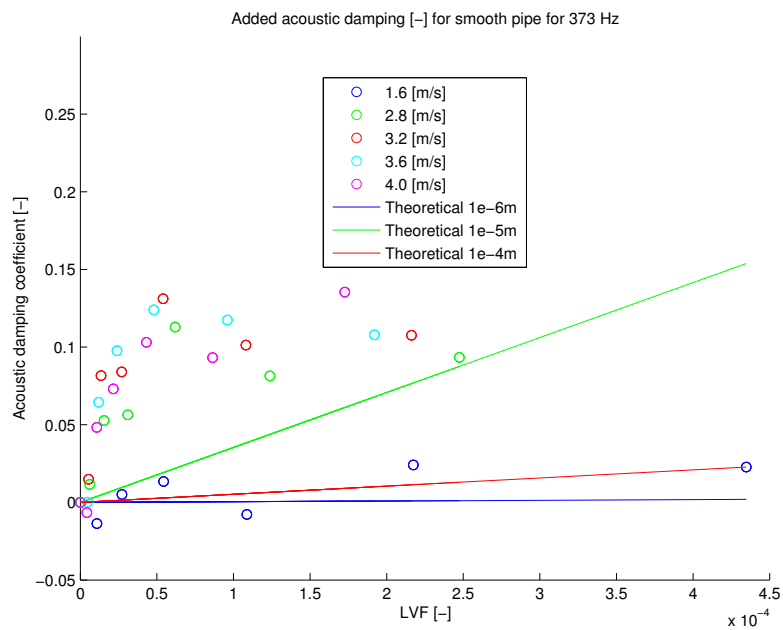


**Figure 5.30** – Added acoustic damping coefficient  $\alpha$  as a function of LVF at a frequency of 373 Hz in a smooth pipe.

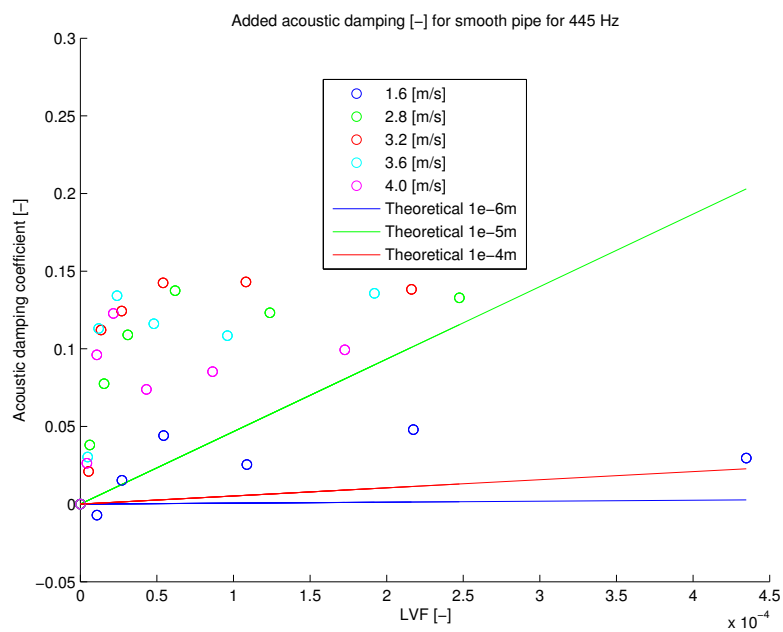


**Figure 5.31** – Added acoustic damping coefficient  $\alpha$  as a function of LVF at a frequency of 445 Hz in a smooth pipe.

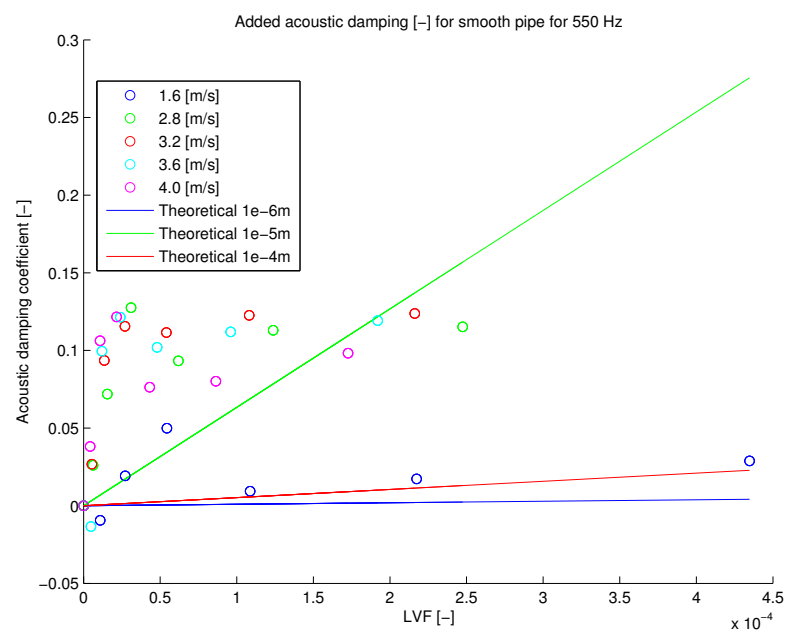


**Figure 5.32** – Added acoustic damping coefficient  $\alpha$  as a function of LVF at a frequency of 550 Hz in a smooth pipe.

**Low LVF Values** To further explore the evolution of the added acoustic damping coefficient, plots for only the lower LVFs are shown in figures 5.33 to 5.35. The plots covers LVF from 0 to  $1 \cdot 10^{-4}$ , that is from 0 to 100 ppmv.

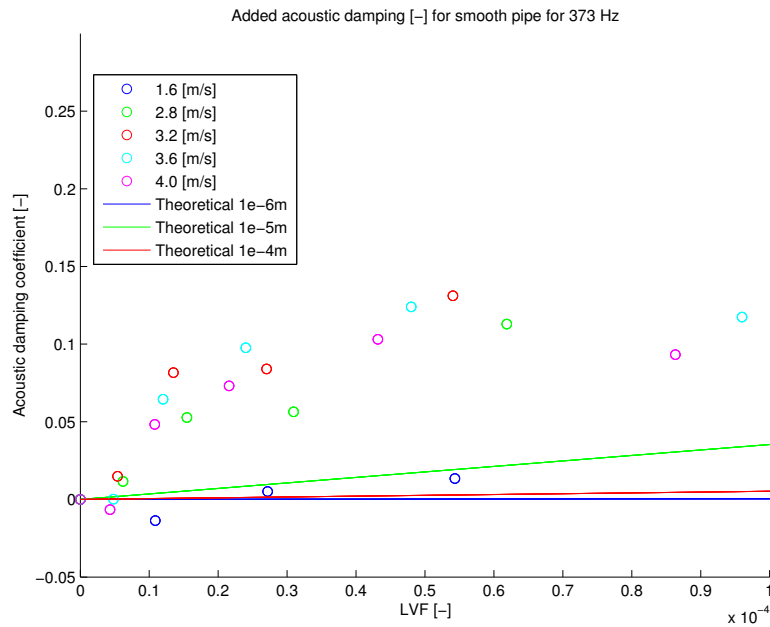


**Figure 5.33** – Added acoustic damping coefficient  $\alpha$  for low LVFs at a frequency of 373 Hz in a smooth pipe.

From these plots the evolution is seen clearer than in figures 5.30 to 5.32. The added acoustic damping coefficient from the experiments is a lot larger than the theoretical value for small LVFs, except for the lowest flow velocity. The lowest flow velocity has a comparable magnitude to the theoretical added acoustic damping and also develops more linearly than the other flow velocities. It is seen again how the added acoustic damping coefficient does not increase linearly with LVF, but that the increase slows down significantly for LVFs larger than  $3 \cdot 10^{-5}$ .

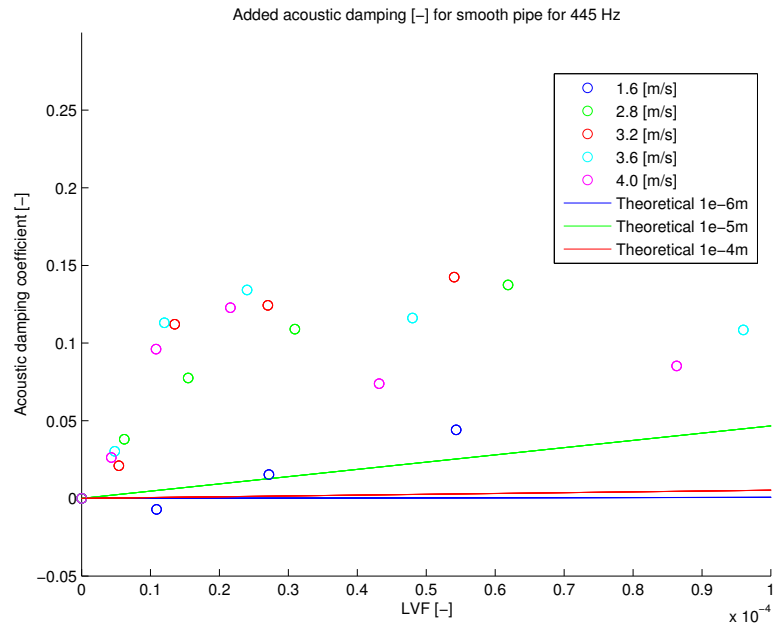


**Figure 5.34** – Added acoustic damping coefficient  $\alpha$  for low LVFs at a frequency of 445 Hz in a smooth pipe.

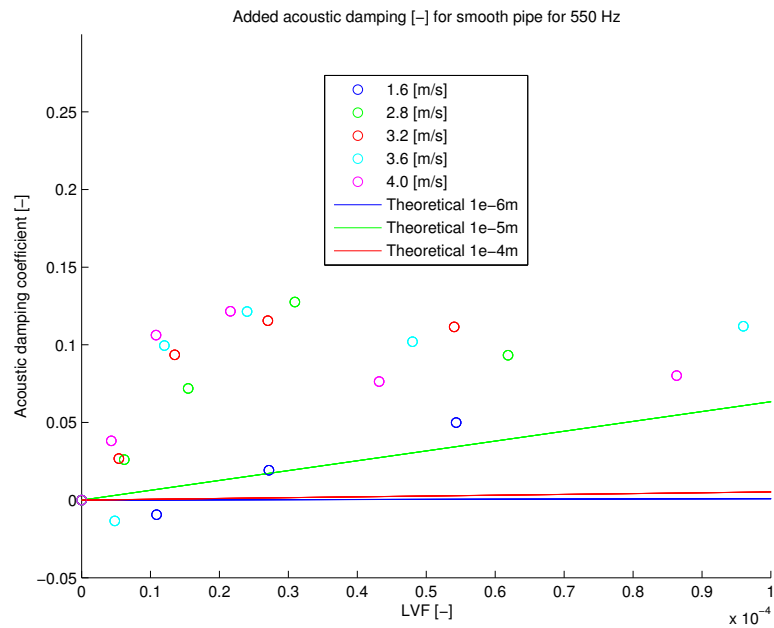


**Figure 5.35** – Added acoustic damping coefficient  $\alpha$  for low LVFs at a frequency of 550 Hz in a smooth pipe.

### 5.3.5.2 Added Acoustic Damping - Closed Corrugated Pipe

The SPLs for the closed corrugated pipe were measured at different frequencies for different flow velocities. Since frequency is an input to calculate the theoretical added acoustic damping, it would hence be different for different flow velocities. The three highest flow velocities had the measurements at approximately the same frequency and are therefore presented in figure 5.36. The frequency for these flow velocities was around 320 Hz and this frequency is therefore used as input to calculate the theoretical damping.

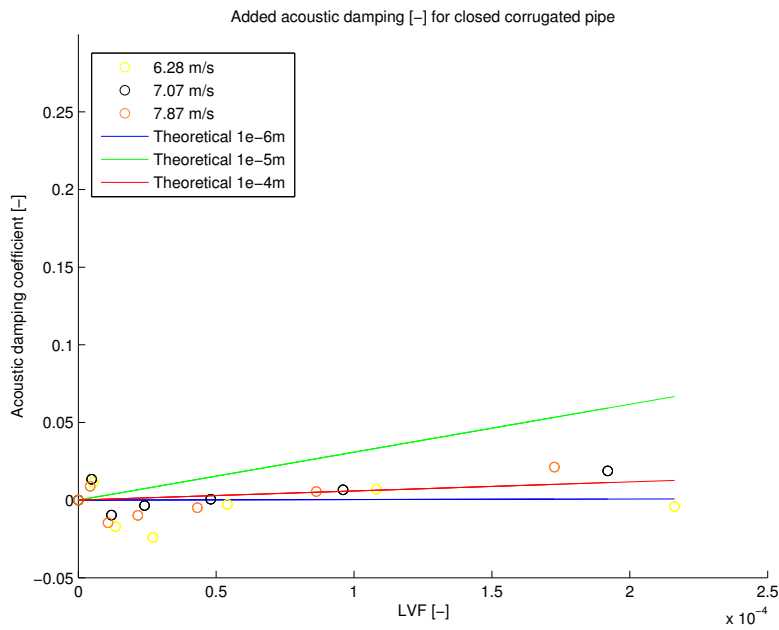


**Figure 5.36** – Added acoustic damping coefficient  $\alpha$  as a function of LVF for closed corrugated pipe. 320 Hz was used as the frequency for the theoretical damping.

Contrary to what we have seen for the smooth pipe, the measured damping is low compared to the theoretical damping. An important observation is that the acoustic damping in fact is negative for some of the first LVF values, something that lacks a reasonable physical explanation. A reason could be that the SPL for no liquid was measured too low and thus shifted the points downwards.

### 5.3.5.3 Added Acoustic Damping - Open Corrugated Pipe

For the open corrugated pipe, the sound frequencies measured were significantly larger than for the closed corrugated and smooth pipe. This meant that the droplet diameter giving the highest damping coefficient changed (ref. Chapter 4). Therefore the three droplet sizes used to calculate the theoretical added damping was changed to  $10\ \mu\text{m}$ ,

50  $\mu\text{m}$  and 100  $\mu\text{m}$  to better illustrate the span of the theoretical value. In addition, as the ratio between liquid and gas mass flow appears in equation 4.9, the gas flow rate has been used as if no ejector effect occurred. The LVFs in the plots are therefore not aligned with reality. The real LVF is smaller than presented in the plot, meaning that the experimental values are shifted to the left.

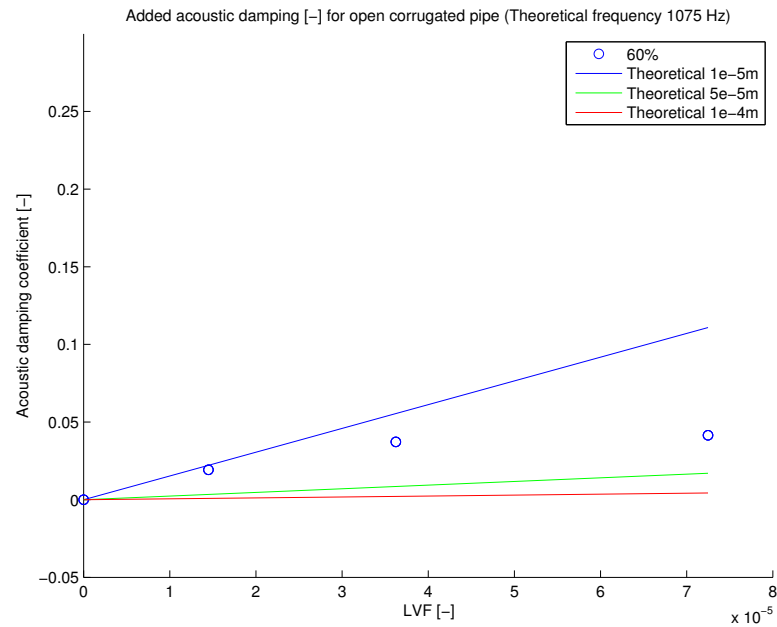


**Figure 5.37** – Added acoustic damping coefficient  $\alpha$  as a function of LVF for open corrugated pipe and 60% flow rate.

In figures 5.37 to 5.39, we observe a reasonable match with theory. That said, one should note that the droplet size is unknown and might even change with the LVF. Thus, the only observation made is that the added acoustic damping is of the same order of magnitude as theory predicts.

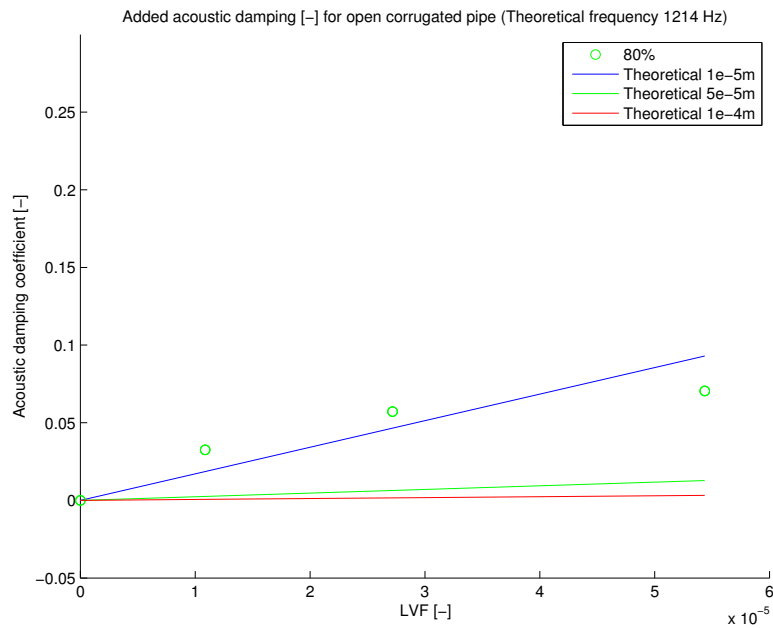


**Figure 5.38** – Added acoustic damping coefficient  $\alpha$  as a function of LVF for open corrugated pipe and 80% flow rate.

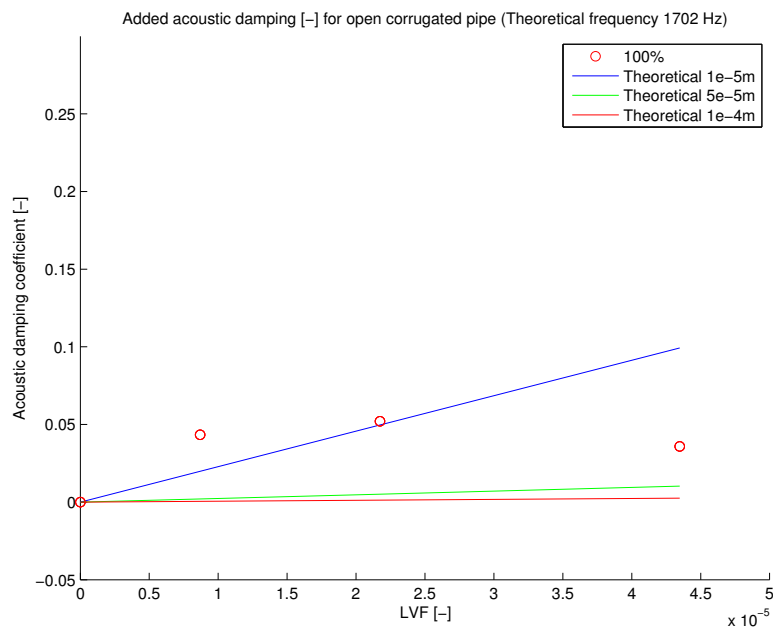


**Figure 5.39** – Added acoustic damping coefficient  $\alpha$  as a function of LVF for open corrugated pipe and 100% flow rate.

### 5.3.6 Evolution Of Resonance Amplitude For Smooth Pipe

To investigate whether the sound amplitude of the smooth pipe increased with time when a resonance frequency is played, we conducted an additional experiment by playing a 373 Hz sound for 8 minutes to see if we could see any signs of the amplitude increasing with time. If the feedback mechanism between the acoustics and the pipe geometry is stronger than the damping of the sound we may experience such an increase of the amplitude. In figure 5.40 the amplitude is plotted as a function of time. Again, the absolute value is not of interest.

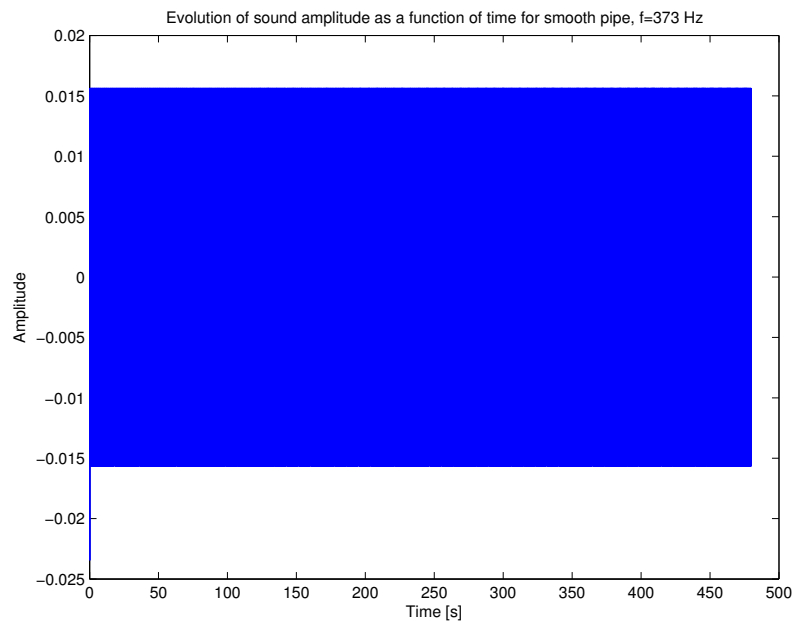


**Figure 5.40** – Amplitude of sound as a function of time for smooth pipe with sound frequency playback at 373 Hz.

From the plot we can not observe any increase in the amplitude, and in fact the amplitude in the end was calculated in Matlab to be identical to the starting amplitude. Even though this test was only conducted for 8 minutes, it suggests that playback of a resonance frequency would not cause the amplitude to increase to infinity. Figure 5.41 shows the Fourier transform where 373 Hz is easily identified. Notice also how other resonance frequencies are affected.



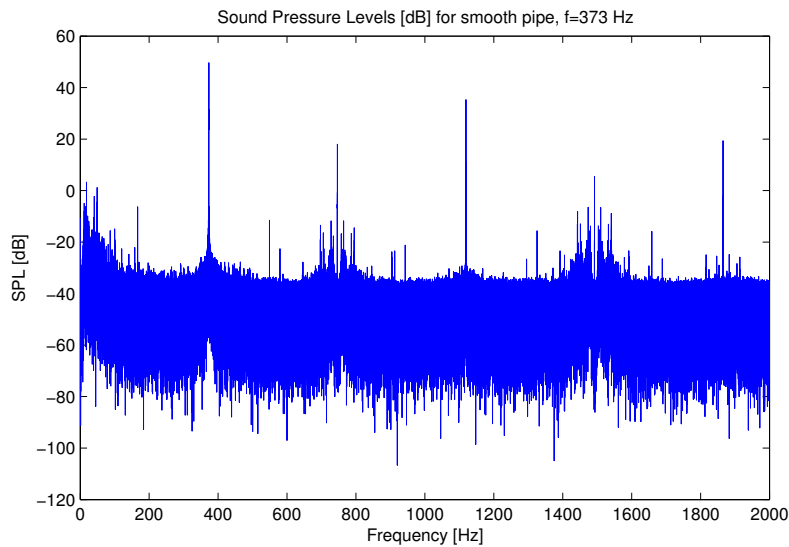


**Figure 5.41** – SPL as a function of frequency for smooth pipe with sound frequency playback at 373 Hz.

## 5.4 Discussion

The experimental results for the smooth pipe revealed no fundamental differences between the three different frequencies, but the highest frequency (550 Hz) had smallest variations in SPL between the four highest flow velocities (figure 5.18). Whether this was due to the frequency being between a local maximum and local minimum in the frequency plot (figure 5.6), or the frequency being the highest, is difficult to state. But being a frequency close to the inflection point of the frequency plot means that small variations in the pipe's natural frequency, for instance if the temperature rises and change the speed of sound, will cause larger variation in the amplitude than for the frequencies close to local maxima and local minima. The reasoning begin that the absolute value of the derivative here is not close to zero as it will be near a local maxima or minima. Hence, it points in the direction that higher frequencies give less variation in amplitude between flow velocities, something that can be investigated further.

The normalized plots for the smooth pipe clearly showed that the added acoustic damping was increasing sharply (and linearly) with the liquid rate for low liquid rates. This trend was broken at higher liquid rates where there were basically no added acoustic damping between the highest liquid rates (the curves flattened out). A possible explanation is that the liquid was not fully entrained as mist flow for the higher liquid rates. During the experiment we observed droplets deposited on the walls, and at the bottom of the pipe in particular. This indicates that the real liquid rate, as in the liquid entrained as droplets in a mist flow, were lower than the liquid rate injected. Liquid droplets on the wall may attenuate sound differently than liquid droplets present in the gas flow.

This could be the reason why the sound amplitude did not decrease (as much) for the higher liquid rates.

The results of the corrugated pipe showed a major difference when compared to the results of the smooth pipe. For the smooth pipe, the reduction of SPL was largest for high flow velocities. For the corrugated pipe, however, the reduction of SPL was largest for low flow velocities (figure 5.21). From Chapter 4, we know that we have more than one sound-attenuating mechanism for a corrugated pipe. The fill-up of liquid in the corrugations decreases the vortex shedding in the corrugations and thus dampen the sound source. In a corrugated pipe, this might be a more powerful sound-attenuating mechanism than mist flow. When running the experiments for the smooth pipe, which was transparent, we clearly saw droplets deposited on the wall. Even though the flow velocities for the corrugated pipe was larger (since the diameter was smaller), this effect was most probably also present in the corrugated pipe as well, meaning the droplets filled up in the corrugations and influenced the sound source of the corrugated pipe. This may have caused the damping to become larger for the lowest flow velocities.

If other means of sound attenuation also have to be taken in to account, i.e. damping from droplets on the wall or in the corrugations, the two phase flow pattern also have to be taken in to account. As mentioned in Chapter 1, a homogenization of the flow should probably happen upstream of the wet gas meter to ensure a uniform LVF over the pipe cross section. This could be insufficient if liquid is deposited on the wall continuously even at the low LVFs we tested in the experiment, resulting in a sort of stratified flow. However, this might not be the case in real world application where the gas and liquid has been mixed for some time, and the only liquid present would be droplets in a mist flow. But it has not been investigated what will happen if we experience a sudden increase in LVF and if all the liquid then still will be present as droplets in mist flow.

For the four highest velocities in the closed corrugated pipe, an increase in the sound amplitude was seen for the lowest liquid rates (figure 5.21). A reason could be that the SPL for no liquid was measured too low and hence setting the starting point too low. If the SPLs were normalized to the values for 1 ml/min liquid rate (and neglecting the one for no liquid injection), a similar trend would have been seen for all flow velocities. For the normalized SPLs to be similar for all liquid rates, the SPL for no liquid injection has to be raised approximately 6 dB. This does not seem reasonable since the variance was so small for these runs and since all flow velocities had approximately the same SPL for no liquid injection.

In figure 5.23 the measured frequencies of the peak sound amplitude are shown. We can observe that the two lowest velocities have the two highest frequencies. This is not according to theory where we would expect the whistling to start at the lowest resonance frequency. As the velocity increases, the amplitude of the sound would increase at this frequency mode before jumping up to the next natural frequency of the pipe. Since the peak amplitude has higher frequencies for the two lowest flow velocities, it may indicate that these measurements were of noise rather than whistling.

To improve the experiments done with the closed corrugated pipe, it would be advisable to install a muffler upstream of the test pipe in order to attenuate the noise, as done by Belfroid et al. [54]. This would of course also be beneficial for the smooth pipe, though there was no problem in measuring the exact frequency from the loud speaker here. Furthermore, the injection pipe had a small diameter compared to the test pipes and the expansion at the exit created noise, especially for high flow rates. This could have been avoided by having an injection tube of the same diameter as the test pipe. Also, the distance between the air and liquid injection points might not have been sufficient for the air flow to be uniform over the cross-section. This could have made it more difficult to entrain all the liquid as droplets. The liquid could also have been injected with an angle towards the air flow to enhance the entrainment.

In Section 5.3.6 we saw that the results indicated that even if the sound is played at the resonance frequency, it does not seem to increase towards infinity with time. The damping mechanisms of the sound waves thus appears to be stronger than the feedback of the system. If this is in fact the case, it would be possible to have a smooth pipe wet gas meter continuously emitting the resonance frequency. Or at the very least, it indicates that the loud speaker can emit the resonance frequency for longer periods without imposing significant structural stress.

As mentioned, the whistling was not heard easily when testing with the closed corrugated pipe, but was heard clearly with the open corrugated pipe, even at low flow velocities. The ejector effect caused more air flow than measured by the rotameter, However, the reason for the closed corrugated pipe not having the same distinct whistling as the open one, was most probably not due to a flow velocity that was not large enough. For the closed corrugated pipe, the maximum flow rate was  $13.9 \text{ m}^3/\text{h}$ , while the lowest flow rate of the open corrugated pipe was 60% of  $6.9 \text{ m}^3/\text{h}$ , plus the contribution from the ejector effect. This contribution was qualitatively measured to be very small, almost negligible, for the lowest flow rate, but increased significantly with the flow rate. Thus, there probably exist another explanation to why the closed corrugated pipe did not have the same distinct whistling. Some further qualitative test indicated that it was important for the air flow to "hit" the corrugations more directly. For instance, if we arranged the closed corrugated pipe in a vertical loop the whistling was more apparent. This was also the case if we put another corrugated pipe at the outlet with a small gap, then the air flow surely "hit" the first corrugations. This serves as a possible explanation to why the whistling was louder for the open corrugated pipe. The air sucked in due to the ejector effect covered the entire cross section of the acrylic cylinder, meaning the air flow was close to the wall at the inlet. Another improvement of the experiment could thus be to increase the distance from the air injection point to the inlet of the test pipe, but this may not have been an issue if the injection pipe had the same diameter as the test pipe.

At the Department of Acoustics at NTNU some dry gas experiments on corrugated pipes have been conducted. Ulf Kristiansen used a vacuum cleaner instead of pressurized air to get air flow in the pipe. This has advantages when it comes to noise generation

and the air flow could be controlled with a flow meter or even an inline rotameter at the outlet. With this setup there would be no doubt that the air flow would be over the entire cross section of the pipe and hence it would interact with the corrugations. Kristiansen also mentioned that from his experiments, he had experienced that only the first few corrugations at the inlet were important to generate whistling. Hence, a possible design of the wet gas meter could be to only have a few corrugations at the inlet of the pipe to generate sound and then measure the attenuation over a smooth pipe. This design could however be more prone to the other sound-attenuating mechanisms in a corrugated pipe, in particular corrugation fill-up. And if the sound source is destroyed, i.e. the corrugations are completely filled up, the wet gas meter would not work. This could of course be a case for the corrugated pipe as well, and further research on how the corrugations fill up over time should be conducted.

## 5.5 Uncertainties

Some of the uncertainties associated with the experiment have already been mentioned in the previous sections. In the preceding section the main sources of uncertainties in the experiment are discussed.

**Not all liquid entrained in gas flow** For low flow velocities as well as for high liquid rates we had some indications that not all the liquid was entrained in the gas flow. In the transparent smooth pipe this was evident with liquid droplets deposited on the wall. We have reason to believe that this also was the case for the corrugated pipes even though the flow velocities were larger. This could be due to the liquid exiting the needles at a certain velocity, making it pass through the gas flow and down to the bottom of the pipe. At the bottom of the pipe, the air velocity was smaller since the injection pipe was approximately in the centre of the pipe. The short distance between the air and the liquid injection point was not sufficient for the air flow to spread out over the entire cross section. Of course, due to the no slip boundary condition usually imposed on fluid flow, the velocity at the walls would be zero anyway.

In the original setup the liquid injection was upstream of the air injection pipe, but this was difficult to achieve with the final setup. If this had been the case, we might have had better mixing of the air and water and possibly less liquid droplet deposited on the wall.

**Not identical frequencies in the measurements** For the corrugated pipe, the frequency with the largest SPL was measured for each run. This frequency was not identical between each runs and it may have influenced the results. However, it seems reasonable to measure the frequency at which the whistling occurs instead of always measuring the same frequency. But the frequency response of the pipe could be different

even between these almost equal whistling frequencies. Hence, a whistling frequency closer to the resonance frequency of the pipe would have a larger amplitude than one further away. This is also true for the smooth pipe, even though we can control the frequency ourselves, the natural frequencies of the pipe might change in time (due to for instance temperature changes) and hence produce different results.

**Fourier transform** The accuracy of the FFT algorithm in Matlab also influence the measurements and it is questionable how well can it differentiate between frequencies that are only a fraction of a Hertz apart. If it is unable to distinguish between such small frequency step it would mean that it is more or less random which frequency the contribution is counted towards. However, the large sample rate (44 100 Hz) of the signal from the microphone may have reduced this potential problem significantly.

**Low-frequency noise** The expansion of the air at the outlet of the injection tube and also background noise from the surroundings may have influenced the measurements. For the closed corrugated pipe, where the whistling frequency was difficult to identify it may have caused measurements of the noise rather than the whistling. The same problem did not occur for the smooth pipe or the open corrugated pipe where it was easy to distinguish the noise from the sound (the whistling in the case of an open corrugated pipe). It could be that measuring the noise works as well as measuring the whistling. The experiment was inconclusive to whether it affected the damping. For instance, take the two lowest flow velocities for the closed corrugated pipe: the evolution of the SPL as a function of liquid rate was similar to those of a smooth pipe, even though we suspect this to be a measurement of the noise rather than the whistling (or a combination of the two).



## Chapter 6

# Simulation Of Flow-Acoustics Model Using COMSOL

In Chapter 3, Popescu and Johansen’s one-dimensional flow-acoustics model for sound generation in a corrugated pipe was derived. This model was simulated using COMSOL Multiphysics. The simulations have been set up to resemble the experiments for the corrugated pipe as much as possible. For instance, the geometries of the corrugated pipe and the flow velocities from the experiments were used. The boundary conditions in COMSOL were set to model an open pipe, that is a corrugated pipe open in both ends.

A probe was placed halfway through the pipe (at 0.5 m) to store the acoustic pressure and acoustic velocity over time. For a detailed explanation regarding the equations, boundary conditions and parameters used, see Appendix E.

### 6.1 The Strouhal Number

The Strouhal number was obtained from Popescu and Johansen’s paper [9]. They performed a CFD simulation of a flow around a single cavity with similar geometry to the one used in our experiment (see table 6.1). The Strouhal number remained constant over a range of velocities. This is in accordance with experimental studies [57]. From the definition of the Strouhal number given in Section 3.3 we have

$$St = \frac{fL}{U}. \quad (3.20 \text{ revisited})$$

where  $f$  [Hz] is the frequency of the vortex shedding,  $L$  [m] the characteristic length and  $U$  [m/s] the velocity of the fluid, we see that the frequency increases linearly with the velocity for a constant Strouhal number (and characteristic length). The characteristic

length in our case is the corrugation pitch length. Popescu and Johansen found the Strouhal number to be approximately 0.6, which is the number used in the simulation.

Geometry description	Modelled [mm]	Popescu and Johansen [mm]
Pipe internal diameter	25.00	25.40
Corrugation pitch length	5.00	5.30
Corrugation depth	3.00	3.11
Corrugation length	2.50	3.12

**Table 6.1** – Modelled corrugated pipe geometry compared to Popescu and Johansen’s geometry.

## 6.2 Simulation Results

The complete set of results for all flow velocities can be found in Appendix E. In table 6.2, the peak frequency for each flow velocity is presented.

Number	Velocity [m/s]	Peak Frequency [Hz]	Fourier Coefficient [-]
1	2.343	45.0	$1.28 \cdot 10^6$
2	3.124	59.5	$2.79 \cdot 10^6$
3	3.905	74.5	$3.7 \cdot 10^6$
4	4.697	89.5	$3.9 \cdot 10^6$
5	5.489	104.5	$1.506 \cdot 10^7$
6	6.281	752.0	$8.95 \cdot 10^7$
7	7.074	135.5	$4.72 \cdot 10^7$
8	7.866	150.0	$9.73 \cdot 10^7$

**Table 6.2** – Frequency results.

The acoustic pressure values seen in figures 6.1, 6.3 and 6.5 are unrealistically high. For example, a sound pressure variation of 10000 Pa (174 dB) for flow velocity 6.281 m/s (figure 6.3) is comparable to a stun grenade [58]. At flow velocity 7.866 m/s, the acoustic pressure averages at 40000 Pa (186 dB), which is extremely loud. The theoretical limit for undistorted sound at atmospheric pressure is 101325 Pa (194 dB), see Chapter 2. Thus, the values are too high to be realistic and the model fails to correctly predict the amplitude of the whistling. In Popescu and Johansen’s paper, they also report very high SPLs (in the area 150-160 dB) [9]. This further underlines the models’ limited ability to predict correct SPLs.

However, despite the acoustic pressure values being predicted too high, the plots can still be compared to each other. Also, the FFT (Fast Fourier Transform) results are not influenced by the amplitude of the plots, since they can be used merely to illustrate



the frequency of the pressure oscillations and consequently the frequency of the sound. Moving on, we discuss some underlying physical phenomena based on the results.

At the five lowest flow velocities, it seems as though there is no feedback system between the pipe's internal acoustics and the flow-induced acoustics. One clear peak frequency is registered in the FFT, and it is obvious that the value of the frequency increases with the velocity, but the magnitude of the acoustic pressure is still quite low compared to other values, ranging from 50 to 700 Pa. For example, see figure 6.1 and 6.2 for the results of flow velocity 4.697 m/s. The overall trend showing the frequency increasing with the flow velocity was also noted by Popescu and Johansen.

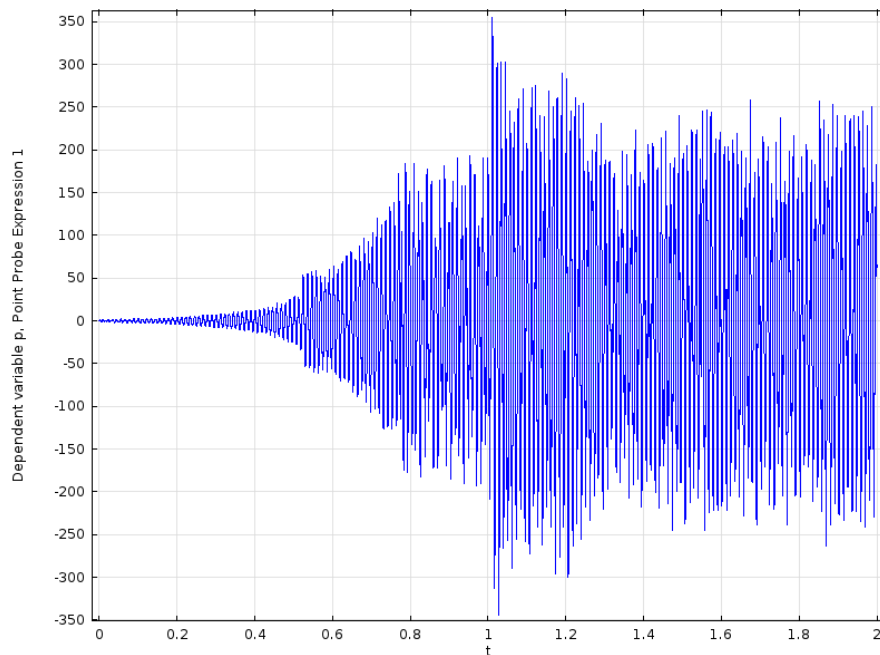


**Figure 6.1** – Time evolution of the acoustic pressure at  $U=4.697$  m/s.

Then, at flow velocity 6.281 m/s, there is a significant change in both the magnitude of the acoustic pressure and the frequency values. The magnitude of the acoustic pressure averages around 10000 Pa and we can observe several frequency peaks (figure 6.3 and 6.4). The phenomenon of several peak frequencies at near resonance conditions was also observed in our experiment. Popescu and Johansen also reported this, stating that the system in these cases goes through a minimum in energy. The system is characterized by more than one dominant frequency before reaching the next frequency mode. Looking at figure 6.3, we see that the acoustic pressure decays over time. This indicates that the whistling cannot be sustained at this velocity and the system is unstable, torn between two states. We have the same picture at flow velocity 7.074 m/s, an unstable system with different peak frequencies. The largest frequency peaks at flow velocity 6.281 m/s and 7.074 m/s are 752 Hz and 135.5 Hz, respectively. However, since the absolute peak

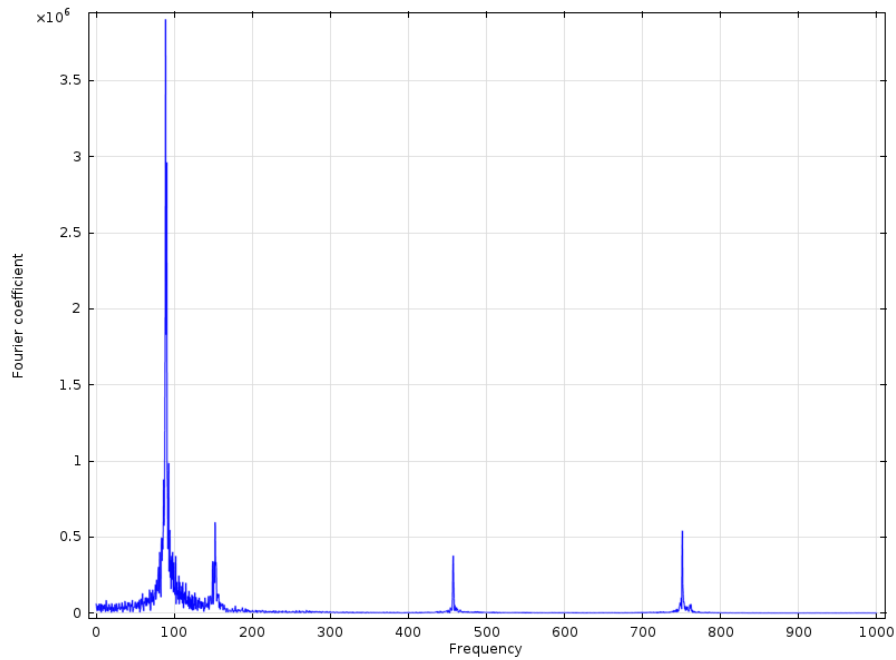


**Figure 6.2** – FFT of the acoustic pressure at  $U=4.697$  m/s.

frequency does not dominate at these flow velocities (figure 6.4), but rather has the same order of magnitude as many others, it does not give added value to the results or the physical explanation.

At flow velocity 7.866 m/s, however, we see that the model has reached whistling conditions and that the feedback system is constant and sustainable (figure 6.5). There is a jump in the acoustic pressure magnitude, now averaging around 40000 Pa. We can therefore say that the model predicts an on-set velocity of whistling somewhere between 7.074 m/s and 7.866 m/s. This was though not supported by the experiment where whistling was heard for far lower flow velocities.

Noteworthy, we have only one dominant frequency which has the value of 150 Hz, see figure 6.6. This closely corresponds to the open corrugated pipe's first natural frequency 2.10, using the effective speed of sound from equation 2.13 (304.8 m/s) and neglecting the end corrections used in equation 2.14:

$$f_{open} = \frac{n \cdot c_{eff}}{2 \cdot L} = 152 \text{ Hz.} \quad (6.1)$$

Thus, we have a lock-in between the pipe's natural frequency and the vortex shedding frequency, creating a resonating feedback system. We ran an additional simulation with a higher flow velocity (8.658 m/s) to check whether the frequency would remain around 150 Hz. This was in fact the case, this time exactly 152 Hz, see figure 6.7.

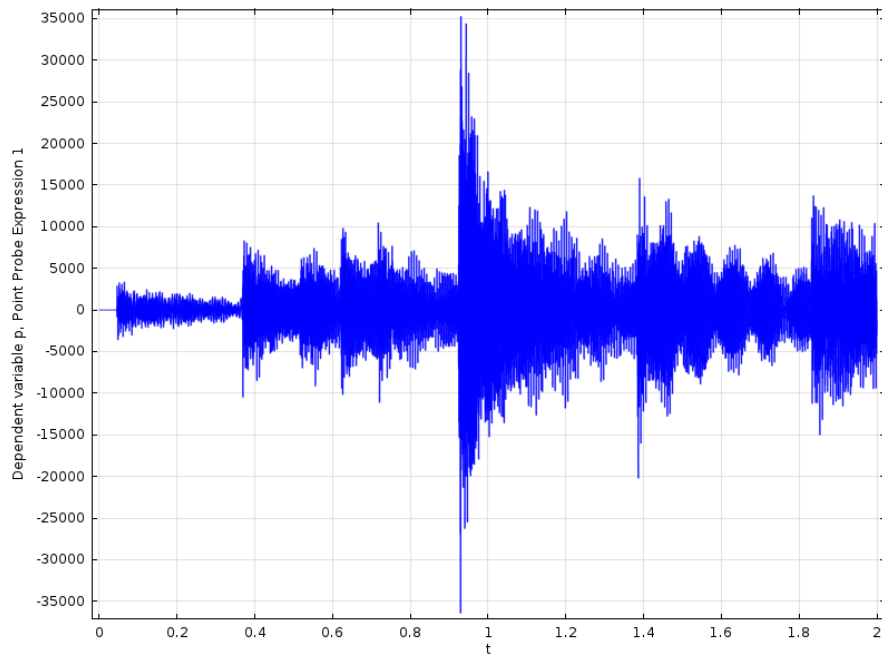


**Figure 6.3** – Time evolution of the acoustic pressure at  $U=6.281$  m/s.

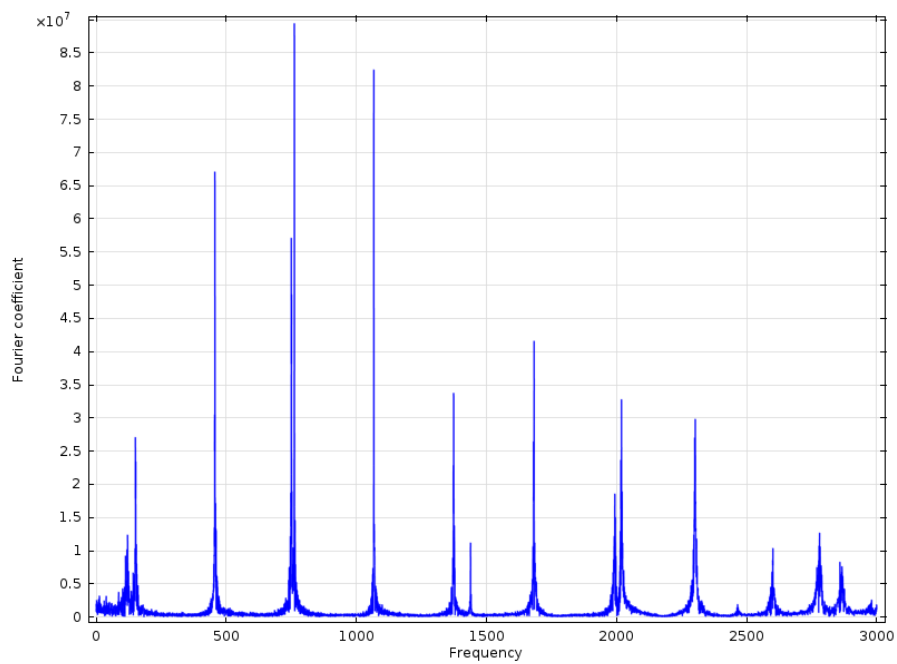


**Figure 6.4** – FFT of the acoustic pressure at  $U=6.281$  m/s.

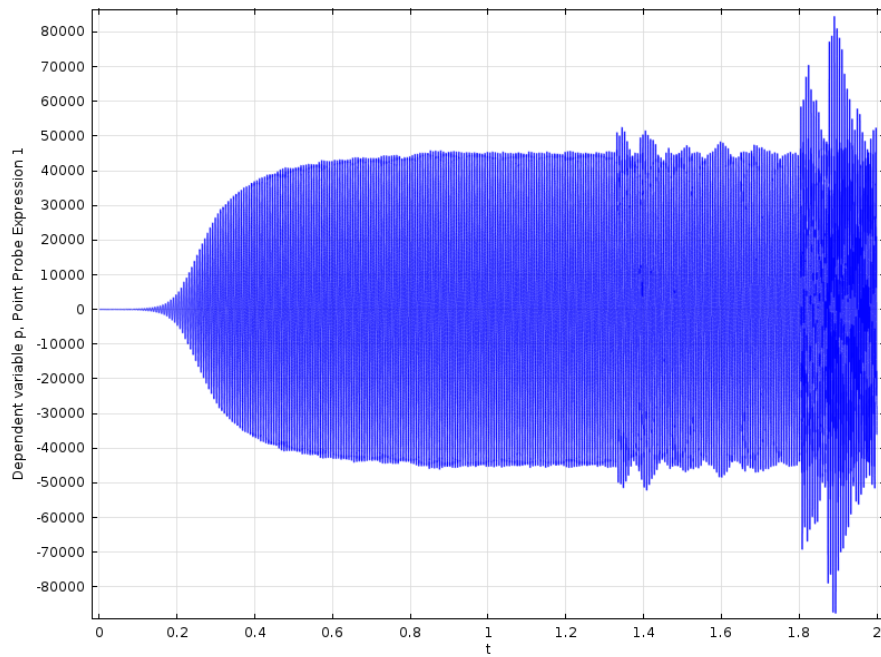


**Figure 6.5** – Time evolution of the acoustic pressure at  $U=7.866$  m/s.

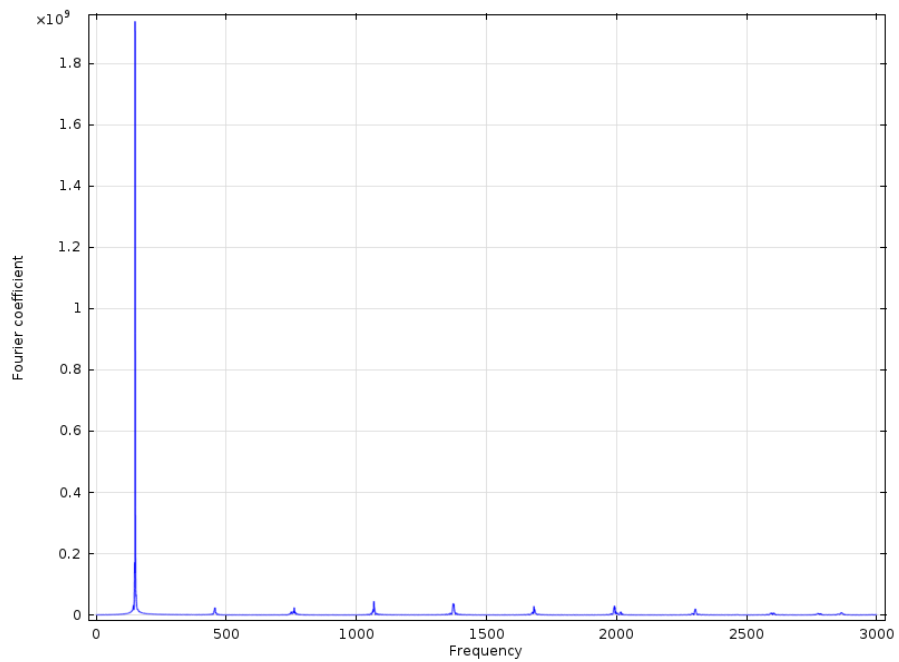


**Figure 6.6** – FFT of the acoustic pressure at  $U=7.866$  m/s.

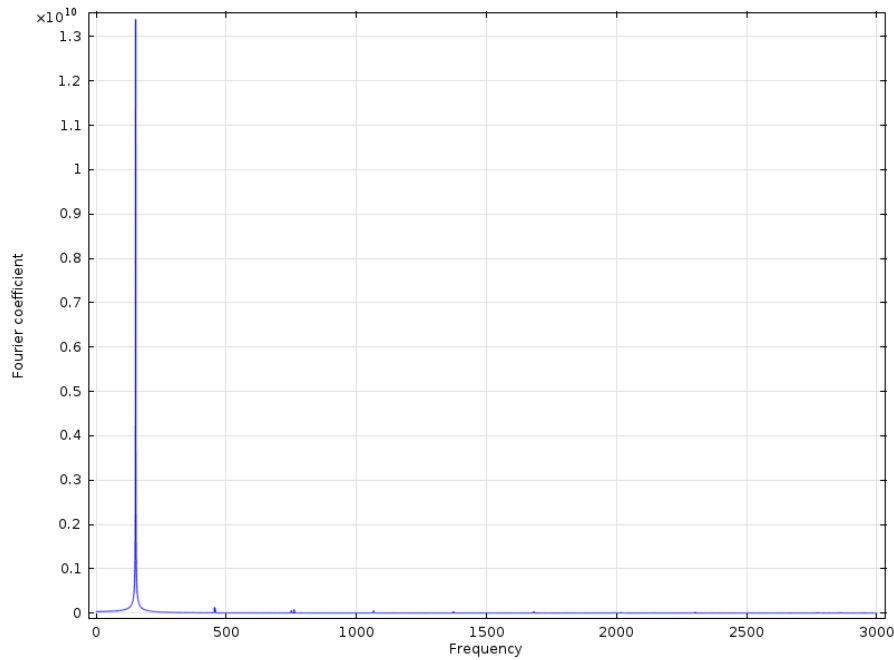


**Figure 6.7** – FFT of the acoustic pressure at  $U=8.658$  m/s.

Figure 6.8 and 6.9 shows the acoustic pressure and acoustic velocity values, respectively, across the pipe at 1 and 2 seconds. Again, the values themselves are not realistic. The shape of the waves, however, are coherent with theory. We clearly have a standing wave, crossing the pipe with half of a wavelength. The acoustic velocity has a  $90^\circ$  shift in phase compared to the acoustic pressure, which also is in accordance with literature, see Chapter 2.

### 6.3 Incorporation Of Added Acoustic Damping

The incorporation of the added acoustic damping  $\alpha$  could be very rewarding if further research is conducted on the wet gas meter. Of course, the current model should first of all return realistic SPL values. But say a rigid model is in place, the ability to simulate acoustic damping would be very beneficial in a future design process.

It would seem intuitive to modify the wave equation to account for added acoustic damping instead of the source equation. This because the added damping from mist flow in theory influences only the sound propagation, not the source (i.e. the corrugation). Some work has been done on this matter; Holm and Näsholm published an article on

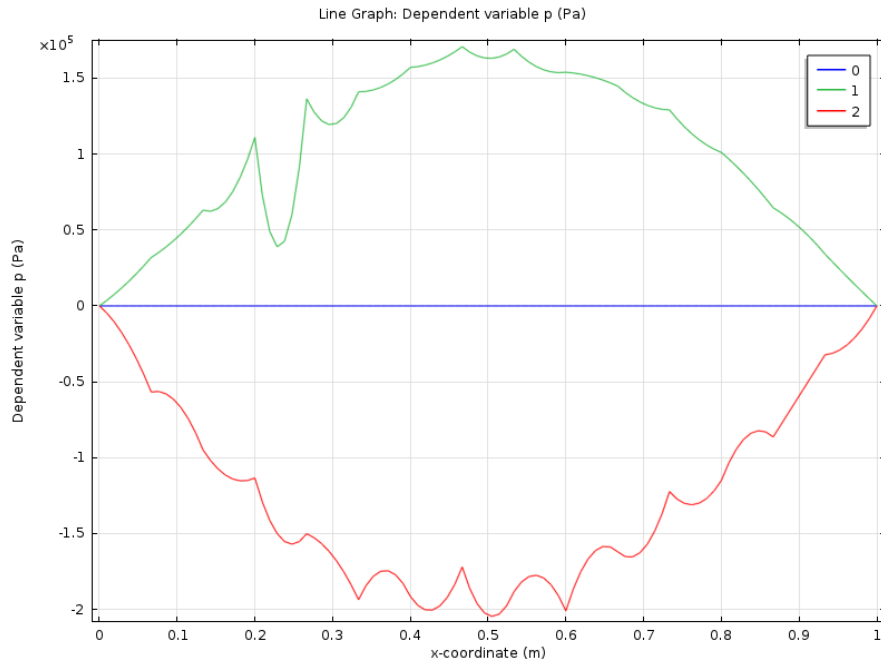


Figure 6.8 – Acoustic pressure wave across the pipe at  $t = 0, 1$  and  $2$  seconds.

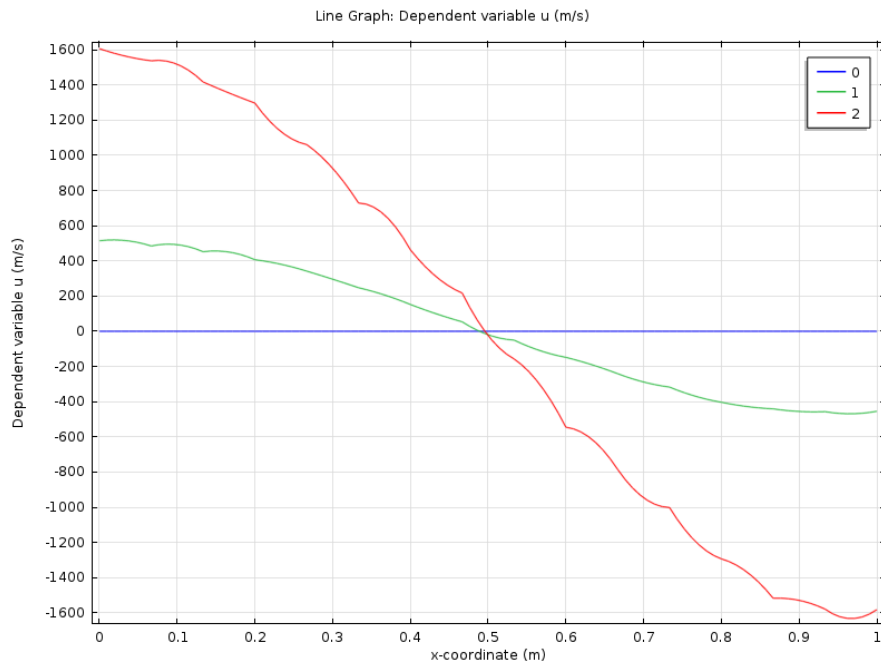


Figure 6.9 – Acoustic velocity wave across the pipe at  $t = 0, 1$  and  $2$  seconds.

wave equation with lossy media [59]. They proposed the equation

$$\nabla^2 u - \frac{1}{c_0^2} \frac{\partial^2 u}{\partial t^2} + \tau_\sigma^\alpha \frac{\partial^\alpha}{\partial t^\alpha} \nabla^2 u - \frac{\tau_\epsilon^\beta}{c_0^2} \frac{\partial^{\beta+2} u}{\partial t^{\beta+2}} = 0. \quad (6.2)$$

In equation 6.2,  $\alpha$  and  $\beta$  can be any fraction, hence this is a wave equation containing fractional derivatives. Fractional derivatives, a branch of fractional calculus, is a newly emerging part of calculus which can be used to describe anomalous diffusion processes [60]. The main principle is that it is possible to perform operations like derivation and integration fractionally and not only discretely at integer values (as in the first, second and third derivative for instance). It appears in the last two terms of equation 6.2 which are the loss terms. They are interpreted in terms of their effect on absorption and sound speed dispersion. The first one contains a second order spatial derivative and a fractional time derivative, whereas the second term contains a higher order fractional time derivative [59]. As for the general wave equation (equation 2.2),  $u$  is the dependent variable and can represent for instance displacement, pressure or density and  $c_0$  [m/s] is the speed of wave propagation. In addition, in equation 6.2  $\tau_\sigma$  [s] and  $\tau_\epsilon$  [s] are the retardation time and relaxation time respectively [59].

The equation is an example of the research going on in this area and gives insight in the future possibilities or mathematical modelling of sound attenuation. Combining this with models of sound generation in corrugated pipe calls for future research and may make it possible to accurately model the sound generation and attenuation in a corrugated pipe in the future.





## Chapter 7

# Discussion

From the theoretical study done in Chapters 2 to 4 strong indications that liquid influence the amplitude of the sound waves were found. Also, from equation 4.9 the relationship between LVF and added acoustic damping due to droplets in a gas flow were assumed to be linear. These hypotheses were tested experimentally. The theoretical study revealed that this area is still in research and the theories presented are widely accepted but the phenomenon is still not fully understood. This was further illustrated by the fact that it currently does not exist mathematical equations capable of precisely describing acoustic damping in a two-phase flow.

In the sensitivity analysis we revealed that the governing equation for added acoustic damping due to droplets in the gas flow is highly dependent on the fluid properties. This means that precise knowledge of the operating conditions as well as the composition of the gas flow have to be known to estimate this value accurately. However, the experiment showed that this equation could not predict the acoustic damping alone. The total added acoustic damping from the liquid injection was found to be significantly larger than what was predicted in theory. That means that even for a smooth pipe, most likely more mechanisms than the droplets in mist flow contributed to the acoustic damping. For a corrugated pipe this has been proposed in literature, but the same result were not expected for the smooth pipe. This may indicate that the gas velocity were too low to fully entrain the droplets in the flow and hence some liquid did not travel through the pipes as mist flow, but were deposited on the wall. This may also explain why the acoustic damping slowed down as the liquid rate increased, i.e. more liquid were not entrained and instead it was deposited at the walls or created a kind of stratified flow. With this in mind, additional experiment can be conducted with higher gas velocities to see if the same pattern emerges there as well.

The result from the experiment then may indicate that not only is the acoustic damping dependent on the fluid properties, but also on the flow pattern. Different mechanisms contribute in different ways to the overall damping. The magnitude of each contribution have not been investigated, thus the difference in acoustic damping from a droplet

suspended in a gas flow and a similar droplet at the wall remains therefore unknown.

The smooth pipe offers an advantage in the form of flexibility to the sound emitted. We are free to choose at which frequency we want to measure the acoustic damping. Although no distinct difference between the frequencies were discovered, we still have the possibility to choose frequencies other than the resonance frequencies. The experiment described in Section 5.3.6 did not indicate that the amplitude at the resonance frequency would increase towards infinity, but this should be investigated further as it may cause structural stress on the pipe. It may, however, be solved by emitted short sound pulses to measure the LVF at discrete times rather than continuously. However, this again will decrease the reliability of the wet gas meter. One goal has to be to quickly discover when the LVF increase beyond certain limits, especially when considering failure of process components and this may not be done as quickly if not a continuous sound can be emitted from the loud speaker.

The same problem actually arise for the corrugated design as well; here the whistling will always be at one of the pipe's natural resonance frequencies. From the experiments done with the open corrugated pipe we did not see any increase in the SPL as the flow rate increase, in fact the highest flow rate had the lowest SPLs. Despite this, we should not forget that the singing riser phenomenon, which this technology strictly speaking is based upon, may induce significant mechanical stress on the pipes. Eventually this means that the whistling of the pipes has to occur in a controlled manner to avoid this. Whether it is sufficient to reduce the gas velocity and consequently the whistling amplitude to a low level or if other means have to be imposed have yet to be answered.

Still, even though we could not conclude this from our experiments, it is reported in literature that the amplitude increases as the flow velocity increases. When the singing moves from one frequency mode to another a decrease in sound amplitude can be seen [9]. This comes from the fact that the power transmitted from the wave is proportional to both the amplitude and frequency squared [61]. Since the singing occurs at one of the pipe's natural frequency modes, as more acoustic power is generated (by higher flow velocity), either the amplitude or the frequency have to increase.

The gas velocity range of the wet gas meter, if an extraction tube is used, can be controlled with the diameter. This may solve challenges considering the amplitude of the singing, at least control the problem. Lower gas velocity induces less acoustic power and less power is transported by acoustic waves. Thus it will take more time before the threshold of fatal mechanical stress is reached, but still the flow in the wet gas meter have to be controlled with a valve to stop the singing from the corrugated pipe. This flexibility is only offered with the extraction tube design. However, the smooth pipe could be installed inline as the imposed mechanical stress can be controlled with the loud speaker.

COMSOL simulations of the acoustic model for a corrugated pipe yielded only partially satisfying results. The down side was that the simulation results did not return realistic values for the acoustic pressure. The model could have been useful for design purposes,

for example in scaling an eventual wet gas meter. One reason for the failure to return realistic amplitude values could be the choice of model parameters, which not always had numerous sources in literature. Another reason could be that COMSOL does not utilize sophisticated enough numerical schemes for these equations. Popescu and Johansen used advanced numerical schemes to solve their model, which were partially developed with this model in mind [9]. It could be that the non-linearity of the model makes COMSOL too general in this particular case.

However, the up side was that the model seemed to simulate the physical phenomena in a correct manner. The frequency increased with the flow velocity before reaching the lock-in frequency of the corrugated pipe. This frequency matched the pipe's natural frequency accurately. Furthermore, the development of a standing wave could readily be seen. The acoustic velocity had a shift of  $90^\circ$  in phase with the acoustic pressure, also coherent with theory.

Despite this, if the simulations of the aero-acoustics in a corrugated pipe is to continue, the model would need a thorough review. If a rigid model is in place, it would very interesting to incorporate acoustic damping in the simulation. The model described in Section 6.3 shows that there is work undergoing on the subject and simulations including acoustic damping might not be that far ahead.

To further pursue this technology an analysis based on the need, the costs and the prospected accuracy offered should be made. From the experiments we got strong indications that the acoustic damping is increased, even for very low LVFs and the main principle is thus demonstrated. Whether the technology can be matured to implementation is still difficult to state, as this is subject to solving the remaining challenges.



## Chapter 8

# Conclusion

The experiment strongly indicated acoustic damping due to liquid, even for very low LVFs. The main principle for the technology (wet gas meter) to work is thus supported. Despite this, the experiment, as well as the sensitivity analysis, also revealed numerous other parameters influencing the acoustic damping. In particular, the properties may change considerably over time, influencing the acoustic damping. If a wet gas meter is to be based on acoustic damping, such issues has to be solved. This calls for precise knowledge of the flow and the ambient conditions.

Furthermore, the experiment could not reveal any significant advantages for either a smooth or corrugated design. While the corrugated pipe has an operational advantage in form of not needing a loud speaker, it may cause the setup to be more vulnerable in measurement accuracy. However, no such clear difference in accuracy was indicated by our experiments. The smooth pipe, on the other hand, offers the possibility to choose the frequency and thus use an exact frequency to measure the damping.

The simulation of the one-dimensional flow-acoustics model was partially satisfying. Some features of the physical phenomena behind sound generation in a corrugated pipe were observed. For example, it predicted the first resonance frequency reasonably well. This can however be predicted from simpler formulas found in literature. The model did also capture the resonance mechanism, thus predicting the lock-in frequency. The main drawback was that it failed to give realistic values for the SPL, meaning that it can not be used to estimate the whistling amplitude. In addition, acoustic damping of two phase flow has yet to be implemented in the model. This calls for an improvement of the model with more sophisticated numerical differentiation schemes and a wave equation taking lossy media into account.

At this early stage of the technology development, there are still several unanswered questions that needs further research. That said, this study strongly suggests that even very low liquid contents increase the acoustic damping and therefore a wet gas meter based upon attenuation of sound waves remains a possibility.



# Bibliography

- [1] S.P.C. Belfroid, J. Golliard, and O. Vijlbrief. Singing mitigation in corrugated tubes with liquid injection. In *Proceedings to the ASME-PVP 2013 conference*, 2013.
- [2] RigZone. Flexible riser. [http://www.rigzone.com/images/howitworks/HIW\\_risers1.jpg](http://www.rigzone.com/images/howitworks/HIW_risers1.jpg). Accessed: 2013-12-05.
- [3] NOV. Flexible riser inner layer. [http://www.nov.com/producingpossibilities/images/risers\\_small.jpg](http://www.nov.com/producingpossibilities/images/risers_small.jpg). Accessed: 2013-12-05.
- [4] SW Rienstra and A Hirschberg. An introduction to acoustics. *Report IWDE*, 2001.
- [5] Bureau Veritas. Joint industry project flexible risers. <http://www.flexible-risers.org/newindex.asp>. Accessed: 2013-09-10.
- [6] Statoil ASA. Multiphase and wet gas meters. <http://www.statoil.com/en/technologyinnovation/fielddevelopment/flowassurance/multiphaseandwetgas/pages/default.aspx>. Accessed: 2013-12-12.
- [7] SPC Belfroid, RJ Swindel, and N Kitney. Flow induced pulsations due to flexible risers. In *Offshore technology conference held in Houston Texas, paper OCT*, volume 19904, 2009.
- [8] Rune Tungen and Even de Lanlay. Early study of two new technologies for solving separation challenges. 2013.
- [9] Mihaela Popescu, Stein Tore Johansen, and Wei Shyy. Flow-induced acoustics in corrugated pipes. *Communications in Computational Physics*, 10(1):120, 2011.
- [10] The Physics Classroom. Categories of waves. <http://www.physicsclassroom.com/class/waves/Lesson-1/Categories-of-Waves>. Accessed: 2014-04-29.
- [11] Wikipedia. Wave. <http://en.wikipedia.org/wiki/Wave>. Accessed: 2014-03-28.
- [12] Pellissippi State Community College. Waves. [http://www.pstcc.edu/departments/natural\\_behavioral\\_sciences/Web%20Physics/Chapter016.htm](http://www.pstcc.edu/departments/natural_behavioral_sciences/Web%20Physics/Chapter016.htm). Accessed: 2014-04-29.

- 
- [13] Dr. Dan Russell. Longitudinal and transverse wave motion. <http://www.acs.psu.edu/drussell/demos/waves/wavemotion.html>. Accessed: 2014-03-31.
- [14] The University Of British Columbia Mathematics Department. Derivation of the wave equation. <http://www.math.ubc.ca/~feldman/apps/wave.pdf>. Accessed: 2014-05-18.
- [15] Avraham Hirschberg. *Noise Sources in Turbulent Shear Flows: Fundamentals and Applications*. Springer Vienna, 2013.
- [16] Rice University. Waves and the wave equation. <http://www.ece.rice.edu/~daniel/262/pdf/lecture02.pdf>. Accessed: 2014-04-29.
- [17] BOSE. Noise cancelling headphones. [http://www.bose.com/controller?url=/shop\\_online/headphones/noise\\_cancelling\\_headphones/quietcomfort\\_15/index.jsp#currentState=qc15\\_custom](http://www.bose.com/controller?url=/shop_online/headphones/noise_cancelling_headphones/quietcomfort_15/index.jsp#currentState=qc15_custom). Accessed: 2014-04-30.
- [18] Simon Fraser University. Pitch. <http://www.sfu.ca/sonic-studio/handbook/Pitch.html>. Accessed: 2014-06-08.
- [19] Wikipedia. Sound pressure. [http://en.wikipedia.org/wiki/Sound\\_pressure](http://en.wikipedia.org/wiki/Sound_pressure). Accessed: 2014-04-29.
- [20] Hong Kong Environmental Protection Department. Characteristics of sound and the decibel scale. [http://www.epd.gov.hk/epd/noise\\_education/web/ENG\\_EPDMTML/m1/intro\\_5.html](http://www.epd.gov.hk/epd/noise_education/web/ENG_EPDMTML/m1/intro_5.html). Accessed: 2014-04-30.
- [21] Pankaj Bhatt. *Maximum Marks Maximum Knowledge in Physics*. Allied Publishers.
- [22] Penn State Behrend. Application-forced spring mass systems and resonance. <http://math.bd.psu.edu/faculty/jprevite/250sp10/250bookSec3.6.pdf>. Accessed: 2014-05-15.
- [23] Akira Hirose and Karl Lonngren. *Fundamentals of Wave Phenomena*. Scitech Publishing, 2010.
- [24] Daniel A. Russell. Standing sound waves (longitudinal standing waves). <http://www.acs.psu.edu/drussell/Demos/StandingWaves/StandingWaves.html>. Accessed: 2014-04-30.
- [25] Johan Liljencrants. End correction at a flue pipe mouth. <http://www.fonema.se/mouthcorr/mouthcorr.htm>. Accessed: 2014-04-30.
- [26] Thomas D Rossing, F Richard Moore, and Paul A Wheeler. *The science of sound*, volume 2. Addison-Wesley Reading, MA, 1990.
- [27] Dr. John Askill. End corrections for resonance tubes. <http://fiziks.net/webpages/endcorrect.htm>. Accessed: 2014-04-30.
- [28] Wikipedia. Helmholtz resonator. [http://en.wikipedia.org/wiki/File:Helmholtz\\_resonator.jpg](http://en.wikipedia.org/wiki/File:Helmholtz_resonator.jpg). Accessed: 2013-12-05.



- [29] Erwin Kreyszig. *Advanced engineering mathematics*. John Wiley & Sons, 2007.
- [30] P Hémon, F Santi, and X Amandolèse. On the pressure oscillations inside a deep cavity excited by a grazing airflow. *European Journal of Mechanics-B/Fluids*, 23(4):617–632, 2004.
- [31] D.G. Crighton. *Modern methods in analytical acoustics: lecture notes*. Springer, 1992.
- [32] Frank M White. *Fluid mechanics*. 5th. Boston: McGraw-Hill Book Company, 2003.
- [33] C. Swan. Shear layer. <http://www.thermopedia.com/content/1118/?tid=104&sn=1159>. Accessed: 2013-12-05.
- [34] Thermopedia. Universal velocity profile. <http://www.thermopedia.com/content/1227/?tid=110&sn=25>. Accessed: 2014-05-04.
- [35] Y Nakamura and N Fukamachi. Sound generation in corrugated tubes. *Fluid Dynamics Research*, 7(5):255–261, 1991.
- [36] APS. Vortex shedding. <http://www.aps.org/units/dfd/pressroom/gallery/images/9-kumar.jpg>. Accessed: 2013-12-05.
- [37] National Programme On Technology Enhanced Learning. Pressure distribution in a free vortex flow. [http://nptel.ac.in/courses/Webcourse-contents/IIT-KANPUR/FLUID-MECHANICS/lecture-14/14-3\\_pressure\\_dist\\_fre\\_vortex\\_flow.htm](http://nptel.ac.in/courses/Webcourse-contents/IIT-KANPUR/FLUID-MECHANICS/lecture-14/14-3_pressure_dist_fre_vortex_flow.htm). Accessed: 2014-05-04.
- [38] Irvine Department Of Earth System Science University Of California. Lecture 4: Circulation and vorticity. <http://www.ess.uci.edu/~yu/class/ess228/lecture.4.vorticity.all.pdf>. Accessed: 2014-05-04.
- [39] Takashi Kanamaru. Van der pol oscillator. [http://www.scholarpedia.org/article/Van\\_der\\_Pol\\_oscillator](http://www.scholarpedia.org/article/Van_der_Pol_oscillator). Accessed: 2013-12-12.
- [40] Bernd R Noack, Frank Ohle, and Helmut Eckelmann. On cell formation in vortex streets. *Journal of Fluid Mechanics*, 227:293–308, 1991.
- [41] G Nakiboğlu, SPC Belfroid, J Golliard, and A Hirschberg. On the whistling of corrugated pipes: effect of pipe length and flow profile. *Journal of Fluid Mechanics*, 672:78–108, 2011.
- [42] George Gabriel Stokes. *On the effect of the internal friction of fluids on the motion of pendulums*, volume 9. Pitt Press, 1851.
- [43] NDT Resource Center. Attenuation of sound waves. <http://www.ndt-ed.org/EducationResources/CommunityCollege/Ultrasonics/Physics/attenuation.htm>. Accessed: 2014-04-04.
- [44] J Happel and H Brenner. *Low reynolds number hydrodynamics*, 1965, 1996.

- 
- [45] University of Cambridge. Sound attenuation. <http://www.msm.cam.ac.uk/phase-trans/2000/amjad/b.pdf>. Accessed: 2014-06-02.
- [46] MCAM Peters, Avraham Hirschberg, AJ Reijnen, and APJ Wijnands. Damping and reflection coefficient measurements for an open pipe at low mach and low helmholtz numbers. *Journal of Fluid Mechanics*, 256:499–499, 1993.
- [47] SPC BELFROID, J GOLLIARD, and A HIRSCHBERG. On the whistling of corrugated pipes: effect of pipe length and flow profile. *J. Fluid Mech*, 672:78–108, 2011.
- [48] Joachim Golliard, Bendiksen, Stefan Belfroid, N. E. Gonzalez-Diez, and C. Frimodt. On the whistling of corrugated pipes with narrow cavities. In *Proceedings to the ASME-PVP 2013 conference*, 2013.
- [49] G Nakiboglu. *Aeroacoustics of corrugated pipes, chapter 5: Aeroacoustic power generated by a compact axisymmetric cavity*. PhD thesis, PhD thesis, Technical University of Eindhoven, 2012.
- [50] Michael S Howe. *Acoustics of fluid-structure interactions*. Cambridge University Press, 1998.
- [51] The Physics Classroom. What is a wave? <http://www.physicsclassroom.com/class/waves/Lesson-1/What-is-a-Wave>. Accessed: 2014-06-02.
- [52] Scott A Shearer and Jeremy R Hudson. Fluid mechanics: Stokes’ law and viscosity. *Measurement Laboratory*, (3), 2008.
- [53] NIST (National Institute of Standards and Technology). Thermodynamic properties of fluid systems. <http://webbook.nist.gov/chemistry/fluid/>. Accessed: 2014-03-18.
- [54] J. Golliard, S.P.C. Belfroid, and O. Vijlbrief. Acoustic damping in smooth and corrugated pipes with and without liquid injection. In *Proceedings to the ASME-PVP 2013 conference*, 2013.
- [55] Nils van der Tuuk OPEDAL, Geir SØRLAND, Johan SJÖBLOM, and Anvendt Teknologi AS. Methods for droplet size distribution determination of water-in-oil emulsions using low-field nmr. 2009.
- [56] Proditec. Ejectors & ejector theory. [http://proditec.cl/images/Teoria\\_y\\_Principios\\_Eyectores.pdf](http://proditec.cl/images/Teoria_y_Principios_Eyectores.pdf). Accessed: 2014-05-20.
- [57] Ulf R Kristiansen and Geir A Wiik. Experiments on sound generation in corrugated pipes with flow. *The Journal of the Acoustical Society of America*, 121:1337, 2007.
- [58] Wikipedia. M84 stun grenade. [http://en.wikipedia.org/wiki/M84\\_stun\\_grenade](http://en.wikipedia.org/wiki/M84_stun_grenade). Accessed: 2014-06-04.

- 
- [59] Sverre Holm and Sven Peter Näsholm. A causal and fractional all-frequency wave equation for lossy media. *The Journal of the Acoustical Society of America*, 130(4):2195–2202, 2011.
- [60] Mauro Bologna. Short introduction to fractional calculus. <http://www.uta.cl/charlas/volumen19/Indice/MAUROrevision.pdf>. Accessed: 2014-06-08.
- [61] Georgia State University Department Of Physics and Astronomy. How much power is transported in a string wave. <http://hyperphysics.phy-astr.gsu.edu/hbase/waves/powstr.html>. Accessed: 2014-06-04.
- [62] Wikipedia. Fourier series. [http://en.wikipedia.org/wiki/Fourier\\_series](http://en.wikipedia.org/wiki/Fourier_series). Accessed: 2014-05-09.
- [63] NTNU. Guidance for risk assessment of master theses. [http://www.ntnu.no/innsida-dokumentlager/HMS/Veiledningstekst\\_risikovurdering\\_masteroppgaver\\_v5\\_2013-10-22\\_engelsk.pdf](http://www.ntnu.no/innsida-dokumentlager/HMS/Veiledningstekst_risikovurdering_masteroppgaver_v5_2013-10-22_engelsk.pdf). Accessed: 2014-06-08.
- [64] NTNU. Laboratory and workshop handbook. <https://innsida.ntnu.no/wiki/-/wiki/English/Laboratory+and+workshop+handbook>. Accessed: 2014-06-08.
- [65] COMSOL. Comsol multiphysics. <http://www.comsol.com/comsol-multiphysics>. Accessed: 2014-05-19.
- [66] COMSOL Multiphysics. 4.3 user's guide, 2012.
- [67] Wikipedia. Lu decomposition. [http://en.wikipedia.org/wiki/LU\\_decomposition](http://en.wikipedia.org/wiki/LU_decomposition). Accessed: 2014-05-19.
- [68] COMSOL. Comsol multiphysics direct iterative solvers. <http://www.comsol.com/blogs/solutions-linear-systems-equations-direct-iterative-solvers/>. Accessed: 2014-05-19.



# List Of Figures

1.1	Flexible risers and the corrugated inner layer [2, 3]. . . . .	1
1.2	Sketch of an extraction tube to measure the liquid content of the gas. . .	4
2.1	Illustration of longitudinal and transverse waves [12]. . . . .	6
2.2	Displacement amplitude of air particles of the fundamental standing waves in (a) closed and (b) open pipes [23]. . . . .	9
2.3	Fundamental modes of a standing wave in a tube closed in one end, show- ing both (a) the displacement of air and (b) the pressure variations [24]. .	10
3.1	Helmholtz resonator based on Hermann von Helmholtz original design [28].	14
3.2	The Helmholtz resonator as an acoustical mass-spring system. . . . .	15
3.3	Sketch of the resonator. . . . .	16
3.4	a) Shear layer over a solid boundary, b) Free shear layer [33]. . . . .	18
3.5	Shear layer instability over a cavity. . . . .	19
3.6	Vortex shedding in the wake of a cylindrical body [36]. . . . .	20
3.7	CFD simulation over a single cavity [8]. . . . .	20
3.8	Block diagram illustrating the feedback mechanism between the flow and the acoustic field [35]. . . . .	23
3.9	Sketch of the corrugation. . . . .	24
4.1	Added acoustic damping as a function of droplet size for different liquid rates. . . . .	35
4.2	3D-plot of acoustic damping as a function of droplet size and liquid rate. .	36
4.3	Ratio between the viscous and thermal term in equation 4.9 as a function of droplet size and liquid rate. . . . .	36
4.4	Added acoustic damping as a function of liquid density for different liquid rates. . . . .	37
4.5	3D-plot of acoustic damping as a function of liquid density and liquid rate.	38
4.6	Ratio between the viscous and thermal term in equation 4.9 as a function of liquid density and liquid rate. . . . .	38
4.7	Added acoustic damping as a function of gas viscosity for different liquid rates. . . . .	39
4.8	3D-plot of acoustic damping as a function of gas viscosity and liquid rate.	40

4.9	Ratio between the viscous and thermal term in equation 4.9 as a function of gas viscosity and liquid rate. . . . .	40
4.10	Added acoustic damping as a function of frequency for different liquid rates.	41
4.11	3D-plot of acoustic damping as a function of frequency and liquid rate. . .	42
4.12	Ratio between the viscous and thermal term in equation 4.9 as a function of frequency and liquid rate. . . . .	42
4.13	Added acoustic damping as a function of frequency for different droplet sizes. . . . .	43
4.14	Added acoustic damping as a function of droplet size for different frequencies. . . . .	44
4.15	3D-plot of acoustic damping as a function of frequency and droplet size. .	44
4.16	Ratio between the viscous and thermal term in equation 4.9 as a function of frequency and droplet size. . . . .	45
4.17	Two-dimensional plot of the ratio between the viscous and thermal term in equation 4.9 as a function of frequency for different droplet sizes. . . .	45
5.1	The probe microphone was borrowed from the Department of Acoustics at NTNU and placed at the outlet of the pipe. . . . .	49
5.2	Sketch of the experimental setup. . . . .	49
5.3	Picture of the test rig. On the lower right hand side the two parallel rotameters can be seen next to the needle and mixing unit. The microphone can be seen at the outlet of the pipe, on the left hand side of the picture.	50
5.4	The mixing unit with the bended pipe and the needle. . . . .	51
5.5	Different needle sizes were used to inject different liquid rates. The rubber on the left hand side of the mixing unit was pulled over the microphone in order to make the end air tight. . . . .	52
5.6	Amplitude of the Fourier transform as function of frequency for the smooth pipe. . . . .	55
5.7	Sketch of a corrugation in the corrugated pipe. . . . .	56
5.8	Amplitude of the Fourier transform as function of frequency for the corrugated pipe. . . . .	56
5.9	The frequency spectrum of the Sound Pressure Level [dB] for the smooth pipe. Flow velocity 3.2 m/s, liquid rate 0 ml/min and frequency 550 Hz. This plot is for run 2. . . . .	58
5.10	Sound pressure level [dB] as a function of liquid rate [ml/min] at a frequency of 373 Hz for different flow velocities. The variance over 3 runs is shown. . . . .	59
5.11	Sound pressure level [dB] as a function of liquid rate [ml/min] at a frequency of 445 Hz for different flow velocities. The variance over 3 runs is shown. . . . .	60
5.12	Sound pressure level [dB] as a function of liquid rate [ml/min] at a frequency of 550 Hz for different flow velocities. The variance over 3 runs is shown. . . . .	61

5.13	Normalized sound pressure level [dB] as a function of liquid rate [ml/min] at a frequency of 373 Hz for different flow velocities, illustrated with lines.	61
5.14	Normalized sound pressure level [dB] as a function of liquid rate [ml/min] at a frequency of 445 Hz for different flow velocities, illustrated with lines.	62
5.15	Normalized sound pressure level [dB] as a function of liquid rate [ml/min] at a frequency of 550 Hz for different flow velocities, illustrated with lines.	62
5.16	Sound pressure level [dB] as a function of LVF at a frequency of 373 Hz for different flow velocities. . . . .	63
5.17	Sound pressure level [dB] as a function of LVF at a frequency of 445 Hz for different flow velocities. . . . .	63
5.18	Sound pressure level [dB] as a function of LVF at a frequency of 550 Hz for different flow velocities. . . . .	64
5.19	The frequency spectrum of the Sound Pressure Level [dB] for the closed corrugated pipe. Flow velocity 6.28 m/s and liquid rate 5 ml/min. This plot is for run 2. . . . .	65
5.20	Average sound pressure level [dB] as a function of liquid rate [ml/min] for different flow velocities for closed corrugated pipe. The variance over 4 runs is also shown as a vertical line. . . . .	66
5.21	Normalized sound pressure level [dB] as a function of liquid rate [ml/min] for different flow velocities for closed corrugated pipe. . . . .	67
5.22	Average sound pressure level [dB] as a function of LVF [-] for different flow velocities for closed corrugated pipe. . . . .	68
5.23	Frequency [Hz] as a function of liquid rate [ml/min] for different flow velocities for closed corrugated pipe. . . . .	68
5.24	The frequency spectrum of the Sound Pressure Level [dB] for open corrugated pipe. Flow rate is equal to 60% of maximum for rotameter 1 and the liquid rate is 1 ml/min. The plot is for run 2. . . . .	69
5.25	Average Sound Pressure Level [dB] as a function of liquid rate [ml/min] for different flow rates for open corrugated pipe. The variance over 3 runs is also shown as a vertical line. . . . .	70
5.26	Normalized Sound Pressure Level [dB] as a function of liquid rate [ml/min] for different flow rates for open corrugated pipe. . . . .	71
5.27	Frequency [Hz] as a function of liquid rate [ml/min] for different flow rates for open corrugated pipe. . . . .	71
5.28	The frequency spectrum of the Sound Pressure Level [dB] for open corrugated pipe. Flow rate is equal to 60% of maximum for rotameter 1 and the liquid rate is 2.5 ml/min. The plot is for run 1. . . . .	72
5.29	Normalized Sound Pressure Level [dB] as a function of liquid rate [ml/min] for an interval $\pm 10$ Hz around the peak frequency. Open corrugated pipe.	73
5.30	Added acoustic damping coefficient $\alpha$ as a function of LVF at a frequency of 373 Hz in a smooth pipe. . . . .	75
5.31	Added acoustic damping coefficient $\alpha$ as a function of LVF at a frequency of 445 Hz in a smooth pipe. . . . .	75

5.32	Added acoustic damping coefficient $\alpha$ as a function of LVF at a frequency of 550 Hz in a smooth pipe. . . . .	76
5.33	Added acoustic damping coefficient $\alpha$ for low LVFs at a frequency of 373 Hz in a smooth pipe. . . . .	77
5.34	Added acoustic damping coefficient $\alpha$ for low LVFs at a frequency of 445 Hz in a smooth pipe. . . . .	78
5.35	Added acoustic damping coefficient $\alpha$ for low LVFs at a frequency of 550 Hz in a smooth pipe. . . . .	78
5.36	Added acoustic damping coefficient $\alpha$ as a function of LVF for closed corrugated pipe. 320 Hz was used as the frequency for the theoretical damping. . . . .	79
5.37	Added acoustic damping coefficient $\alpha$ as a function of LVF for open corrugated pipe and 60% flow rate. . . . .	80
5.38	Added acoustic damping coefficient $\alpha$ as a function of LVF for open corrugated pipe and 80% flow rate. . . . .	81
5.39	Added acoustic damping coefficient $\alpha$ as a function of LVF for open corrugated pipe and 100% flow rate. . . . .	81
5.40	Amplitude of sound as a function of time for smooth pipe with sound frequency playback at 373 Hz. . . . .	82
5.41	SPL as a function of frequency for smooth pipe with sound frequency playback at 373 Hz. . . . .	83
6.1	Time evolution of the acoustic pressure at $U=4.697$ m/s. . . . .	91
6.2	FFT of the acoustic pressure at $U=4.697$ m/s. . . . .	92
6.3	Time evolution of the acoustic pressure at $U=6.281$ m/s. . . . .	93
6.4	FFT of the acoustic pressure at $U=6.281$ m/s. . . . .	93
6.5	Time evolution of the acoustic pressure at $U=7.866$ m/s. . . . .	94
6.6	FFT of the acoustic pressure at $U=7.866$ m/s. . . . .	94
6.7	FFT of the acoustic pressure at $U=8.658$ m/s. . . . .	95
6.8	Acoustic pressure wave across the pipe at $t = 0, 1$ and 2 seconds. . . . .	96
6.9	Acoustic velocity wave across the pipe at $t = 0, 1$ and 2 seconds. . . . .	96
A.1	The first four partial sums of the Fourier series of a square wave [62]. . . . .	121
E.1	Fundamental modes of a standing wave in a tube closed in one end, showing both the displacement of air and the pressure variations [24]. . . . .	172
E.2	Time evolution of the acoustic pressure at $U=2.343$ m/s. . . . .	177
E.3	FFT of the acoustic pressure at $U=2.343$ m/s. . . . .	177
E.4	Time evolution of the acoustic pressure at $U=3.124$ m/s. . . . .	178
E.5	FFT of the acoustic pressure at $U=3.124$ m/s. . . . .	178
E.6	Time evolution of the acoustic pressure at $U=3.905$ m/s. . . . .	179
E.7	FFT of the acoustic pressure at $U=3.905$ m/s. . . . .	179
E.8	Time evolution of the acoustic pressure at $U=4.697$ m/s. . . . .	180
E.9	FFT of the acoustic pressure at $U=4.697$ m/s . . . . .	180



---

E.10	Time evolution of the acoustic pressure at $U=5.489$ m/s. . . . .	181
E.11	FFT of the acoustic pressure at $U=5.489$ m/s. . . . .	181
E.12	Time evolution of the acoustic pressure at $U=6.281$ m/s. . . . .	182
E.13	FFT of the acoustic pressure at $U=6.281$ m/s. . . . .	182
E.14	Time evolution of the acoustic pressure at $U=7.074$ m/s. . . . .	183
E.15	FFT of the acoustic pressure at $U=7.074$ m/s. . . . .	183
E.16	Time evolution of the acoustic pressure at $U=7.866$ m/s. . . . .	184
E.17	FFT of the acoustic pressure at $U=7.866$ m/s. . . . .	184
E.18	Time evolution of the acoustic pressure at $U=8.658$ m/s. . . . .	185
E.19	FFT of the acoustic pressure at $U=8.658$ m/s. . . . .	185



# List Of Tables

2.1	Sound Pressure Level [dB] of some common sounds [20]. . . . .	8
4.1	Paramteres used in the sensitivity analysis. Air and water at 1 atm and 15°C have been used for gas and liquid properties respectively [32, 53]. . .	33
4.2	Relationship between liquid rates used in the analysis, LVF and ppmv. . .	34
5.1	Equipment used in the experiment. . . . .	48
5.2	Test matrix for smooth pipe. . . . .	50
5.3	Test matrix for corrugated pipe with upstream end closed. . . . .	52
5.4	Test matrix for corrugated pipe with both ends open. Air flow rates given in percentage of 6.9 m <sup>3</sup> /h. . . . .	52
5.5	Average variance and standard deviation for the measured SPL [dB] in the experiments. . . . .	53
5.6	Resonance frequencies [Hz] of the smooth pipe. . . . .	54
5.7	Geometric properties of the corrugated pipe. . . . .	56
5.8	Resonance frequencies [Hz] of the corrugated pipe. Speed of sound calculated without the bolt. . . . .	57
5.9	Resonance frequencies [Hz] of the corrugated pipe. Speed of sound calculated with the bolt. . . . .	57
6.1	Modelled corrugated pipe geometry compared to Popescu and Johansen’s geometry. . . . .	90
6.2	Frequency results. . . . .	90
E.1	Convection-Diffusion equation with variable $u$ . . . . .	171
E.2	Convection-Diffusion equation with variable $p$ . . . . .	171
E.3	Convection-Diffusion equation with variable $u$ . . . . .	171
E.4	COMSOL script. . . . .	174
E.5	COMSOL values. . . . .	175



# Appendix A

## Fourier Analysis

In analysis of periodic signals, Fourier analysis and the Fourier transformation are of significant importance. Fourier series are infinite series replicating general periodic signals with simple sine and cosine functions [29]. Furthermore, in the digital age we currently live in, the discrete Fourier transform can analyse the frequencies in digital signals such as voice or music using the fast Fourier transform algorithm. A brief introduction to the Fourier transforms is given to support the analysis of the sound signals in the experiment. The derivation is found in Kreyszig "Advanced Engineering Mathematics" [29].

### A.1 Fourier Transform Of Continuous Functions

A periodic function is defined as

$$f(x + np) = f(x) \text{ for } n = 1, 2, 3, \dots \quad (\text{A.1})$$

meaning that the function repeats itself over a certain distance (or time). Equation A.1 also implies that if the function  $f(x)$  had period  $p$  it also has period  $2p$ . For a general function  $f(x)$  of period  $2L$ , it can be represented by the Fourier series

$$f(x) = a_0 + \sum_{n=1}^{\infty} \left( a_n \cos \frac{n\pi}{L} x + b_n \sin \frac{n\pi}{L} x \right) \quad (\text{A.2})$$

where the Fourier coefficients are given by the Euler formulas:

$$a_0 = \frac{1}{2L} \int_{-L}^L f(x) dx \quad (\text{A.3})$$

$$a_n = \frac{1}{L} \int_{-L}^L f(x) \cos \frac{n\pi x}{L} dx \quad (\text{A.4})$$

$$b_n = \frac{1}{L} \int_{-L}^L f(x) \sin \frac{n\pi x}{L} dx. \quad (\text{A.5})$$

The interpretation of the Fourier coefficients is the magnitude of this frequency (given as  $f_n = n/2L$ ) in the signal. Figure A.1 shows the first five partial sums of the Fourier series of a square wave [62]. It can clearly be seen how the Fourier series replicate the original function.

## A.2 Discrete Fourier Transform

In Matlab, a built-in function takes the discrete fast Fourier transform of a vector with a given sample rate. The sample rate is the time between each value in the vector. Equations A.2 to A.5 can only be used for a function defined continuously over some interval. Digital signals on the other hand are given as values at finite many points. Certain modification has to be done to extend Fourier analysis to this case. The regular Fourier transform have to be replaced by the discrete Fourier transform and an important conditions is that the values are sampled with fixed intervals. I.e. at times

$$t_k = \frac{2\pi k}{N}, k = 0, 1, 2, \dots, N - 1 \quad (\text{A.6})$$

where  $2\pi$  (for simplicity) is the period of the sampled function,  $f(t)$ , and  $N$  is the number of measurements. The goal is to determine a complex trigonometric polynomial,  $q(t)$  that interpolates  $f(t)$  at the nodes in equation A.6. In other words,

$$f(t_k) = q(t_k) = \sum_{n=0}^{N-1} c_n e^{int_k}, k = 0, 1, 2, \dots, N - 1. \quad (\text{A.7})$$

The object now is to determine the coefficients  $c_n$  to satisfy equation A.7, then an analysis of the frequencies spectrum in the discrete signal can be done. To determine these, sums are used instead of integrals. Equation A.7 is multiplied by  $e^{-imt_k}$  and the sum over  $k$  from 0 to  $N - 1$  is taken. The order of summation is interchanged and  $t_k$  is replaced from equation A.6 to get

$$\sum_{k=0}^{N-1} f(t_k) e^{-imt_k} = \sum_{k=0}^{N-1} \sum_{n=0}^{N-1} c_n e^{i(n-m)t_k} = \sum_{k=0}^{N-1} \sum_{n=0}^{N-1} c_n e^{i(n-m)2\pi k/N}. \quad (\text{A.8})$$

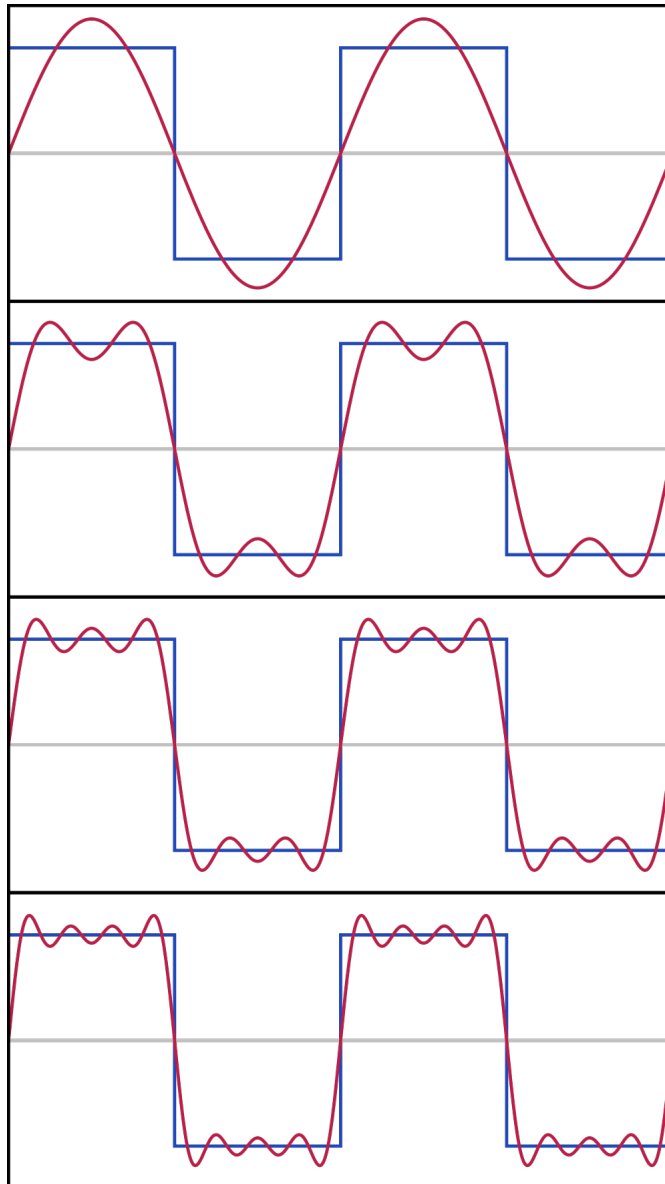


**Figure A.1** – The first four partial sums of the Fourier series of a square wave [62].

It can be proven that the right hand side of equation A.8 is equal to  $c_m N$ . For simplicity set

$$e^{i(n-m)2\pi k/N} = \left( e^{i(n-m)2\pi/N} \right)^k = r^k. \quad (\text{A.9})$$

For integers  $n = m$  we get  $r = e^0 = 1$ , hence the sum of these terms over  $k$  equals  $N$  (the number of these terms). On the other hand for  $n \neq m$ ,  $r$  is no longer equal to one,

but the geometric sum gives

$$\sum_{k=0}^{N-1} r^k = \frac{1 - r^N}{1 - r} = 0 \quad (\text{A.10})$$

because  $r^N = 1$ . This can be shown by the fact that

$$r^N = e^{i(n-m)2\pi k} = \cos 2\pi k(n - m) + i \sin 2\pi k(n - m) = 1 + 0 = 1. \quad (\text{A.11})$$

Hence the right hand side of equation A.8 equals  $c_m N$  [29]. Since only the terms where  $n = m$  matters, we can write  $n$  for  $m$  in equation A.8 . The formula for calculating the discrete complex Fourier coefficients is then given as

$$c_n = \frac{1}{N} \sum_{k=0}^{N-1} f(t_k) e^{-int_k}, \quad n = 0, 1, 2, \dots, N - 1. \quad (\text{A.12})$$

Notice the clear resemblance with equations A.4 and A.5. The fast Fourier transform (FFT) algorithm, used in for instance Matlab, successively halves the problem size  $N$  and hence the factor  $1/N$  is dropped from the definition of the discrete Fourier transform. This is also the reason why one usually define the window length,  $N$ , to be extended with zeros to become a power of two to increase the speed of the algorithm. And also the reason why the coefficients have to be divided by the time vector length to get the "correct" coefficient, as seen in the Matlab files in Appendix B. The discrete Fourier transform of a discrete signal  $\vec{f} = [f_0 \cdots f_{n-1}]^T$  is then the vector  $\vec{\hat{f}} = [\hat{f}_0 \cdots \hat{f}_{n-1}]$  with the components given as [29]

$$\hat{f}_n = N c_n = \sum_{k=0}^{N-1} f(t_k) e^{-int_k}, \quad n = 0, 1, 2, \dots, N - 1. \quad (\text{A.13})$$

Each complex coefficient hence corresponds to a given frequency and the vector of the discrete Fourier transforms gives the frequency spectrum of the signal.



# Appendix B

## Matlab Files

### B.1 Sensitivity Analysis

#### B.1.1 Droplet Size

```
1 %% PARAMETRIC STUDY OF ACOUSTIC DAMPING DUE TO DROPLETS
2 %
3 % Mix: Air and Water
4 % Water properties: http://webbook.nist.gov/chemistry/fluid/
5 % Air properties:
6 %
7 % Parameters studied:
8 % LIQUID INJECTION RATE
9 % DROPLET SIZE
10 %
11 % Frequency fixed to 1000 Hz = 6*pi*1000 rad/s
12 % =====
13 % =====
14
15 clear all; close all; clc; % Cleaning up
16
17 gridNumber = 100; % Number of points in the ...
   parameter
18
19 %% GAS PROPERTIES (AIR) @1 atm, 15C
20 c_gas = 343.3; % Speed of sound [m/s]
21 my = 1.802e-05; % Gas viscosity [Pa*s]
22 rho_g = 1.225; % Gas density [kg/m^3]
23 gamma = 1.4; % Isentropic constant [-]
24 cp = 1007; % Specific heat of gas [J/kgK]
25 cv = cp/gamma; % Specific heat of gas [J/kgK]
26 kappa = 0.02476; % Thermal conductivity of ...
   gas [W/mK]
```

```

27
28 %% LIQUID PROPERTIES (WATER) @1 atm, 15C
29 rho_l = 999.10; % Liquid density [kg/m^3]
30 cs = 4.1885e3; % Specific heat of ...
    droplets [J/kgK]
31
32 %% GENEREAL PROPERTIES
33 omega = 200; % Frequency [Hz]
34 lambda = (c_gas/omega); % Wave length [m]
35 dp = linspace(1e-10,100e-6,gridNumber); % Droplet diameter [m]
36 pipe_d = 35e-3; % Pipe diameter [m]
37 m = ((4*pi*(dp/2).^3)/3)*rho_l; % Droplet mass [kg]
38 LRStep = 0.5; % Step size in liquid rate ...
    vector [ml/min]
39 liquidRate = 0:LRStep:100; % Injected liquid [ml/min]
40 U = 3; % Gas velocity [m/s]
41 gasMass = ((pi*(pipe_d/2)^2)*rho_g*U); % Mass of gas [kg/s]
42 liquidMass = (liquidRate./(60*1000*1000))*rho_l; % Mass of liquid [kg/s]
43 alphaP = liquidMass/gasMass; % Liquid Mass Fraction [-]
44 LVF = alphaP*rho_g/rho_l; % Liquid Volume Fraction [-]
45
46 %% CALCULATING THE ACOUSTIC DAMPING COEFFICIENT
47 % Initialize matrices
48 alpha = zeros(length(liquidRate),length(dp));
49 viscous = zeros(length(liquidRate),length(dp));
50 thermal = zeros(length(liquidRate),length(dp));
51
52 for i=1:length(liquidRate)
53
54 tauN = m./(6*pi*mu.*(dp./2));
55 tauT = m.*cs./(4*pi*kappa.*(dp./2));
56
57 % CALCULATING THE VISCOUS AND THERMAL DAMPING
58 viscous(i,:) = (omega.*tauN)./(1+(omega.*tauN).^2);
59 thermal(i,:) = ((gamma-1).*cs.*omega.*tauT)./(cp.*(1+(omega.*tauT).^2));
60
61 alpha(i,:) = ((alphaP(i))./(2*lambda)).*(viscous(i,:) + thermal(i,:));
62 end
63
64 %% PLOTTING
65
66 % Defining plot indices for easier plotting and legend
67 %plotIndices = [1/LRStep floor(length(liquidRate)/4) ...
    floor(length(liquidRate)/2)...
68 % floor(3*length(liquidRate)/4) length(liquidRate)];
69 plotIndices = [1/LRStep 2.5/LRStep 5/LRStep 10/LRStep 20/LRStep...
70 40/LRStep length(liquidRate)-1] + 1;
71
72 figure(1)
73 plot(dp,alpha(plotIndices,:))
74 xlabel('Droplet Size [m]')
75 ylabel('Alpha [-]')
76 title('Damping coefficient as function of droplet size')

```

```
77 legend([num2str(liquidRate(plotIndices)'),...
78         kron(ones(size(liquidRate(plotIndices))), ' ml/min '),...
79         'location', 'Best')
80
81 figure(2)
82 surf(dp, liquidRate, alpha, 'Edgecolor', 'none');
83 xlabel('Droplet Size [m]')
84 ylabel('Liquid Rate [ml/min]')
85 zlabel('Alpha [-]')
86 title('Alpha as function of liquid rate and droplet size')
87
88 % RATIO BETWEEN VISCOUS AND THERMAL DAMPING
89 visTheRatio = viscous./thermal;
90
91 % Plotting
92 figure(3)
93 surf(dp, liquidRate, visTheRatio, 'Edgecolor', 'none');
94 xlabel('Droplet Size [m]')
95 ylabel('Liquid Rate [ml/min]')
96 zlabel('Ratio Between Viscous and Thermal Damping')
97 title('Ratio of Viscous and Thermal as function of droplet size')
98
99 figure(4)
100 plot(dp, visTheRatio(plotIndices, :))
101 xlabel('Droplet Size [m]')
102 ylabel('Ratio Between Viscous and Thermal Damping [-]')
103 title('Ratio of Viscous and Thermal as function of droplet size')
104 legend([num2str(liquidRate(plotIndices)'),...
105         kron(ones(size(liquidRate(plotIndices))), ' ml/min '),...
106         'location', 'Best')
```

## B.1.2 Liquid Density

```

1 %% PARAMETRIC STUDY OF ACOUSTIC DAMPING DUE TO DROPLETS
2 %
3 %
4 % Mix: Methane and Water
5 % liquid and gas properties found on: ...
   http://webbook.nist.gov/chemistry/fluid/
6 %
7 % Parameters studied:
8 % LIQUID INJECTION RATE
9 % LIQUID DENSITY
10 %
11 % Droplet size set to 100e-6 meter (diameter)
12 % =====
13 % =====
14
15 clear all; close all; clc; % Cleaning up
16
17 gridNumber = 100; % Number of points in the ...
   parameter
18
19 %% GAS PROPERTIES (AIR) @1 atm, 15C
20 c_gas = 343.3; % Speed of sound [m/s]
21 my = 1.802e-05; % Gas viscosity [Pa*s]
22 rho_g = 1.225; % Gas density [kg/m^3]
23 gamma = 1.4; % Isentropic constant [-]
24 cp = 1007; % Specific heat of gas [J/kgK]
25 cv = cp/gamma; % Specific heat of gas [J/kgK]
26 kappa = 0.02476; % Thermal conductivity of ...
   gas [W/mK]
27
28 %% LIQUID PROPERTIES (WATER) @1 atm, 15C
29 rho_l = 1000; % Liquid density [kg/m^3]
30 cs = 4.1885e3; % Specific heat of ...
   droplets [J/kgK]
31
32 %% GENEREAL PROPERTIES
33 omega = 200; % Frequency [Hz]
34 lambda = (c_gas/omega); % Wave length [m]
35 dp = 100e-6; % Droplet diameter [m]
36 pipe_d = 35e-3; % Pipe diameter [m]
37 m = ((4*pi*(dp/2).^3)/3)*rho_l; % Droplet mass [kg]
38 LRStep = 0.5; % Step size in liquid rate ...
   vector [ml/min]
39 liquidRate = 0:LRStep:100; % Injected liquid [ml/min]
40 U = 3; % Gas velocity [m/s]
41 gasMass = ((pi*(pipe_d/2)^2))*rho_g*U; % Mass of gas [kg/s]
42
43 tauN = m./(6.*pi.*my.*(dp./2));
44 tauT = m.*cs./(4*pi*kappa.*(dp./2));
45

```

```

46 %% CALCULATING THE ACOUSTIC DAMPING COEFFICIENT
47 % Initialize matrices
48 alpha = zeros(length(liquidRate),length(rho_l));
49 viscous = zeros(length(liquidRate),length(rho_l));
50 thermal = zeros(length(liquidRate),length(rho_l));
51 liquidMass = zeros(length(liquidRate),length(rho_l));
52 alphaP = zeros(length(liquidRate),length(rho_l));
53 LVF = zeros(length(liquidRate),length(rho_l));
54
55 for i=1:length(liquidRate)
56 liquidMass(i,:) = (liquidRate(i)/...
57     (60*1000*1000)).*rho_l;           % Mass of liquid [kg/s]
58 alphaP(i,:) = liquidMass(i,+)/gasMass; % Liquid Mass Fraction [-]
59 LVF(i,:) = alphaP(i,).*rho_g./rho_l; % Liquid Volume ...
60     Fraction [-]
61
62 %% CALCULATING THE VISCOUS AND THERMAL DAMPING
63 viscous(i,:) = (omega.*tauN)./(1+(omega.*tauN).^2);
64 thermal(i,:) = ((gamma-1).*cs.*omega.*tauT)./(cp.*(1+(omega.*tauT).^2));
65 alpha(i,:) = ((alphaP(i,))./(2*lambda)).*(viscous(i,:) + thermal(i,:));
66 end
67
68 %% PLOTTING
69
70 % Defining plot indices for easier plotting and legend
71 plotIndices = [1/LRStep 2.5/LRStep 5/LRStep 10/LRStep 20/LRStep...
72     40/LRStep length(liquidRate)-1] + 1;
73
74 figure(1)
75 plot(rho_l,alpha(plotIndices,:))
76 xlabel('Liquid Density [kg/m3]')
77 ylabel('Alpha [-]')
78 title('Damping coefficient as function of liquid density')
79 legend([num2str(liquidRate(plotIndices)'),...
80     kron(ones(size(liquidRate(plotIndices)')), ' ml/min '),...
81     'location','NorthEast')]
82
83 figure(2)
84 surf(rho_l,liquidRate,alpha,'Edgecolor','none');
85 xlabel('Liquid Density [kg/m3]')
86 ylabel('Liquid Rate [ml/min]')
87 zlabel('Alpha [-]')
88 title('Alpha as function of liquid rate and liquid density')
89
90 %% RATIO BETWEEN VISCOUS AND THERMAL DAMPING
91 visTheRatio = viscous./thermal;
92
93 % Plotting
94 figure(3)
95 surf(rho_l,liquidRate,visTheRatio,'Edgecolor','none');
96 xlabel('Liquid Density [kg/m3]')
97 ylabel('Liquid Rate [ml/min]')

```

```
98 zlabel('Ratio Between Viscous and Thermal Damping')
99 title('Ratio of Viscous and Thermal as function of liquid rate and ...
      liquid density')
100
101 figure(4)
102 plot(rho_l,visTheRatio(plotIndices,:))
103 xlabel('Liquid Density [kg/m3]')
104 ylabel('Ratio Between Viscous and Thermal Damping [-]')
105 title('Ratio of Viscous and Thermal as function of liquid density')
106 legend([num2str(liquidRate(plotIndices)'),...
107         kron(ones(size(liquidRate(plotIndices))), ' ml/min '),...
108         'location','Best')
```

## B.1.3 Gas Viscosity

```

1 %% PARAMETRIC STUDY OF ACOUSTIC DAMPING DUE TO DROPLETS
2 %
3 % Mix: Air and Water
4 % Water properties: http://webbook.nist.gov/chemistry/fluid/
5 % Air properties:
6 %
7 % Parameters studied:
8 % LIQUID INJECTION RATE
9 % GAS VISCOSITY
10 %
11 % Droplet size set to 100e-6 meter (diameter)
12 % =====
13 % =====
14
15 clear all; close all; clc; % Cleaning up
16
17 gridNumber = 100; % Number of points in the ...
    parameter
18
19 %% GAS PROPERTIES (AIR) @1 atm, 15C
20 c_gas = 343.3; % Speed of sound [m/s]
21 my = 1e-7:1e-06:1e-4; % Gas viscosity [Pa*s]
22 rho_g = 1.225; % Gas density [kg/m^3]
23 gamma = 1.4; % Isentropic constant [-]
24 cp = 1007; % Specific heat of gas [J/kgK]
25 cv = cp/gamma; % Specific heat of gas [J/kgK]
26 kappa = 0.02476; % Thermal conductivity of ...
    gas [W/mK]
27
28 %% LIQUID PROPERTIES (WATER) @1 atm, 15C
29 rho_l = 999.10; % Liquid density [kg/m^3]
30 cs = 4.1885e3; % Specific heat of ...
    droplets [J/kgK]
31
32 %% GENEREAL PROPERTIES
33 omega = 200; % Frequency [rad/s]
34 lambda = (c_gas/omega); % Wave length [m]
35 dp = 100e-6; % Droplet diameter [m]
36 pipe_d = 35e-3; % Pipe diameter [m]
37 m = ((4*pi*(dp/2).^3)/3)*rho_l; % Droplet mass [kg]
38 LRStep = 0.5; % Step size in liquid rate ...
    vector [ml/min]
39 liquidRate = 0:LRStep:100; % Injected liquid [ml/min]
40 U = 3; % Gas velocity [m/s]
41 gasMass = (pi*(pipe_d/2)^2)*rho_g*U; % Mass of gas [kg/s]
42 liquidMass = (liquidRate./(60*1000*1000))*rho_l; % Mass of liquid [kg/s]
43 alphaP = liquidMass/gasMass; % Liquid Mass Fraction [-]
44 LVF = alphaP*rho_g/rho_l; % Liquid Volume Fraction [-]
45
46 %% CALCULATING THE ACOUSTIC DAMPING COEFFICIENT

```

```

47 % Initialize matrices
48 alpha = zeros(length(liquidRate),length(my));
49 viscous = zeros(length(liquidRate),length(my));
50 thermal = zeros(length(liquidRate),length(my));
51
52 for i=1:length(liquidRate)
53
54 tauN = m./(6.*pi.*my.*(dp./2));
55 tauT = m.*cs./(4*pi*kappa.*(dp./2));
56
57 % CALCULATING THE VISCOUS AND THERMAL DAMPING
58 viscous(i,:) = (omega.*tauN)./(1+(omega.*tauN).^2);
59 thermal(i,:) = ((gamma-1).*cs.*omega.*tauT)./(cp.*(1+(omega.*tauT).^2));
60
61 alpha(i,:) = ((alphaP(i))./(2*lambda)).*(viscous(i,:) + thermal(i,:));
62 end
63
64 %% PLOTTING
65
66 % Defining plot indices for easier plotting and legend
67 plotIndices = [1/LRStep 2.5/LRStep 5/LRStep 10/LRStep 20/LRStep...
68     40/LRStep length(liquidRate)-1] + 1;
69
70 figure(1)
71 plot(my,alpha(plotIndices,:))
72 xlabel('Gas Viscosity [Pa*s]')
73 ylabel('Alpha [-]')
74 title('Damping coefficient as function of viscosity')
75 legend([num2str(liquidRate(plotIndices))],...
76     kron(ones(size(liquidRate(plotIndices))), ' ml/min '),...
77     'location','Best')
78
79 figure(2)
80 surf(my,liquidRate,alpha,'Edgecolor','none');
81 xlabel('Gas Viscosity [Pa*s]')
82 ylabel('Liquid Rate [ml/min]')
83 zlabel('Alpha [-]')
84 title('Alpha as function of liquid rate and viscosity')
85
86 % RATIO BETWEEN VISCOUS AND THERMAL DAMPING
87 visTheRatio = viscous./thermal;
88
89 % Plotting
90 figure(3)
91 surf(my,liquidRate,visTheRatio,'Edgecolor','none');
92 xlabel('Gas Viscosity [Pa*s]')
93 ylabel('Liquid Rate [ml/min]')
94 zlabel('Ratio Between Viscous and Thermal Damping')
95 title('Ratio of Viscous and Thermal as function of liquid rate and ...
96     viscosity')
97
98 figure(4)
99 plot(my,visTheRatio(plotIndices,:))

```



```
99 xlabel('Gas Viscosity [Pa*s]')
100 ylabel('Ratio Between Viscous and Thermal Damping [-]')
101 title('Ratio of Viscous and Thermal as function of viscosity')
102 legend([num2str(liquidRate(plotIndices)'),...
103         kron(ones(size(liquidRate(plotIndices))), ' ml/min '),...
104         'location', 'Best')
```

## B.1.4 Sound Frequency

### B.1.4.1 Liquid Rate

```

1 %% PARAMETRIC STUDY OF ACOUSTIC DAMPING DUE TO DROPLETS
2 %
3 %
4 % Mix: Methane and Water
5 % liquid and gas properties found on: ...
   http://webbook.nist.gov/chemistry/fluid/
6 %
7 % Parameters studied:
8 % FREQUENCY
9 % LIQUID RATE
10 %
11 % Droplet size set to 100e-6 m (diameter)
12 % =====
13 % =====
14 clear all; close all; clc; % Cleaning up
15
16 gridNumber = 100; % Number of points in the ...
   parameter
17
18 %% GAS PROPERTIES (AIR) @1 atm, 15C
19 c_gas = 343.3; % Speed of sound [m/s]
20 my = 1.802e-05; % Gas viscosity [Pa*s]
21 rho_g = 1.225; % Gas density [kg/m^3]
22 gamma = 1.4; % Isentropic constant [-]
23 cp = 1007; % Specific heat of gas [J/kgK]
24 cv = cp/gamma; % Specific heat of gas [J/kgK]
25 kappa = 0.02476; % Thermal conductivity of ...
   gas [W/mK]
26
27 %% LIQUID PROPERTIES (WATER) @1 atm, 15C
28 rho_l = 999.10; % Liquid density [kg/m^3]
29 cs = 4.1885e3; % Specific heat of ...
   droplets [J/kgK]
30
31 %% GENEREAL PROPERTIES
32 omega = linspace(0,2000,gridNumber); % Frequency [Hz]
33 lambda = (c_gas./omega); % Wave length [m]
34 dp = 100e-6; % Droplet diameter [m]
35 pipe_d = 35e-3; % Pipe diameter [m]
36 m = ((4*pi*(dp/2).^3)/3)*rho_l; % Droplet mass [kg]
37 LRStep = 0.5; % Step size in liquid rate ...
   vector [ml/min]
38 liquidRate = 0:LRStep:100; % Injected liquid [ml/min]
39 U = 3; % Gas velocity [m/s]
40 gasMass = ((pi*(pipe_d/2)^2))*rho_g*U; % Mass of gas [kg/s]
41 liquidMass = (liquidRate./(60*1000*1000))*rho_l; % Mass of liquid [kg/s]
42 alphaP = liquidMass/gasMass; % Liquid Mass Fraction [-]

```

```

43 LVF = alphaP*rho_g/rho_l; % Liquid Volume Fraction [-]
44
45 %% CALCULATING THE ACOUSTIC DAMPING COEFFICIENT
46 % Initialize matrices
47 alpha = zeros(length(liquidRate),length(omega));
48 viscous = zeros(length(liquidRate),length(omega));
49 thermal = zeros(length(liquidRate),length(omega));
50
51 for i=1:length(liquidRate)
52
53 tauN = m./(6*pi*my.*(dp./2));
54 tauT = m.*cs./(4*pi*kappa.*(dp./2));
55
56 % CALCULATING THE VISCOUS AND THERMAL DAMPING
57 viscous(i,:) = (omega.*tauN)./(1+(omega.*tauN).^2);
58 thermal(i,:) = ((gamma-1).*cs.*omega.*tauT)./(cp.*(1+(omega.*tauT).^2));
59
60 alpha(i,:) = ((alphaP(i))./(2*lambda)).*(viscous(i,:) + thermal(i,:));
61 end
62
63 %% PLOTTING
64
65 % Defining plot indices for easier plotting and legend
66 plotIndices = [1/LRStep 2.5/LRStep 5/LRStep 10/LRStep 20/LRStep...
67 40/LRStep length(liquidRate)-1] + 1;
68
69 figure(1)
70 plot(omega,alpha(plotIndices,:))
71 xlabel('Frequency [Hz]')
72 ylabel('Alpha [-]')
73 title('Damping coefficient as function of droplet size')
74 legend([num2str(liquidRate(plotIndices))',...
75 kron(ones(size(liquidRate(plotIndices))),' ml/min '),...
76 'location','NorthEast')
77
78 figure(2)
79 surf(omega,liquidRate,alpha,'Edgecolor','none');
80 xlabel('Frequency [Hz]')
81 ylabel('Liquid Rate [ml/min]')
82 zlabel('Alpha [-]')
83 title('Alpha as function of liquid rate and droplet size')
84
85 % RATIO BETWEEN VISCOUS AND THERMAL DAMPING
86 visTheRatio = viscous./thermal;
87
88 % Plotting
89 figure(3)
90 surf(omega,liquidRate,visTheRatio,'Edgecolor','none');
91 xlabel('Frequency [Hz]')
92 ylabel('Liquid Rate [ml/min]')
93 zlabel('Ratio Between Viscous and Thermal Damping')
94 title('Ratio of Viscous and Thermal as function of droplet size')
95

```

```
96 figure(4)
97 plot(omega,visTheRatio(plotIndices,:))
98 xlabel('Frequency [Hz]')
99 ylabel('Ratio Between Viscous and Thermal Damping [-]')
100 title('Ratio of Viscous and Thermal as function of frequency')
101 legend([num2str(liquidRate(plotIndices)'),...
102        kron(ones(size(liquidRate(plotIndices)')), ' ml/min ')],...
103        'location','Best')
```

## B.1.4.2 Droplet Size

```

1 %% PARAMETRIC STUDY OF ACOUSTIC DAMPING DUE TO DROPLETS
2 %
3 % Mix: Air and Water
4 % Water properties: http://webbook.nist.gov/chemistry/fluid/
5 % Air properties:
6 %
7 % Parameters studied:
8 % FREQUENCY
9 % DROPLET SIZE
10 %
11 % Liquid Injection Rate set to 20 ml/min
12 % =====
13 % =====
14
15 clear all; close all; clc; % Cleaning up
16
17 gridNumber = 101; % Number of points in the ...
    parameter
18
19 %% GAS PROPERTIES (AIR) @1 atm, 15C
20 c_gas = 343.3; % Speed of sound [m/s]
21 my = 1.802e-05; % Gas viscosity [Pa*s]
22 rho_g = 1.225; % Gas density [kg/m^3]
23 gamma = 1.4; % Isentropic constant [-]
24 cp = 1007; % Specific heat of gas [J/kgK]
25 cv = cp/gamma; % Specific heat of gas [J/kgK]
26 kappa = 0.02476; % Thermal conductivity of ...
    gas [W/mK]
27
28 %% LIQUID PROPERTIES (WATER) @1 atm, 15C
29 rho_l = 999.10; % Liquid density [kg/m^3]
30 cs = 4.1885e3; % Specific heat of ...
    droplets [J/kgK]
31
32 %% GENEREAL PROPERTIES
33 omega = linspace(0,2000,gridNumber); % Frequency [Hz]
34 lambda = (c_gas./omega); % Wave length [m]
35 dp = linspace(1e-10,100e-6,gridNumber); % Droplet diameter [m]
36 m = ((4*pi*(dp/2).^3)/3)*rho_l; % Droplet mass [kg]
37 pipe_d = 35e-3; % Pipe diameter [m]
38 liquidRate = 20; % Injected liquid [ml/min]
39 U = 3; % Gas velocity [m/s]
40 gasMass = (pi*(pipe_d/2)^2)*rho_g*U; % Mass of gas [kg/s]
41 liquidMass = (liquidRate./(60*1000*1000))*rho_l; % Mass of liquid [kg/s]
42 alphaP = liquidMass/gasMass; % Liquid Mass Fraction [-]
43 LVF = alphaP*rho_g/rho_l; % Liquid Volume Fraction [-]
44
45 %% CALCULATING THE ACOUSTIC DAMPING COEFFICIENT
46 % Initialize matrices
47 alpha = zeros(length(dp),length(omega));

```

```

48 viscous = zeros(length(dp),length(omega));
49 thermal = zeros(length(dp),length(omega));
50 tauN = zeros(length(dp),1);
51 tauT = zeros(length(dp),1);
52
53 for i=1:length(dp)
54
55 tauN(i) = m(i)/(6*pi*my.*(dp(i)./2));
56 tauT(i) = m(i).*cs./(4*pi*kappa.*(dp(i)./2));
57
58 % CALCULATING THE VISCOUS AND THERMAL DAMPING
59 viscous(i,:) = (omega.*tauN(i))./(1+(omega.*tauN(i)).^2);
60 thermal(i,:) = ...
        ((gamma-1).*cs.*omega.*tauT(i))./(cp.*(1+(omega.*tauT(i)).^2));
61
62 alpha(i,:) = ((alphaP)/(2*lambda)).*(viscous(i,:) + thermal(i,:));
63 end
64
65 %% PLOTTING
66
67 % Defining plot indices for easier plotting and legend
68 plotIndices = [2 floor(length(dp)/4) floor(length(dp)/2)...
69               floor(3*length(dp)/4) length(dp)];
70
71 figure(1)
72 plot(omega,alpha(plotIndices,:))
73 xlabel('Frequency [Hz]')
74 ylabel('Alpha [-]')
75 title('Damping coefficient as function of frequency for different ...
        droplet sizes')
76 legend([num2str(dp(plotIndices))',...
77         kron(ones(size(dp(plotIndices)')), ' m ')],...
78         'location','Best')
79
80 figure(2)
81 plot(dp,alpha(:,plotIndices))
82 xlabel('Droplet Size [m]')
83 ylabel('Alpha [-]')
84 title('Damping coefficient as function of droplet size for different ...
        frequencies')
85 legend([num2str(omega(plotIndices))',...
86         kron(ones(size(omega(plotIndices)')), ' Hz ')],...
87         'location','Best')
88
89 figure(3)
90 surf(omega,dp,alpha,'Edgecolor','none');
91 xlabel('Frequency [Hz]')
92 ylabel('Droplet Size [m]')
93 zlabel('Alpha [-]')
94 title('Alpha as function of frequency and droplet size')
95
96 % RATIO BETWEEN VISCOUS AND THERMAL DAMPING
97 visTheRatio = viscous./thermal;

```

```
98
99 % Plotting
100 figure(4)
101 surf(omega, dp, visTheRatio, 'Edgecolor', 'none');
102 xlabel('Frequency [Hz]')
103 ylabel('Droplet Size [m]')
104 zlabel('Ratio Between Viscous and Thermal Damping')
105 title('Ratio of Viscous and Thermal as function of frequency and ...
        droplet size')
106
107 figure(5)
108 plot(omega, visTheRatio(plotIndices, :))
109 xlabel('Frequency [Hz]')
110 ylabel('Ratio Between Viscous and Thermal Damping [-]')
111 title('Ratio of Viscous and Thermal as function of frequency')
112 legend([num2str(dp(plotIndices)'), ...
113         kron(ones(size(dp(plotIndices)'), ' m '), ...
114             'location', 'Best')
```

## B.2 Experiment

### B.2.1 Creating Sound

```

1 %% MAKING SOUND
2 %
3 % This script produces sounds at given frequencies
4 % =====
5 % =====
6
7 clear all; close all; clc;
8
9 sampleRate = 44100;           % Sample rate [Hz]
10 time1 = 20*60;                % Time [s]
11 freq = 373;
12
13 t=0:1/sampleRate:time1 - 1/sampleRate;
14 y1 = sin(2*pi*freq*t);
15
16 audiowrite('373Hz.flac',y1,sampleRate)

```

```

1 %% FREQUENCY SPAN
2 %
3 % Creating a sound file that spans frequencies for the experiment
4 % =====
5 % =====
6
7 clear all; close all; clc;
8
9 sampleRate = 44100;           % Defining sound sample rate [hz]
10 ΔTime = 1;                   % Time step between frequency steps [s]
11 frequencyStep = 1;           % Frequency step [Hz]
12 startFrequency = 60;          % Starting frequency [Hz]
13 endFrequency = 1000;          % End frequency [Hz]
14
15 % Creating a time vector for each frequency based on the sample rate
16 t=0:1/sampleRate:ΔTime - 1/sampleRate;
17
18 % Initializing the sound vector
19 y = zeros(1,((endFrequency - startFrequency)/frequencyStep + ...
20             1)*length(t));
21
22 start = 1;                     % Starting point for the frequency step
23
24 % For-loop going through all the frequencies and adding them to the
25 % y-vector
26
27 for i=1:(endFrequency-startFrequency)/frequencyStep + 1
28     y(start:length(t)*i) = sin(2*pi*(startFrequency + ...

```



```
        (i-1)*frequencyStep)*t);
28     start = start + length(t);
29 end
30
31 % Writing the sound to file
32 audiowrite('60to1000Hz.flac',y,sampleRate)
```

## B.2.2 Recording Sound

```

1 %% SOUND RECORDING WITH MATLAB
2 %
3 % This script records input from audio input
4 %
5 % =====
6 % =====
7
8 clear all; close all; clc; % Cleaning up
9
10 % Experiment code (expCode)
11 % C = corrugated, S = smooth
12 % <underscore>
13 % (F)x = Flow Rate 1,2,3,...,10
14 % (L)x = Liquid Rate 1,2,3,...,7
15 expCode = 'S_F4L3H1';
16 numRun = '1'; % Experiment run no.
17
18 soundFrequency = 373; % The frequency of the sound (only for ...
    smooth pipe)
19 % Used to calculated average dB around this
20 % frequency
21
22 sampleRate = 44100; % Sample rate [Hz]
23 bits = 8; % Record quality [bits]
24 monoStereo = 1; % Mono = 1, Stereo = 2
25 time = 20; % Record time [s]
26 deviceID = 0; % Device ID of microphone (Check audiodevinfo)
27
28 % Create an audiorecorder object that records sound
29 recObj = audiorecorder(sampleRate,bits,monoStereo,deviceID);
30
31 disp('Starting recording...');
32 recordblocking(recObj,time); % <time> seconds recording
33 disp('Recording stopped');
34
35 % Play back the recording
36 %play(recObj);
37
38 % Store the audio data in an array
39 y = getaudiodata(recObj);
40
41 % Plot the audio sample
42 t = 0:1/sampleRate:time-1/sampleRate;
43 plot(t,y);
44
45 %
46 % Frequency transform
47 m = length(y); % Window length
48 n = pow2(nextpow2(m)); % Transform length
49 fourier1 = fft(y,n)/m; % DFT

```

```

50 f = (0:n-1)*(sampleRate/n);           % Frequency range
51 amplitude = 2*abs(fourier1);          % Amplitude of Fourier transform
52
53 h(1) = figure(2);
54 plot(f,amplitude)
55 xlim([0 2000])                        % Limits the plotting range to ...
    interesting frequencies
56 xlabel('Frequency [Hz]')
57 ylabel('Amplitude')
58 title('\bf Periodogram')
59
60 %% Decibel plot
61 % USE TOGETHER WITH AMPLITUDE
62 decibelFourier = 20*log10(abs(amplitude));
63 h(2) = figure(3);
64 %semilogx(f,decibelFourier)
65 plot(f,decibelFourier)
66 xlim([0 2000])                        % Limits the plotting range to ...
    interesting frequencies
67 xlabel('Frequency [Hz]')
68 ylabel('Amplitude [dB]')
69 title('\bf Sound Pressure Levels')
70
71 %% Calculate the maximum amplitude and its frequency
72 % Have to be double checked against plot
73
74 [maxDecibel, maxFrequency] = ...
    resonanceMax(decibelFourier,900,2000,sampleRate);
75 maxAverageDecibel = resonanceAverage(decibelFourier,soundFrequency-10,...
    soundFrequency+10,sampleRate);
76
77
78 %% SAVE WORKSPACE AND FIGURES
79 %
80 saveDirectory = ...
    strcat('/Users/rtungen/Desktop/MATLAB_Experiment/SMOOTH/NEW/',...
    expCode,'/Run',numRun,'/');
81
82
83 % Make the folders
84 mkdir(saveDirectory);
85
86 workspaceName = strcat('workspace',expCode,'_',numRun);
87 figureName = strcat('frequencyPlots',expCode,'_',numRun);
88
89 savefig(h, strcat(saveDirectory,figureName));
90 save(strcat(saveDirectory,workspaceName));

```

### B.2.2.1 Supporting Functions

```

1 %% FIND RESONANCE FREQUENCIES
2 %
3 % This function returns the frequency and amplitude of the maximum value
4 % of a Fourier transform within a given range.
5 %
6 % The input is the amplitude (or decibel amplitude) vector and the
7 % frequency range we are interested in, in addition to the sample rate.
8 %
9 % =====
10 % =====
11
12 function [value, frequency] = resonanceMax(y,minFreq,maxFreq,sampleRate)
13
14 % Convert frequency to index
15 indexToFreq = sampleRate/length(y);
16
17 minIndex = floor(minFreq/indexToFreq);      % Start index for max function
18 maxIndex = ceil(maxFreq/indexToFreq);      % End index for max function
19
20 % Finding the maximum within the range
21 % Index is the index of the maximum with minIndex equal to 1
22 [value, index] = max(y(minIndex:maxIndex));
23
24 % Converting back from index to frequency and return this
25 frequency = (index+minIndex-1)*indexToFreq;

```

```

1 %% FIND RESONANCE FREQUENCIES
2 %
3 % This function returns the average amplitude
4 % of a Fourier transform within a given range.
5 %
6 % The input is the amplitude (or decibel amplitude) vector and the
7 % frequency range we are interested in, in addition to the sample rate.
8 %
9 % =====
10 % =====
11
12 function value = resonanceAverage(y,minFreq,maxFreq,sampleRate)
13
14 % Convert frequency to index
15 indexToFreq = sampleRate/length(y);
16
17 minIndex = floor(minFreq/indexToFreq);      % Start index for mean ...
18     function
19 maxIndex = ceil(maxFreq/indexToFreq);      % End index for mean function
20
21 % Finding the mean of the range
22 value = mean(y(minIndex:maxIndex));

```

## B.2.3 Plotting Experimental Values

### B.2.3.1 Smooth Pipe

```

1 %% READ EXCEL DATA TO MATLAB
2 %
3 % [ === SMOOTH PIPE === ]
4 %
5 % This script imports data from the excel sheet for the experiment
6 % and plots the results.
7 %
8 % =====
9 % =====
10
11 close all; clear all; clc;
12
13 filename =...
14 '/Users/rtungen/Dropbox/NTNU/Masteroppgave/Experiment/Testmatrix.xlsx';
15 sheet = 'SmoothNEW';
16
17 % Number of liquid rates, frequencies and air flows
18 numFreq = 3;
19 startMatrix = [1,22,29,36,43;...
20     116,137,144,151,158;...
21     232,253,260,267,274]; % The row where each flow rate start in ...
22                               Excel sheet
23 numAir = 5;
24 numLiq = 7;
25
26 [~, expID] = xlsread(filename,sheet,'A36:A315');
27 flowRate = xlsread(filename,sheet,'B36:C315');
28 flowVelocity = xlsread(filename,sheet,'D36:D315');
29 liquidRate = xlsread(filename,sheet,'G36:G315');
30 LVF = xlsread(filename,sheet,'I36:I315');
31 SPL = xlsread(filename,sheet,'J36:Q315');
32 frequency = xlsread(filename,sheet,'R36:X315');
33 peakInterval = xlsread(filename,sheet,'Y36:AE315');
34 alpha = xlsread(filename,sheet,'AH36:AH315');
35
36
37 %% PLOTTING 373 Hz
38
39 flowrateColor = ['b','g','r','c','m','y','k','b'];
40
41 % SCATTER PLOT OF THE AVERAGE dB-LEVELS FOR 373 Hz
42 fig3 = figure(3);
43 hold on
44 for i=1:numAir
45     scatter(LVF(startMatrix(1,i):startMatrix(1,i)+numLiq-1),...
46             SPL(startMatrix(1,i):startMatrix(1,i)+numLiq-1,6),flowrateColor(i))
47 end
48 xlabel('LVF [-]')

```

```

47 ylabel('SPL [dB]')
48 title('Sound Pressure Level [dB] for smooth pipe at 373 Hz')
49 flowVelocityLegend = legend('1.6 [m/s]', '2.8 [m/s]', '3.2 [m/s]', '3.6 ...
    [m/s]', ...
50     '4.0 [m/s]', 'Location', 'Best');
51 hold off
52
53 % Copy the legend for use in the scatter plot with error bars
54 copyLegendFlowVel1 = copyobj(flowVelocityLegend, fig3);
55 copyLegendFlowVel2 = copyobj(flowVelocityLegend, fig3);
56 copyLegendFlowVel3 = copyobj(flowVelocityLegend, fig3);
57
58 % Figure 1 plots the normalized average of frequency 1 (373 Hz)
59 fig1 = figure(1);
60 hold on
61 for i=1:numAir
62     plot(liquidRate(startMatrix(1,i):startMatrix(1,i)+numLiq-1), ...
63         SPL(startMatrix(1,i):startMatrix(1,i)+numLiq-1,8), flowrateColor(i))
64 end
65 xlabel('Liquid Rate [ml/min]')
66 ylabel('SPL [dB]')
67 title('Normalized Sound Pressure Level [dB] for smooth pipe at 373 Hz')
68 legend('1.6 [m/s]', '2.8 [m/s]', '3.2 [m/s]', '3.6 [m/s]', ...
69     '4.0 [m/s]', 'Location', 'Best');
70 hold off
71
72 % AVERAGE SPL FOR 373 Hz WITH ERROR BARS EQUAL TO VARIANS
73 fig2 = figure(2);
74 hold on
75 for i=startMatrix(1,1):startMatrix(1,end)
76     plot([liquidRate(i) liquidRate(i)], ...
77         [(SPL(i,6) - SPL(i,7)) (SPL(i,6) + SPL(i,7))], 'Color', 'k');
78 end
79
80 for i=1:numAir
81     scatter(liquidRate(startMatrix(1,i):startMatrix(1,i)+numLiq-1), ...
82         SPL(startMatrix(1,i):startMatrix(1,i)+numLiq-1,6), flowrateColor(i))
83 end
84 hold off
85 xlabel('Liquid Rate [ml/min]')
86 ylabel('SPL [dB]')
87 title('Sound Pressure Level [dB] for smooth pipe at 373 Hz')
88 axis([-0.5 40.5 40 85])
89 legend('Varians of 3 runs', 'Location', 'Best')
90 set(copyLegendFlowVel1, 'Parent', fig2, 'Position', [0.6651 0.4 0.1572 ...
91     0.1810]);
92
93 %% PLOTTING 445 Hz
94
95 % Figure 1 plots the normalized average of frequency 1 (373 Hz)
96 fig4 = figure(4);
97 hold on
98 for i=1:numAir

```

```

98 plot(liquidRate(startMatrix(2,i):startMatrix(2,i)+numLiq-1),...
99     SPL(startMatrix(2,i):startMatrix(2,i)+numLiq-1,8),flowrateColor(i))
100 end
101 xlabel('Liquid Rate [ml/min]')
102 ylabel('SPL [dB]')
103 title('Normalized Sound Pressure Level [dB] for smooth pipe at 445 Hz')
104 legend('1.6 [m/s]', '2.8 [m/s]', '3.2 [m/s]', '3.6 [m/s]', ...
105     '4.0 [m/s]', 'Location', 'Best')
106 hold off
107
108 % AVERAGE SPL FOR 445 Hz WITH ERROR BARS EQUAL TO VARIANS
109 fig5 = figure(5);
110 hold on
111 for i=startMatrix(2,1):startMatrix(2,end)
112 plot([liquidRate(i) liquidRate(i)],...
113     [(SPL(i,6) - SPL(i,7)) (SPL(i,6) + SPL(i,7))], 'Color', 'k');
114 end
115 for i=1:numAir
116 scatter(liquidRate(startMatrix(2,i):startMatrix(2,i)+numLiq-1),...
117     SPL(startMatrix(2,i):startMatrix(2,i)+numLiq-1,6),flowrateColor(i))
118 end
119 hold off
120 xlabel('Liquid Rate [ml/min]')
121 ylabel('SPL [dB]')
122 title('Sound Pressure Level [dB] for smooth pipe at 445 Hz')
123 axis([-0.5 40.5 40 85])
124 legend('Varians of 3 runs', 'Location', 'Best')
125 set(copyLegendFlowVel2, 'Parent', fig5, 'Position', [0.6651 0.4 0.1572 ...
126     0.1810]);
127
128 % SCATTER PLOT OF THE AVERAGE dB-LEVELS FOR 445 Hz
129 fig6 = figure(6);
130 hold on
131 for i=1:numAir
132 scatter(LVF(startMatrix(2,i):startMatrix(2,i)+numLiq-1),...
133     SPL(startMatrix(2,i):startMatrix(2,i)+numLiq-1,6),flowrateColor(i))
134 end
135 xlabel('LVF [-]')
136 ylabel('SPL [dB]')
137 title('Sound Pressure Level [dB] for smooth pipe at 445 Hz')
138 legend('1.6 [m/s]', '2.8 [m/s]', '3.2 [m/s]', '3.6 [m/s]', ...
139     '4.0 [m/s]', 'Location', 'Best')
140 hold off
141
142 %% PLOTTING 550 Hz
143
144 % Figure 1 plots the normalized average of frequency 1 (373 Hz)
145 fig7 = figure(7);
146 hold on
147 for i=1:numAir
148 plot(liquidRate(startMatrix(3,i):startMatrix(3,i)+numLiq-1),...
149     SPL(startMatrix(3,i):startMatrix(3,i)+numLiq-1,8),flowrateColor(i))

```

```

150 end
151 xlabel('Liquid Rate [ml/min]')
152 ylabel('SPL [dB]')
153 title('Normalized Sound Pressure Level [dB] for smooth pipe at 550 Hz')
154 legend('1.6 [m/s]', '2.8 [m/s]', '3.2 [m/s]', '3.6 [m/s]', ...
155        '4.0 [m/s]', 'Location', 'Best')
156 hold off
157
158 % AVERAGE SPL FOR 445 Hz WITH ERROR BARS EQUAL TO VARIANS
159 fig8 = figure(8);
160 hold on
161 for i=startMatrix(3,1):startMatrix(3,end)
162 plot([liquidRate(i) liquidRate(i)],...
163      [(SPL(i,6) - SPL(i,7)) (SPL(i,6) + SPL(i,7))], 'Color', 'k');
164 end
165
166 for i=1:numAir
167 scatter(liquidRate(startMatrix(3,i):startMatrix(3,i)+numLiq-1),...
168        SPL(startMatrix(3,i):startMatrix(3,i)+numLiq-1,6), flowrateColor(i))
169 end
170 hold off
171 xlabel('Liquid Rate [ml/min]')
172 ylabel('SPL [dB]')
173 title('Sound Pressure Level [dB] for smooth pipe at 550 Hz')
174 axis([-0.5 40.5 40 85])
175 legend('Varians of 3 runs', 'Location', 'Best')
176 set(copyLegendFlowVel3, 'Parent', fig8, 'Position', [0.6651 0.4 0.1572 ...
177             0.1810]);
178
179 % SCATTER PLOT OF THE AVERAGE dB-LEVELS FOR 445 Hz
180 fig9 = figure(9);
181 hold on
182 for i=1:numAir
183 scatter(LVF(startMatrix(3,i):startMatrix(3,i)+numLiq-1),...
184        SPL(startMatrix(3,i):startMatrix(3,i)+numLiq-1,6), flowrateColor(i))
185 end
186 xlabel('LVF [-]')
187 ylabel('SPL [dB]')
188 title('Sound Pressure Level [dB] for smooth pipe at 550 Hz')
189 legend('1.6 [m/s]', '2.8 [m/s]', '3.2 [m/s]', '3.6 [m/s]', ...
190        '4.0 [m/s]', 'Location', 'Best')
191 hold off
192
193 %% COMPARING alpha WITH THEORY
194 %
195 dropletSize = [1e-6, 1e-5, 1e-4]; % Calculate theoretical ...
196 value for % three droplet sizes [m]
197 pipeDiameter = 35e-3; % Pipe diameter [m]
198
199 % Initialize matrices
200 alphaTheory = zeros(length(frequency), length(dropletSize));
201 theoryLegend1 = zeros(1, length(dropletSize));

```



```

201 theoryLegend2 = zeros(1,length(dropletSize));
202 theoryLegend3 = zeros(1,length(dropletSize));
203 expLegend1 = zeros(1,length(numAir));
204 expLegend2 = zeros(1,length(numAir));
205 expLegend3 = zeros(1,length(numAir));
206
207 for j=1:length(dropletSize)
208
209     for i=1:length(frequency)
210         alphaTheory(i,j) = ...
                alphaAirWater(frequency(i,6),dropletSize(j),liquidRate(i),...
                flowVelocity(i),pipeDiameter);
211     end
212 end
213
214
215 % Comparison between expermint and theory of acoustic damping for 373 Hz
216 fig10 = figure(10);
217 hold on
218 for j=1:length(dropletSize)
219     for i=1:numAir
220         expLegend1(i) = ...
                scatter(LVF(startMatrix(1,i):startMatrix(1,i)+numLiq-1),...
                alpha(startMatrix(1,i):startMatrix(1,i)+numLiq-1),...
                flowrateColor(i));
221
222
223
224         theoryLegend1(j) = ...
                plot(LVF(startMatrix(1,i):startMatrix(1,i)+numLiq-1),...
                alphaTheory(startMatrix(1,i):startMatrix(1,i)+numLiq-1,j),...
                flowrateColor(j));
225
226     end
227 end
228
229 xlabel('LVF [-]')
230 ylabel('Acoustic damping coefficient [-]')
231 title('Added acoustic damping [-] for smooth pipe for 373 Hz')
232 legend([expLegend1 theoryLegend1],'1.6 [m/s]','2.8 [m/s]',...
233        '3.2 [m/s]','3.6 [m/s]','4.0 [m/s]','Theoretical 1e-6m',...
234        'Theoretical 1e-5m','Theoretical 1e-4m','Location','Best')
235 axis([0 4.5e-4 -0.05 0.3])
236 hold off
237
238 % Comparison between expermint and theory of acoustic damping for 445 Hz
239 fig11 = figure(11);
240 hold on
241 for j=1:length(dropletSize)
242     for i=1:numAir
243         expLegend2(i) = ...
                scatter(LVF(startMatrix(2,i):startMatrix(2,i)+numLiq-1),...
                alpha(startMatrix(2,i):startMatrix(2,i)+numLiq-1),...
                flowrateColor(i));
244
245
246
247         theoryLegend2(j) = ...
                plot(LVF(startMatrix(2,i):startMatrix(2,i)+numLiq-1),...
                alphaTheory(startMatrix(2,i):startMatrix(2,i)+numLiq-1,j),...
248

```

```

249         flowrateColor(j));
250     end
251 end
252 xlabel('LVF [-]')
253 ylabel('Acoustic damping coefficient [-]')
254 title('Added acoustic damping [-] for smooth pipe for 445 Hz')
255 legend([expLegend2 theoryLegend2], '1.6 [m/s]', '2.8 [m/s]', ...
256        '3.2 [m/s]', '3.6 [m/s]', '4.0 [m/s]', 'Theoretical 1e-6m', ...
257        'Theoretical 1e-5m', 'Theoretical 1e-4m', 'Location', 'Best')
258 hold off
259
260 % Comparison between expermiemt and theory of acoustic damping for 550 Hz
261 fig12 = figure(12);
262 hold on
263 for j=1:length(dropletSize)
264     for i=1:numAir
265         expLegend3(i) = ...
266             scatter(LVF(startMatrix(3,i):startMatrix(3,i)+numLiq-1), ...
267                    alpha(startMatrix(3,i):startMatrix(3,i)+numLiq-1), ...
268                    flowrateColor(i));
269         theoryLegend3(j) = ...
270             plot(LVF(startMatrix(3,i):startMatrix(3,i)+numLiq-1), ...
271                 alphaTheory(startMatrix(3,i):startMatrix(3,i)+numLiq-1, j), ...
272                 flowrateColor(j));
273     end
274 end
275 xlabel('LVF [-]')
276 ylabel('Acoustic damping coefficient [-]')
277 title('Added acoustic damping [-] for smooth pipe for 550 Hz')
278 legend([expLegend3 theoryLegend3], '1.6 [m/s]', '2.8 [m/s]', ...
279        '3.2 [m/s]', '3.6 [m/s]', '4.0 [m/s]', 'Theoretical 1e-6m', ...
280        'Theoretical 1e-5m', 'Theoretical 1e-4m', 'Location', 'Best')
281 hold off

```

### B.2.3.2 Closed Corrugated Pipe

```

1 %% READ EXCEL DATA TO MATLAB
2 %
3 % [ === CLOSED CORRUGATED PIPE === ]
4 %
5 % This script imports data from the excel sheet for the experiment
6 % and plots the results.
7 %
8 % =====
9 % =====
10
11 close all; clear all; clc;
12
13 filename =...
14 '/Users/rtungen/Dropbox/NTNU/Masteroppgave/Experiment/Testmatrix.xlsx';
15 sheet = 'Corrugated';
16
17 % Number of liquid rates, frequencies and air flows
18 numFreq = 1;
19 startMatrix = [1,8,15,22,29,36,43,50]; % The row where each flow ...
    rate start in Excel sheet
20 numAir = 8;
21 numLiq = 7;
22
23 %% READ EXCEL SHEET
24 [~, expID] = xlsread(filename,sheet,'A25:A80');
25 flowRate = xlsread(filename,sheet,'B25:C80');
26 flowVelocity = xlsread(filename,sheet,'D25:D80');
27 liquidRate = xlsread(filename,sheet,'G25:G80');
28 LVF = xlsread(filename,sheet,'I25:I80');
29 SPL = xlsread(filename,sheet,'J25:Q80');
30 frequency = xlsread(filename,sheet,'R25:X80');
31 peakInterval = xlsread(filename,sheet,'Y25:AE80');
32 alpha = xlsread(filename,sheet,'AH25:AH80');
33
34 %% PLOTTING
35
36 %flowrateColor = ['b','g','r','c','m','y','k','b'];
37 flowrateColor = [[0 0 1];[0 1 0];[1 0 0];[0 1 1];[1 0 1];...
38 [1 1 0];[0 0 0];[1 0.5 0.2]];
39 % SCATTER PLOT OF THE AVERAGE dB-LEVELS
40 fig3 = figure(3);
41 hold on
42 for i=1:numAir
43 scatter(LVF(startMatrix(i):startMatrix(i)+numLiq-1),...
44 SPL(startMatrix(i):startMatrix(i)+numLiq-1,6),36,flowrateColor(i,:))
45 end
46 xlabel('LVF [-]')
47 ylabel('SPL [dB]')
48 title('Sound Pressure Level [dB] for closed corrugated pipe')
49 flowVelocityLegend = legend('2.34 m/s','3.12 m/s','3.90 m/s',...

```

```

50     '4.70 m/s','5.40 m/s','6.28 m/s','7.07 m/s','7.87 m/s',...
51     'Location','Best');
52 hold off
53
54 % Copy the legend for use in the scatter plot with error bars
55 copyLegendFlowVel1 = copyobj(flowVelocityLegend,fig3);
56 copyLegendFlowVel2 = copyobj(flowVelocityLegend,fig3);
57 copyLegendFlowVel3 = copyobj(flowVelocityLegend,fig3);
58
59 % Figure 1 plots the normalized SPL average
60 fig1 = figure(1);
61 hold on
62 for i=1:numAir
63     plot(liquidRate(startMatrix(i):startMatrix(i)+numLiq-1),...
64         SPL(startMatrix(i):startMatrix(i)+numLiq-1,8),'Color',...
65         flowrateColor(i,:))
66 end
67 xlabel('Liquid Rate [ml/min]')
68 ylabel('SPL [dB]')
69 title('Normalized Sound Pressure Level [dB] for closed corrugated pipe')
70 legend('2.34 m/s','3.12 m/s','3.90 m/s',...
71     '4.70 m/s','5.40 m/s','6.28 m/s','7.07 m/s','7.87 m/s',...
72     'Location','Best')
73 hold off
74
75 % AVERAGE SPL WITH ERROR BARS EQUAL TO VARIANS
76 fig2 = figure(2);
77 hold on
78 for i=1:numAir
79     for j=0:numLiq-1
80         plot([liquidRate(startMatrix(i)+j) liquidRate(startMatrix(i)+j)],...
81             [(SPL(startMatrix(i)+j,6) - SPL(startMatrix(i)+j,7))...
82             (SPL(startMatrix(i)+j,6) + SPL(startMatrix(i)+j,7))], 'Color', ...
83             'k');
84     end
85 end
86 for i=1:numAir
87     scatter(liquidRate(startMatrix(i):startMatrix(i)+numLiq-1),...
88         SPL(startMatrix(i):startMatrix(i)+numLiq-1,6),36,flowrateColor(i,:))
89 end
90 hold off
91 xlabel('Liquid Rate [ml/min]')
92 ylabel('SPL [dB]')
93 title('Sound Pressure Level [dB] for closed corrugated pipe')
94 axis([-0.5 40.5 35 65])
95 rune = legend('Varians of 4 runs','Location','Best');
96 set(copyLegendFlowVel1,'Parent',fig2,'Position',[0.6651 0.6 0.1286 ...
97     0.1119]);
98
99 fig4 = figure(4);
100 hold on
101 for i=1:numAir

```

```

101     for j=1:3
102         scatter(LVF(startMatrix(i):startMatrix(i)+numLiq-1),...
103             SPL(startMatrix(i):startMatrix(i)+numLiq-1,j),36,...
104             flowrateColor(i,:))
105     end
106 end
107 hold off
108 xlabel('LVF [-]')
109 ylabel('SPL [dB]')
110 title('Sound Pressure Level [dB] for all runs on closed corrugated pipe')
111 set(copyLegendFlowVel2,'Parent',fig4,'Position',[0.6651 0.6 0.1286 ...
112     0.1119]);
113
114 fig5 = figure(5);
115 hold on
116 for i=1:numAir
117     for j=1:3
118         scatter(liquidRate(startMatrix(i):startMatrix(i)+numLiq-1),...
119             frequency(startMatrix(i):startMatrix(i)+numLiq-1,j),36,...
120             flowrateColor(i,:))
121     end
122 end
123 hold off
124 xlabel('Liquid Rate [ml/min]')
125 ylabel('Frequency [Hz]')
126 title('Sound Frequency [Hz] for closed corrugated pipe')
127 set(copyLegendFlowVel3,'Parent',fig5,'Position',[0.6651 0.6 0.1286 ...
128     0.1119]);
129 %% COMPARING alpha WITH THEORY
130 %
131 dropletSize = [1e-6,1e-5,1e-4];           % Calculate theoretical ...
132     value for                               % three droplet sizes [m]
133 pipeDiameter = 25e-3;                     % Pipe diameter [m]
134
135 frequencyTheory = 320;                    % Frequency used to calculate
136                                             % theoretical damping [Hz]
137                                             % Because using the
138                                             % experimental gives messy
139                                             % plots
140
141 % Initialize matrices
142 alphaTheory = zeros(length(frequency),length(dropletSize));
143 theoryLegend1 = zeros(1,length(dropletSize));
144 expLegend1 = zeros(1,length(numAir)-5);
145
146 for j=1:length(dropletSize)
147
148     for i=1:length(frequency)
149         alphaTheory(i,j) = ...
150             alphaAirWaterCorrugated(frequencyTheory,dropletSize(j),...

```

```
150     liquidRate(i),flowVelocity(i),pipeDiameter);
151     end
152 end
153
154 % Comparison between expermint and theory of acoustic damping
155 fig6 = figure(6);
156 hold on
157 for j=1:length(dropletSize)
158     for i=6:numAir
159         expLegend1(i-5) = ...
160             scatter(LVF(startMatrix(i):startMatrix(i)+numLiq-1),...
161                 alpha(startMatrix(i):startMatrix(i)+numLiq-1),36,...
162                 flowrateColor(i,:));
163         theoryLegend1(j) = ...
164             plot(LVF(startMatrix(i):startMatrix(i)+numLiq-1),...
165                 alphaTheory(startMatrix(i):startMatrix(i)+numLiq-1,j),...
166                 'Color',flowrateColor(j,:));
167     end
168 end
169 xlabel('LVF [-]')
170 ylabel('Acoustic damping coefficient [-]')
171 title('Added acoustic damping [-] for closed corrugated pipe')
172 legend([expLegend1 theoryLegend1],'6.28 m/s','7.07 m/s','7.87 m/s',...
173         'Theoretical 1e-6m','Theoretical 1e-5m','Theoretical ...
174         1e-4m','Location','Best')
```

### B.2.3.3 Open Corrugated Pipe

```

1 %% READ EXCEL DATA TO MATLAB
2 %
3 % [ === OPEN CORRUGATED PIPE === ]
4 %
5 % This script imports data from the excel sheet for the experiment
6 % and plots the results.
7 %
8 % =====
9 % =====
10
11 close all; clear all; clc;
12
13 filename =...
14 '/Users/rtungen/Dropbox/NTNU/Masteroppgave/Experiment/Testmatrix.xlsx';
15 sheet = 'CorrugatedOpen';
16
17 % Number of liquid rates, frequencies and air flows
18 numFreq = 1;
19 startMatrix = [1,8,15]; % The row where each flow rate start in ...
    Excel sheet
20 numAir = 3;
21 numLiq = 4;
22
23 %% READ EXCEL SHEET
24 [~, expID] = xlsread(filename, sheet, 'A25:A42');
25 flowRate = xlsread(filename, sheet, 'B25:C42');
26 flowVelocity = xlsread(filename, sheet, 'D25:D42');
27 liquidRate = xlsread(filename, sheet, 'G25:G42');
28 LVF = xlsread(filename, sheet, 'I25:I42');
29 SPL = xlsread(filename, sheet, 'J25:Q42');
30 frequency = xlsread(filename, sheet, 'R25:X42');
31 peakInterval = xlsread(filename, sheet, 'Y25:AF42');
32 alpha = xlsread(filename, sheet, 'AH25:AH42');
33
34 %% PLOTTING
35
36 flowrateColor = [[0 0 1];[0 1 0];[1 0 0];[0 1 1];[1 0 1];...
37 [1 1 0];[0 0 0];[1 0.5 0.2]];
38
39 % SCATTER PLOT OF THE AVERAGE dB-LEVELS
40 fig3 = figure(3);
41 hold on
42 for i=1:numAir
43 scatter(LVF(startMatrix(i):startMatrix(i)+numLiq-1),...
44 SPL(startMatrix(i):startMatrix(i)+numLiq-1,6),36,flowrateColor(i,:))
45 end
46 xlabel('LVF [-]')
47 ylabel('SPL [dB]')
48 title('Sound Pressure Level [dB] for open corrugated pipe')
49 flowVelocityLegend = legend('60%', '80%', '100%', 'Location', 'Best');

```

```

50 hold off
51
52 % Copy the legend for use in the scatter plot with error bars
53 copyLegendFlowVel1 = copyobj(flowVelocityLegend,fig3);
54 copyLegendFlowVel2 = copyobj(flowVelocityLegend,fig3);
55 copyLegendFlowVel3 = copyobj(flowVelocityLegend,fig3);
56 copyLegendFlowVel4 = copyobj(flowVelocityLegend,fig3);
57
58 % Figure 1 plots the normalized average of frequency 1 (373 Hz)
59 fig1 = figure(1);
60 hold on
61 for i=1:numAir
62 plot(liquidRate(startMatrix(i):startMatrix(i)+numLiq-1),...
63      SPL(startMatrix(i):startMatrix(i)+numLiq-1,8), 'Color',...
64      flowrateColor(i,:))
65 end
66 xlabel('Liquid Rate [ml/min]')
67 ylabel('Normalized SPL [-]')
68 title('Normalized Sound Pressure Level [dB] for open corrugated pipe')
69 legend('60%', '80%', '100%', 'Location', 'Best');
70 hold off
71
72 % AVERAGE SPL FOR 373 Hz WITH ERROR BARS EQUAL TO VARIANS
73 fig2 = figure(2);
74 hold on
75 for i=1:numAir
76     for j=0:numLiq-1
77         plot([liquidRate(startMatrix(i)+j) liquidRate(startMatrix(i)+j)],...
78              [(SPL(startMatrix(i)+j,6) - SPL(startMatrix(i)+j,7))...
79               (SPL(startMatrix(i)+j,6) + SPL(startMatrix(i)+j,7))], 'Color', ...
80              'k');
81     end
82 end
83 for i=1:numAir
84 scatter(liquidRate(startMatrix(i):startMatrix(i)+numLiq-1),...
85         SPL(startMatrix(i):startMatrix(i)+numLiq-1,6),36,flowrateColor(i,:))
86 end
87 hold off
88 xlabel('Liquid Rate [ml/min]')
89 ylabel('SPL [dB]')
90 title('Sound Pressure Level [dB] for open corrugated pipe')
91 legend('Varians of 3 runs', 'Location', 'Best')
92 axis([-0.5 5.5 38 56])
93 set(copyLegendFlowVel1, 'Parent', fig2, 'Position', [0.6651 0.6 0.1286 ...
94             0.1119]);
95
96 fig4 = figure(4);
97 hold on
98 for i=1:numAir
99     for j=1:3
100        scatter(LVF(startMatrix(i):startMatrix(i)+numLiq-1),...
101              SPL(startMatrix(i):startMatrix(i)+numLiq-1, j),36,...

```



```

101     flowrateColor(i,:))
102     end
103 end
104 hold off
105 xlabel('LVF [-]')
106 ylabel('SPL [dB]')
107 title('Sound Pressure Level [dB] for all runs open corrugated pipe')
108 set(copyLegendFlowVel2,'Parent',fig4,'Position',[0.6651 0.3 0.1286 ...
109     0.1119]);
110
111 fig5 = figure(5);
112 hold on
113 for i=1:numAir
114     for j=1:3
115         scatter(liquidRate(startMatrix(i):startMatrix(i)+numLiq-1),...
116             frequency(startMatrix(i):startMatrix(i)+numLiq-1,j),36,...
117             flowrateColor(i,:))
118     end
119 end
120 hold off
121 xlabel('Liquid Rate [ml/min]')
122 ylabel('Frequency [Hz]')
123 title('Sound Frequency [Hz] for open corrugated pipe')
124 set(copyLegendFlowVel3,'Parent',fig5,'Position',[0.6651 0.6 0.1286 ...
125     0.1119]);
126 %% PLOTTING PEAK INTERVAL WITH ERROR BARS
127 % Neglecting the lowest flow rates which have some abnormal values
128 legend1 = zeros(1,length(numAir)-1);
129 legend2 = zeros(1,length(numAir)-1);
130
131 fig9 = figure(9);
132 hold on
133 for i=2:numAir
134     legend1(i-1) = ...
135         plot(liquidRate(startMatrix(i):startMatrix(i)+numLiq-1),...
136             peakInterval(startMatrix(i):startMatrix(i)+numLiq-1,8),'Color',...
137             flowrateColor(i,:));
138
139     for j=1:3
140         legend2(i-1) ...
141             =scatter(liquidRate(startMatrix(i):startMatrix(i)+numLiq-1),...
142                 peakInterval(startMatrix(i):startMatrix(i)+numLiq-1,j)...
143                 /peakInterval(startMatrix(i),6),36,flowrateColor(i,:));
144     end
145 end
146 xlabel('Liquid Rate [ml/min]')
147 ylabel('Normalized SPL [-]')
148 title('Normalized Sound Pressure Level [dB] for an interval +/- 10 Hz ...
149     from peak frequency for open corrugated pipe')
150 legend([legend1 legend2],'80%','100%','80%','100%','Location','Best');
151 hold off

```

```

149
150 %% COMPARING alpha WITH THEORY
151 %
152 dropletSize = [1e-5,5e-5,1e-4];           % Calculate theoretical ...
      value for
153                                           % three droplet sizes [m]
154 pipeDiameter = 25e-3;                     % Pipe diameter [m]
155
156 % Initialize matrices
157 alphaTheory = zeros(length(frequency),length(dropletSize));
158 theoryLegend1 = zeros(1,length(dropletSize));
159 expLegend1 = zeros(1,length(numAir));
160 frequencyTheory = zeros(1,length(frequency));
161
162 averageExpFreqs = [1075 1214 1702];
163 % Frequency used to calculate theoretical damping [Hz]. Because using the
164 % experimental gives messy plots
165 for i=1:numAir
166 frequencyTheory(startMatrix(i):startMatrix(i)+numLiq-1) = ...
      averageExpFreqs(i);
167 end
168
169 % Calculating the theoretical damping
170 for j=1:length(dropletSize)
171
172     for i=1:length(liquidRate)
173         alphaTheory(i,j) = ...
            alphaAirWaterCorrugated(frequencyTheory(i),dropletSize(j),...
174             liquidRate(i),flowVelocity(i),pipeDiameter);
175     end
176
177 end
178
179 % Comparison between expermint and theory of acoustic damping 60% flow
180 % rate with theoretical frequency set to 1075
181 fig6 = figure(6);
182 hold on
183 for j=1:length(dropletSize)
184     expLegend1 = scatter(LVF(startMatrix(1):startMatrix(1)+numLiq-1),...
185         alpha(startMatrix(1):startMatrix(1)+numLiq-1),36,...
186         flowrateColor(1,:));
187
188     theoryLegend1(j) = ...
        plot(LVF(startMatrix(1):startMatrix(1)+numLiq-1),...
189         alphaTheory(startMatrix(1):startMatrix(1)+numLiq-1,j),'Color',...
190         flowrateColor(j,:));
191 end
192 xlabel('LVF [-]')
193 ylabel('Acoustic damping coefficient [-]')
194 title('Added acoustic damping [-] for open corrugated pipe ...
      (Theoretical frequency 1075 Hz)')
195 legend([expLegend1 theoryLegend1],'60%',...

```

```

196     'Theoretical 1e-5m','Theoretical 5e-5m','Theoretical ...
        1e-4m','Location','NorthEast')
197 axis([0 0.8e-4 -0.05 0.3])
198 hold off
199
200 % Comparison between expermiemt and theory of acoustic damping 60% flow
201 % rate with theoretical frequency set to 1214
202 fig7 = figure(7);
203 hold on
204 for j=1:length(dropletSize)
205     expLegend1 = scatter(LVF(startMatrix(2):startMatrix(2)+numLiq-1),...
206         alpha(startMatrix(2):startMatrix(2)+numLiq-1),36,...
207         flowrateColor(2,:));
208
209     theoryLegend1(j) = ...
210         plot(LVF(startMatrix(2):startMatrix(2)+numLiq-1),...
211             alphaTheory(startMatrix(2):startMatrix(2)+numLiq-1,j),'Color',...
212             flowrateColor(j,:));
213 end
214 xlabel('LVF [-]')
215 ylabel('Acoustic damping coefficient [-]')
216 title('Added acoustic damping [-] for open corrugated pipe ...
        (Theoretical frequency 1214 Hz)')
217 legend([expLegend1 theoryLegend1],'80%',...
        'Theoretical 1e-5m','Theoretical 5e-5m','Theoretical ...
        1e-4m','Location','NorthEast')
218 axis([0 0.6e-4 -0.05 0.3])
219 hold off
220
221 % Comparison between expermiemt and theory of acoustic damping 60% flow
222 % rate with theoretical frequency set to 1702
223 fig8 = figure(8);
224 hold on
225 for j=1:length(dropletSize)
226     expLegend1 = scatter(LVF(startMatrix(3):startMatrix(3)+numLiq-1),...
227         alpha(startMatrix(3):startMatrix(3)+numLiq-1),36,...
228         flowrateColor(3,:));
229
230     theoryLegend1(j) = ...
231         plot(LVF(startMatrix(3):startMatrix(3)+numLiq-1),...
232             alphaTheory(startMatrix(3):startMatrix(3)+numLiq-1,j),'Color',...
233             flowrateColor(j,:));
234 end
235 xlabel('LVF [-]')
236 ylabel('Acoustic damping coefficient [-]')
237 title('Added acoustic damping [-] for open corrugated pipe ...
        (Theoretical frequency 1702 Hz)')
238 legend([expLegend1 theoryLegend1],'100%',...
        'Theoretical 1e-5m','Theoretical 5e-5m','Theoretical ...
        1e-4m','Location','NorthEast')
239 axis([0 0.5e-4 -0.05 0.3])
240 hold off

```

### B.2.3.4 Supporting Functions

```

1 function alpha = alphaAirWater(omega,dp,liquidRate,U,pipe_d)
2 % Mix: Air and Water
3 % liquid and gas properties found on: ...
   http://webbook.nist.gov/chemistry/fluid/
4 %
5 % Function to return alpha_0 for given properties
6 %
7 % =====
8 % =====
9
10 gridNumber = 100; % Number of points in the ...
   parameter
11
12 %% GAS PROPERTIES (AIR) @1 atm, 15C
13 c_gas = 343.3; %Speed of sound [m/s]
14 c_eff = 1; % Effective speed of sound
   % for corrugated pipe
15
16 my = 1.802e-05; %Gas viscosity [Pa*s]
17 rho_g = 1.225; %Gas density [kg/m^3]
18 gamma = 1.4;
19 cp = 1007; %Specific heat of gas [J/kgK]
20 cv = cp/gamma; %Specific heat of gas [J/kgK]
21 kappa = 0.02476; %Thermal conductivity of ...
   gas [W/mK]
22
23 %% LIQUID PROPERTIES (WATER) @1 atm, 15C
24 rho_l = 999.10; %Liquid density [kg/m^3]
25 cs = 4.1885e3; %Specific heat of droplets ...
   [J/kgK]
26
27 %% GENERALEAL PROPERTIES
28 %omega = 200; %Frequency [Hz]
29 lambda = (c_gas/omega); %Wave length [m]
30 %dp = linspace(1e-10,100e-6,gridNumber); %Droplet diameter [m]
31 %pipe_d = 35e-3; %Pipe diameter [m]
32 m = ((4*pi*(dp/2).^3)/3)*rho_l; %Droplet mass [kg]
33 %liquidRate = 0:50:2000; %Injected liquid [ml/min]
34 %U = 3; %Gas velocity [m/s]
35 gasMass = (pi*(pipe_d/2)^2)*rho_g*U; %Mass of gas [kg/s]
36 liquidMass = (liquidRate./(60*1000*1000))*rho_l; %Mass of liquid [kg/s]
37 alphaP = liquidMass/gasMass; %Liquid Mass Fraction [-]
38 LVF = alphaP*rho_g/rho_l; %Liquid Volume Fraction [-]
39
40 %% CALCULATING THE ACOUSTIC DAMPING COEFFICIENT
41
42 tauN = m./(6*pi*my.*(dp./2));
43 tauT = m.*cs./(4*pi*kappa.*(dp./2));
44
45 % CALCULATING THE VISCOUS AND THERMAL DAMPING
46 viscous = (omega.*tauN)./(1+(omega.*tauN).^2);

```

```

47 thermal = ((gamma-1).*cs.*omega.*tauT)./(cp.*(1+(omega.*tauT).^2));
48
49 alpha = ((alphaP)./(2*lambda)).*(viscous + thermal);

```

```

1 function alpha = alphaAirWaterCorrugated(omega,dp,liquidRate,U,pipe_d)
2 % Mix: Air and Water
3 % liquid and gas properties found on: ...
   http://webbook.nist.gov/chemistry/fluid/
4 %
5 % Function to return alpha for given properties for corrugated pipe
6 % Using effective speed of sound instead of regular speed of sound
7 %
8 % =====
9 % =====
10
11 %% GAS PROPERTIES (AIR) @1 atm, 15C
12 c_gas = 343.3; %Speed of sound [m/s]
13
14 my = 1.802e-05; %Gas viscosity [Pa*s]
15 rho_g = 1.225; %Gas density [kg/m^3]
16 gamma = 1.4;
17 cp = 1007; %Specific heat of gas [J/kgK]
18 cv = cp/gamma; %Specific heat of gas [J/kgK]
19 kappa = 0.02476; %Thermal conductivity of ...
   gas [W/mK]
20
21 %% LIQUID PROPERTIES (WATER) @1 atm, 15C
22 rho_l = 999.10; %Liquid density [kg/m^3]
23 cs = 4.1885e3; %Specific heat of droplets ...
   [J/kgK]
24
25 %% GENEREAL PROPERTIES
26 %omega = 200; %Frequency [Hz]
27 pipeLength = 1; % Length of corrugated ...
   pipe [m]
28 pitchLength = 5e-3;
29 cavityWidth = 2.5e-3;
30 cavityDepth = 3e-3;
31 numCorr = floor(pipeLength/pitchLength); % Number of corrugations [-]
32 totalCavityVolume = numCorr*(pi*((pipe_d/2+cavityDepth)^2 -...
   (pipe_d/2)^2)*cavityWidth); % Total volume of the ...
   corrugations [m^3]
34 innerVolume = pipeLength*pi*(pipe_d/2)^2;
35 totalVolume = totalCavityVolume + innerVolume; % Total volume of pipe ...
   [m^3]
36
37 c_eff = c_gas*sqrt(innerVolume/totalVolume); % Effective speed of ...
   sound [m/s]
38
   % for corrugated pipe
39 lambda = (c_eff/omega); %Wave length [m]
40 %dp = linspace(1e-10,100e-6,gridNumber); %Droplet diameter [m]
41 %pipe_d = 35e-3; %Pipe diameter [m]

```


```
42 m = ((4*pi*(dp/2).^3)/3)*rho_l;           %Droplet mass [kg]
43 %liquidRate = 0:50:2000;                   %Injected liquid [ml/min]
44 %U = 3;                                     %Gas velocity [m/s]
45 gasMass = ((pi*(pipe_d/2)^2)*rho_g*U;      %Mass of gas [kg/s]
46 liquidMass = (liquidRate./(60*1000*1000))*rho_l; %Mass of liquid [kg/s]
47 alphaP = liquidMass/gasMass;               %Liquid Mass Fraction [-]
48 LVF = alphaP*rho_g/rho_l;                 %Liquid Volume Fraction [-]
49
50 %% CALCULATING THE ACOUSTIC DAMPING COEFFICIENT
51
52 tauN = m./(6*pi*my.*(dp./2));
53 tauT = m.*cs./(4*pi*kappa.*(dp./2));
54
55 % CALCULATING THE VISCOUS AND THERMAL DAMPING
56 viscous = (omega.*tauN)./(1+(omega.*tauN).^2);
57 thermal = ((gamma-1).*cs.*omega.*tauT)./(cp.*(1+(omega.*tauT).^2));
58
59 alpha = ((alphaP)./(2*lambda)).*(viscous + thermal);
```

## Appendix C

# Risk Assessment Of Laboratory Work

A risk assessment were used to evaluate the risk concerning the laboratory work. This comes in addition to the mandatory HSE course that is required to get access to the lab. To evaluate the risks we used the standard setup from The Department of Energy and Process Engineering at NTNU as template [63]. The laboratory work were initially classified as harmless and hence the risk assessment presented is therefore not as comprehensive as it would have been if the experiment involved for instance high pressure, high temperature or toxic gases.

Nonetheless, an identification of the potential hazardous accidents is valuable as it clearly states a variety of potential threats to humans, environment and equipment. This is as valid for more harmless work that it is for experiments involving higher consequences should something fail. NTNU and SINTEF's laboratory and workshop handbook were used as reference regarding both the risk assessment and if we were unsure how to handle a specific incident [64].

NTNU	<b>Hazardous activity identification process</b>				Prepared by	Number	Date
					HSE section	HMSRV2601	22/03/2011
		Approved by	Page	Replaces			
		The Rector		01/12/2006			

Unit: (Department)

EPT

Date: 12.06.14

Line manager:

Ole-Jørgen Nydal

Participants in the identification process (incl. function):

Even de Lanlay (student), Rune Tungen (student)

Short description of the main activity/main process:

Master project for students Even de Lanlay and Rune Tungen. "Evaluation of design concepts for a separation monitoring technology"

Is the project work purely theoretical? (YES/NO)

NO Answer "YES" implies that supervisor is assured that no activities

requiring risk assessment are involved in the work. If YES, briefly describe the activities below. The risk assessment form need not be filled out.

ID nr.	Activity/process	Responsible person	Existing documentation	Existing safety measures	Laws, regulations etc.	Comment
1	Use of pressurized air	Even	NTNU Laboratory and workshop handbook, chapter 6 and 7	HSE Lab course. Turn off when not in use. Make sure it is turned off when changing outlet equipment. Empty hose before changing outlet equipment.		Difficult to remove air pistol (etc.) when hose is filled with air, can cause dangerous situations since significant force then is used.
2	Turning on pressurized air (passing underneath multiphase flow pipes)	Even	NTNU Laboratory and workshop handbook, chapter 2 and 6	Protective eyewear, possibly helmet		Protective eyewear is mandatory in the area of the multiphase loop. Helmet not mandatory, but could be used
3	Loud noise from experiment	Rune	NTNU Laboratory and workshop handbook, chapter 3	Earbuds	HMSRV1210E, Norwegian Working Environment Act §4.4	Take care of other people frequenting the perimeter as well and offer them earbuds.
4	Work after normal working hours	Rune	NTNU Laboratory and workshop handbook, chapter 8	Never work alone. Send SMS to supervisor when entering the lab and when leaving.	HMSRV0704E	
5	Physical stress on personnel	Even	NTNU Laboratory and workshop handbook, chapter 8	Find a good and ergonomic sitting position. Perform stretching and move around once every hour.	HMSRV0704E, HMSRV1206E	
6	Hazards caused by experiments in the near vicinity	Even		Information flow - knowledge of other ongoing experiments		Experiment conducted close to the multiphase loop
7	Locked out after normal working hours because of forgotten key card	Rune		Never take key card out of pocket		



NTNU		<b>Risk assessment</b>		Prepared by	Nummer	Date
				HSE section	HMSRV2603	04/02/2011
HMS./KS				Approved by	Page	Replaces
				The Rector		09/02/2010

Unit: (Institute) EPT Date: 12.06.14

Line manager: Ole-Jørgen Nydal

Participants in the identification process (incl. function): Even de Lanlay (student), Rune Tungen (student)

Risk assessment of: Master project for students Even de Lanlay and Rune Tungen. "Evaluation of design concepts for a separation monitoring technology"

ID nr.	Activity from the identification process form	Potential undesirable incident/strain	Likelihood: (1-5)	Consequence:			Risk value (human)	Risk value (environ.)	Risk value (econo.)	Comments/status Suggested measures
				Human (A-E)	Environment (A-E)	Economy/material (A-E)				
1	Use of pressurized air	Sudden ejection of air	2	C	B	B	C2	B2	B2	Empty hose before removing equipment
2	Turning on pressurized air (passing underneath multiphase flow pipes)	Hit head against the overhanging pipes	2	B	A	A	B2	A2	A2	Wear helmet, walk slow
3	Loud noise from experiment	Damage hearing ability	5	B	A	A	B5	A5	A5	Use earbuds, offer ear protection to people nearby
4	Work after normal working hours	No one to contact immediately if accident occurs	4	B	A	A	B4	A4	A4	
5	Physical stress on personnel	Becoming complacent with HSE regulations	3	C	A	A	C3	A3	A3	Take breaks
6	Hazards caused by experiments in the near vicinity	Splashing of fluids, mechanical breakdown, noise	2	C	B	C	C2	B2	C2	Get information about ongoing experiments
7	Locked out after normal working hours because of forgotten key card	Delay of experiment	3	A	A	B	A3	A3	B3	Never remove key card from pocket

Risk value = Likelihood (1, 2, ...) x consequence (A, B, ...). Risk value A1 means very low risk. Risk value E5 means very large and serious risk

Value	Likelihood		Consequence				
	Criteria	Grading	Human	Environment	Economy/material		
1	Minimal: Once every 50 year or less	E	Very critical May produce fatality/ies	Very prolonged, non-reversible damage	Shutdown of work >1 year.		
2	Low: Once every 10 years or less	D	Critical Permanent injury, may produce serious health damage/sickness	Prolonged damage. Long recovery time.	Shutdown of work 0.5-1 year.		
3	Medium: Once a year or less	C	Dangerous Serious personal injury	Minor damage. Long recovery time	Shutdown of work < 1 month		
4	High: Once a month or less	B	Relatively safe Injury that requires medical treatment	Minor damage. Short recovery time	Shutdown of work < 1 week		
5	Very high: Once a week	A	Safe Injury that requires first aid	Insignificant damage. Short recovery time	Shutdown of work < 1 day		

MATRIX FOR RISK ASSESSMENT

CONSEQUENCE	Very critical	E2	E3	E4	E5
	Critical	D2	D3	D4	D5
Dangerous	C1	C2	C3	C4	C5
Relatively safe	B1	B2	B3	B4	B5
Safe	A1	A2	A3	A4	A5
	Minimal	Low	Medium	High	Very high
LIKELIHOOD					

Explanation of the colors used in the risk matrix.

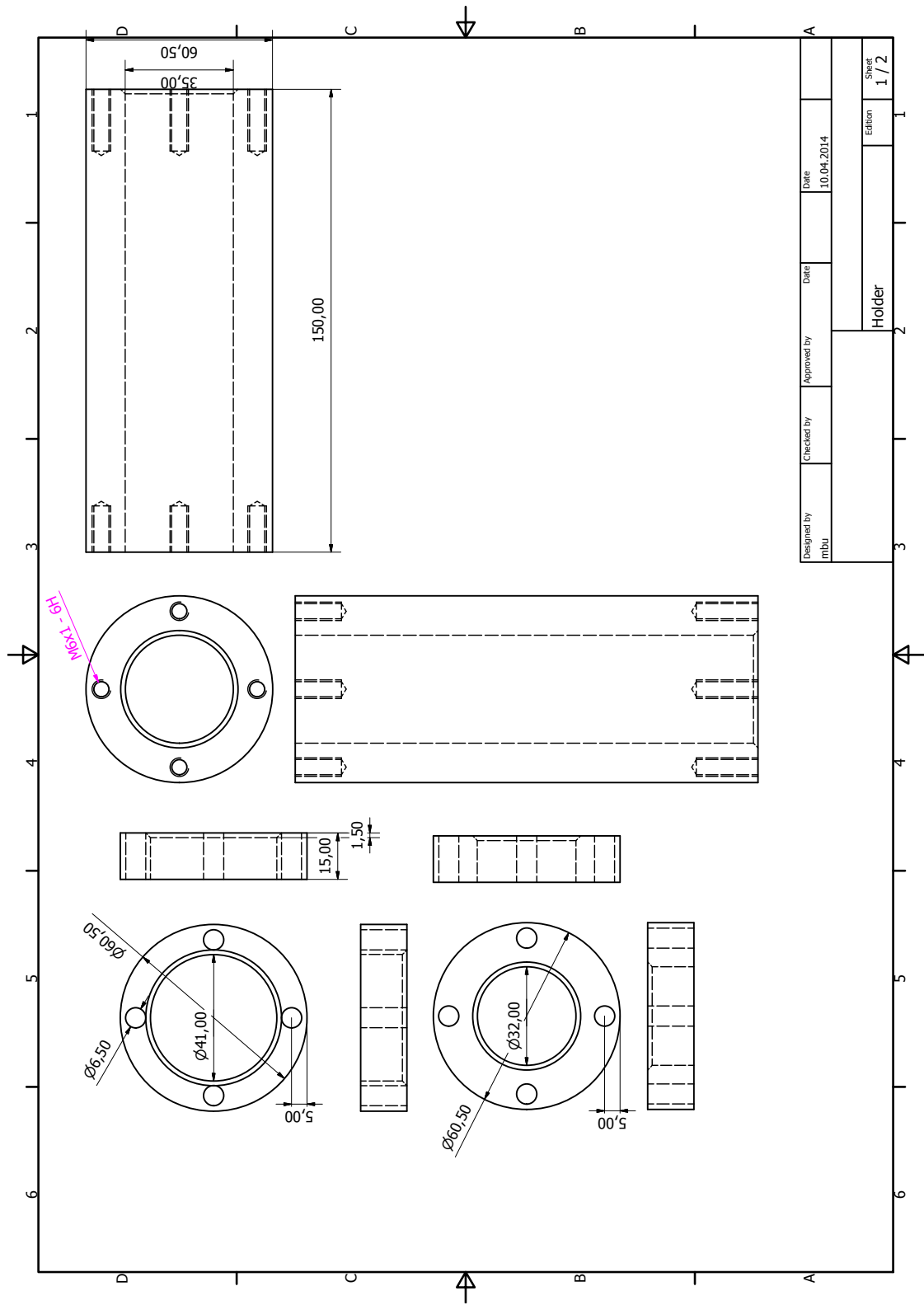
Color	Description
Red	Unacceptable risk. Safety measures must be implemented.
Yellow	Measures to reduce risk shall be considered.
Green	Acceptable risk.

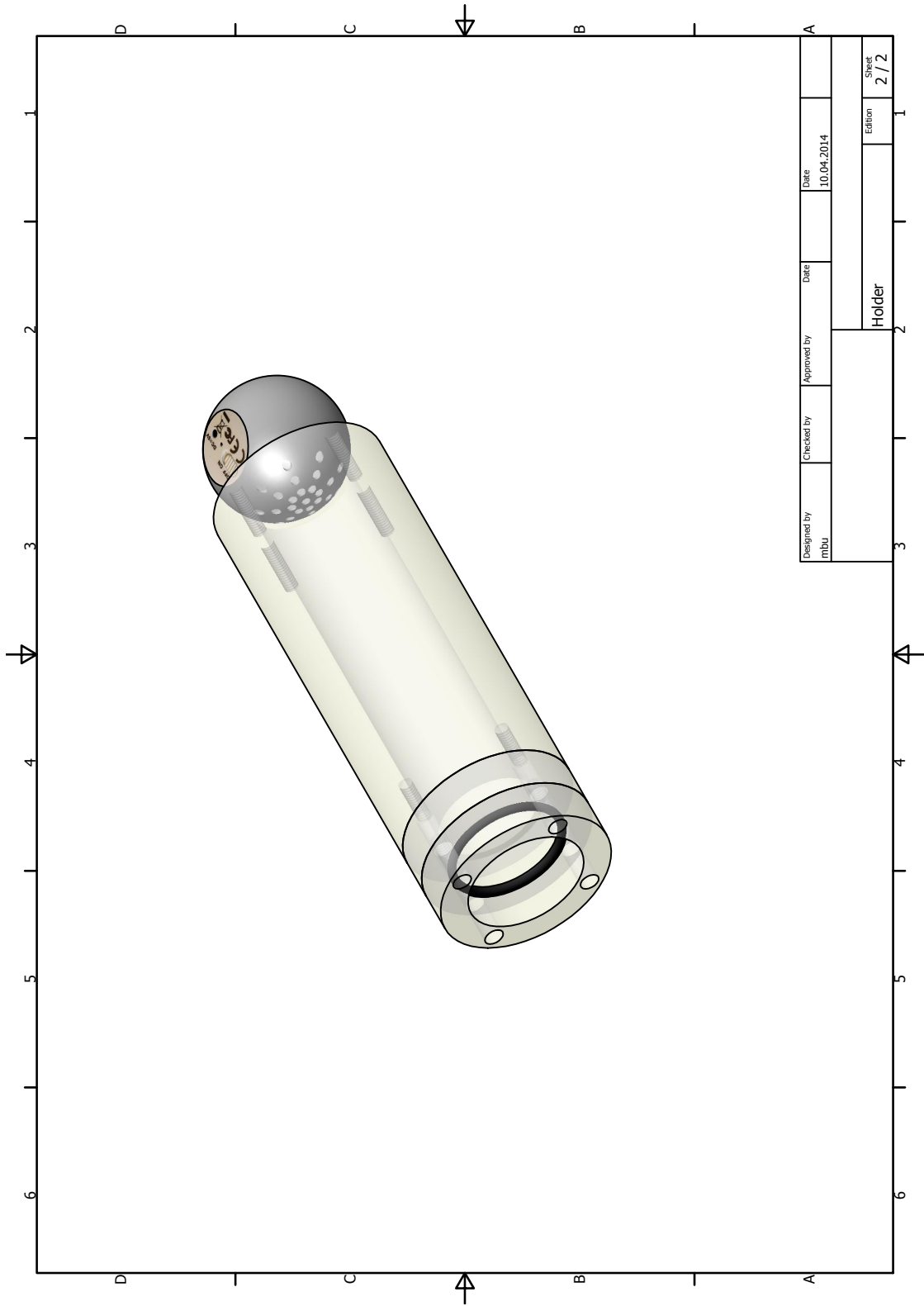
## Appendix D

# Work Drawings For The Experiment

The experimental setup was made in cooperation with Martin Bustadmo and his work drawings for the acrylic cylinder are presented here. The first drawing shows all the components and their corresponding dimensions. To connect the acrylic cylinder to the test pipe, i.e. the smooth of the corrugated pipes, O-rings were made.

In the second drawing, a 3D picture of the finished bolt and the loud speaker is shown. Here, the two O-rings connecting the acrylic cylinder and the test pipe is clearly shown. Between them, a rubber ring is placed to make the connection as air tight as possible.







## Appendix E

# COMSOL Simulation Setup And Results

The simulation of Popescu and Johansen's one-dimensional flow-acoustics model was done using COMSOL Multiphysics. COMSOL Multiphysics is a software platform based on advanced numerical methods, for modeling and simulating physics-based problems [65]. We used Equation Based Modeling in COMSOL in order to solve the system consisting of three PDE's. In COMSOL, built-in equations were modified to replicate the equations given in Popescu and Johansen's model.

### E.1 Equations

#### E.1.1 General Equations

Popescu and Johansen's model is a system of three coupled partial differential equations. The derivation is found in Chapter 3. The following set of equations account for the sound propagation in the pipe:

$$\begin{cases} \frac{\partial(\rho_0 u)}{\partial t} + U \frac{\partial(\rho_0 u)}{\partial z} + \frac{\partial p}{\partial z} = F(z, t), \\ \frac{\partial p}{\partial t} + U \frac{\partial p}{\partial z} + \rho_0 c_0^2 \frac{\partial u}{\partial z} = 0 \end{cases} \quad (3.47 \text{ revisited})$$

where  $u$  [m/s] is the acoustic velocity,  $p$  [Pa] the acoustic pressure,  $U$  [m/s] the velocity,  $\rho_0$  [kg/m<sup>3</sup>] the reference density and  $c_0$  [m/s] the speed of sound.

The source term is:

$$F(z, t) = G \frac{\partial p_s}{\partial z} \quad (3.48 \text{ revisited})$$

where  $p_s$  [Pa] is the acoustic pressure in the corrugations and  $G$  is a coefficient defined in Section 3.6.

The third equation accounts for the acoustic pressure in the corrugations:

$$\ddot{p}_s + 2A\eta_r \left\{ \left( \frac{p_s}{B\rho_0 U^2} \right)^2 - 1 \right\} \omega \dot{p}_s + \omega^2 p_s - v \frac{\partial^3 p_s}{\partial t \partial z^2} = \xi \omega \dot{p} \quad (3.44 \text{ revisited})$$

where the reduced damping  $\eta_r$  [-] is

$$\eta_r = \omega_r^2 \omega \frac{V}{2\pi c^3} \quad (3.45 \text{ revisited})$$

and the excitation term  $\xi$  [-] is

$$\xi = \frac{\omega}{\omega_r} \frac{|p|}{|p + p_s|}. \quad (3.46 \text{ revisited})$$

$A$  and  $B$  are coefficients defined in Section 3.5.

### E.1.2 COMSOL Equations

To account for equation 3.47, two Convection-Diffusions equations are used in COMSOL. They have the following form:

$$\begin{cases} d_a \frac{\partial u}{\partial t} + \nabla(-c\nabla u) + \beta\nabla u = f, \\ d_a \frac{\partial p}{\partial t} + \nabla(-c\nabla p) + \beta\nabla p = f \end{cases} \quad (E.1)$$

where  $u$  is the acoustic velocity,  $p$  the acoustic pressure and

$$\nabla = \frac{\partial}{\partial x}. \quad (E.2)$$

Table E.1 and table E.2 show how equation E.1 is manipulated in COMSOL to match equation 3.47 for  $u$  and  $p$ .

To account for equation 3.44, a Coefficient Form PDE is used. It has the following form:

$$e_a \frac{\partial^2 ps}{\partial t^2} + d_a \frac{\partial ps}{\partial t} + \nabla(-c\nabla ps - \alpha ps + \gamma) + \beta\nabla ps + a ps = f \quad (E.3)$$

where  $ps$  is the acoustic pressure and  $\nabla$  defined as in equation E.2.

Table E.3 shows how the Coefficient Form PDE equation with variable  $ps$  is manipulated.



Convection-Diffusion equation	COMSOL script	General form
Source term $f$	$-px + G * psx$	$-\frac{dp}{dz} + G \frac{dp_s}{dz}$
Diffusion coefficient $\beta$	0	0
Convection coefficient $c$	$U * rho$	$U \rho_0$
Damping or mass coefficient $d_a$	$rho$	$\rho_0$

**Table E.1** – Convection-Diffusion equation with variable  $u$ .

Convection-Diffusion equation	COMSOL script	General form
Source term $f$	$-rho * (c^2) * ux$	$-\rho_0 c^2 \frac{du}{dz}$
Diffusion coefficient $\beta$	0	0
Convection coefficient $c$	$U$	$U$
Damping or mass coefficient $d_a$	1	1

**Table E.2** – Convection-Diffusion equation with variable  $p$ .

Coefficient form PDE	COMSOL script	General form
Diffusion coeff. $c$	0	0
Absorption coeff. $a$	$w^2$	$\omega^2$
Source term $f$	$(w/w_{cavity}) * (abs(p)/abs(p + ps)) * w * pt$	$\frac{\omega}{\omega_r} \frac{ p }{ p+ps } \omega \frac{dp}{dt}$
Mass coeff. $e_a$	1	1
Damping or mass coeff. $d_a$	$2 * eta * A * ((ps/(B * rho * U^2))^2 - 1) * w$	$2\eta_r A \left\{ \left( \frac{ps}{B\rho_0 U^2} \right)^2 - 1 \right\} \omega$
Conserv. flux conv. coeff. $\alpha$	0	0
Convection coeff. $\beta$	0	0
Conservative flux source $\gamma$	$-v * d(psx, t)$	$-v \frac{\partial^3 ps}{\partial t \partial z^2}$

**Table E.3** – Convection-Diffusion equation with variable  $u$ .

## E.2 Boundary Conditions

The boundary conditions we use in COMSOL are strongly linked to the wave theory presented in Chapter 2. For an open pipe, which we are modeling, there exist pressure nodes at each end of the pipe. Mathematically, with a pipe of length  $L$ , the acoustic pressure boundary condition is given by

$$p(0, t) = p(L, t) = 0. \quad (\text{E.4})$$

The velocity of the air particles (acoustic velocity) has the same shape and phase as the displacement. At the antinode, the air particles undergo a displacement equal to two times the amplitude of the graph in figure E.1, while at the node, no displacement occurs.

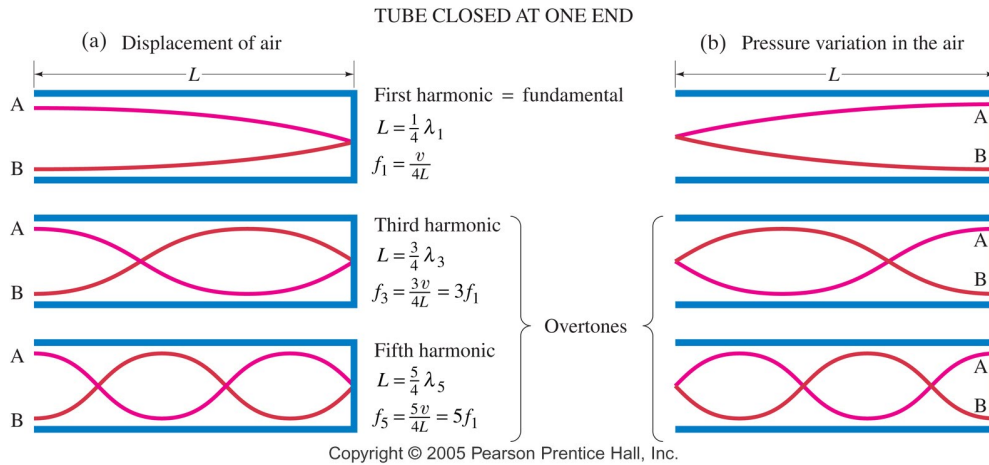


**Figure E.1** – Fundamental modes of a standing wave in a tube closed in one end, showing both the displacement of air and the pressure variations [24].

All of the other points have less displacement than the antinode. Since the velocity is equal to the derivate of the displacement with respect to time, the velocity of the air particles is directly proportional to the displacement. This because the time for one oscillation (i.e. the frequency) is constant. Hence, the graph of the displacement and the velocity of the air particles are equal. At the open ends of the pipe, i.e. an antinode, the derivative of the velocity (and also the displacement) with respect to space is equal to zero. Thus,

$$\frac{\partial u}{\partial x}(0, t) = \frac{\partial u}{\partial x}(L, t) = 0. \quad (\text{E.5})$$

In addition to the four boundary conditions for the pressure and velocity, four initial conditions should be specified as well. At the starting point we have no displacement of

the air particles and no pressure oscillations:

$$p(x, 0) = u(x, 0) = 0. \quad (\text{E.6})$$

The derivative of the pressure oscillation at the starting point is also equal to zero:

$$\frac{\partial p}{\partial t}(x, 0) = \frac{\partial u}{\partial t}(x, 0) = 0. \quad (\text{E.7})$$

In addition to the boundary conditions for the wave propagation quantified by equation 3.47, we need boundary conditions for equation 3.44. Since equation 3.44 describes acoustic pressure as well, we apply the same boundary conditions as for the acoustic pressure in equation 3.47:

$$p_s(0, t) = p_s(L, t) = 0. \quad (\text{E.8})$$

Concerning the initial condition, COMSOL requires a starting value other than zero to launch the simulation. We choose

$$p_s(x, 0) = 1. \quad (\text{E.9})$$

as initial condition. The exact value of the initial condition is irrelevant since the values of  $p_s$  grow well beyond the value of 1.

The boundary condition for the acoustic pressure (variables  $p$  and  $p_s$ ) used in COMSOL is the Dirichlet Boundary Condition, which in COMSOL is quantified in the form

$$\begin{aligned} p &= r \\ p_s &= r \\ g_{reaction} &= -\mu \end{aligned} \quad (\text{E.10})$$

The Dirichlet Boundary condition specifies a value of  $p$  at the boundaries of the domain:  $p = r$  and  $p_s = r$  [66]. We set  $p = 0$  and  $p_s = 0$ .

For the acoustic velocity (variable  $u$ ), we used the Zero Flux boundary condition, which in COMSOL is quantified in the form

$$\vec{n} \cdot (c\nabla u + \alpha u - \gamma) = 0 \quad (\text{E.11})$$

The Zero Flux boundary condition is a Neumann boundary condition equal to zero, meaning the derivative of the acoustic velocity is equal to zero. In COMSOL, the Zero Flux boundary condition is the default boundary condition and prescribes a zero flux (insulation) across the boundary [66].

### E.3 Parameters

The geometry used in COMSOL is a one-dimensional interval of 1 m, corresponding to the length of the corrugated pipe used in our experiment. The properties for air at 15 °C and atmospheric pressure is obtained from McGraw and Hill [32]. The Strouhal number is obtained from Popescu and Johansen’s CFD simulation of a flow over a single cavity with geometry almost equal to the one used in our experiment [9]. Table E.4 and E.5 show the script used in COMSOL and the value of the variables, respectively.

Name	COMSOL script
$U$	3[m/s]
$\rho$	1.225[kg/m <sup>3</sup> ]
$m_y$	1.802e - 5[Pa * s]
$v$	$m_y/\rho$
$c$	343.3[m/s]
$c_{eff}$	$c * \text{sqrt}(\text{vol}_{\text{pipeSmooth}}/\text{vol}_{\text{pipeCorr}})$
$\text{correction}_{fac}$	0.46
$\lambda$	$c_{eff}/w$
$w_{cavity}$	$c_{eff} * \text{sqrt}((Ac)/(\text{vol}_{\text{corrugation}} * (2 * H_{\text{mark}} + Hc)))$
$St$	0.6
$w$	$(St * U)/\text{pitchLength}$
$\eta$	$(w_{cavity}^2 * w * \text{vol}_{\text{pipePitch}})/(2 * \pi * c_{eff}^3)$
$A$	0.5 * ( $\text{boundaryLayer}/\text{pipeRadius}$ )
$B$	$\text{pipe}_d/(\text{cavWidth} + 0.00125)$
$G$	$\text{cavWidth}/\text{pitchLength}$
$\text{pipeLength}$	1[m]
$\text{pipeRadius}$	$\text{pipe}_d/2$
$\text{pipe}_d$	25[mm]
$\text{vol}_{\text{pipeSmooth}}$	$\pi * (\text{pipeRadius}^2) * \text{PipeLength}$
$\text{corr}_{\text{pipeLength}}$	1[m]
$\text{number}_{\text{corr}}$	$\text{corr}_{\text{pipeLength}}/\text{pitchLength}$
$\text{vol}_{\text{pipeCorr}}$	$\text{vol}_{\text{pipeSmooth}} + (\text{number}_{\text{corr}} * \text{vol}_{\text{corrugation}})$
$\text{vol}_{\text{pipePitch}}$	$(\pi * (\text{pipeRadius}^2) * \text{cavWidth}) + \text{vol}_{\text{corrugation}}$
$\text{pitchLength}$	5[mm]
$Hc$	3[mm]
$H_{\text{mark}}$	$Hc/10$
$\text{cavWidth}$	2.5[mm]
$Ac$	$2 * \pi * (((\text{pipeRadius} + Hc)^2 - (\text{pipeRadius})^2) + (\text{cavWidth} * (\text{pipeRadius} + Hc)))$
$\text{Vol}_{\text{corrugation}}$	$\pi * \text{cavWidth} * ((\text{pipeRadius} + Hc)^2 - \text{pipeRadius}^2)$
$\text{boundaryLayer}$	$\text{pipeRadius}/10$

Table E.4 – COMSOL script.

Name	Value	Description
$U$	3 [m/s]	Velocity
$\rho$	1.225 [kg/m <sup>3</sup> ]	Air density
$\mu$	1.802e-5 [Pa · s]	Air viscosity
$\nu$	1.4710e-5 [m <sup>2</sup> /s]	Air kinematic viscosity
$c$	343.3 [m/s]	Speed of sound
$c_{eff}$	304.77 [m/s]	Effective speed of sound
$correction_{fac}$	0.46 [-]	Correction factor
$\lambda$	0.84659 [m]	Wave length
$w_{cavity}$	1.7368e5 [1/s]	Natural frequency cavity
$St$	0.6 [-]	Strouhal number
$w$	360.0 [1/s]	Resonance frequency
$\eta$	0.11519 [-]	Reduced damping
$A$	0.05 [-]	Coefficient A
$B$	6.6667 [-]	Coefficient B
$G$	0.5 [-]	Coefficient G
$pipeLength$	1 [m]	Pipe length
$pipeRadius$	0.0125 [m]	Pipe radius
$pipe_d$	0.025 [m]	Pipe diameter
$vol_{pipeSmooth}$	4.9087e-4 [m <sup>3</sup> ]	Volume of smooth pipe
$corr_{pipeLength}$	1 [m]	Corrugated pipe length
$number_{corr}$	200 [-]	Number of corrugations
$vol_{pipeCorr}$	6.2282e-4 [m <sup>3</sup> ]	Volume corrugated pipe
$vol_{pipePitch}$	1.8869e-6 [m <sup>3</sup> ]	Volume pipe w/ pitch length
$pitchLength$	0.005 [m]	Pitch length
$H_c$	0.003 [m]	Corrugation height
$H_{mark}$	3.0e-4 [m]	Added height
$cavWidth$	0.0025 [m]	Corrugation width
$Ac$	7.7126e-4 [m <sup>2</sup> ]	Area of corrugation
$vol_{corrugation}$	6.5973e-7 [m <sup>3</sup> ]	Volume of corrugation
$boundaryLayer$	0.00125 [m]	Boundary layer thickness

Table E.5 – COMSOL values.

## E.4 Solvers

The PARDISO solver was used for our simulations. The PARDISO solver is a fully coupled, direct solver which uses LU decomposition. LU decomposition factors a matrix as the product of a lower triangular matrix and an upper triangular matrix. The LU decomposition can be viewed as the matrix form of Gaussian elimination [67].

COMSOL offers the choice between three direct solvers; MUMPS, PARDISO and SPOOLES. They differ primarily in their relative speed, where PARDISO tends to be the fastest [68]. MUMS is cluster-capable, but this was unnecessary for our simulations.

We tightened the relative tolerance of the solver from 0.01 to 0.001, which allowed us to get more accurate results. The mesh refinement was set to "normal".

The computer used for the simulations is a stationary HP PC with 16 GB of RAM. It was borrowed from the Department of Energy and Process Engineering at NTNU. We used remote computing to control the stationary PC, in order to manage the simulation from our own laptops (Apple MacBook Pro). One simulation took approximately 6 hours.

## E.5 Results

The time evolution of the acoustic pressure in the pipe for all the simulated velocities and the associated Fourier transforms are shown in figure E.2 to E.19.

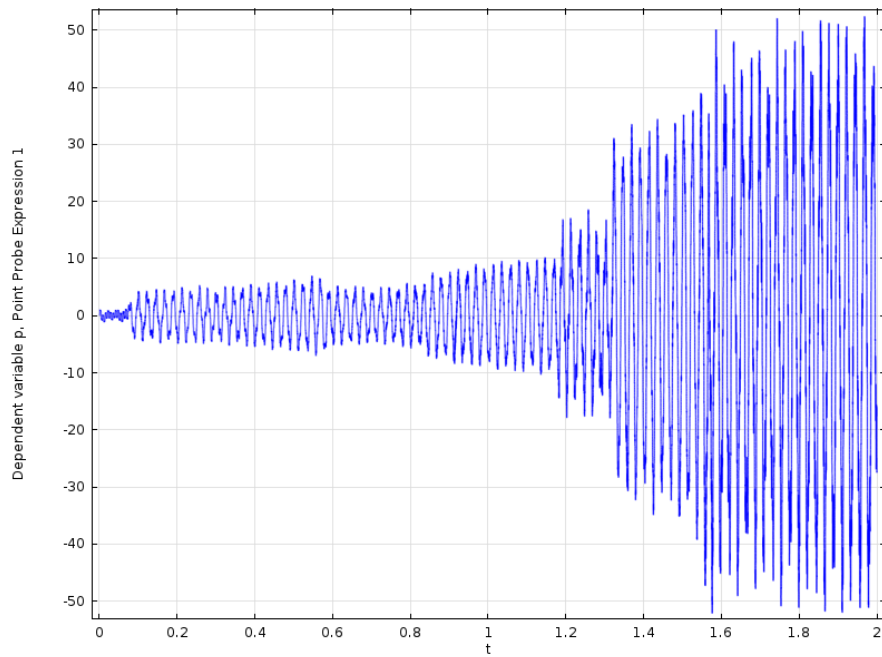


**Figure E.2** – Time evolution of the acoustic pressure at  $U=2.343$  m/s.

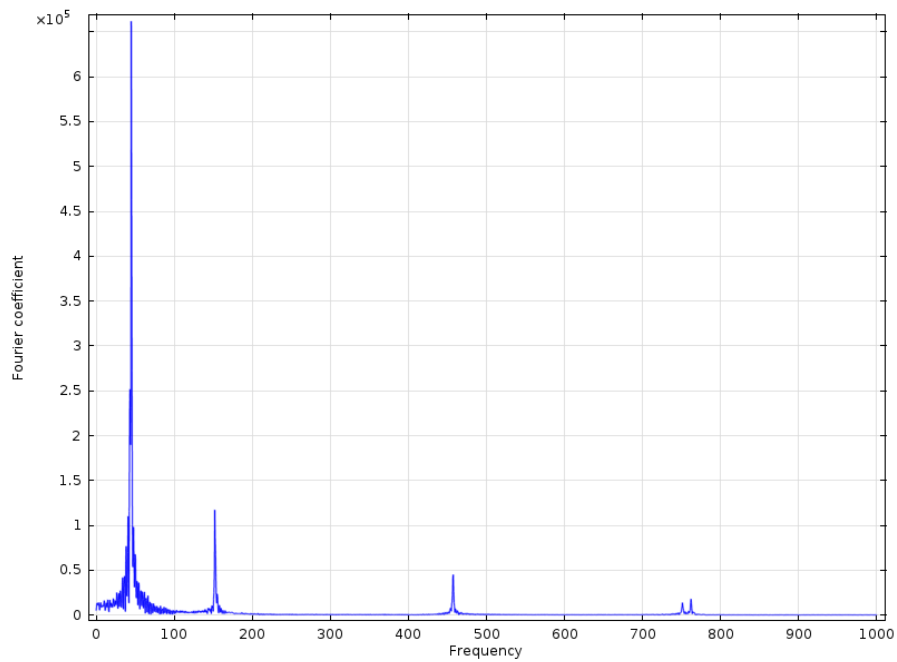


**Figure E.3** – FFT of the acoustic pressure at  $U=2.343$  m/s.

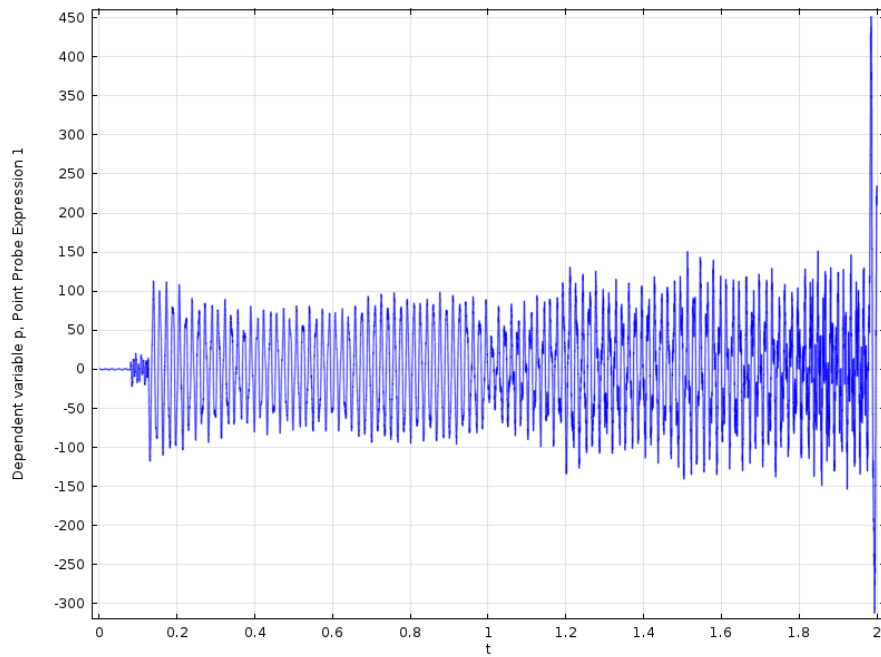


**Figure E.4** – Time evolution of the acoustic pressure at  $U=3.124$  m/s.

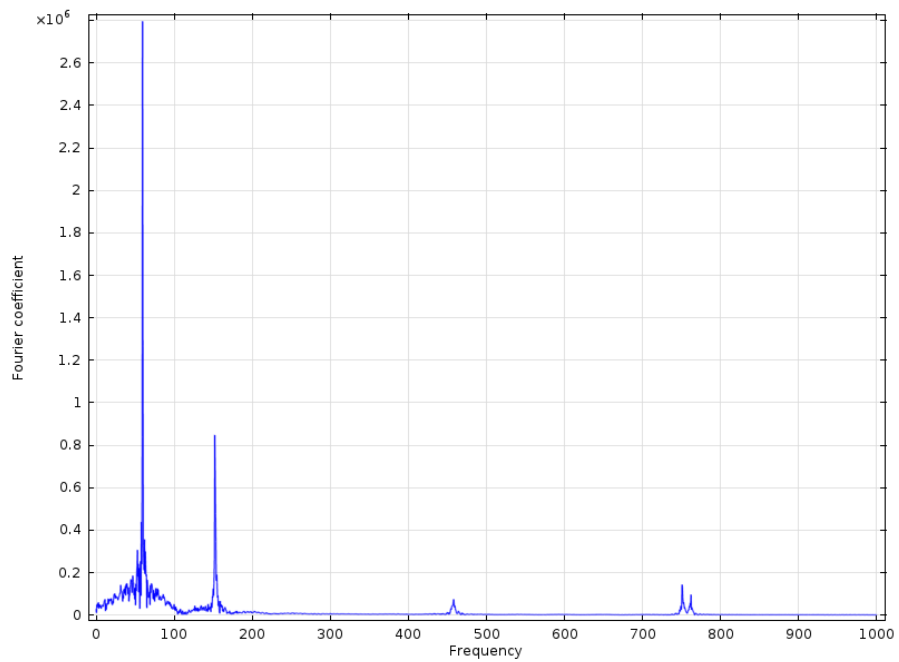


**Figure E.5** – FFT of the acoustic pressure at  $U=3.124$  m/s.



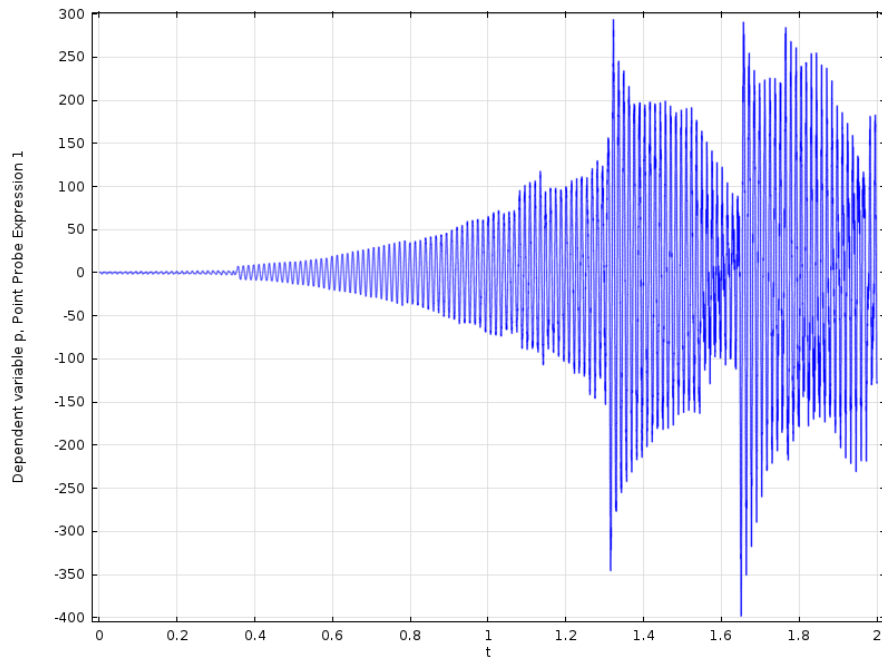


**Figure E.6** – Time evolution of the acoustic pressure at  $U=3.905$  m/s.

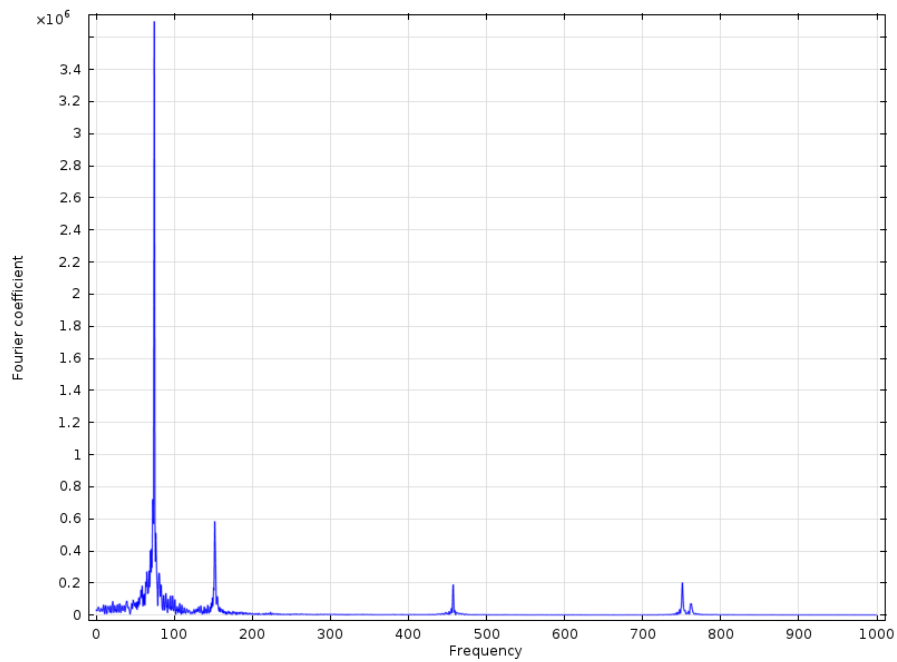


**Figure E.7** – FFT of the acoustic pressure at  $U=3.905$  m/s.

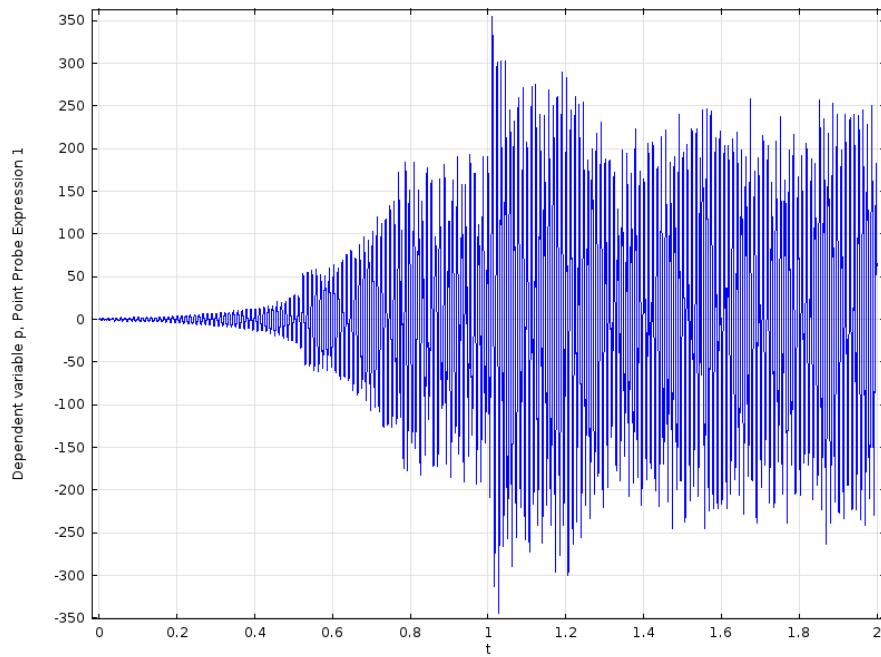


**Figure E.8** – Time evolution of the acoustic pressure at  $U=4.697$  m/s.

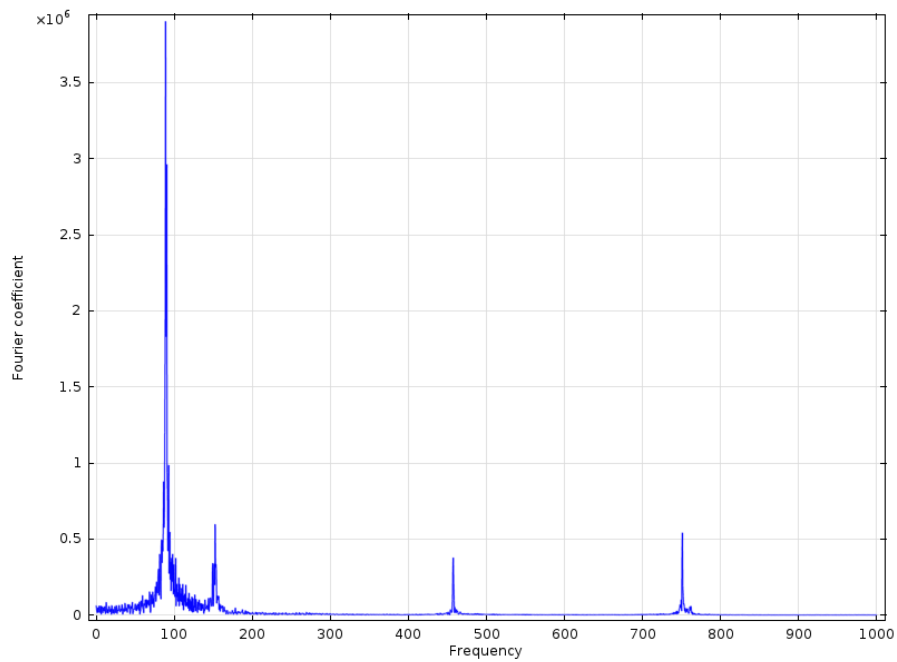


**Figure E.9** – FFT of the acoustic pressure at  $U=4.697$  m/s

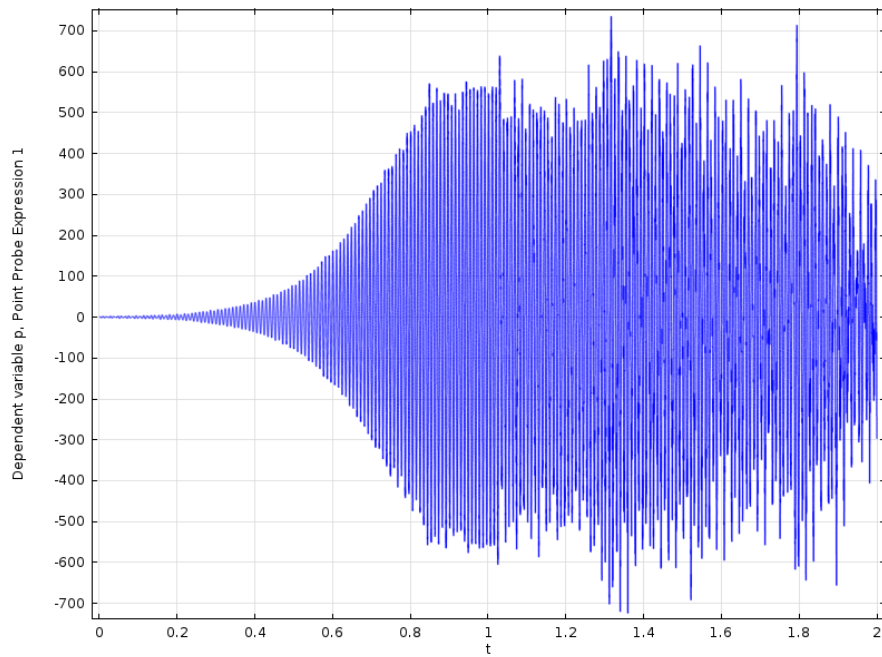


**Figure E.10** – Time evolution of the acoustic pressure at  $U=5.489$  m/s.

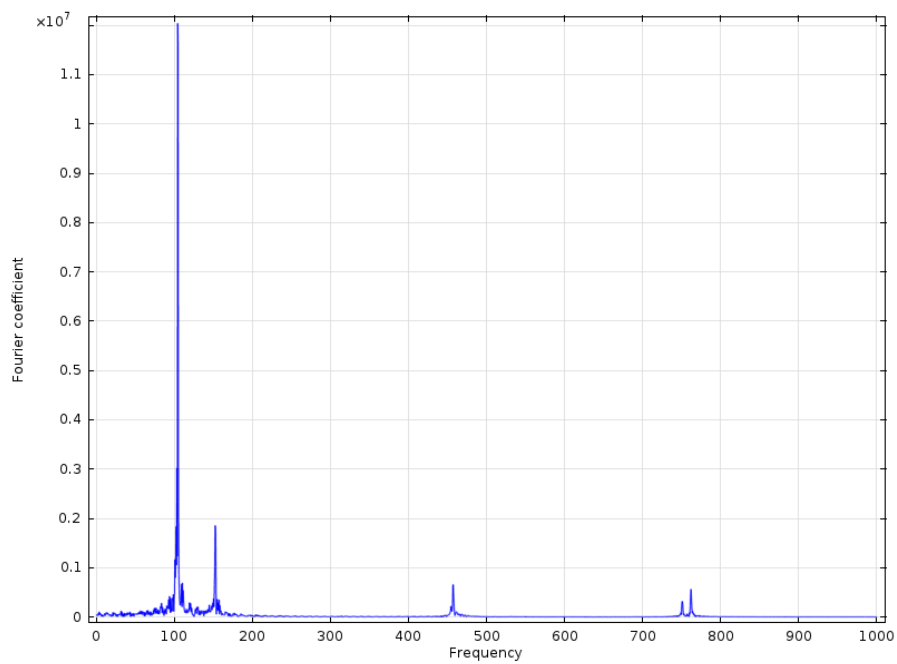


**Figure E.11** – FFT of the acoustic pressure at  $U=5.489$  m/s.

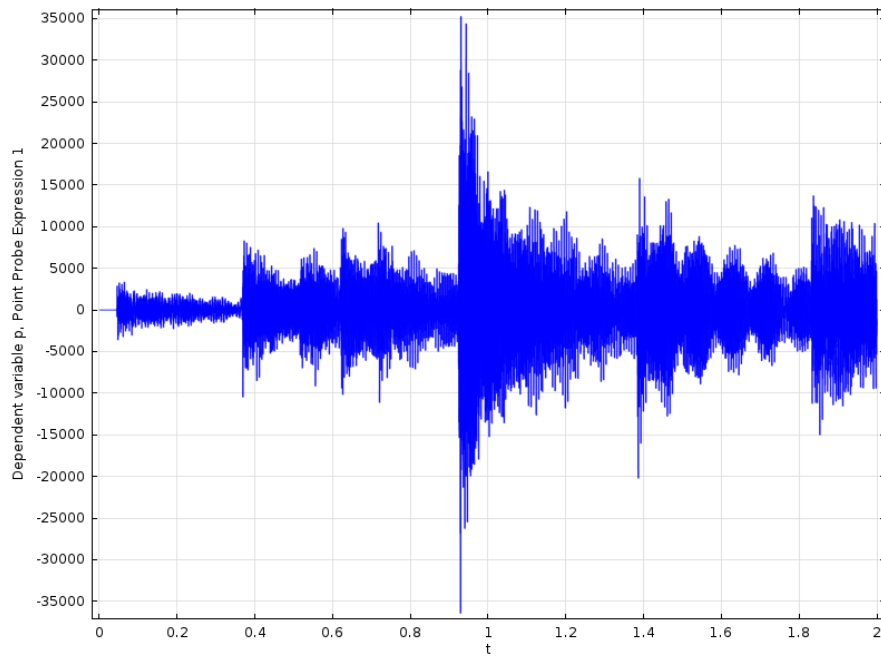


**Figure E.12** – Time evolution of the acoustic pressure at  $U=6.281$  m/s.

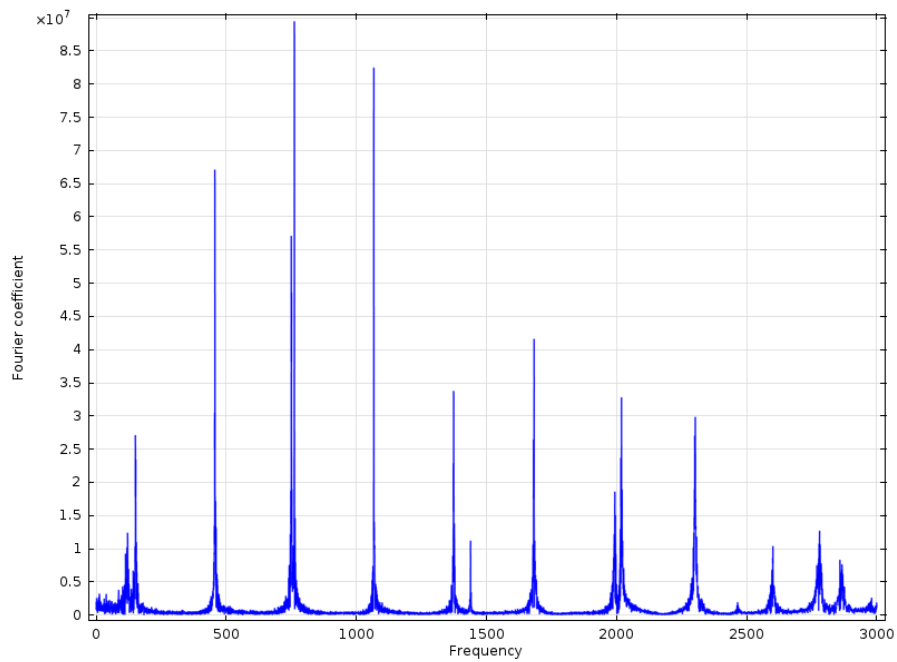


**Figure E.13** – FFT of the acoustic pressure at  $U=6.281$  m/s.

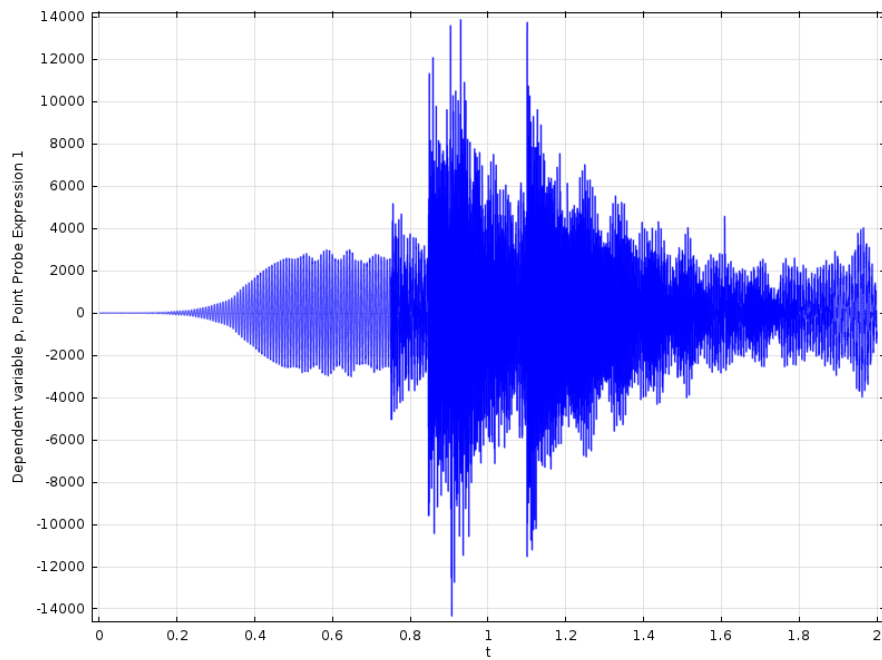


**Figure E.14** – Time evolution of the acoustic pressure at  $U=7.074$  m/s.

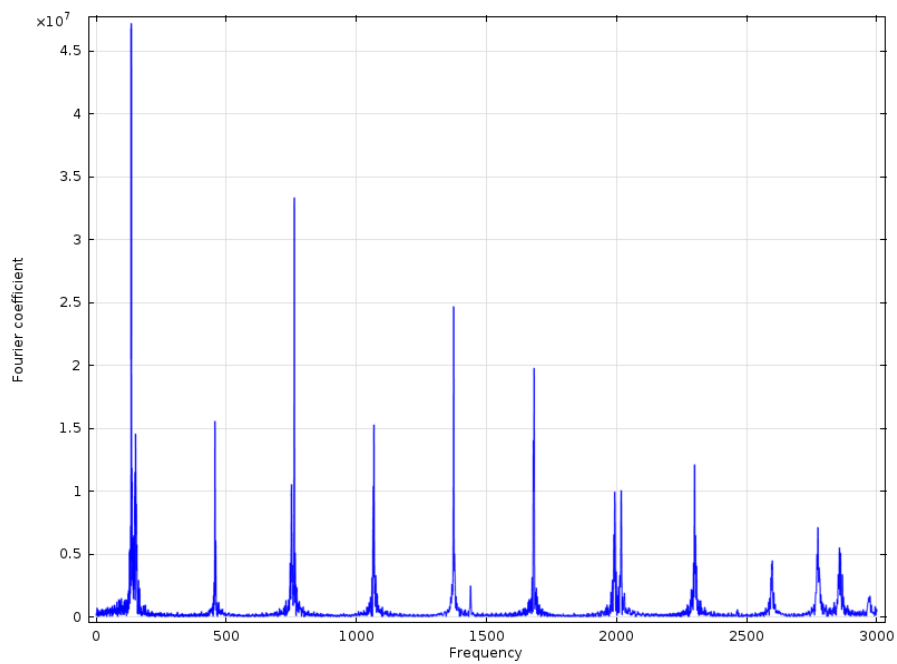


**Figure E.15** – FFT of the acoustic pressure at  $U=7.074$  m/s.

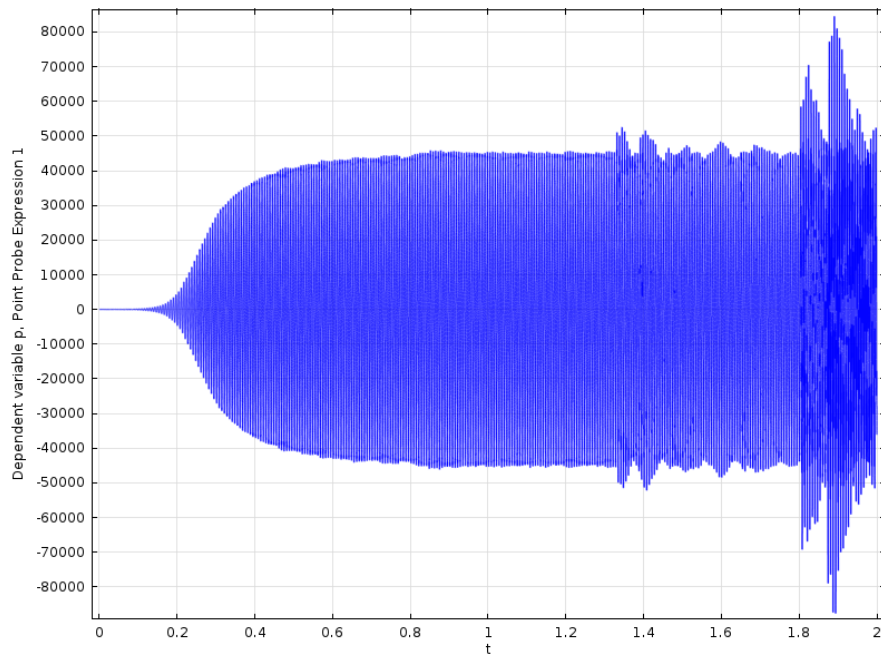


**Figure E.16** – Time evolution of the acoustic pressure at  $U=7.866$  m/s.

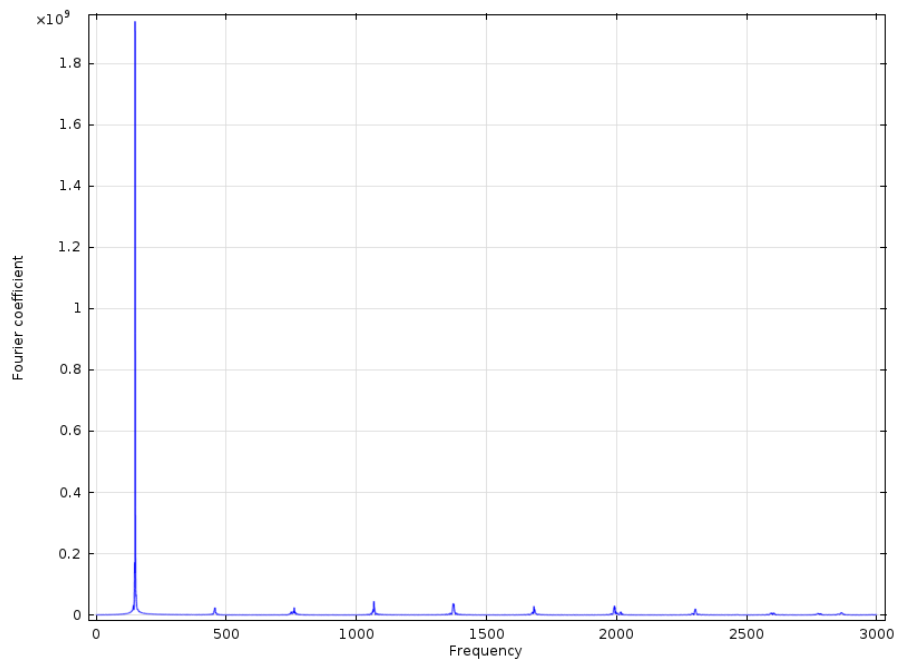


**Figure E.17** – FFT of the acoustic pressure at  $U=7.866$  m/s.

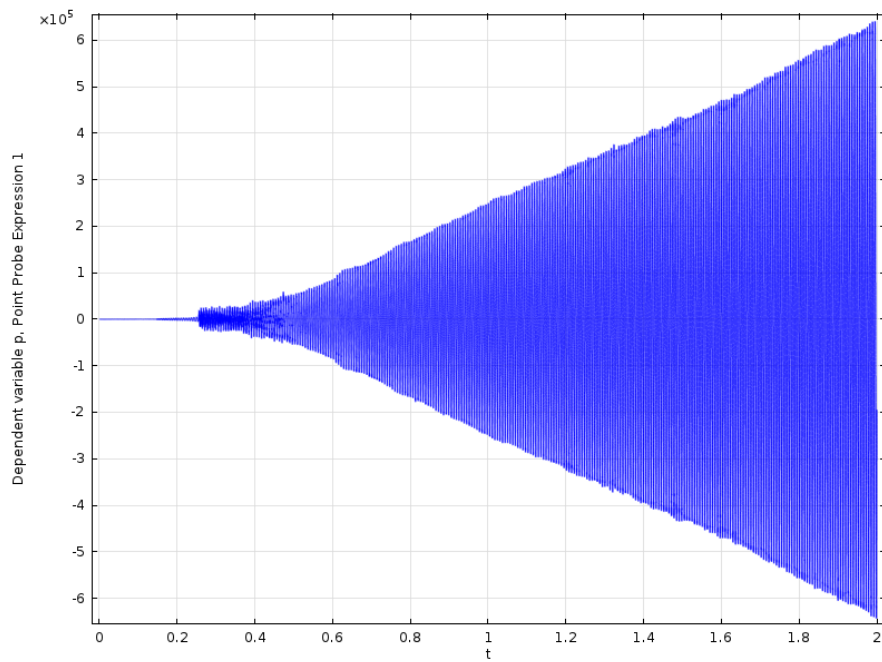


**Figure E.18** – Time evolution of the acoustic pressure at  $U=8.658$  m/s.

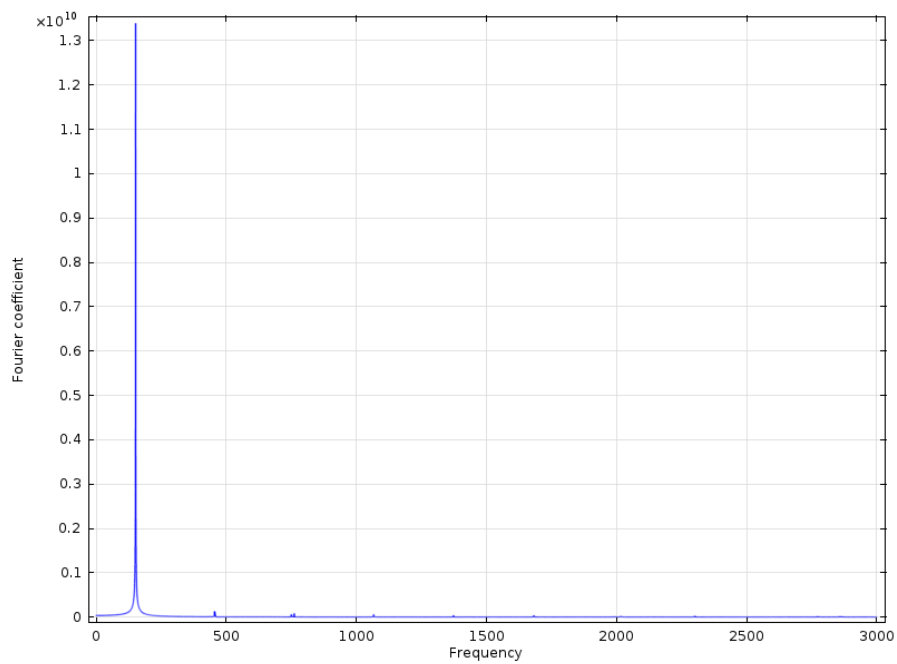


**Figure E.19** – FFT of the acoustic pressure at  $U=8.658$  m/s.